A study of structure and bonding in polymers produced by glow discharge polymerization with particular refrence to the use of E.S.C.A.

Mohamad Zaki Abrahman

UNIVERSITY OF DURHAM

A thesis entitled

A STUDY OF STRUCTURE AND BONDING IN POLYMERS PRODUCED BY GLOW DISCHARGE POLYMERIZATION WITH PARTICULAR REFERENCE TO THE USE OF E.S.C.A.

submitted by

Mohamad Zaki AbRahman B.Sc.(Hons.)
(National University of Malaysia)

A Candidate for the Degree of Doctor of Philosophy

Graduate Society October 1981

بسم الله الرحمن الرحيم

To

My wife Faudziah Hj.Yusoff,
my son Ahmad Faudwaz and
my parents.

ACKNOWLEDGEMENTS

I would like to express my thanks to a large number of individuals for help and assistance without which this work would not have been possible. The first and greatest thanks in this acknowledgement must be given to my supervisor, Professor David T. Clark for his constant guidance, encouragement and enthusiasm during the course of this research. I am indebted to Dr. Alan Dilks, now of Xerox, Co. Webster, New York, for his early advice and practical assistance.

Thanks are also due to Hugh Munro and Alan Harrison for useful help and discussions of the theoretical studies described in Chapter 5. This appreciation is extended to Dick Hutton, Bill Brennan and Rosemary Wilson for their help and advice throughout. I am also grateful to all other members of the group for friendship and co-operation over the past three years.

I am indebted to Mr. R. Coult and Mrs. M. Cocks for performing the microanalytical work and to Mrs. Elizabeth Nevins for her assistance in preparing most of the figures in this thesis. I also gratefully acknowledge Dr. W. J. Feast who kindly supplied the monomer used in the study presented in Chapter 7.

Gratitude is also expressed to the Agricultural University of Malaysia for their generous financial support for my family and I, and to the Science Research Council for provision of equipment.

Finally, but not least, I am always indebted to my parents' distant encouragement during my stay in Durham, England.

Mohamad Zaki AbRahman

1981.

MEMORANDUM

The work described in this thesis was carried out in the University of Durham between October 1978 and September 1981. It has not been submitted for any other degree, and is the original work of author except where acknowledged by reference.

Work in this thesis has formed the whole, or part, of the following publications:-

1. Plasma Polymerization. IV. A Systematic Investigation of the Inductively Coupled R.F. Plasma Polymerization of Pentafluorobenzene, D.T. Clark and M.Z. AbRahman, J. Polym. Sci., Polym. Chem. Ed., in press 1981

2. Plasma Polymerization. V. A Systematic Investigation of the Inductively Coupled R.F. Plasma Polymerization of the Isomeric Tetrafluorobenzenes, D.T. Clark and M.Z. AbRahman, J. Polym. Sci., Polm. Chem. Ed., in press 1981

3. Plasma Polymerization. VI. An ESCA Investigation of the R.F. Plasma Polymerization of Perfluoro-2-butyltetrahydrofuran, D.T. Clark and M.Z. AbRahman, J. Polym. Sci., Polym. Chem. Ed., submitted for publication

4. Plasma Polymerization. VII. An ESCA Investigation of the R.F. Plasma Polymerization of Perfluorobenzene and Pefluorobenzene/Hydrogen Mixtures, D.T. Clark and M.Z. AbRahman, J. Polym. Sci., Polym. Chem. Ed., submitted for publication

5. Plasma Polymerization. VIII. A Comparative Study of the Plasma Polymers Produced from Inductively Coupled Plasmas Excited in the Fluorobenzenes, D.T. Clark and M.Z. AbRahman, J. Polym. Sci., Polym. Chem. Ed., to be submitted

SUMMARY

X-ray photoelectron spectroscopy (ESCA) has been used to investigate the structure, bonding and reactivity of polymers synthesized by R.F. (radio-frequency), glow discharge polymerization (plasma polymerization). Polymer films have been prepared, predominantly using fluorine containing monomers, under a variety of conditions which entailed input powers in the range 1 W -- 50 W and initial pressures of 50 μ -- 500 μ .

The composition, gross structural features and rate of deposition of plasma polymer films obtained from a series of fluorobenzene monomers have been studied by ESCA as a function of the operating parameters. A comparison has been drawn with the data obtained from studies of internal stress, critical surface tension and coefficient of friction for the polymers. Plasma polymers derived from perfluorobenzene/hydrogen mixtures studied in situ are also described. The rates of polymer deposition are discussed as a function of the composite parameter W/FM (W, input power; F, flow rate; M, molecular weight of monomer). Heats of formation have been computed at the MNDO SCF MO level for some structural isomers of the tetrafluorobenzene ring systems, and the results related to the experimental data.

The work has been extended to include the data from a systematic study of polymerized perfluoro-2-butyltetrahydrofuran prepared by plasma techniques. A preliminary study of the polymer films obtained from (1), $CF_2=CF-CF_2-COOCH_3$; (2), $CF_2=CF-C(CF_3)_2OH$; (3), $CF(CF_3)_2OH$ and (4), $CBrCl_2CHBrCl$; by ESCA is also presented.

CONTENTS

CHAPTER ONE

CHAPTER ONE

PLASMA POLYMERIZATION IN GLOW DISCHARGES - A REVIEW

Abstract

A review of the fundamental aspects of low temperature electrical discharge polymerization is presented along with a description of kinetics and mechanisms of plasma polymerization. The application of discharge techniques, the techniques employed to characterize polymer films and some of potential uses of plasma films are also pointed out.

1.1 Introduction

There has been a growing awareness over the past three decades of the importance of plasma chemistry as a means of polymer synthesis.[1-4] The field as a whole however has had a long and chequered history. The first genuine experiment in plasma polymerization dates from 1796 when Dutch chemists subject ethylene to spark discharges and obtained oils.[5] Deposits were often found in early discharge experiments[6,7] and since these were usually insoluble in common solvents and strongly adhered to the walls of vessels were largely regarded as a nuisance. In 1956 however Goodman[8] demonstrated that a 1-micron thick plasma polymerized styrene film deposited on titanium foil made a satisfactory dielectric for a nuclear battery.

Since then, a number of potential uses of plasma polymerized films have been investigated. The application of plasma techniques in polymer synthesis and in the surface modification and degradation of polymers is an area of active development. In industrial laboratories, plasma synthesis of polymers has been a particularly active area of research because of the capability of producing thin uniform pinhole-free films with superior physical, chemical, electrical and mechanical properties. The interest in the use of plasma techniques in the surface modification of polymers may be divided into three different areas, namely; plasma polymerization at surfaces, surface modifications effect by direct and radiative energy transfer, and the use of plasmas for selectively etching or removing organic polymeric phases.

The principle changes brought about by exposure of a polymer to a plasma are in the surface wettability, the molecular weight of a surface layer and the chemical composition of the surface. For the most part, the effects of the plasma treatment are confined to a layer $< 1\ \mu$

in depth below the surface. As a result the bulk properties of the treated polymer are unchanged. Exposure of a polymer to a plasma can also be used to create reactive sites on the polymer surfaces. The changes in the surface composition can be produced by rearrangement and elimination reactions which lead to unsaturation or by attachment of groups (e.g. $-NH_2$, -COOH, etc.) to polymer surfaces. These sites can then be involved in subsequent reactions to further modify the surface chemistry.[9]

This review chapter briefly considers the preparation, characterization, application and also properties and structures of plasma polymerized materials. Some consideration will also be given to the kinetics and mechanisms of plasma polymerization process in organic materials. Although the emphasis in plasma polymerization to date relates essentially to organic-based systems, it is undoubtedly true that some of the most important potential applications are in the field of inorganic systems. Hollahan and McKeever[10] reported that polymers were formed in an electrodeless discharge sustained in mixtures of CO, H_2 and N_2 and the structure of those materials were found to resemble that of proteins.

Before further discussion concerning the formation of plasmas, it is worthwhile to briefly consider the general method involved in forming a plasma polymerized polymer. This entails a gas or vapour of the starting material being introduced in a low vacuum systems, which undergoes excitation due to the effect of an applied electric field. The reactive species so formed lead to the production of plasma polymerized materials. This subject will be discussed in greater detail in the section 1.4.

1.2 Fundamental Aspects of Plasmas

The phenomenon of gas discharges has been apparent since the earliest times in two characteristic forms, lightning and the Aurora Borealis (Northern light) or Aurora Australis (Southern light). Lightning occurs at a pressure of one atmosphere and Franklin (1750) conceived the idea that lightning was not essentially different from the electric sparks that van Musschenbroek had obtained between the terminals of his Leyden jars.[11] The Auroras occur in the rarefied gas of the uppermost layer of the atmosphere. They are the result of high speed bombardment of the rarefied gas by ionized hydrogen gas (protons and electrons) and accompanied by the disturbances in the outer 'magnetosphere' by some interaction with the solar wind.[12]

The early studies of the discharges in gases really began after the discoveries of the induction coil by Ruhmkroff[13] in 1851, that a continuous high voltage source could be obtained and the technique for fusing platinum electrodes into glass by Geissler in 1858. Using the induction coil and Geissler's technique Plücker (1859), Hittorf (1869), Goldstein (1876) and Crookes (1879) were able to investigate the properties of the cathode rays emitted from discharge tubes. In 1897 Thomson shown that cathode rays were sub-atomic particles (electrons) approximately a thousand times lighter than a hydrogen atom. By the early 1900's it had been established, due largely to the work of Townsend[14] that conductivity in electrical discharges resulted from ionization of the gas molecules by collision. After the nature of the elementary charged particles; the electron, the positive ion and the negative ion were clearly recognized the way was opened for considerable advances in gaseous discharge research. In 1928 Langmuir[15] coined the word plasma to denote the ionized gases formed in an electrical discharges.

1.2.1 Definition

A gas discharge can be obtained by subjecting a gas in the discharge tube to an electric field under appropriate conditions (e.g. pressure and power). Some of the gas molecules will be ionized into positive ions and free electrons. Under these circumstance the state of gas is known as a plasma.

A plasma may also be defined as a gaseous state or a partially ionized gas composed of atoms, molecules, ions, metastables and the excited states of these species and electrons such that the concentration of positively and negatively charge species is roughly the same. A plasma must therefore be electrically neutral. This criterion is satisfied when the dimensions of the discharged gas volume are significantly greater than the Debye length λ_D , and[2]

$$\lambda_D = \left(\frac{E_0 k T_e}{n e^2} \right)^{1/2} \qquad (1.2.1)$$

which defines the distance over which a charge imbalance may exist, where: E_0 is the permitivity of free space,

k is the Boltzmann constant,

T_e is the electron temperature,

n is the electron density and

e is the charge on the electron.

Theoretically, a plasma, which has colloquially been referred to as 'the fourth state of matter' may be characterized in terms of the average electron temperature and the charge density within the system. This state of matter which may be found in nature and can also be created

in the laboratories, by such diverse techniques as flames, electrical discharges, electron beams, lasers or nuclear fusion. Figure 1.2.1 summarizes the various plasma systems, either occurring naturally or produced in laboratories.[16]

The region (in Figure 1.2.1) which has proved to be of greatest interest to plasma chemists is that labeled 'glow discharge'. The plasmas produced in the glow discharges are characterized by average electron energies in the range of 1 - 10 eV and electron densities of 10^9 - 10^{12} cm.$^{-3}$ In a glow discharge, the ratio of electron temperature, T_e, and gas temperature, T_g, lie in the range 10 - 100. Such plasmas categorized as being cool, therefore correspond to a Boltzmann equivalent temperature for the massive species of roughly ambient.

Free electrons within the glow discharge gain energy from an imposed electrical field, and subsequently lose it through collision with neutral molecules in the gas. Collision between electrons and molecules leads to the formation of a variety of chemically reactive species, some of which are precursors in the plasma polymerization.

1.2.2 Electron Energy Distribution Functions

The rate of atomic processes in a glow discharge depends mainly on the energy distributions of the interacting particles, and this energy distribution depends primarily upon the behavior of the electrons accelarated by the imposed electric field. Collisions that occur within a plasma may be divided into two types, namely, elastic and inelastic collisions. The latter involved electron collisions with other particles in the plasma leading to excitation and ionization processes. For elastic collision only a very small energy transfer from the electrons take place.[16]

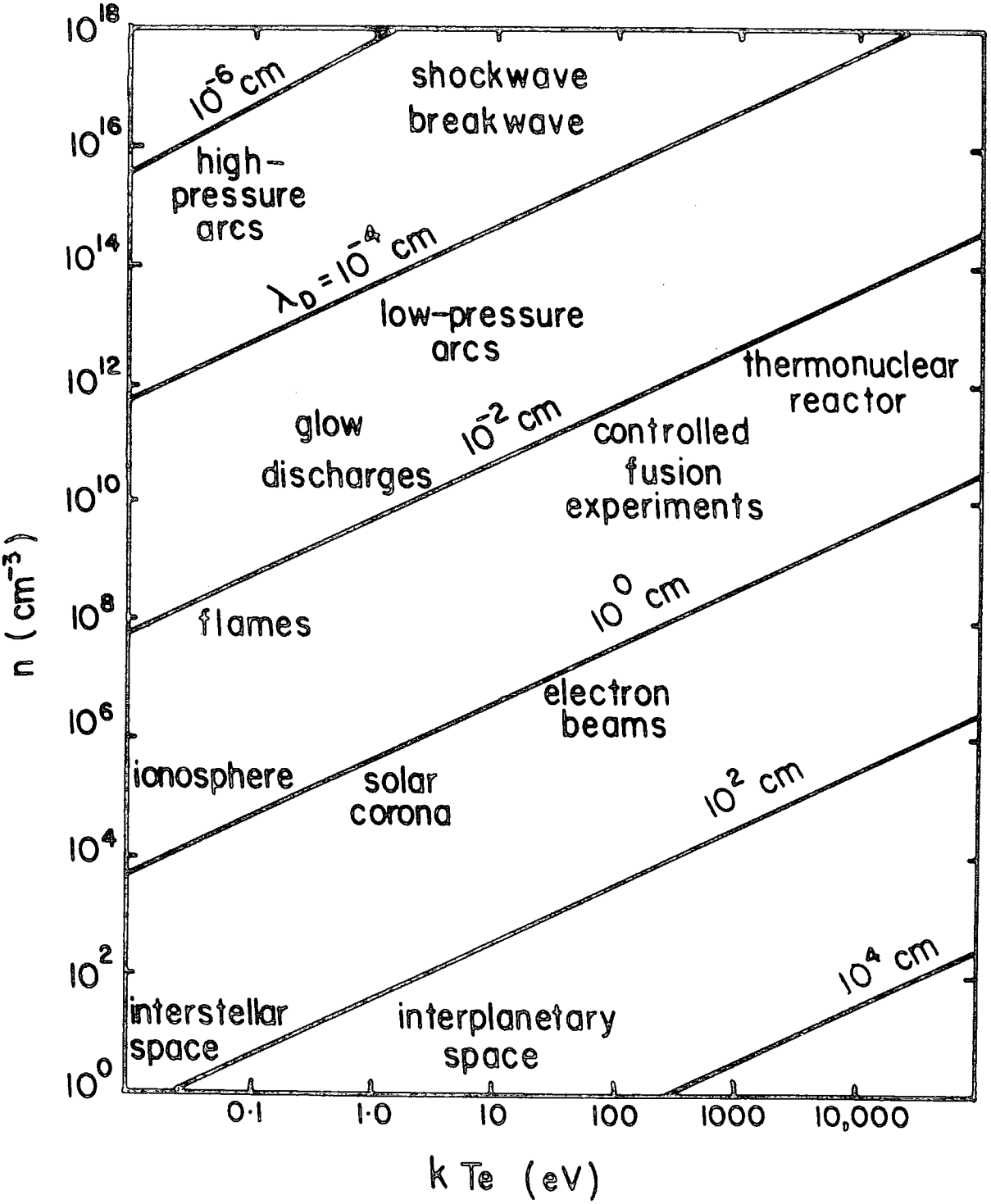

Figure 1.2.1 Plasmas Found in Nature and in The Laboratory

On the assumption that strong interactions between the electrons enables them to attain statistical and thermal equilibrium, the energy distributions of the electrons are likely to be Maxwellian. This may be expressed as; [17]

$$f_m(\epsilon) = 2{\cdot}07 \langle\epsilon\rangle^{-3/2} \epsilon^{1/2} e^{-1{\cdot}5\epsilon/\langle\epsilon\rangle} \qquad (1.2.2)$$

and the electron temperature T_e, is defined as;

$$\langle\epsilon\rangle = \tfrac{3}{2} k T_e \qquad (1.2.3)$$

Equation 1.2.2 gives a good approximation of the velocity distribution of gas molecules in the absence of an electric field or in a high frequency field. However, when only elastic collisions occur, and with the application of an electrical field, the velocity distribution of the electrons becomes Druyvesteyn,[17-18] and may also be expressed in terms of electron energy ϵ , and its mean value, $\langle \epsilon \rangle$ as;

$$f_D(\epsilon) = 1{\cdot}04 \langle\epsilon\rangle^{-3/2} \epsilon^{1/2} e^{-0{\cdot}55\epsilon^2/\langle\epsilon\rangle^2} \qquad (1.2.4)$$

Figure 1.2.2 illustrates the form of the Maxwellian and Druyvesteyn distribution for average electron energies of 1.0, 2.0, and 3.0 eV, which are found to be close approximations for the inert gas plasmas. Equation 1.2.2 still gives a close approximation to velocity distribution, for an electron temperature T, concentration n, and electric field E, if the following conditions are satisfied:[18]

$$\lambda \frac{\delta T}{\delta r} \ll T \qquad (1.2.5)$$

$$\lambda \frac{\delta n}{\delta r} \ll n \qquad (1.2.6)$$

$$E e \lambda \ll kT \qquad (1.2.7)$$

where, λ is the electron mean free path,

e is the electronic charge,

r is the spatial coordinate

Figure 1.2.2 Energy Distributions of electrons in an inert gas glow discharge.

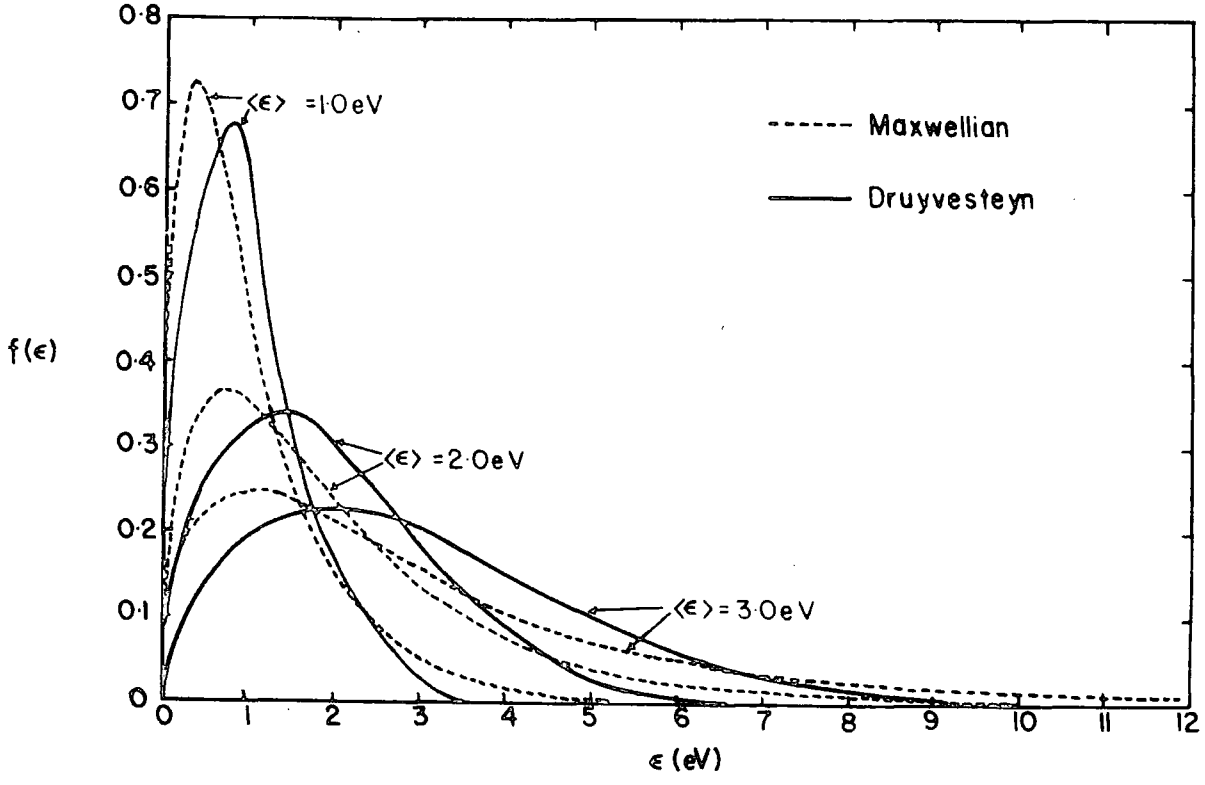

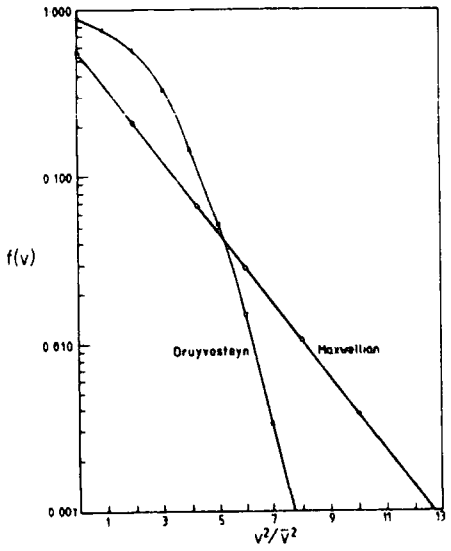

Figure 1.2.3 Maxwellian and Druyvesteyn distribution function having the same mean-squared velocity

Figure 1.2.3 shows a comparison of Maxwellian and Druyvesteyn distributions in velocity having the same mean energy.[19] It is apparent that from the Figure 1.2.2 and Figure 1.2.3, for the same mean energy, the Maxwellian distribution provides a higher fraction of high energy electrons then the Druyvesteyn distribution.

The average velocity, $\bar{C}$ of an electron between collisions is given by:[18]

$$\bar{C} = \left(\frac{M e^2 E \lambda}{m^3}\right)^{1/4} \qquad (1.2.8)$$

where, M is the mass of the heavier particle,

e is the electron charge,

E is the electric field,

λ is the electron mean free path and

m is the electronic mass.

By assuming, $\bar{c}^2 = \overline{c^2}$, electron temperature, T_e (equation 1.2.3) a Maxwellian distribution of electron energy may be obtained:

$$\langle \epsilon \rangle = {}^3/_2 k T \approx {}^1/_2 mc^2 \qquad (1.2.9)$$

where k is the Boltzmann's constant and

c is the random velocity.

In an electrical discharge electron velocities are generally much higher than the ion or molecular velocities. At a temperature of about 300 K the electron temperature is often of the orders of 20,000 K.

Since the calculation of electron velocity distribution is only possible for a small system e.g. H_2, the form of the distribution in 'real systems' has been analyzed experimentally by probe measurement[20] and direct electron sampling.[21] The distribution in both cases corresponds closely to that predicted theoretically for simple systems. In Chapter 5, these electron energy distribution functions have been applied for the detailed discussion of the mechanism of polymer formation in a R.F. (radio-frequency) glow discharge in the isomeric tetrafluoro-benzenes.

1.2.3 Reactive Species in Plasmas

A variety of species may be found in a plasma excited by an electrical discharge arising from collisions involving electrons accelerated by electrical field. These species may include electrons, ions, metastables, neutral molecules and free radicals in ground, and excited states together with photons of various energies. These species are potentially chemically active. Table 1.2.1 displays some typical

value of energies associated with glow discharges together with some typical bond energies for organic systems.[22]

Table 1.2.1

Energies associated with a glow discharge.

	eV
Electrons	0 - 20
Ions	0 - 2
Metastables	0 - 20
U.V./visible	3 - 40

bond energies:-

C—H	4·3	C=O	8·0
C—N	2·9	C—C	3·4
C—Cl	3·4	C=C	6·1
C—F	4·4	C≡C	8·4

With a wide variety of ions, radicals and excited states available from excitation of plasmas, even from simple monomers, it is evident that a variety of mechanisms are available for polymerization reactions in a glow discharge.[23] As an example of the very large number of chemical reactions that may occur, Table 1.2.2 shows data for an oxygen discharge.[16]

Table 1-2-2 Elementary Reactions Occurring in Oxygen Discharges

	Reaction		
I	Ionization	1	$e + O_2 \rightarrow O_2^+ + 2e$
		2	$e + O \rightarrow O^+ + 2e$
II	Dissociative ionization	3	$e + O_2 \rightarrow O^+ + O + 2e$
III	Dissociative attachment	4	$e + O_2 \rightarrow O^- + O$
		5	$e + O_2 \rightarrow O^- + O^+ + e$
IV	Dissociation	6	$e + O_2 \rightarrow 2O + e$
V	Metastable formation	7	$e + O_2 \rightarrow O_2(^1\Delta_g) + e$
VI	Charge transfer	8	$O^+ + O_2 \rightarrow O_2^+ + O$
		9	$O_2^+ + O \rightarrow O^+ + O_2$
		10	$O_4^+ + O_2 \rightarrow O_2^+ + O$
		11	$O_2^+ + 2O_2 \rightarrow O_4^+ + O_2$
		12	$O^- + O_2 \rightarrow O_2^- + O$
		13	$O^- + O_3 \rightarrow O_3^- + O$
		14	$O^- + 2O_2 \rightarrow O_4^- + O_2$
		15	$O_2^- + O \rightarrow O^- + O_2$
		16	$O_2^- + O_2 \rightarrow O_3^- + O$
		17	$O_2^- + O_3 \rightarrow O_3^- + O_2$
		18	$O_2^- + 2O_2 \rightarrow O_4^- + O_2$
		19	$O_3^- + O_2 \rightarrow O_4^- + O_3$
		20	$O_4^- + O \rightarrow O_3^- + O_2$
		21	$O_4^- + O_2 \rightarrow O_2^- + 2O_2$
VII	Detachment	22	$O^- + O \rightarrow O_2 + e$
		23	$O^- + O_2 \rightarrow O + O_2 + e$
		24	$O^- + O_2(^1\Delta_g) \rightarrow O_3 + e$
		25	$O_2^- + O \rightarrow O_3 + e$
		26	$O_2^- + O_2 \rightarrow 2O_2 + e$
		27	$O_2^- + O_2(^1\Delta_g) \rightarrow 2O_2 + e$
VIII	Electron-ion recombination	28	$e + \left\{ \begin{matrix} O^+ \\ O_2^+ \\ O_3^+ \\ O_4^+ \end{matrix} \right\} \rightarrow \left\{ \begin{matrix} O \\ 2O \\ O + O_2 \\ 2O_2 \end{matrix} \right\}$
IX	Ion-ion recombination	29	$\left\{ \begin{matrix} O^- \\ O_2^- \\ O_3^- \\ O_4^- \end{matrix} \right\} + \left\{ \begin{matrix} O^+ \\ O_2^+ \\ O_3^+ \\ O_4^+ \end{matrix} \right\} \rightarrow \left\{ \begin{matrix} O \\ O_2 \end{matrix} \right\}$
X	Atom recombination	30	$2O + O_2 \rightarrow 2O_2$
		31	$3O + O \rightarrow O_2$
		32	$O + O_2 \rightarrow \frac{3}{2}O_2$
		33	$O + O_3 \rightarrow 2O_2$
		34	$O \xrightarrow{\text{wall}} \frac{1}{2}O_2$

1.2.4 Electromagnetic Emissions from Plasmas

The term 'glow discharge' arises from the observation of the emission of light from discharges. Table 1.2.3 the colours observed from the plasma excited in inert gases under a variety of conditions are listed.[24]

Table 1.2.3

	Discharge Colours	
Inert gas	<0.15 Torr	>0.15 Torr
He	Peacock blue	Lilac †
Ne	Crimson	Cerise
Ar	Purple	Purple/blue
Kr	Purple	Purple/blue
Xe	Purple	Purple/blue

† Pink at 0.5 Torr

The optical radiation from low pressure discharges contains components in the microwave, the infrared (IR), the visible, the ultraviolet (uV) and the vacuum ultraviolet (v uV). The infrared radiation can be strongly absorbed in the plasma but generally is dissipated through thermal reactions which produce heat and are of no interest in plasma chemistry. In general, plasmas are copious sources of electromagnetic radiation particularly in the ultraviolet and vacuum ultraviolet.[25] A relatively smaller output in the visible region gives rise to the characteristic colours of the plasma as already noted.

Detailed studies have been reported of simple inert gas plasmas as a function of power and pressure.[24] The published results show that in the case of argon the emission of photons is predominantly associated with the Ar(I) resonance lines at 1048.2 Å and 1066.7 Å originating from transitions of the neutral atoms, $3p^5 4s \longrightarrow 3d^6$, and with the Ar(II) resonance lines at 932.1 Å and 919.8 Å resulting from transitions of single ionized system, $3s3p^6 \longrightarrow 3s^2 3p^5$.

As further example Table 1.2.4 lists the transitions observed in low temperature and low pressure nitrogen plasmas in respect of electromagnetic output in the microwave, infrared, visible and uV portions of the electromagnetic spectrum.[26]

Table 1.2.4

Molecule	Transition	λ(Å)	Region
N_2^+	$A^2\Pi_u \longrightarrow X^2\Sigma_g$ (rotational)	11000	microwave
N_2	$B^3\Pi_g \longrightarrow A^3\Sigma_u^+$ (vibrational)	10500	IR
N_2^+	$B^2\Sigma_u^+ \longrightarrow X^2\Sigma_g^+$ (electronic)	3900	uv/visible
N_2	$C^3\Pi_u \longrightarrow B^3\Pi_g$ (electronic)	3400	uv

1.3 Plasma Polymerization

1.3.1 Introduction

The process of polymer formation in a glow discharge is generally referred to as plasma polymerization or glow discharge polymerization. This process may be carried out by injecting an organic or organometallic vapour into a glow discharge in an inert gas, such as argon, or by creating a glow discharge in a pure organic or organometallic vapour. Under these conditions the deposition of polymeric films onto an exposed surface is often observed.

Since the molecular structure of the starting material (monomer) is not in general retained in the polymer structure, a polymer formed by plasma polymerization cannot be identified by the starting material. This contrasts with the situation for conventional polymerization. The distinctive feature of plasma polymerizationa as opposed to conventional polymerization is that a variety of organic compounds which do not contain particular functional groups may be polymerized. Although the formation of polymers in a glow discharge has been known for many years, the detailed mechanisms of polymer formation by glow discharge techniques and their structure are very complex.[2] The presence of many elementary reactions leads to the production of polymer films of highly crosslinked and branched nature, and which tend to be insoluble in most common solvents.

The considerable current interest in the general properties of polymer films formed in glow discharges has lead to detailed consideration of the mechanism of film formation. The process of plasma polymerization in glow discharges has been classified by Yasuda[27] into "plasma-induced polymerization" and "plasma-state polymerization." The latter process is illustrated by Competitive Ablation and Polymerization (CAP) mechanism

and is shown schematically in Figure 1.3.1.

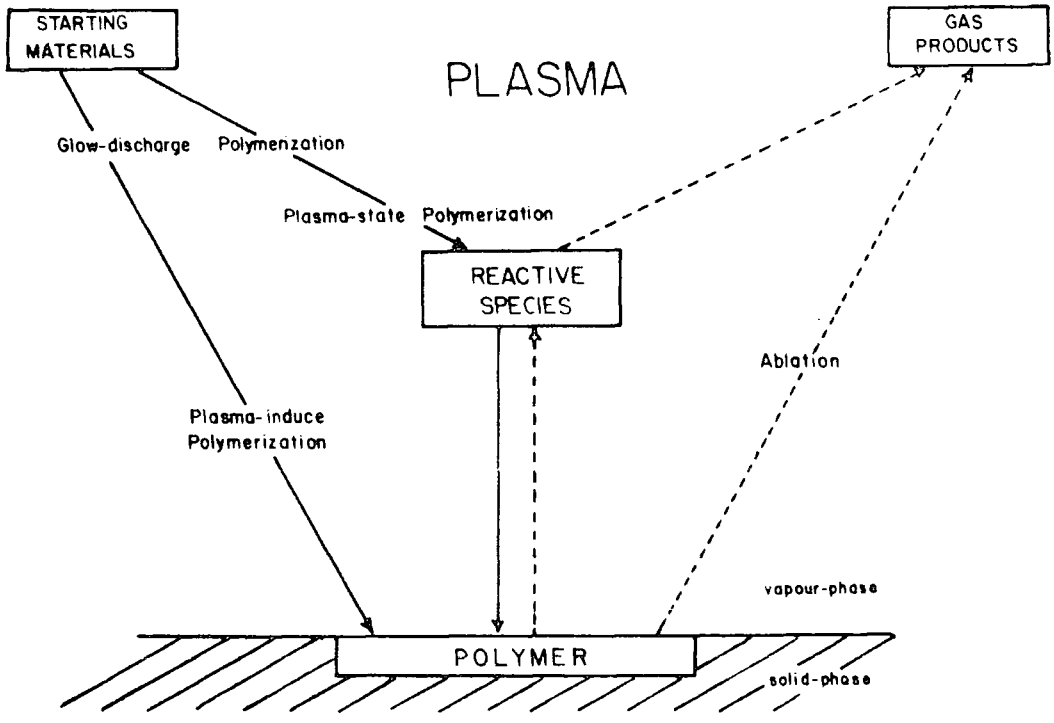

Figure 1.3.1 CAP (COMPETITIVE ABLATION AND POLYMERIZATION) SCHEME OF GLOW DISCHARGE POLYMERIZATION

The processes involved in the polymer formation referred to as plasma-state polymerization occur only via a plasma state, and may be explained by the following mechanism:

Initiation or reinitiation

$$M_i \longrightarrow M_i^*$$

$$M_k \longrightarrow M_k^*$$

Propagation and Termination

$$M_i^* + M_k \longrightarrow M_i - M_k^*$$

$$M_i + M_k^* \longrightarrow M_i - M_k$$

where, i and k are the numbers of repeating units (starting material, i = k = 1), M^* represents a reactive species that may occur in a plasma which is derived from M, while M can also be a fragment or even an atom detached from the original starting material.

Plasma-induced polymerization may be schematically represented by a chain propagation mechanism:

Propagation

$$M^* + M \longrightarrow MM^*$$

$$M_i^* + M \longrightarrow M_{i+1}^*$$

Termination

$$M_i^* + M_k^* \longrightarrow M_i - M_k$$

From the mechanistic scheme, the plasma-induced polymerization is essentially the same as conventional addition polymerization. In this process the starting materials must contain polymerizable structure such as olefinic double bonds, triple bonds or cyclic structures.[27]

Although, the overall polymerization in a glow discharge consists of both plasma-induced polymerization and plasma-state polymerization the mechanism of polymer formation is system dependent. Since all these species present in the plasma are extremely sensitive to the condition of glow discharge, the mechanism of polymer formation is very complex process.

The properties and structures of the polymer are controlled by the balance between polymerization and ablation arising during its formation in the plasma.

The ablation process phenomenon has been observed by Kay[28] for the glow discharge polymerization of CF_4. No plasma polymer deposition occurred under his normal investigation conditions. However, the deposition of the polymer is observed by the introduction of H_2 into monomer flow system. And when the H_2 flow is stopped the ablation or etching of the deposited polymer occurs.

It should be noted that the overall CAP mechanism of polymer formation is extremely dependent on the discharge conditions. Yasuda and coworker[29] have introduced a significantly meaningful composite discharge power parameter W/FM, which may be used to correlate the phenomena of the polymerization occurring in the glow discharge.

where, W is the discharge power (watt)

F is the monomer flow rate (mole per unit time) and

M is the molecular weight of monomer.

It has become apparent that the parameters are important for describing and controlling the experimental conditions of plasma polymerization may be encoded in the composite W/FM parameter. When the gas or vapour of the material to be plasma polymerized is introduced into a vacuum system and the glow discharge is initiated, the deposition of polymer is observed. Since the rate of deposition of the polymer in the glow discharge depends on the nature of the glow discharge the result of the deposition rate obtained is often examined and interpreted in terms of parameters (e.g. discharge power and flow rate).

1.3.2 Kinetics of Plasma Polymerizations

The nature of the polymer formed in a glow discharge strongly depends on the experimental parameters (or operational factors) such as flow rate, pressure, power, frequency and reactor configurations for a given starting material. These operational factors that effect plasma polymerization are interrelated to each other in a complex manner. None of the factors can be singled out as being an independent variable or the most importance factor of the process. The major effects of plasma polymerization which are dependent on some of their operational factors are listed in Table 1.3.1 below.

Table 1.3.1

a) Rate of polymer deposition
   - i) discharge power
   - ii) flow rate

b) Distribution of polymer deposition
   - i) the operating pressure
   - ii) the reactivity of a starting material
   - iii) the geometrical arrangement of inlet of starting material, outlet of the system and region of energy input

c) Properties of polymers
   - i) the types of reactor
   - ii) the location within a reactor where polymer deposition occurs.

Generally the deposition of polymer in the glow discharge depends on the monomer flow rate or discharge power, this is illustrated

in Figure 1.3.2 below.

Figure 1.3.2 Deposition rate of plasma polymers vs. flow rate or discharge power.

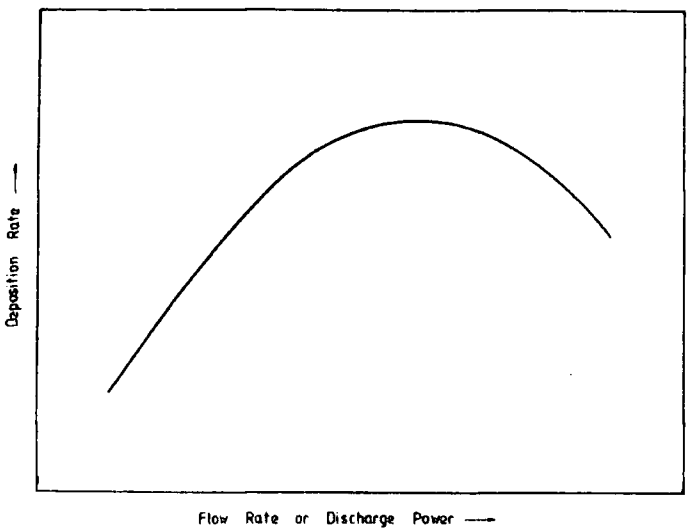

At low flow rates, the deposition rate is limited only by the availability of monomer supply. While at high flow rate the polymerization rates depends on the residence time of the monomers in the reactor. At intermediate flow rates these two competing processes result in a maximum polymer deposition rate. A similar pattern also occurs in considering the deposition rate as a function of discharge power. The polymer deposition rate generally increases with the discharge power until it reaches a maximum. With a further rise in discharge power, ablation process increase in importance and there is then a decrease in the deposition rate of polymer. Examples of such phenomena will be described in Chapters 5,6 and 7.

Figure 1.3.3 also illustrates the above phenomena, in addition it also illustrates the effect of increased unsaturation in the monomers on the rate of deposition.[30]

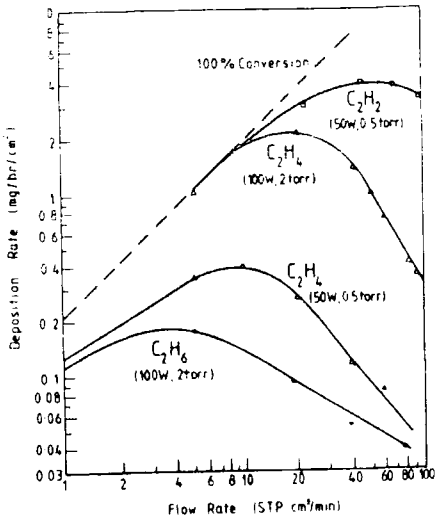

Figure 1.3.3 Rates of plasma polymerization of C_2H_2, C_2H_4, C_2H_6 as a function of flow rate/discharge power

It is evident that under similar conditions, acetylene polymerized faster than ethylene which in turn polymerized even faster than the saturated ethane.

The effect of molecular weight in a homologous series of hydrocarbons on polymerization rate have been studied[30] and representative data are shown in Figure 1.3.4. For three olefinic hydrocarcons, (e.g. ethylene, propylene and isobutylene) the polymerization rate decreases with increasing molecular weight.

Figure 13.4 Deposition rate vs. flow rate for the olefinic hydrocarbons

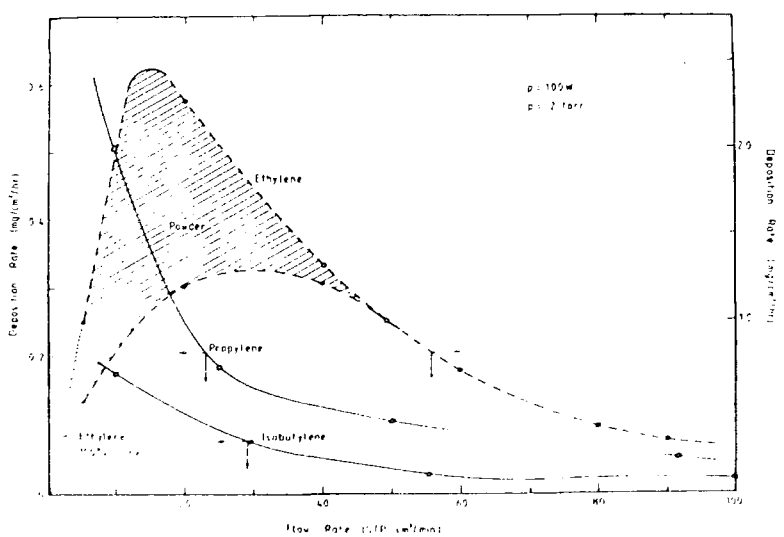

It should be noted that the use of electrodeless glow discharge will produce results different than those with internal electrodes. The effect of frequency on polymerization has not been studied in great detail but typical data[31] are summarized in Figure 1.3.5. This is an interesting effect for polymerization, since most of the plasma polymerizations have been carried out in the frequency range for 50Hz to 13.56Hz using the capacitively coupled system. While for the inductively coupled discharge system the frequency was at 13.56MHz.

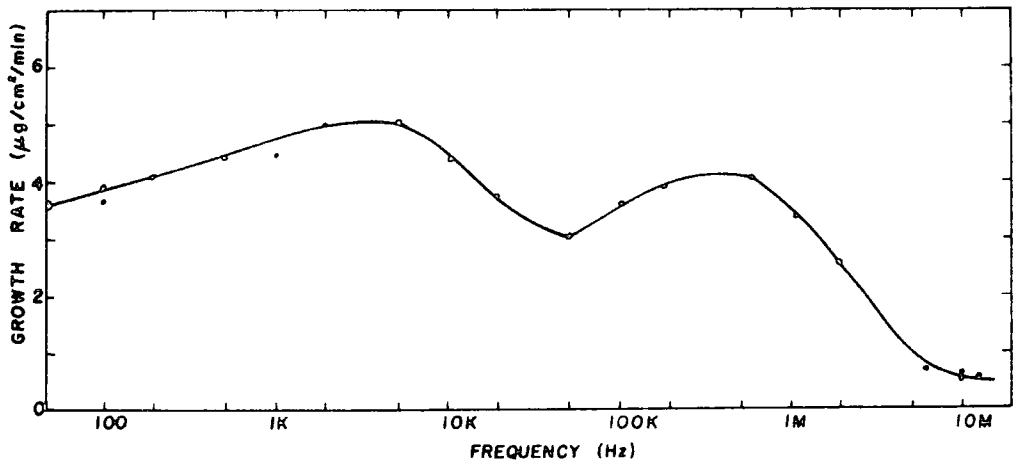

Figure 1.3.5 The rate of plasma polymerization of ethane as a function of discharge frequency.

Generally, it has been noted that the polymerization rate is lower in pulse discharges than in continuous-wave discharges with few exceptions.[32-33]

Deposition rate is also dependent on reactor configuration and on molecular structure. For monomers containing aromatic groups, nitrogen (e.g. -NH, $-NH_2$, -CN), silicon and olefinic double bonds are found to be more polymerizable in comparison with those containing

oxygen (e.g. -C=O, -O-, -OH), chlorine, aliphatic hydrocarbons and cyclic hydrocarbons which tend to decompose.[34]

1.3.3 Mechanisms of Plasma Polymerizations

The discussion above has emphasized that the polymerization in a glow discharge is strongly dependent on the experimental conditions. From previous investigations[35-39] on the mechanisms of polymerization in glow discharges, it is clear that the following may play a major role in the plasma polymerization mechanism:

a) positive ions

b) free radicals

c) substrates

Westwood[40] studied polymerization in an electroded system and observed that the deposition of polymer occurred mainly at the cathode. He suggested that positive ions in the plasma cause the polymerization. A series of experiments have been carried out on the species occurring in R.F. discharges of organic and organomatallic vapour.[41-42] The presence of the highly unsaturated ions in the plasma can be explained in favour of the cationic species mechanism.

The presence of free radicals trapped in the film were observed in the studies by Denaro and coworkers[43], and have also been detected by the e.s.r.[44] technique. Exposure of plasma polymer films to the atmosphere often results in surface oxidation and this has been detected successfully using ESCA and IR spectroscopy. This phenomena has been interpreted as favouring a free radical mechanism.

Although the interest has predominantly been of the plasma polymers deposited onto substrate, polymer formation proceeds via both gas phase and surface reactions simultaneously. The main conclusion from

previous investigations of the mechanism of plasma polymerization may be summarized as follows:

a) Organic monomer is adsorbed onto the surface on a electrode, and polymerization proceeds by the bombardment of positive ions. This mechanism is predominant in the direct methods of glow discharge polymerization process.

b) Polymerization occurs at the surface of the substrate and also in the gas phase in electrodeless systems.

A numbers of workers[38,45-46] have developed kinetic models for plasma polymerization. The kinetic scheme for the plasma polymerization of hydrocarbons which describes the relationship between gas phase and substrate has been presented by Tibbitt and coworkers.[47]

1.3.4 Reactions involved in Glow Discharge Polymerization

Although the plasma chemistry of organic compounds has provided an interesting new way to synthesize the compounds which possess very unique properties with great potential for application, the present knowledge of the reaction in plasma chemistry of organic materials is rather incomplete. It is however, from various kinds of investigation, possible to present general types of reactions which are very commom in glow discharge polymerization. Typical reactions which occur in a glow discharge can be summarized as follows: [2]

a) Generation of atoms, ions or radicals

b) Isomerization

c) Elimination of atoms or small groups

d) Bimolecular reactions.

Atoms of hydrogen, oxygen or nitrogen can be generated if their molecules are subjected to a glow discharge. These atoms react with molecules in the glow discharge either by abstraction of atoms from these molecules resulting the formation of radicals or by addition which can lead to the formation of new molecules or radicals.

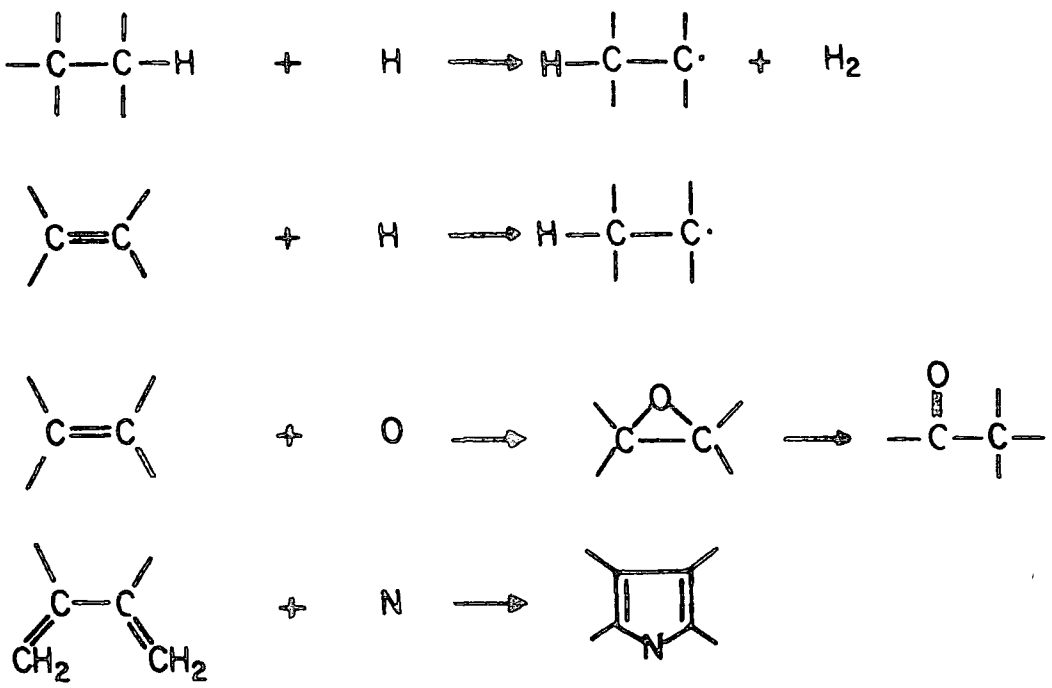

Isomerization reactions have been studied in the particular case of the isomers of stilbene. When the trans-isomer is distilled through a glow discharge, two predominant products I and II were obtained and their relative yields depending on the glow discharge parameters (e.g. discharge power, flow rate, etc.)[48]

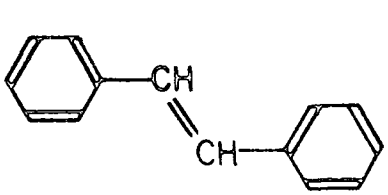

trans-stilbene

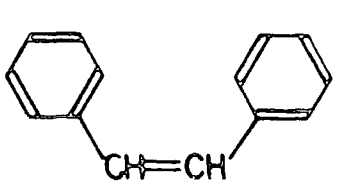

I
cis-stilbene

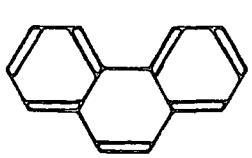

II
pheanthrene

In aromatic compounds especially, isomerization may occur by the migration of substituents and by rearrangement:

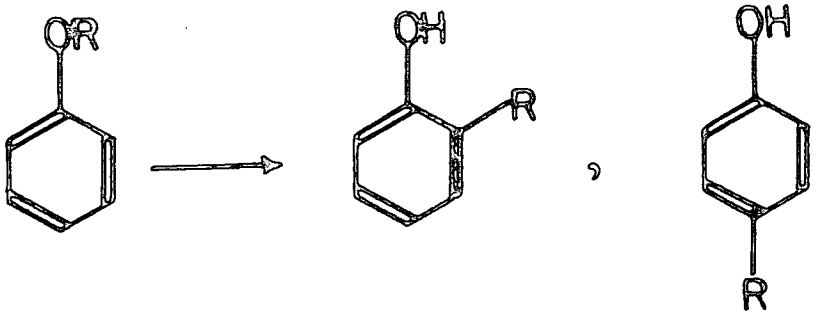

migration

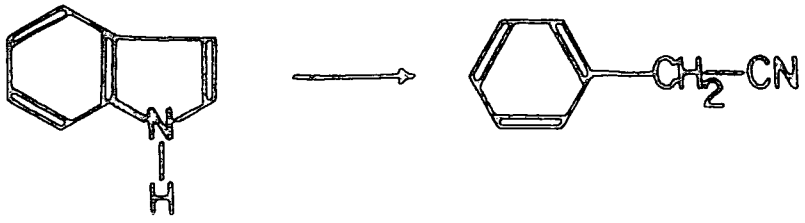

rearrangement

Collisions between electrons of low energies with molecules in the glow discharge may eliminate small groups or atoms. Elimination reactions can occur in plasma by dehydrogenation and the removal of small molecules such as H_2O, HBr, HCN or CO. Elimination reactions may also produce various types of radical intermediates, and these may stabilized by hydrogen abstraction, cyclization, dimerization or polymerization.[48]

1.4 Plasma Techniques

In general, the electrical discharges used to produce a plasma may be divided into two types:[1]

(1) The destructive discharges

The plasma produced by the destructive discharge type commonly known as the 'hot' or 'equilibrium' plasma, referring to the high gas temperature and having roughly the same temperature as electrons. Because of this characteristic it is unstable for plasma polymerization,

as most of the organic compounds have low thermal stability and the polymer produced would be rapidly degraded. Typical examples of such plasmas are arcs and plasma torches, and these are of more interest to physicists.

(2) Non destructive discharges

The term 'cold' or 'non-equilibrium' may be appropriate to describe the plasma produced from a non destructive discharge. This type of plasma, which has been elaborated upon in detail in section 1.2 is characterized by a low gas temperature and high electron temperature. The plasma obtained in the various types of glow discharges and silent discharges are examples of this type of plasma and are of primary interest to chemists.

For AC or DC electrical sources, the elements of glow discharge experiment and their aspects of interest are illustrated schematically in Table 1.4.1[22]

Table 1.4.1

Elements of a Glow Discharge Experiment

Electrical Power	→	Coupling Mechanism	→	Plasma Enviroment
D.C.		Resistive		Current
A.C.		Capacitive		Pressure
R.F.		Inductive		Gas Flow & Temp.
Microwave				Reactant Phases
				Electric & Magnetic Fields

In Table 1.4.1 it is also shown that two different methods can be classified for the formation of a plasma polymer; namely the direct and indirect methods. In the direct method, which was resistive coupling, the glow discharge is initiated between electrodes. Whilst in the indirect method it may be either capacitively or inductively coupled, in which the plasma can be formed by means of electrodes placed externally to the reactor or by an electrodeless discharges with copper coils being wound round the external surface of a cylindrical reactor respectively.

The arrangement of reactors for the indirect method are illustrated in Figure 1.4.1 and can only be employed using frequencies higher than 1 MHz.[48]

Figure 1.4.1 Some arrangements of reactors for electrodeless discharges

Capacitive coupling

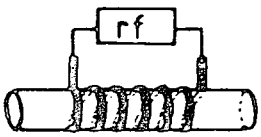

Inductive coupling

The rate of polymer deposition is greater with the direct method and it is also easier to control the film thickness. One of the problems using the direct method compared to the indirect method is that the polymer is deposited on the electrodes and may thus become contaminated.

At low pressure and by the use of internal electrodes, however the glow discharge experiment can be performed over a wide range of frequencies from AC to the RF region. Yasuda and coworker[49] have employed frequencies of 60Hz (AC), 10KHz (AF; Audio frequency) and 13.56MHz (RF). The distribution of power density in the glow region of glow discharge is modified in a magnetic field and so the glow discharge may be operated over a wider range of power levels, where it is magnetically focussed between the electrodes.

In general, DC and low frequency discharge are characterized in terms of the voltage and current supplied to the electrodes (see Figure 1.4.2). At low gas pressure of about 1 Torr a voltage of 10 - 100 V/cm is required to sustain the glow discharge.[50]

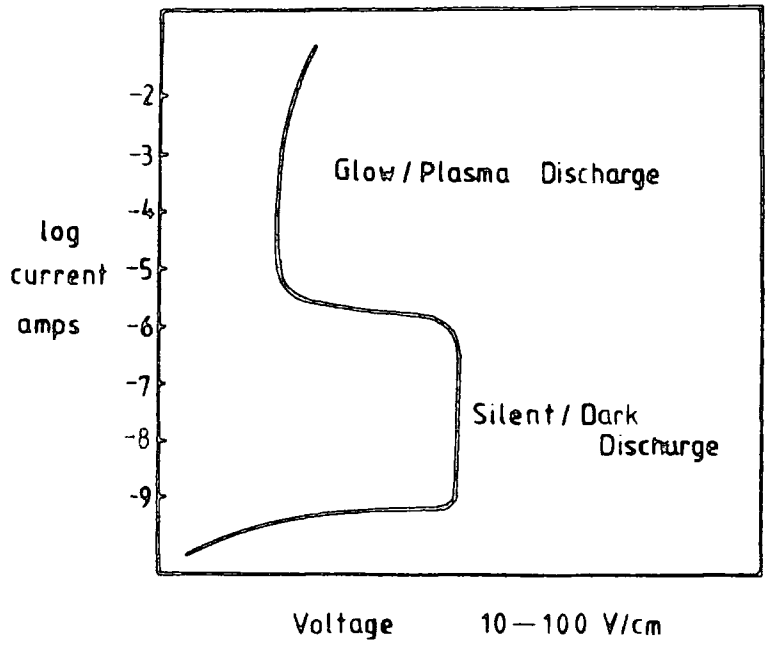

Figure 1.4.2. Schematic current - voltage relationship of a low pressure gas discharge

Typical glow discharge experiment involve power of a few tens of watts or less, although it may vary from 0.1W to a few kilowatts.

Operating pressure using R.F. discharge can range from ~0.01 Torr to 1.0 Torr, and up to 1 atmosphere for DC discharge. Using R.F. power it is possible to obtain stable glow discharge operating at low average power loading by pulsing the power input. When working with DC discharges at higher power levels ($>$ 50 W) some special cooling system for the electrodes is necessary.

Since the plasmas produced by R.F. glow discharges have been shown to have great flexibility and to give closer control over operating parameters, together with the practical consideration such as simplicity, stability, ease of construction and relatively low cost, the plasma polymerizations carried out in this thesis have used this method.

1.4.1 Advantages and Disadvantages of the Glow Discharge Technique

The principle advantages and disavantages of the glow discharge technique are summarized in Table 1.4.2.

Table 1.4.2

Advantages

1. Applicable to batch or continuous processing
2. Low initial capital outlay
3. Suitable applied to a wide range of systems
4. Close control over experimental conditions.

Disadvantages

1. Cannot produce film to a specific formula
2. Thich films are brittle and discoloured.

Only the advantages set out in Table 1.4.2 which are of value to synthesis will be considered.

The wide flexibility in the design and geometry of reactor which may be used in glow discharge experiments to synthesize polymer films or to modify polymer surfaces, it is possible to accommodate either batch or continuous operations depending upon the particular instance. This facility may prove to be of great importance, especially when considering the integration of the technique in industrial processing or treatments.

The glow discharge polymerization is essentially a one step process, which often proves to be cost effective in terms of power consumption and labour requirements. This contrasts with the conventional solution technique which often employ several steps and require highly pure solvents. Such synthetic procedures are normally carried out at temperature higher than ambient.

The obvious advantages of the glow discharge technique compared with conventional polymer synthesis are that the plasma polymerized materials are deposited in the 'clean' environment of a partial vacuum, and may be readily coated onto virtually any substrates.

Low-pressure glow discharge are conveniently sustained by employing a high frequency electric field derived from R.F. or microwave generators. The commercially available R.F. equipment is relatively inexpensive and specifically designed for plasma chemistry studies. A complete arrangement in the R.F. glow discharge experiments consists of a generator, an impedence matching network, some means of measuring the R.F. power, and a reactor attached to a vacuum line.

The glow discharge technique facilitates great control over operating parameter (pressure, flow rate and power), and the appropriate conditions can readily be established for a wide range of starting materials to be plasma polymerized.[1-4]

1.5 Plasma Polymer Characterization Techniques

Since the polymers produced by plasma polymerization are system dependent, the variation in the operating parameter (e.g. power, pressure, etc.) often produce significant changes in the structure and properties of the polymers. As an example[51] (see Figure 1.5.1), ethylene may polymerized at a frequency of 13.56 MHz. and produce a powder, film or oily product depending on the glow discharge experiment.

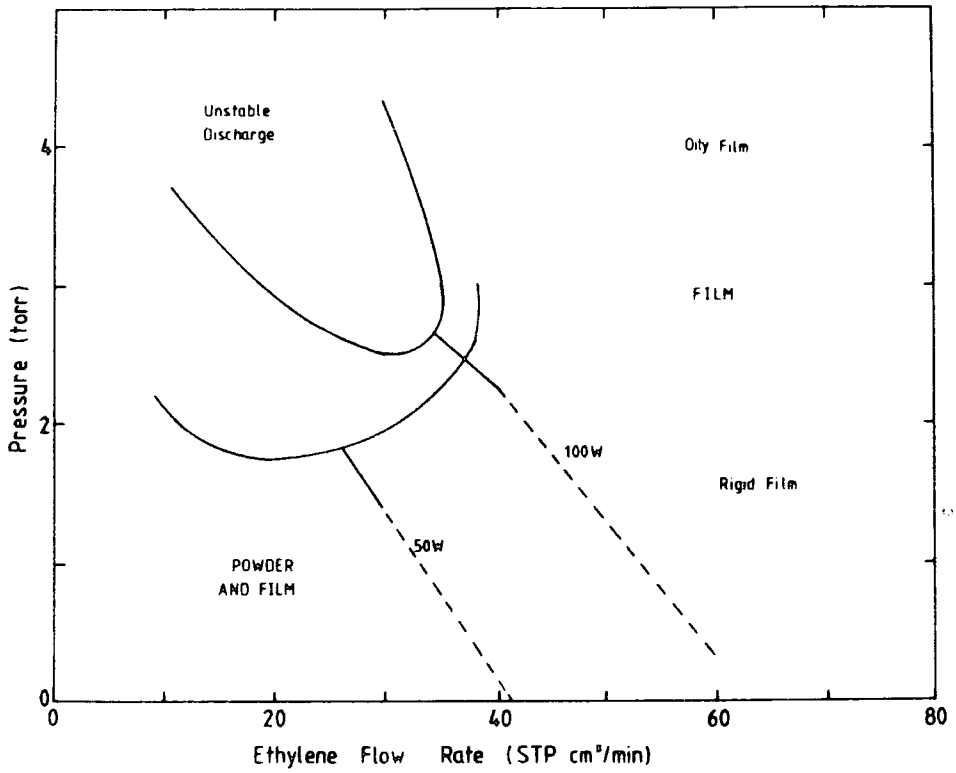

Figure 1.5.1 Characteristic map for plasma polymerized ethylene as a function of operating condition.

In this section a brief discussion of the characterization techniques which have been employed to investigate the properties of plasma polymerized polymers are considered. Some of the analytical techniques which have been used to study the bulk and the surface properties are displayed in Table 1.5.1 below.

Table 1.5.1

A. Bulk properties
   1. Microanalysis
   2. Electron spin resonance spectroscopy (e.s.r)
   3. Gas chromatography
   4. Nuclear magnetic resonance (NMR)
   5. Differential scanning calorimetry and thermal gravimetric analysis
   6. Infrared spectroscopy (IR)
   7. Dielectric properties

B. Surface properties
   1. ESCA
   2. Contact angle
   3. Reflectance IR
   4. Electron microscopy

In this thesis the surface characterizations are considered in somewhat more detail (see later Chapters), however, it is worthwhile to briefly summarize some of the results obtained from bulk studies.

Generally, the chemical composition of the plasma polymerized polymer bear no simple relationship to that of the starting material. And the stoichiometry ratio of the polymer may depends on the condition under which the plasma polymerization reaction is carried out. In a

later Chapter 6, the stoichiometry of plasma polymerized polymers produced by R.F. glow discharges in the fluorobenzenes are investigated using microanalysis and ESCA. The results show that the stoichiometric ratio of carbon to fluorine are roughly the same as for the starting materials,(perfluoro, pentafluoro and tetrafluorobenzenes). But for the isomeric difluoroethylenes[52] the polymers are close to 0.5 in terms of C : F ratio compared to a ratio of 1 for the starting monomers.

Electron spin resonance spectroscopy has been used to determined the spin density of the free radicals in the plasma polymerized material.[44,51] Trapped radicals have low mobilities which may be due to the highly crosslinked structure of the polymers. The free radicals may either be formed through incorporation of radicals from the plasma or created by the interaction of reactive plasma species and radiation with the depositing films. Titration of plasma polymerized styrene with DPPH has shown that in this particular case one in every twenty of polymer molecule is a radical.[43]

The structure of the plasma polymerized polymers have been investigated using pyrolysis/gas chromatography (P/GC).[53-54] Using this technique one can study the highly branched and crosslinked nature and irregularity of the polymer structure.

The oily products from plasma polymerization have been investigated using gel permeation chromatography[41] and vapour phase osmometry[51], and have been shown to be branched oligomers. NMR studies may also be used to investigate the oily product where these are completely soluble. The presence of short alkane segments and various types of vinyl groups have shown to be the predominant structural groups in the polymers as observed by NMR and also by IR.[38,55-58]

Recently high resolution solid state NMR spectroscopy[59-60] have also been used in the study of plasma polymerized films. The structural information obtained from the study of plasma polymerized ethane, ethylene and acetylene has shown that ~50% of the unsaturated carbon and ~21% of saturated carbon is not directly bonded hydrogen, which suggests a high degree of branching and crosslinking of the plasma polymer films. For the plasma polymerized toluene and 10% methyl ^{13}C enriched toluene[60], it is evident from the solid state NMR data that a major process in the plasma involves elimination of a toluene methyl hydrogen to form a benzyl radical, which attachs to the growing polymers.

Differential scanning calorimetry and thermal gravimetric analysis have shown that plasma polymers have no phase transition until decomposition occurs reflecting in general the thermal stability of these materials.[58] It has also been taken as evidence for the crosslinked nature of the plasma polymerized polymer. The complete absence of crystallinity in the plasma polymer has been examined using x-ray diffraction technique.[61]

Turning to the surface characterization technique, Table 1.5.1 (section B) displays some techniques which are commonly employed to study the surface of plasma polymerized materials and modified films. Most of the investigation on polymer surfaces carried out in this thesis are concerned with the used of ESCA, contact angle determination and reflectance IR studies.

The application of ESCA to the study of structure and bonding in polymer surfaces has been fully appreciated. However some of the important information levels available from ESCA studies which may be of use in the investigation of plasma polymerized polymers and modified surfaces are summerized in Table 1.5.2 below.

Table 1.5.2

1. Elemental analysis
2. Functional group analysis
3. Shake-up studies to investigate unsaturation
4. Angular studies
5. Kinetic studies

The polarity of polymer surfaces can be examined by the measurement of contact angles with suitable liquids.[62-64] A discussion concerning contact angle studies will also be considered in Chapter 6. Results from the determination of contact angles will give more or less directly the value of their surface free energy and provide complementary information for discussion of the data obtained with ESCA.

Reflectance IR spectroscopy has been used extensively to obtain further information on the surface structure of the system and the reactivity of the polymer.

The gross morphological features of plasma polymerized polymer surfaces have been investigated using electron microscopy by a number of workers.[65-67] Generally the technique has been used to examine the homogeneity of the polymer films. Using this technique the effect of the surface roughness of the substrate. On the formation of plasma

polymerized ethylene has been investigated. The results show that plasma polymerized ethylene deposited onto a smooth surface (mica) also gives a very smooth surface. Whilst on a rougher substrate (Teflon) a powdery surface was obtained.[66]

1.6 Application of Plasma Polymerized Films

Having discussed in detail the principles and the techniques involved in the formation of plasma polymerized materials and the analytical techniques used to study these, it is worthwhile to point out some of the potential applications of these materials in respect of industrial interest. The fact that the plasma polymerized films show widespread promise in a variety of applications has increasingly stimulated research effect in this field of study.

Considerable attention has been focussed on the utilization of plasma polymerized films as hyperfilteration membranes. Yasuda and coworkers have prepared plasma polymerized films from nitrogen containing monomers and from a mixture of acetylene, carbon monoxide and water vapour. The plasma polymerized films produced from both experiments have shown similar properties as reverse osmosis membranes for water flux and high salt rejection, but the latter has an advantage of being chlorine resistant. The uses of plasma polymerization techniques for preparing semipermeable membranes have been briefly discussed by Hollahan and coworkers.[2]

Plasma polymerized thin films have been used as insulating layers for semiconductors. Mearns[69] has published a review which includes the uses of plasma polymerization in the production of thin insulating films.

The most interesting applications of plasma polymerization techniques for producing thin films are in the field of surface coatings. Their applications are very promising ranging from the potential for use as coatings for laser fusion targets to the application as coatings to reduce friction in elastomer seals used in the oil industry. The particular properties of plasma polymerized films, such as good dielectric, anti-reflection and anti-corrosive properties suggest may use in coatings technology.[3]

Again, with very widespread potential uses, it is important to note that the uses of plasma polymerized films are because of their unique and uniform films with superior physical, chemical, electrical and mechanical properties which cannot be obtained by conventional methods. Rewiew of the applications of plasma polymerized films can be found in the literature.[2-4,68-70]

CHAPTER TWO

CHAPTER TWO

ELECTRON SPECTROSCOPY FOR CHEMICAL APPLICATION (ESCA)

Abstract

The fundamentals of the ESCA experiment are briefly reviewed. Along with this a discussion of the more important experimental observables, and the chemical shifts as interpreted theoretically are outline. A description of typical sample preparation by technique and of the instrumentation employed is also given.

CHAPTER TWO

ELECTRON SPECTROSCOPY FOR CHEMICAL APPLICATION (ESCA)

2.1 Introduction

In common with most other spectroscopic methods x-ray photoelectron spectroscopy is a technique originally developed by physicists and is now extensively utilized by both inorganic and organic chemists as a tool for the investigation of structure, bonding and reactivity.[71]

It was in 1886 and 1887 Heinrich Hertz performed the experiments[72] that first observed the photoelectric effect and confirmed the existence of electromagnetic waves. He accidentally discovered that an electric discharge between two electrodes occurs more readily when ultravoilet light falls on one of the electrodes. In 1900 Lenard,[73] following up some experiments of Hallwachs, showed that the absorption of light by the metal is followed by the emission of electrons from the metal.

The experiments on the photoelectric effect show that the energy of photoelectrons is independent of the intensity but proportional to the frequency of the incident radiation, ν , and the number of photoelectrons emitted per second is proportional to the intensity of the incident radiation. The classical wave theory of light cannot be applied in order to explain this phenomena. But in 1905 Einstein[74] who first realized the light quantum concept introduced by Max Planck in 1900, was able to explain the photoelectric effect. He suggested that in some respects light was more like a stream of particles, now called 'photons', each possessing energy $h\nu$, where h is the Planck constant. In the photoelectric effect, each of these photons gives up its energy to an electron in the metal. Part of the photon energy is used in just removing the electron from the metal surface and the remainder appears as the kinetic

energy (KE) of the photoelecteon, given by the equation:

$$h\nu = KE + W \qquad (2.1.1)$$

where W is the 'work function', the minimum energy needed to remove the electron from the metal's surface.

The emission of electrons from various elements by the x-ray irradiation of thin foil was studied by Robinson [75](in England) and de Broglie[76] (in France). The distribution of electron energies for the transmitted photoelectrons was recorded photographically and analyzed using a homogeneous magnetic field. Since the radiation source consisted of a continuous spectrum (bremsstrahlung) with the characteristic line spectrum of the anode material superimposed, the electron distributions obtained were characterized by long tails with distinct edges at the high energy end. Measurement of these edge positions give a determination of the energy levels of the electron orbital in the atom and therefore with a knowledge of the exciting x-ray line, binding energies of the photo-electrons were calculated.

Except for a few isolated attempts [77-79] to extend the work of Robinson and de Broglie, x-ray photoelectron spectroscopy went into recession, as at that time the edge positions were not well defined. It was not until the early 1950's when Siegbahn and coworkers [80] at Uppsala University, Sweden, developed an iron-free magnetic double-focussing electron analyzer for high resolution studies of β-ray energies.

In 1954 the instrument was ready to use to record high resolution photoelectron spectra excited by x-ray and they observed that the sharp line could be resolved from the edge of each electron veil (see Fig. 2.1.1). This line represents the kinetic energy of photoelectrons which do not undergo any energy loss and, therefore corresponds to the binding energy

of the atomic level from which they come and could be measured to a precision of a few tenths of an electron volt (eV).

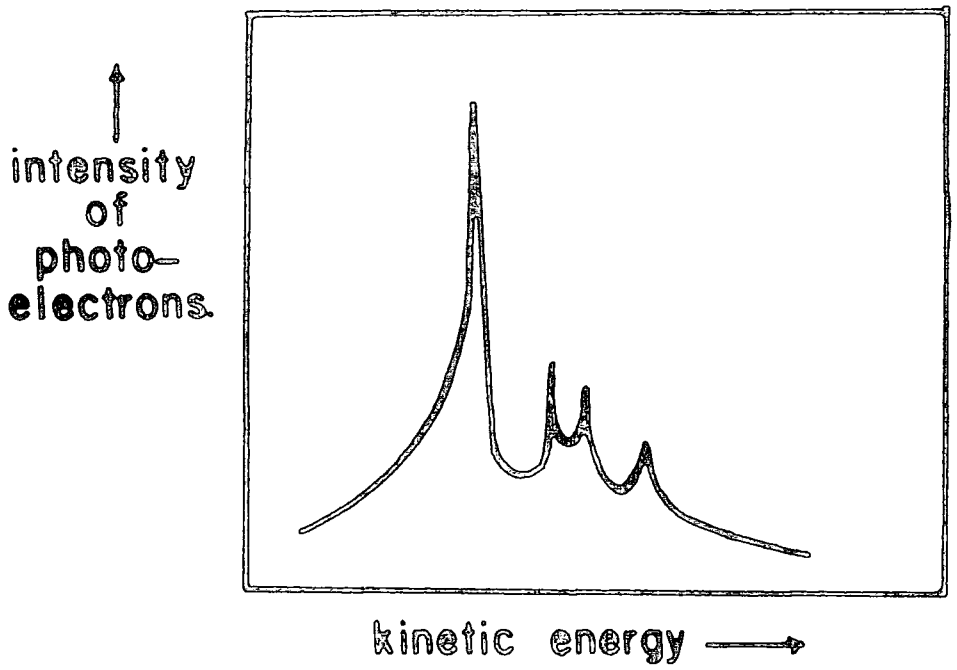

Figure 2.1.1 Electron Spectra of MgO with $Cu_{K\alpha}$ X-Ray

Using this new technique in 1958, Siegbahn and coworkers[81] first studies chemical shifts for copper and it oxides. However, its general utility was fully appreciated only as recently as 1964, after they observed the two distinct 1s peaks from the different oxidation states of sulphur in sodium thiosulphate.[82-83]

Over the past 30 years the technique of photoelectron spectroscopy has largely been developed by Siegbahn and his coworkers[84] and much of the early work has been extensively documented in 1968 in 'ESCA, Atomic, Molecular and Solid State Structure Studied by Means of Electron Spectroscopy.' Later works by this group were well documented in a series of publications.[85-89]

As an electron spectroscopic technique, the basis of ESCA " Electron Spectroscopy for Chemical Application " originally coined by Siegbahn, is the measurement of the energies of electrons photoemitted from a sample in a vacuum following ionization by incident photons. For ionization by x-ray photons the technique is also known as X-ray Photoelectron Spectroscopy (XPS), and in addition the terms; High Energy Photoelectron Spectroscopy (HEPS), Induced Electron Emission Spectroscopy (IEES) and Photoelectron Spectroscopy of the Inner Shell (PESIS) have also been used.

2.2 Processes Involved in ESCA

2.2.1 Photoionization

When an atom in a molecule or lattice is irradiated with a monoenergetic beam of soft x-ray, then electrons with specific kinetic energies can be photoejected.[84]

The most commonly employed x-ray sources in current use are $Al_{K\alpha_{1,2}}$ and $Mg_{K\alpha_{1,2}}$ with corresponding photon energies of 1486.6 eV and 1253.7 eV respectively. In principle all electrons, from the core to the valence levels may be ejected though these latter are usually studied[90] using Ultravoilet Photoelectron Spectroscopy (UPS) with He (I) radiation, 21.22 eV or He (II) radiation, 40.8 eV. Typically, the life-times of the core hole state of the photoemission processes is complete in the range 10^{-13} - 10^{-17} secs.[91] Emphasizing the extremely short time scales involved in ESCA compared with most other spectroscopic techniques.

For an isolated molecule, such as in gas phase the total kinetic

---

Originally designated " ..... for Chemical Analysis ".

energy (KE) of the ejected photoelectron is given by

$$KE = h\nu - BE - E_r \qquad (2.2.1)$$

where h is Planck's constant,

ν is the frequency of the x-ray radiation,

BE is the binding energy of the photoemitted electron, and

E_r is the recoil energy of the atom or molecule.

Using $Al_{K\alpha_{1,2}}$ (1486.6 eV), Siegbahn and co-workers[84] have calculated that the recoil energy of atoms decreases with increasing atomic number e.g. H = 0.9 eV, Li = 0.1 eV, Na = 0.04 eV, K = 0.02 eV and Rb = 0.01 eV. Generally the recoil energy is considered to be negligible for routine studies when using typical x-ray sources for example $Mg_{K\alpha_{1,2}}$ and $Al_{K\alpha_{1,2}}$. Therefore the equation 2.2.1 for a free molecule reduces to equation 2.2.2

$$KE = h\nu - BE \qquad (2.2.2)$$

However recent studies by Cederbaum and Domcke[92] have shown that modification of the vibrational band envelopes of light atoms may also occur when using high energy photon sources. As an example using $Ag_{K\alpha}$ ($\sim$22KeV) the recoil energy of Li is 2 eV and it is evident that E_r term is a significant for the light atoms and must be taken into account in these cases.

When dealing with solids the binding energy are referred to the Fermi level. This level for a conducting sample is defined as the highest occupied level, and sometimes referred to as the 'electron chemical potential' and is located at the interface of the valence band

---

Binding energy (BE) is defined as the positive energy required to remove an electron to infinite (vacuum level) with zero kinetic energy.

and the conduction band.[84] The relationship between the binding energies for solid and gaseous samples will be dealt with more detail in section 2.4.1 of this chapter.

2.2.2 Auger Emission and X-Ray Fluorescence

The photoejection of a core electron from an atom leaves a hole in that atom and the de-excitation of the hole state can occur via both Auger emission and x-ray fluorescence processes.[84] These fundamental processes are represented schematically in Figure 2.2.1.

Figure 2.2.1 Photoionization, Auger and X-ray Fluorescence

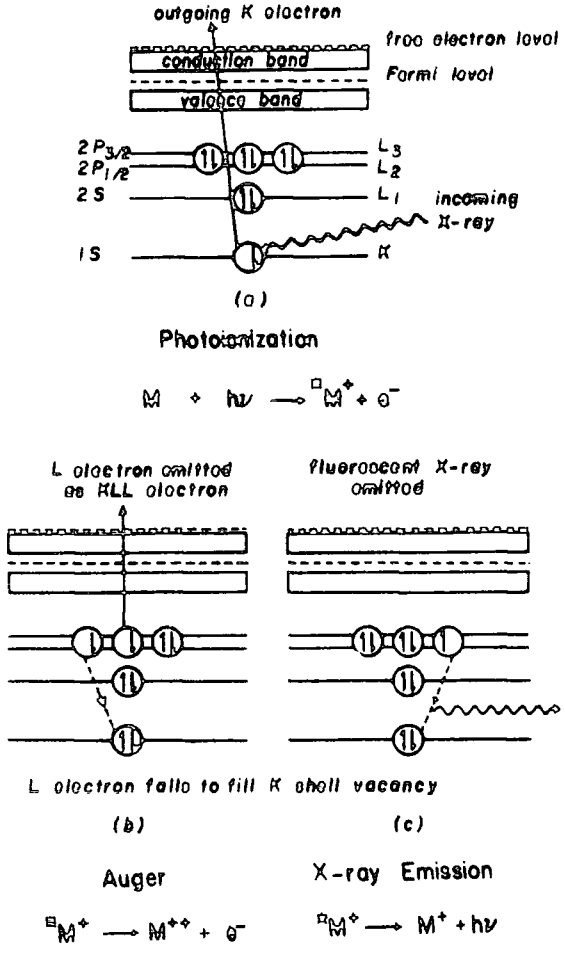

Auger electron emission may be viewed as a two step process involving the ejection of an electron from an inner orbital by a photon followed by an electron dropping down from a higher orbital to the vacancy in the inner orbital with the simultaneous emission of a second electron.[93-97]

When the electron drops from a valence orbital the Auger spectrum is related to the energies of both valence and core orbitals. Where the electronic vacancy in the inner orbital is filled by an electron from another inner orbital, a Coster-Kronig transition,[95] the Auger spectrum is related to the inner orbital transition. Such spectra are often very well resolved,[95-96] but unfortunately cause a broadening of the spectrum due to the very short lifetime of the process. For a Coster-Kronig transition to occur the energy different between the two orbital must be sufficiently large to eject an electron from a higher orbital. Because of this limitation Coster-Kronig processes are only observed in elements of atomic number less than 40.

Auger electron are also recorded in ESCA spectra, and since their kinetic energies are independent of how the initial core hole is created, they may readily be distinguished from photoelectrons by changing the energy of the exciting radiation.

In general, the energy $E_z(KLM)$ of KLM Auger electron emitted from an element of atomic number z in a solid can be estimated from the one core electron energies by:[98]

$$E_z(KLM) = E_z(K) - E_z(L) - E_{z+1}(M) \qquad (2.2.3)$$

Since this equation is of an empirical nature, a more precise calculation of the Auger electrons can be made from the following equation:[99-100]

$$E_z(KLM;s) = E_z(K) - E_z(L) - E_z(M) - \xi(LM;s) + R(LM) \qquad (2.2.4)$$

where s denote the final state with holes in the L and M orbitals, $\mathcal{E}_R(LM;s)$ is the interaction energy between the L and M holes in the final state s, and R(LM) is the total relaxation energy.

The other mode of de-excitation, x-ray emission, is not very efficient for lighter elements and is negligible for energies less than 500 eV, but is a higher probability process for atoms with atomic numbers greater than ~35.

The probability of Auger emission and x-ray fluorescence as a function of atomic number[84] is illustrated in Figure 2.2.2. It can be seen that Auger emission is important for the lighter elements and x-ray fluorescence for the heavier elements.

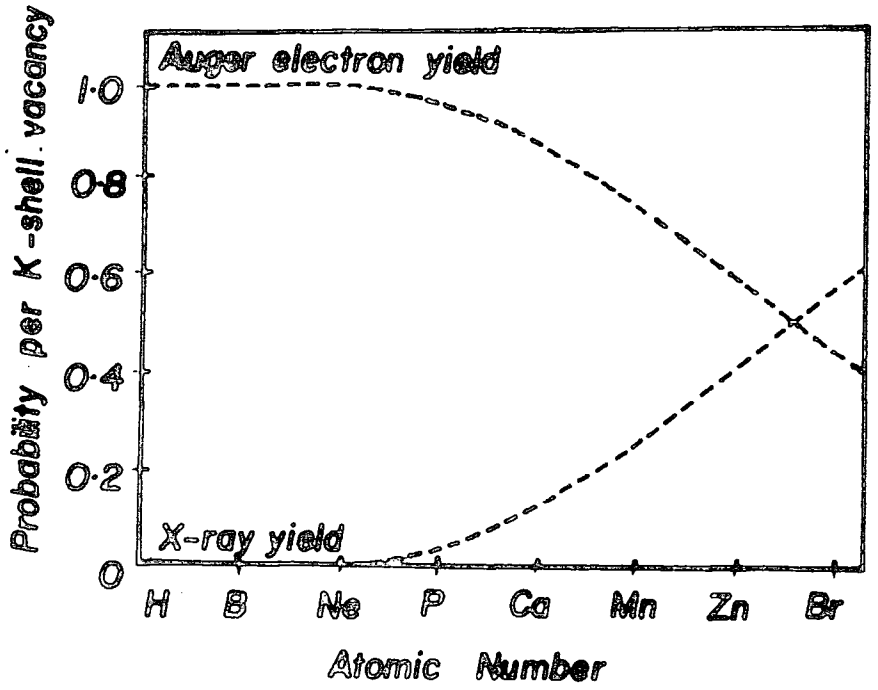

Figure 2.2.2 Yields of the Auger and X-ray Fluorescence processes as a function of atomic number

Auger electrons are usually excited with an electron beam (typically 3 to 10 KeV at 1 to 30 μA) because such beams are easily obtained, focussed, and produce a relative large number of Auger electrons. X-ray, proton and heavy ion excitation can be also used but in most cases the Auger signals produced are much weaker. As the escape depth of electrons in the energy range 20 - 2000 eV is only about 5 atomic layers or approximately $\sim$10 Å,[101] the Auger electron spectroscopy is particularly for surface analysis of metals or semiconductors. However, the incident beam of electrons in Auger spectroscopy is approximately three orders of magnitude greater in flux than a normal ESCA photon beam, and radiation damage is therefore a severe problem[102] when studying polymer surfaces.

The emission of x-ray instead of electrons leads to x-ray fluorescence (secondary-emission analysis) and the energies of emitted x-ray give information of the differences in energy levels in the samples. X-ray fluorescence spectroscopy is an excellent method of quantitative analysis for elements with atomic number greater than ten.[103] Concentration down to 0.1% for most elements and 0.01% for heavier elements have been detected.

For Auger electron and x-ray emission, the detailed spectrum depends on the final state of the ion; In the case of x-rays emission it is the singly charged ion and the doubly charged ion for Auger processes. The decrease in x-ray fluorescence with decreasing energy is due to the fact that it is an electromagnetic (dipole) process and depends mostly on the acceleration of the orbiting electron. The Auger process, however is dependent upon the electrostatic forces accompanied by a vacancy in the inner orbital.

2.2.3 Electronic Relaxation

The removal of a core electron, which is almost completely shielding as far as the valence electrons are concerned, is accompanied by substantial electronic reorganization (referred to as electronic relaxation), predominantly associated with the valence electron.[104-107] Theoretical and experimental studies have shown that for a given core level the magnitude of relaxation energy (RE) is a sensitive function of the electronic environment of a molecule.[108-112] It is considerable importance in determining not only the absolute binding energy of a core electron but also in determining the line shapes of observed peaks by means of vibrational fine structure. Binding energies of the emitted photo-electrons, depend on the properties of both initial and the final wave functions. Therefore, in the calculation of the absolute binding energies using Koopmans' theorem,[113] which is ignores relaxation energies, in many cases, give incorrect or too large binding energies. Whilst, using LCAO MO SCF calculation on both the neutral molecule and core ionized states, Hartree-Fock formalism (ΔSCF),[111-112,114-115] provides a good degree of accuracy calculation of the binding energy. The problem in the solution of these equations (apart from the very high cost in computer time) is that the Hartree-Fock operator itself depends on the one electron eigen-function.

Relaxation energies associated with core ionization of first row atoms are considerable (e.g. $\sim$13 eV)[111,116] and are caused by the reorganization of the valence electron in response to the decreased shielding of the nuclear charge. This reorganization changes the spatial distribution of the remaining n-1 electrons, a factor which is taken into account in the ΔSCF method but not in Koopmans' Theorem. Since the core electrons have larger screening coefficient than the valence electrons,

the change in potential at the nucleus is therefore much larger when a core electron is ionized. This is shown by the fact that relaxation energies for the valence electrons are approximately an order of magnitude smaller than for core electrons. As an example, the calculated values of relaxation energies for the C_{1s} and π orbital in CO calculated within ΔSCF formalism are 11.4 eV and 1.8 eV respectively.[111,116] It has been shown that the difference in relaxation energies for closely related molecules are small and therefore make only minor changes to shift in binding energy.[111]

2.2.4 Shake-up and Shake-off

Although core electrons are essentially localized in the proximity of the nucleus, and do not take any part in bonding, the major contribution to the total energy of an atom or molecule arises from the core electrons, which closely monitor valence electron distributions.[84] As well as the relaxation processes described in the previous section, the sudden perturbation of the valence electron cloud accompanying core ionization give rise to a finite probability for photoionization to be accompanied by simultaneous emission of a valence electron from an occupied orbital to a virtual orbital (shake-up) or ionization of a valence electron (shake-off) as illustrated in Figure 2.2.3.

These relaxation processes result in excited states of the core ionized species, and give rise to satellite peaks on the low kinetic energy side of the direct photoionization peak. Therefore, a revision of equation 2.2.2 is needed to account for these multi-electron processes:

$$KE = h\nu - BE + \bar{E} \qquad (2.2.5)$$

where $\bar{E}$ is the energy of the multi-electron process.

Figure 2.2.3 Photoionization, Shake-up and Shake-off

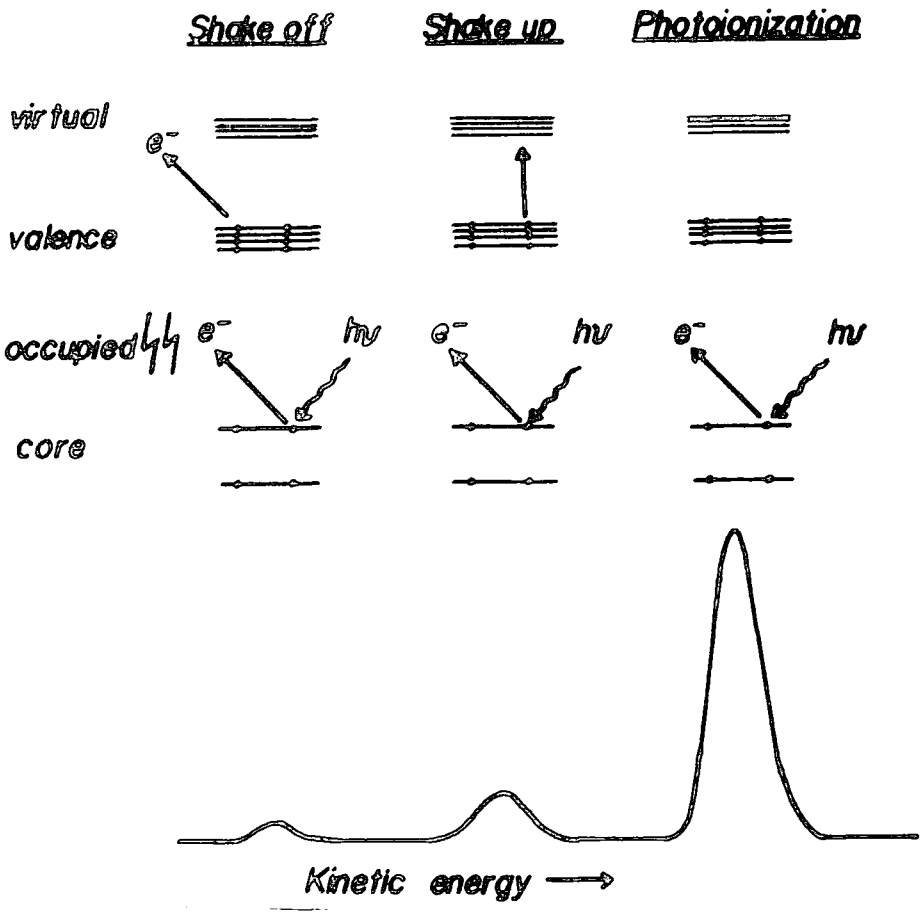

In the sudden approximation, transition intensities are directly related to the sums of one centre overlap terms involving the occupied orbitals of the hole-state species.[117] It may be shown that excitation of states obeys monopole selection rules:

$$(\Delta J = \Delta L = \Delta S = \Delta M_J = \Delta M_L = \Delta M_S = 0) \qquad (2.2.6.)$$

and in some ways may be viewed as an analogue of ultraviolet spectroscopy in ESCA.

The probability of exciting an electron from the orbital denoted by nlj of the neutral atom to the orbital n'lj of the ion, is given by:

$$P_{n'lj \leftarrow nlj} = N \left| \int \psi^{*}_{nlj} \psi'_{n'lj} \, d\tau \right|^2 \qquad (2.2.7)$$

where N is the number of electrons in orbital nlj and Ψ_{nlj}, $\Psi_{n'lj}$ are the wavefunctions of orbital nlj, n'lj in the atom and ion respectively.

Shake-up Transitions

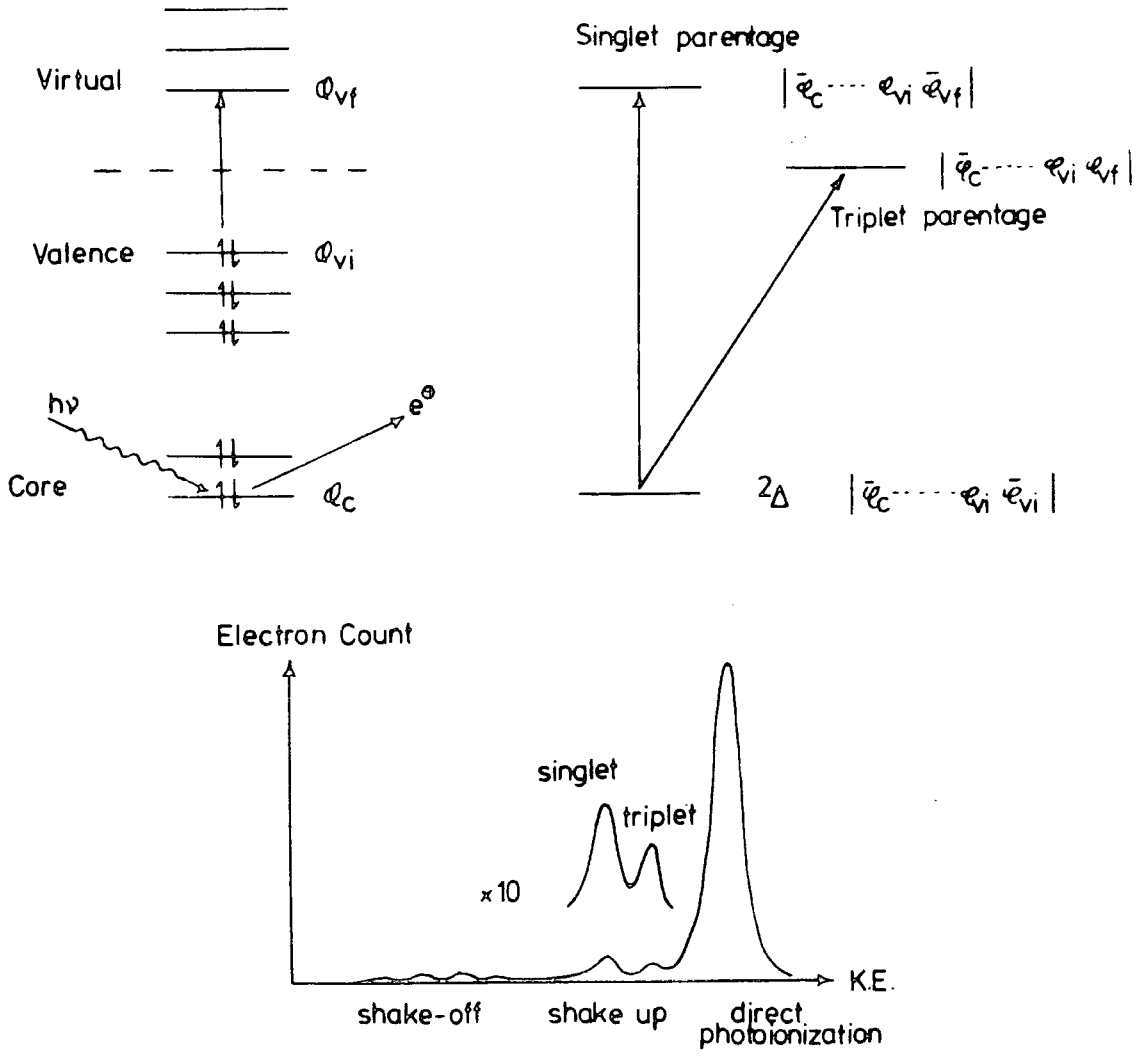

Figure 2.2.4 Schemetic Illustration of Singlet-Triplet shake-up

Considering excitations involving a core hole state in the doublet manifold, as depicted in Figure 2.2.4, it is apparent that within a simple orbital model, there are two possible states that can be generated.

Either unpaired electron in the valence orbital and that excited to the virtual orbital will have opposite spins ("singlet origin"), or they both have the same spin, whilst the remaining core electron has the opposite spin ("triplet origin"). The triplet state is lower in energy than that of singlet origin, however since both represent doublet states, transitions from the ground state of the core hole state may be viewed as both being allowed. In principle, therefore, it should be possible to experimentally observe the energy separations and intensities for the components of the shake-up states of a given excitation configuration.

The theretical relationship between shake-up, shake-off and electronic relaxation energies has been discussed by Manne and Åberg.[106] They showed that the weighted mean of the direct photoionization, shake-up and shake-off peaks corresponds to the binding energy of the unrelaxed system (given by Koopmans' theorem), and this is schematically in Figure 2.2.5.

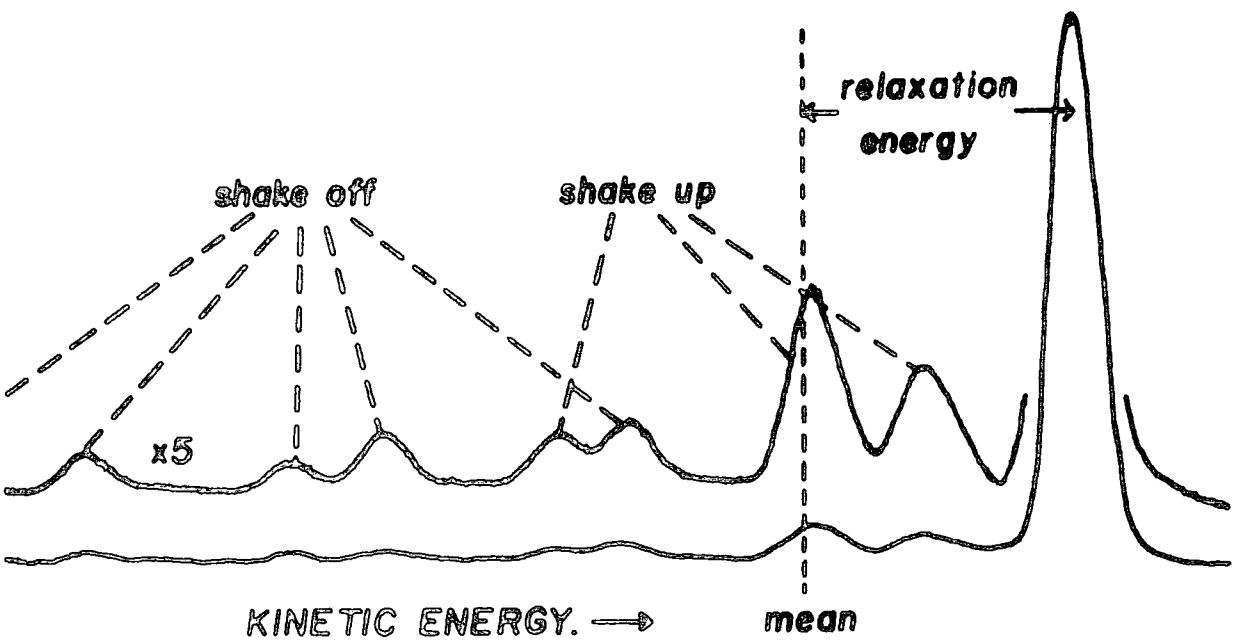

Figure 2.2.5 Relationship between relaxation energy and relative intensities of photoionization, shake-up and shake-off peaks

The transition probabilities for high energy shake-off processes are relatively small compared to shake-up processes, and the transitions of highest probability fall reasonably close to the weighted mean. In principle, the relaxation energy should be available from experimental data of direct photoionization, shake-up and shake-off, but in practice this is not feasible. This problem arises by the general 'inelastic tail' which is due to the direct photoelectrons, followed by energy loss by a variety of inelastic processes. This produces a broad energy band which peaks (for organic systems) at approximately 20 eV below the direct ionization peak.

Shake-up and shake-off structure has been studied in organic and inorganic materials with particular attention to the transition elements. A recent review of shake-up effect has been published.[118]

2.2.5 Energy Loss Processes

In the case of a gas phase study, the electron distribution found to the binding energy side of a primary photoionization peak is due entirely to shake-up and shake-off. When working at high gas pressure and with solids (or liquid) non-discrete energy losses become important. With some metals (especially conductors) there is an enhanced probability for loss of a specific amount of energy due to interaction between the photoelectrons and other electrons in the surface region of the sample, and produces a distinct rather sharp band at $\sim$21 eV below the kinetic energy of the parent peak.[119] For metals, these are the so-called "plasmon losses", the inelastic losses of the photoionization electrons.[120]

An inelastic loss can also arise from the interaction with secondary electron emission resulting from autoionization process.[121]

2.3 Instrumentation

The work in this thesis was carried out on both an AEI ES200AA/B and an Kratos ES300 spectrometers. But for almost all of the ESCA studies the former was used extensively. In this section on ESCA instrumentation will consider only the apparatus appropriate to the AEI ES200 spectrometer. There are a number of commercial ESCA instruments presently available on the market since the first ESCA instrumentation appeared in 1969.

A schematic of the essential components of an ESCA spectrometer is shown in Figure 2.3.1 and is largely self explanatory, including:

1. x-ray source
2. Sample chamber
3. Electron energy analyzer
4. Electron detection.

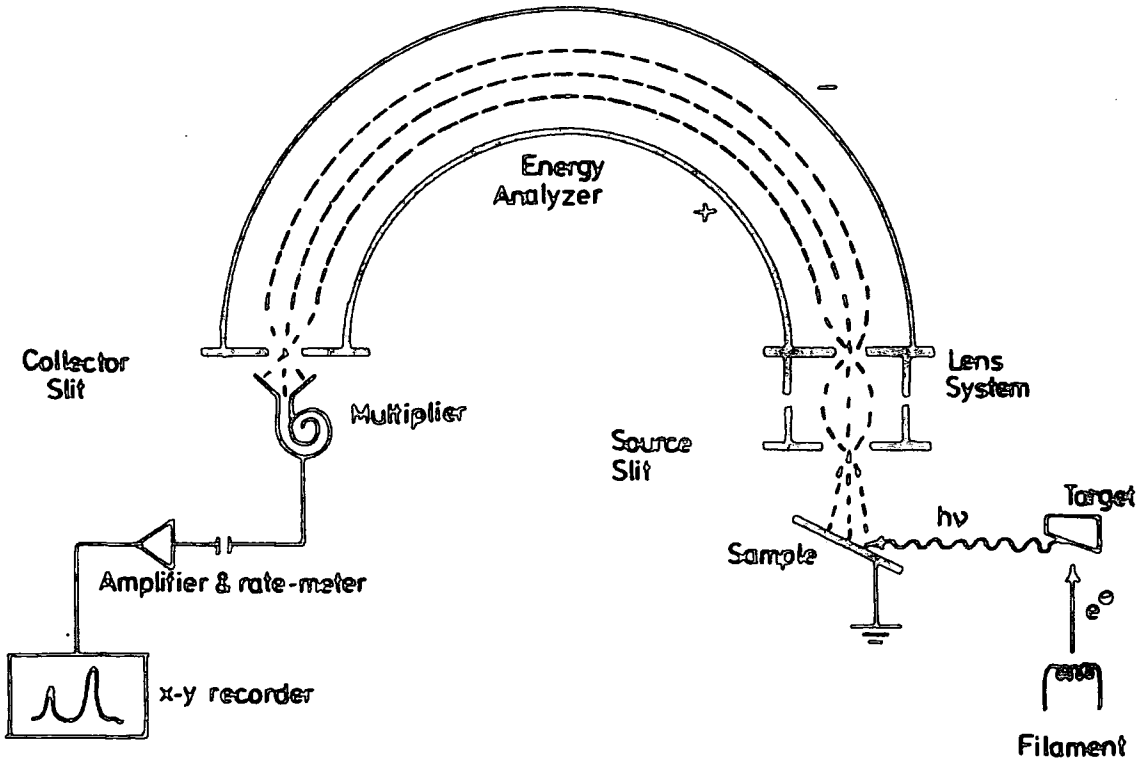

Figure 2.3.1 Some of the components of the ES200 spectrometer

2.3.1 X-ray Source

The high voltage supply is from a Marconi Elliott GX 14 unit, with integrally variable voltage and current output, 0 - 60 kV and 0 - 80 mA respectively. This high voltage generator may be operated in the pressure range $<10^{-5}$ Torr. The spectrometer is equipped with two x-ray photon sources of hidden filament or Henke design,[122] non-monochromatized $Mg_{K\alpha_{1,2}}$ and monochromatized $Al_{K\alpha_{1,2}}$ with typical operating conditions of 12 kV, 15 mA and 15 kV, 35 mA respectively. The x-ray flux is of the order of 0.1 millirad/sec.[123] which cause little or no radiation damage to the majority of polymeric systems.

The x-ray gun forms part of the source region but is isolated by means of a thin aluminium foil window, mounted in the face of the tube between target and the sample holder to avoid interference due to stray electrons from the filament. In order to reduce the risk of scattered electrons exciting x-ray radiation from the Al window, the gun filament is earthed and the target operates at high positive voltage $\backsim$ +10 - +15 KV. A target is characterized by the photon energy of its characteristic line and by the width of the line. The component linewidth for non-monochromatic x-ray source in the particular cases of Mg and Al are $\backsim$0.7 eV and $\backsim$0.9 eV respectively.[84] The photon energy determines the highest binding energy of electrons within an atom that may be excited (investigated). The photon (line) energy also determines the kinetic energy of the photoelectrons and this in turn determines the depth in the sample from which the photoelectrons emerge.

A typical non-monochromatic x-ray spectrum (a tungsten anode) is shown in Figure 2.3.2. The spectrum consists of the characteristic line spectrum superimposed on a continuum (bremsstrahlung), the shape

of which depend only of the energy of electrons and not on the anode material.

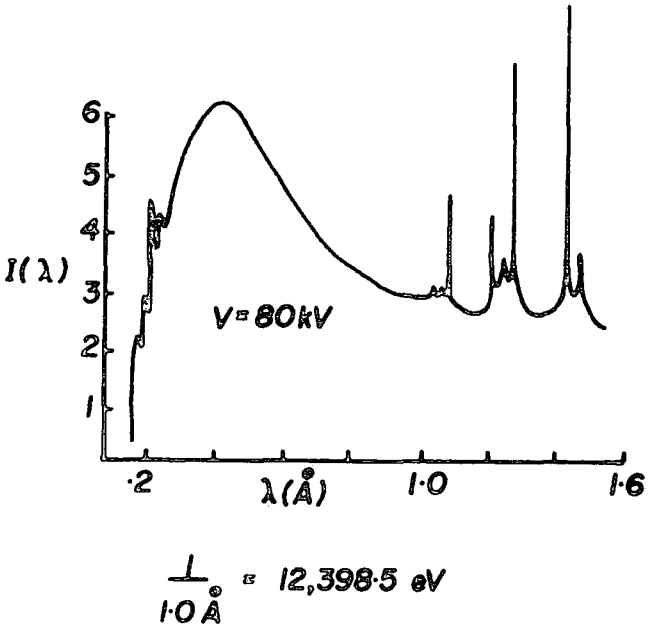

Figure 2.3.2 X-ray spectrum of a tungsten target

The λ_o cut-off at short wave-lengths is inversely proportional to the kinetic energy, E and follows the equation:

$$h\nu_o = E \qquad (2.3.1)$$

where h is Planck's constant.

The total x-ray energy per electron, E_T, is proportional to the integral over λ of the continuum and is given by:

$$E_T = kZE^2 \qquad (2.3.2)$$

where k 0.7×10^{-4} for E_T and E in meV, and Z is the atomic number of the anode material. The fraction of the electron kinetic energy converted in x-ray energy is:

$$\frac{E}{E} = kZE \qquad (2.3.3)$$

For a magnesium anode (Z = 12) and E = 0.05 meV $\frac{E}{E_T}$ is about 4×10^{-3}%.

The line spectra obtained from Mg and Al anodes used in ESCA are from the K series transitions and in particular the $K\alpha_{1,2}$ line. The composition of these lines (and intensities) relative to the $K\alpha_{1,2}$ line are given in Table 2.3.1.

Table 2.3.1 X-ray satellite energies (lines) and intensities)

	$K\alpha$	1,2	3	4	5	6
Mg	displacement (eV)	0	8.4	10.2	17.5	20.0
	relative height	100	8.0	4.1	0.55	0.45
Al	displacement (eV)	0	9.8	11.8	20.0	23.4
	relative height	100	6.4	3.2	0.4	0.3

$Al_{K\alpha}$ radiation can be monochromatized using a crystal diffraction technique[85] to eliminate satellites and remove the continuum producing pure $K\alpha_{1,2}$ radiation. Crystals of the appropriate lattice spacing are not available for the monochromatization of $Mg_{K\alpha}$ radiation. For $Al_{K\alpha}$ essentially three techniques are available: (a) 'slit filtering' (b) 'dispersion compensation' and (c) 'fine focussing'. By these techniques a line-width of $\sim$0.2 eV for the x-ray source can be attained. These options are displayed in Figure 2.3.3. The first two, namely slit filtering and dispertion compensation have been commercially exploited. The fine-focussing technique[124] uses a highly focussed x-ray source and required rotating anode in order to produce sufficient x-ray intensity.

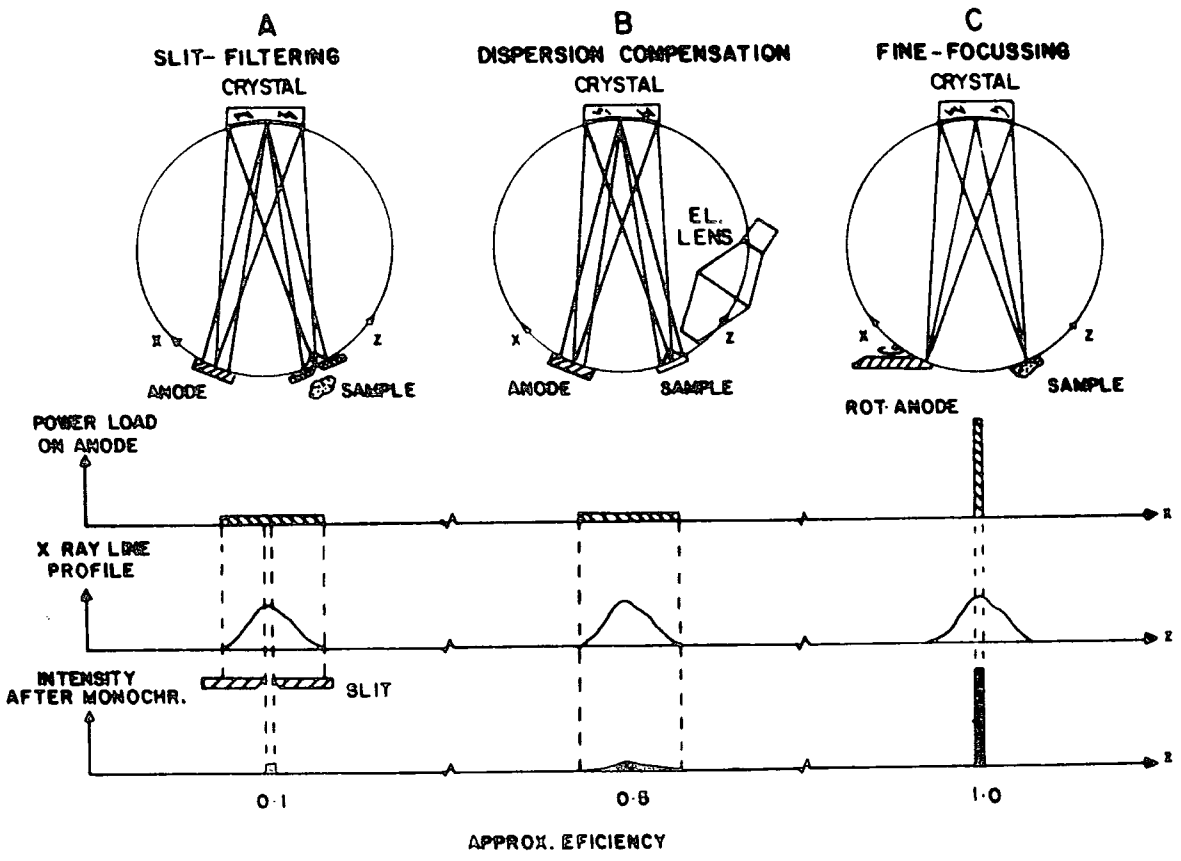

Figure 2.3.3 Techniques for monochromatization of x-rays

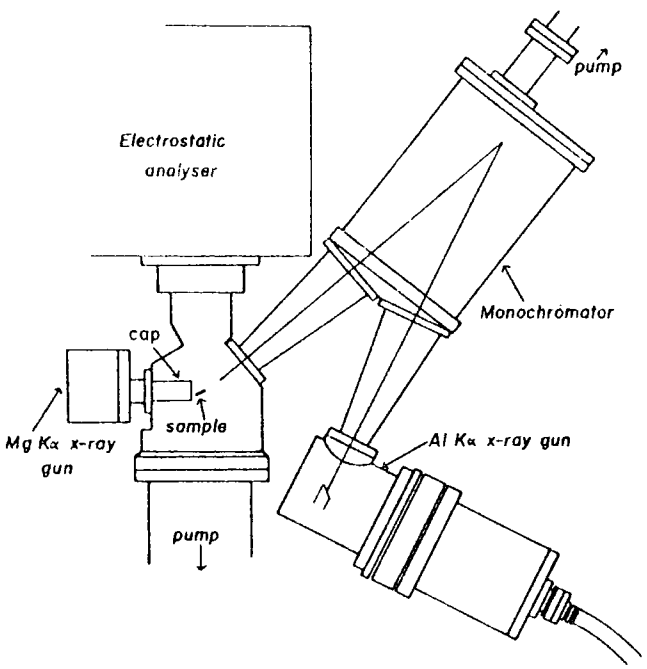

Figure 2.3.4 AEI ES200A/B Spectrometer

2.3.2 Sample Chamber

A schematic drawing of the ES200AA/B spectrometer showing the relative position of the sample, excitation source and analyzer is shown in Figure 2.3.4.

The sample chamber has several access ports for sample introduction and treatment facilities. By using the probe, samples may be introduced easily into sample chamber via an insertion system and high vacuum gate valve. Angular dependent studies can also be carried out by rotating the probe. Typical operating pressure in the sample region would be $< 10^{-7}$ Torr.

2.3.3 Sample Preparation and Handling

With several access ports provision is made to enable samples to be heated and cooled in-situ and ancillary sample preparation chamber allows greater flexibility in terms of sample preparation or pretreatment (e.g. argon ion or electron bombardment, ultravoilet irradiation, in-situ plasma polymerization, etc.).

Solid samples are conveniently studied as films or powders mounted on the tip of sample probe by means of double sided 'Scotch' insulating tape. For solids that are sufficiently soluble, then thin films may be deposited directly on a gold backing by conventional dip or bar coating, or spin casting. Since ESCA in such a surface sensitive technique, it is important to use clean apparatus and pure solvents containing no non-volatile residues which would segregate at the surface on evaporation of the solvent.

The facility for cooling the sample probe tip allows liquid and volatile solid samples to be studied in a condensed phase introducing them from a reservoir shaft or direct inlet passed through a second insertion lock. The probe on this instrument has a variable temperature control and may be operated at temperature from -150°C to +400°C.

With provision of differential pumping, samples may be studied directly in the gaseous state. Siegbahn has developed two techniques where liquids and solutions may be studied as submillimeter beams [86] or as films an wire loop[126] passing through the x-ray beam and continually being wetted by the liquid.

When a sample has been exposed under the x-ray in the ESCA instrument about an hour, it is often observed that there is an appreciable build up of hydrocarbon contamination. It has been found that the major source of hydrocarbon contamination of samples comes from hydrocarbon 'boiling off' the x-ray cap and the window.[127] To remedy this the x-ray cap has been equipped with a cooling jacket through which either cold water or liquid nitrogen may be passed.

2.3.4 Electron Energy Analyzer

The electron energy analyzer on the AEI ES200AA/B is a hemispherical double focussing electrostatic analyzer, which was originally described by Purcell[128] in 1938, enclosed within two mu-metal cans for magnetic shielding. The electron energy analyzer should have a resolution of 1 in 10^4 in order to carry out ESCA studies. The resolution of the analyzer is given by:

$$\frac{\Delta E}{E} = \frac{R}{W} \qquad (2.3.4)$$

where E is the energy of the electrons,

R is the mean radius of the hemisphere, and

W is the combined width of entrance and exit slits.

Therefore to improve the resolution three things can be done:

i) reduce the slit widths W, which also reduces the signal intensity,

ii) increase the mean radius R of the hemisphere which increases the engineering cost and the overall pumping requirements,

iii) reduce the kinetic energy of electrons before they enter the analyzer.

A compromise has therefore to be made on these three and so the slit widths are adjusted to obtain sufficient signal intensities while the ES200AA/B uses a retarding lens to slow the electrons down before they enter the analyzer. This enables the size of the two hemispheres to be kept to a reasonable size so as to reduce mechanical distortions and to keep engineering costs down. The retarding lens used in fact serves two purposed:

i) By reducing the kinetic energy of the electrons the resolution requirements on the analyzer are reduced.[129]

ii) The lens system allows the analyzer to be located at a convenient distance physically from the source chamber which permits a maximum flexibility in sample handling.

Electrons entering the analyzer with the required kinetic energy may be foccussed at the detector slit by one of two methods:

i) Electronically scanning the retarding potential applied to the lens while keeping the hemispherical potential constant, or

ii) Simultaneously scanning the retarding potential applied to the lens and the hemispherical potential and keeping a constant ratio between the two, which is the method used on the ES200AA/B employed here.

The overall resolution, $\Delta E_m/E$ also depend on the contributions from sources other than the analyzer. For a solid sample and with Gaussian line shapes ΔE_m is given by:

$$(\Delta E_m)^2 = (\Delta E_x)^2 + (\Delta E_{cl})^2 + (\Delta E_s)^2 + (\Delta E_{ss})^2 \qquad (2.3.5)$$

where ΔE_{cl} is the natural width of the electron energy distribution in the level being studied,

ΔE_s is the line broadening due to spectrometer irregularities, and

ΔE_{ss} is the line broadening due to the solid state effect in the solids.

2.3.5 Electron Detection and Data Acquisition

The electrons passing through the collector slit are detected by an electron multiplier, and the pulses obtained are amplified and fed into the counting electronics. Spectra may be generated by one of two methods:

i) The kinetic energy of photoelectron is scanned continuously from a fixed kinetic energy until another predetermined higher kinetic energy is reached. The signal from the amplifier may be fed into a rate meter or recorded on an X-Y recorder directly against the kinetic energy of the electrons. In these case a graph of electron counts per second versus kinetic energy of the electrons is obtained.

ii) The kinetic energy of the photoelectrons passing through the analyzer is scanned stepwise from a fixed kinetic energy to another higher predetermined kinetic energy. The increments are

typically 0.1 eV and at each increment the counts may be measured for a fixed time or a fixed number of counts may be timed. The data obtained from the step scans is stored in a multi-channel analyzer. Many scans can be accumulated to average random fluctuations in background. Using this method this signal to noise ratio increase as the square root of the number of scans.

In both of these methods where the data acquisition is relating long (of the order of an hour) care must be taken to avoid long term sample changes. For example, hydrocarbon contamination may alter peak ratio and time dependent sample charging may produce erroneous spectra.

2.4 Features of ESCA Spectra

2.4.1 Binding Energies

Since the core electrons are essentially localized on atoms, their energies are characteristic for a given element.[71] Thus, with a knowledge of the binding energies of core levels in an element, it is possible to detect and identify the gross elemental composition in a sample.[71] Typical examples of approximate core electron binding energies for some elements are shown in Table 2.4.1. Therefore with $Mg_{K\alpha_{1,2}}$ and $Al_{K\alpha_{1,2}}$ photon sources there are sufficient energy to study the 1s and valence levels of first elements, the 2s,2p and valence level of second row elements and so on. In general there is no advantage in studying the most tightly bound core levels of a given element (e.g. 1s level of gold; see Section 2.4.4), since this may well have a very large natural line width and the required higher energy photon source inevitably has a large line width.

Table 2.4.1 Approximate core binding energies for 1st and 2nd row elements (eV)

	Li	Be	B	C	N	O	F	Ne
1s	55	111	188	284	399	532	686	867
	Na	Mg	Al	Si	P	S	Cl	Ar
1s	1072	1305	1560	1839	2149	2472	2823	2303
2s	63	89	118	149	189	229	270	320
$2p_{1/2}$	31	52	74	100	136	165	202	247
$2p_{3/2}$	31	52	73	99	135	164	200	245

It is important to understand the relationship that exists between the binding energy observed experimentally by ESCA for a solid, as opposed to free molecule (e.g. a gas), and the value calculated theoretically by ab initio LCAO MO SCF treatments, (see also Section 2.4.2). For a conducting sample it is more convenient to refer the binding energies to the Fermi level.[71] The Fermi level E_f in a metal is defined as the highest occupied level, and may be expressed by:[84]

$$\int_0^{E_f} N(E)\, dE = N \qquad (2.4.1)$$

where $N(E) = Z(E).F(E)$; $Z(E)$ is the density of states of electrons, that is the number of energy levels between E and $E + \Delta E$, $F(E)$ is the Fermi probability distribution, the probability that a Fermi particle in a system at thermal equilibrium will be in a state with energy E:

$$F(E) = 1/\left[e^{(E - E_f)/kT} + 1 \right] , \quad (kT \ll E_f) \qquad (2.4.2)$$

N is the total number of electrons in the system and the electrons fill the available states up to the Fermi level.

The work function for a solid, ϕ_s, is defined as the energy gap between the free electron (or vacuum) level and the Fermi level in the solid. Since the sample and spectrometer are in electrical contact, their Fermi levels are the same. However, the vacuum levels for the solid and the spectrometer may be different, and then the electron will experience either an accelerating or retarding potential equal to $\phi_s - \phi_{spec}$, where ϕ_{spec} is the work function of spectrometer.[130-131] The kinetic energy, KE of the photoelectron when it enter the analyzer therefore will in general be different from the kinetic energy KE' which it had on emerging from the sample. Taking zero binding energy to be at the Fermi level of the sample gives:

$$BE = h\nu - KE - \phi_{spec} \qquad (2.4.3)$$

This is schematically illustrated in Figure 2.4.1.

Figure 2.4.1 **Binding Energy reference level in solids**

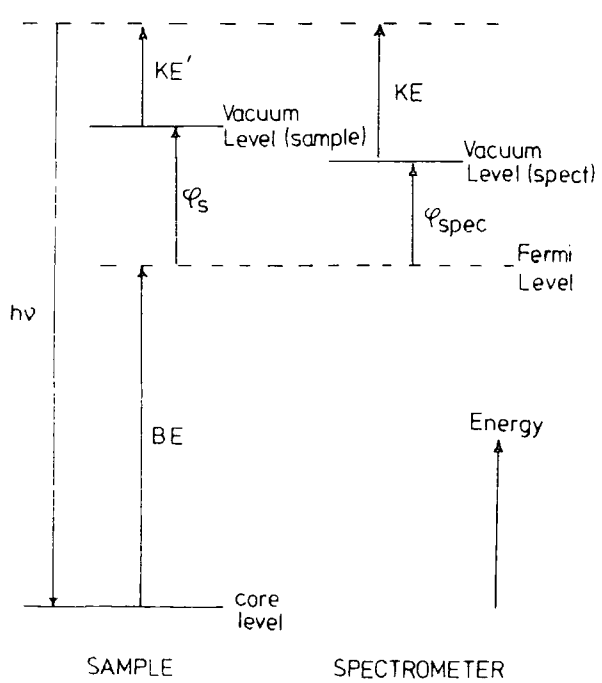

The binding energy referred to the Fermi level does not depend on the work function of the sample, but only on that of the spectrometer, ϕ_{spec}, this gives a constant correction to all binding energy. In practice, the problem of extracting absolute binding energy is circumvented by the use of reference standards for calibration of the binding energy scale.[132] (see also Section 2.4.5).

2.4.2 Chemical Shifts

Variations of binding energy within a given core level are a sensitive function of the electronic environment of an atom.[84-85] Differences in electronic environment of a given atom in a molecule give rise to a small range binding energies, or chemical shifts, often representative of a particular structural feature. The classic illustration of chemical shift being the C_{1s} spectrum of ethyl trifluoroacetate[85] (Figure 2.4.2). Some typical values of chemical shift are also given on page 69.

The theoretical interpretation of chemical shift has been carried out by four distinct approachs:

1. Koopmans' Theorem
2. Core Hole Calculation (ΔSCF)
3. Equivalent Core Model
4. Madelung Charge Potential Model.

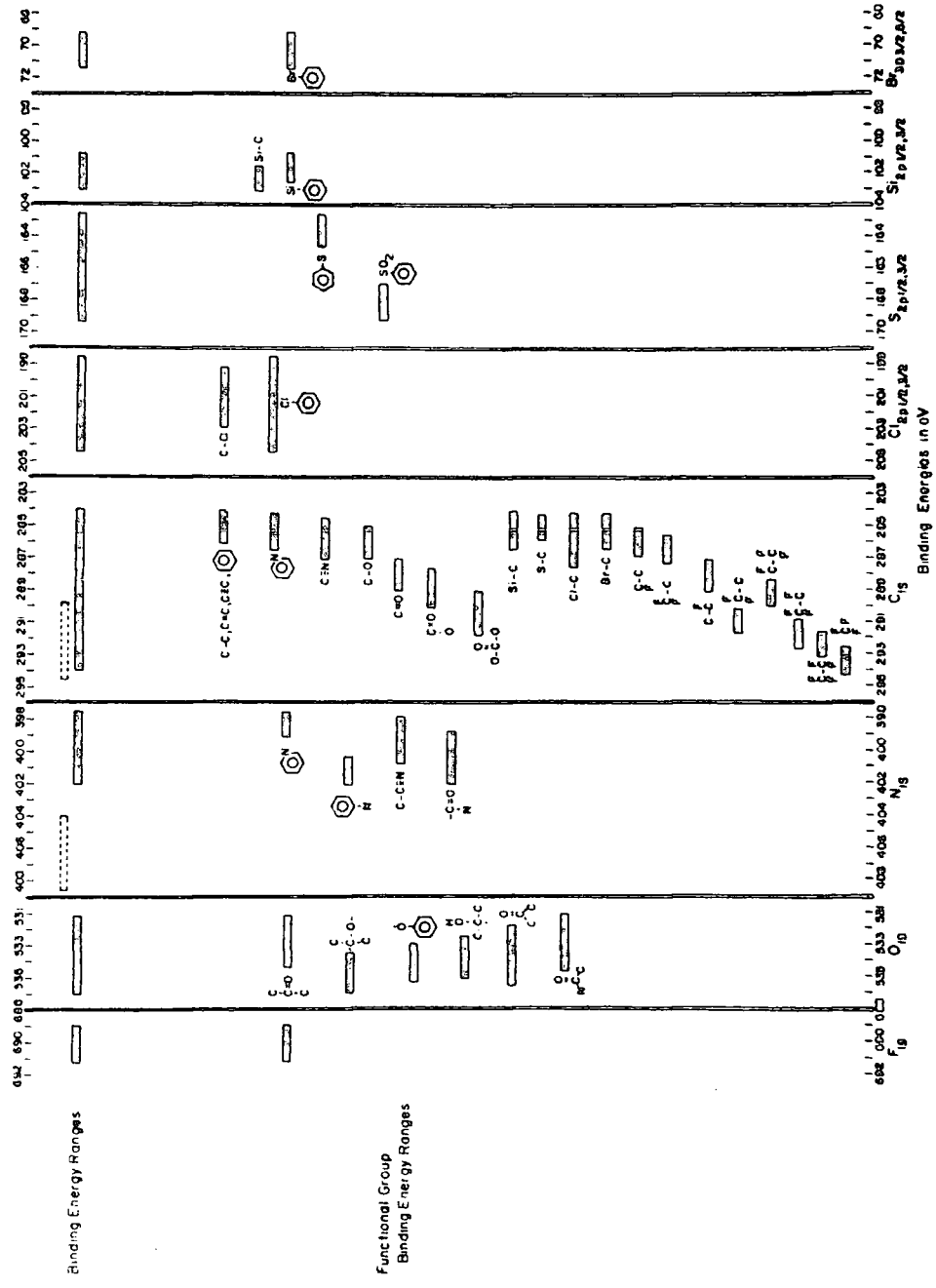
Binding Energy Ranges
Functional Group
Binding Energy Ranges
Binding Energies in eV

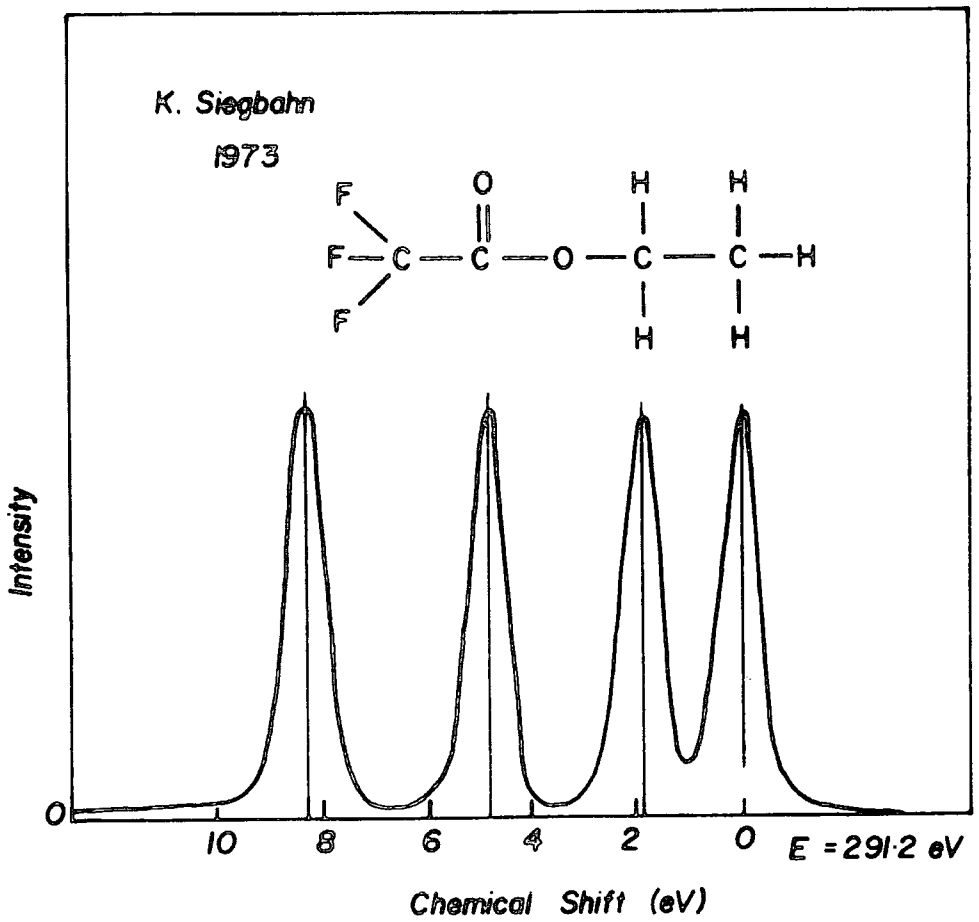

Figure 2.4.2 C_{1s} Spectrum of ethyl trifluoroacetate

2.4.2.1 Koopmans' Theorem

Koopmans' theorem[113] calculations of absolute binding energy rely solely on the ground state properties of a wave function, which showed that the energy difference, binding energy (or ionization potential) is just the orbital energy of the atom. Thus, the calculation neglects relaxation energies and also relativistic and correlation energies which occurs on photoionization. The contributions from relativistic[133] and correlation[134] effects are small for light elements up to Ne, and can be neglected for practical purposes, but the neglect of relaxation energy means that absolute binding energies calculated by this method are over-estimated. Nevertheless, the Koopmans' theorem has many useful qualitative

and semi-quantitative applications, and may provide a reasonable quantitative description of shift in binding energy within a series of molecules.

2.4.2.2 Core Hole State Calculation

This method, ΔSCF, the absolute binding energy is calculated as the difference between the energies of the ground state and ionized state of an atom or molecule.[111,114-115] Like Koopmans' Thoerem, this method neglects relativistic and correlation energies but does take into account relaxation energy.

The relation between the experimental, Koopmans' and Δ SCF binding energy is schematically shown in Figure 2.4.2 and the relaxation energy, RE is given by:

$$RE = BE_{Koopmans'} - BE_{\Delta SCF} \qquad (2.4.2)$$

Figure 2.4.2 **The relation between Koopmans' Theorem, Δ SCF and Experimental Binding Energy**

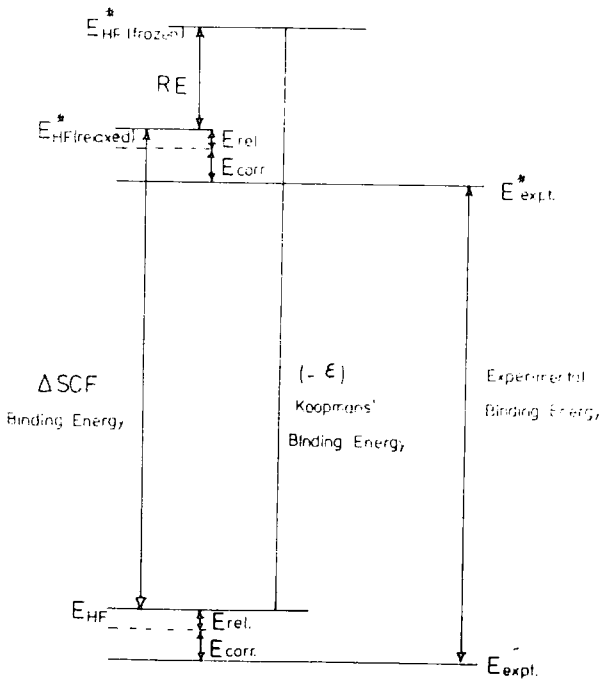

Bagus[104] first performed ΔSCF calculation for various ions of Ne and Ar. Schwartz[135] has carried out the calculation of this type on molecules (the first-row hydrides) and these results are compared to the experimental value obtained by Siegbahn and co-workers[85] in Table 2.4.2.

Table 2.4.2 1s Electron Binding Energies (eV)

Molecule	Orbital Energy (Koopmans' Theorem)	Core Hole State	Experimental
BH_3	207.3	197.5	-
CH_4	304.9	291.0	290.7
NH_3	422.8	405.7	405.6
H_2O	559.4	539.4	539.7
NF	715.2	693.3	-
Ne	891.4	868.8	870.2

It is clear that the core hole state calculations are in good overall agreement with the experimental datas (e.g. Table 2.4.2).

Then, the binding energy may be precisely be defined as:

$$BE = \Delta E_{\Delta SCF} + \Delta E_{Corr} + \Delta E_R \qquad (2.4.5)$$

where $\Delta E_{\Delta SCF}$ is the difference in the Hartree-Fock energies between the ground and core hole state, (Δ SCF binding energy),

ΔE_{Corr} is the difference in correlation energies, and

ΔE_R is the difference in relativistic energies.

It is important to note that when a core electron is ejected from a molecule, there will be a change in the geometry of the core hole state and this has been demonstrated by Siegbahn and co-workers.[136] Therefore the term, $\Delta E_{vib.}$, the difference between the vertical and adiabatic ionization potential, should be included in equation (2.4.5). However as the calculated binding energy corresponding to the minima for neutral molecule and the hole state differ by only $\Delta 0.3$ eV from the computed from the geometry appropriate to the neutral molecule.[137] It is clear therefore that the assumption of an unchanging nuclear framework on core ionization is a good approximation. It has also been investigated that $\Delta E_{vib.}$ is small enough to be ignored.[138]

2.4.2.3 Equivalent Cores Model

The equivalent cores model was developed by Jolly and Hendrickson[139] to calculate shifts in core electron binding energies from ground state thermodynamic data. The model assumes that " when a core electron is removed from an atom in a molecule or ion, the valence electrons relax as if the nuclear charge on the atom had increase by one unit. " Thus atomic cores that have the same charge are considered to chemically equivalent and interchangeable with the complete cores of the next element in the periodic table. The following example illustrates how the principle may be used to estimate the gas phase shift in C_{1s} binding energy between carbon atoms in methane and fluoromethane.

The carbon 1s binding energy in methane, BE_{CH_4} is given by the energy of the process

(i) $$CH_4 \longrightarrow {}^{*}CH_4^{+} + e^{-} \qquad \Delta E = BE_{CH_4}$$

where * indicates a vacancy in a core orbital (C_{1s} in this case).

(ii) $$^{*}CH_4^{+} + N^{5+} \longrightarrow NH_4^{+} + {}^{*}C^{5+} \qquad \Delta E = \delta_o$$

This reaction is the exchange of the $^{*}C^{5+}$ core and the equivalent N^{5+} core. According to the principle of equivalent cores the energy of this reaction, δ_o, is zero. Summing reaction (i) and (ii) gives

(iii) $$CH_4 + N^{5+} \longrightarrow NH_4^{+} + {}^{*}C^{5+} + e^{-} \qquad \Delta E = BE_{CH_4} + \delta_o$$

A similar reaction may be written for CH_3F, or any other compound containing a carbon atom.

(iv) $$CH_3F + N^{5+} \longrightarrow NH_3F^{+} + {}^{*}C^{5+} + e^{-} \qquad \Delta E = BE_{CH_3F} + \delta_1$$

The differences between reaction (iv) and (iii) than gives

(v) $$CH_3F + NH_4^{+} \longrightarrow NH_3F^{+} + CH_4 \qquad \Delta E = BE_{CH_3F} - BE_{CH_4} + (\delta_1 - \delta_o)$$

The strong form of the equivalent cores approximation states that $\delta_1 = \delta_o = 0$ and thus the gas phase shift in the C_{1s} binding energy between methane and fluoromethane is given by the energy of reaction (v).

However, provided that $\delta_1 = \delta_o$ that is the energy of core exchange is the same and independent of molecular environment, reaction (v) still gives the shift in binding energy. This assumption is known as the weak form of the equivalent cores approximation.

Some typical gas phase data are shown in Table 2.4.3, and in general indicate good agreement between experimentally observed shifts and those calculated from thermodynamic data.

Table 2.4.3 Experimental and Thermodynamic Binding Energy Shifts. (eV)

Atomic Core Level	Compound	Experimental Shift	Thermodynamic Data Shift
N_{1s}	NH_3	0	0
N_{1s}	$(CH_3)_2NH$	- 0.7	0.7
N_{1s}	CH_3NH_2	- 0.3	0.4
N_{1s}	N_2	4.35	3.5
N_{1s}	NO	5.5	4.4
C_{1s}	CH_4	0	0
C_{1s}	CO	5.4	4.1
C_{1s}	CO_2	6.8	6.9
C_{1s}	CF_4	11.0	12.3
$Xe_{3d_{5/2}}$	Xe	0	0
$Xe_{3d_{5/2}}$	XeF_2	2.95	2.7
$Xe_{3d_{5/2}}$	XeF_4	5.5	5.4
$Xe_{3d_{5/2}}$	$XeOF_4$	7.0	6.3
$Xe_{3d_{5/2}}$	XeF_6	7.9	7.85

The principle restriction to the use of the equivalent cores method is the absence and/or unreliability of thermodynamic data especially with regard to the positive ions involved in the reactions. The theoretical validity however, of the equivalent cores concept has been well documented by Clark and Adams[140-141] in their studies on simple molecules. When the experimental thermodynamic data required to calculate binding energy shifts are not available, SCF calculations on the molecules and ions in their ground states may be used to abtain the required heat of reaction. Pople and co-workers[142-143] have shown that for reaction involving closed shell species even minimal basis set (STO 3G) calculations, which are relatively inexpensive with regard to computer time, can reliably reproduce heats of reaction. It is also possible to use semi-empirical calculations, which are also computationally inexpensive, to calculate heats of reaction and then predict in a qualitative manner the chemical shifts. Thermodynamic data refer to isoelectronic cations with their nuclei in the equilibrium position, but since photoionization is a rapid process compared to nuclear motion it is more realistic to consider cations with the same geometry as the parent molecule. Also, by using the same geometry for the molecules and isoelectronic cations in ab initio calculations, many of the two electrons integrals may be retained and this greatly reduce the amount of computing time required.

2.4.2.4 Madelung Charge Potential Model

The charge potential model relates core electron binding energies with the charge on the atom from which core ionization takes place and the potential from the charges in the remainder of the molecule.[85]

Siegbahn and coworkers[85] initially interpreted the chemical shifts in ESCA in terms of an ionic model. If a charge is removed from

or added to the valence level of a molecule the electrostatic potential within the valence orbital is changed. If an amount of charge (q) is removed from the valence electron distribution of atom to infinity, the potential energy is lowered by the amount:

$$\Delta E = \frac{q}{r} \qquad (2.4.6)$$

where r is the radius of valence orbital. When the electron is not removed to infinity but to a finite distance R, from the molecule, the lowering of the potential energy (shift) is given by:

$$\Delta E = \left(\frac{1}{r} - \frac{1}{R} \right) q \qquad (2.4.7)$$

In the case of ionic crystal model the lattice effects have to be considered, but as far as core electrons are concerned, since the orbital overlap is negligible small, then to a first approximation neighbouring atoms can be regared as point charges. Therefore a summation of the potential from the point charges in crystal will determine the potential, V_i, at the centre of atom i, and thus the binding energy of the core electron;

$$V_i = \sum_{j \neq i} \frac{q_j}{r_{ij}} \qquad (2.4.8)$$

where r_{ij} are the centre-to-centre inter-ionic distances and q_j is the charge on ion j.

Siegbahn and co-workers[85] have then extended this model to covalent compounds by considering the change in potential as arising from a one centre component associated with the change in the number of valence electrons on the atom and a two centre component originating from the electron distribution in the remainder of the molecule.

Therefore the binding energies, E_i are:

$$E_i = E^o + kq_i + \sum_{j \neq i} \frac{q_i}{r_{ij}} \qquad (2.4.9)$$

and thus the chemical shift, ΔE are

$$\Delta E = E_i - E^o = kq_i + \sum_{j \neq i} \frac{q_i}{r_{ij}} \qquad (2.4.10)$$

where, E^o is a reference binding energy,

q_i is the charge on atom i,

r_{ij} are the interatomic distances and

k is the average interaction between a core and valence electron on the atom.

The use of a point charge model assumes that there is no overlap between the core electron density on atom i and the valence electron densities on the other atoms in the molecule. Using this assumption all valence electron CNDO/2 SCF MO calculations[144] have been carried out on quite complex molecules in relating to the ESCA chemical shift. Good description have been obtained but since the charge potential model may be related to Koopmans' theorem[113] which neglects electronic relaxation, therefore, it suffer from the same defects.

The use of the charge potential model in studies of structure and bonding in molecules is illustrated in Figure 2.4.3. Starting on A, if the geometry and appropriate charge distribution (e.g. CNDO/2) are available, then the experimental shift may be used to obtained values of k and E^o for a given level in a particular element. It is

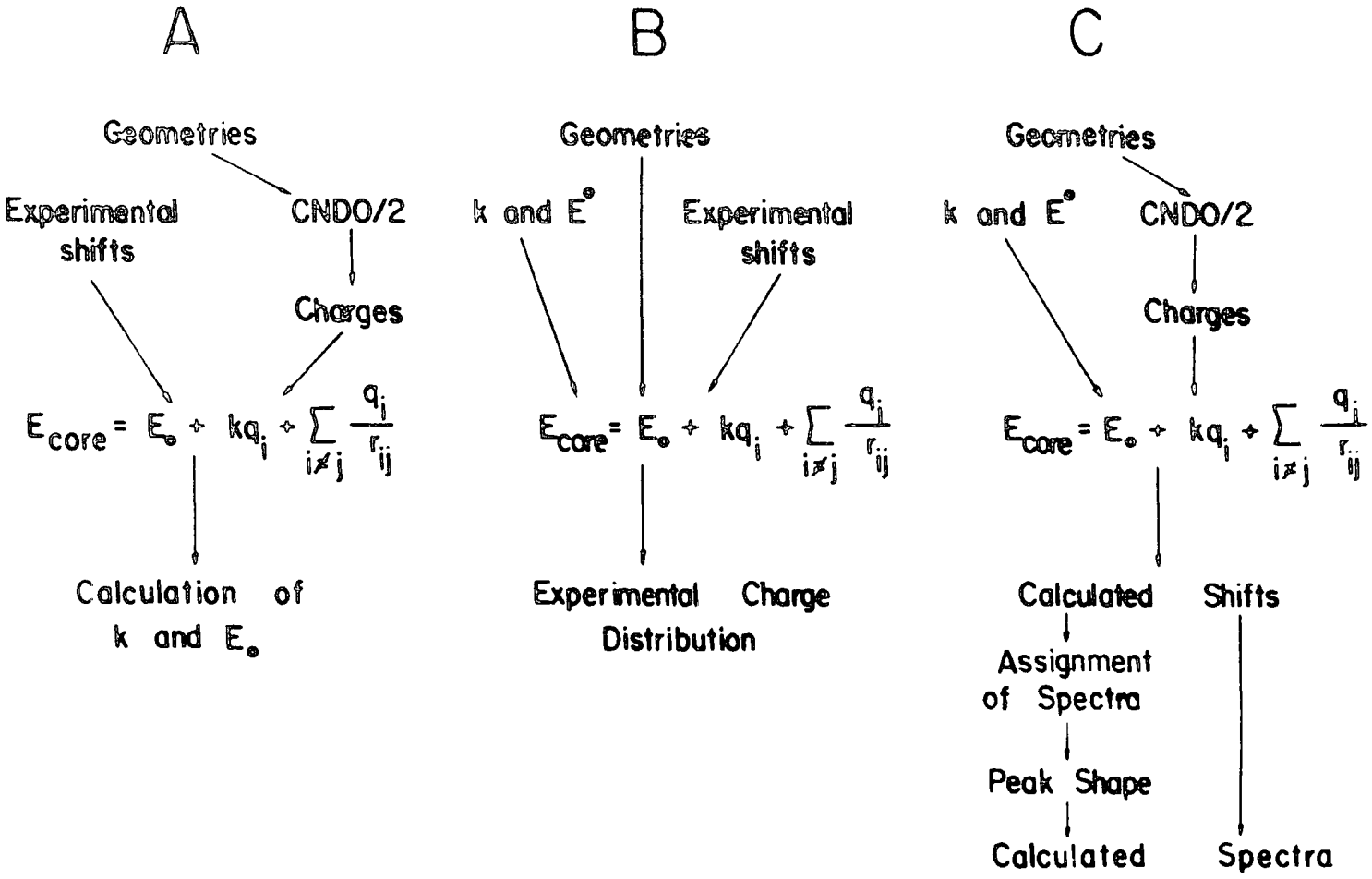

Uses of the Charge Potential Model

Figure 2.4.3

therefore feasible to 'invert' the charge potential model by using the geometry, appropriate of k and E^{o} (as determined from studies on related system), the measured binding energies may be used to obtained 'experimental' charge distribution as in B. An example of this is outlined more fully for a simple halocarbon in Figure 2.4.4.

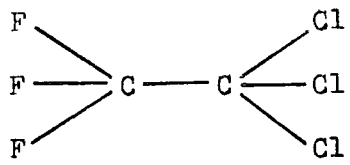

F	$\underline{C}F_3$	$\underline{C}Cl_3$	Cl
690	294	283	187

Experimentally Determined	Known		Required
E^F	E_o^F	k^F	q^F
E^{CF_3}	E_o^C	k^C	q^{CF_3}
E^{CCl_3}	E_o^{Cl}	k^{Cl}	q^{CCl_3}
C^{Cl}	Molecular Geometry (e.g. bond angles and lengths)		q^{Cl}

Figure 2.4.4 Application of the inverted charge potential model to simple hydrocarbon

Schematically the equations for F_{1s}, C_{1s} and Cl_{2p} levels are as follows

$$\underline{E}_{1s} \quad \begin{matrix} E^F \\ \vdots \end{matrix} = E_o^F + k^F q_F + \frac{2q_F}{r_{C-F}} + \frac{3q_{Cl}}{r_{FCl}} + \frac{q_{CF_3}}{r_{F-CF_3}} + \frac{q_{CCl_3}}{r_{F-CCl_3}}$$

$$\vdots$$

$$\underline{C}_{1s}\, E^{C}_{CF_3} = E^{C}_{o} + kq_{CF_3} + \frac{3q_F}{r_{C-F}} + \frac{3q_{Cl}}{r_{C-Cl}} + \frac{q_{CCl_3}}{r_{C-C}}$$

$$\underline{Cl}_{2p} E^{Cl} = E^{Cl}_{o} + kq_{Cl} + \frac{3q_F}{r_{Cl-F}} + \frac{2q_{Cl}}{r_{Cl-C_1}} + \frac{q_{CF_3}}{r_{Cl-C_1}} + \frac{q_{CCl_3}}{r_{Cl-C_2}}$$

$$\vdots$$

$$\vdots$$

Also $3q_F + 3q_{Cl} + q_{CF_3} + q_{CCl_3} = 0$

It is also possible as shown in C to use the charge potential model to assign peaks within a spectrum. This is particularlly useful when assigning binding energies, which differ only slightly, to various atom within a molecule. Clark and coworkers have made extensive use of this method of assigning binding energies.[145-147] Calculated charge distributions can also be usefully employed in investigating sample charging.

2.4.3 Fine Structure

2.4.3.1 Spin-Orbit Splitting

If photoionization occurs from an orbital with an orbital quantum number l greater than 1 (e.g. p, d and f) then a doublet structure wil be observed in the XPS spectrum.[84] This rises from coupling between the spin S, and the orbital momenta L, giving rise to two possible values of the total angular momentum J for hole state formed.

For the lighter elements, up to about the lanthanides, it can be shown that the total angular momentum, J, may be obtained by

summing the first the individual spin momenta and the individual orbital angular momenta separately. The resulting total spin momentum S_T and orbital angular momentum L_T are then coupled to give a total momentum:

$$J_T = S_T + L_T \qquad (2.4.11)$$

This type of coupling scheme is known as a Russell-Saunders[148] coupling, occurs in the lighter elements where the spin-orbit coupling is weak, compared to electrostatic interaction. Where the spin-orbit coupling energy is strong with respect to the electrostatic interaction then the individual spin and orbital momenta couple to give a resultant ji. The coupling of the individual momenta, j, with the electrostatic interactions will give a final momentum J_T. This situation occurs for the heavier elements, where spin and orbital momentum couple individually and the resultants couple is known as jj coupling scheme.[148]

The intensities of the peaks in the doublet are proportional to the ratios of the degeneracies of the state (2J + 1). The relevant intensity ratios are displayed in Table 2.4.4.

Table 2.4.4 Intensity Ratios for Different Levels

	Orbital Quantum number l	Total Quantum Number $J = (l \mp S)$		Intensity Ratio (2J+1)/(2J+1)
s	0	1/2		No splitting
p	1	1/2	3/2	1:2
d	2	3/2	5/2	2:3
f	3	5/2	7/2	3:4

Examples of experimentally observed peaks from C_{1s}, Cl_{2p}, Ag_{3d} and Au_{4f} are shown in Figure 2.4.5 below.

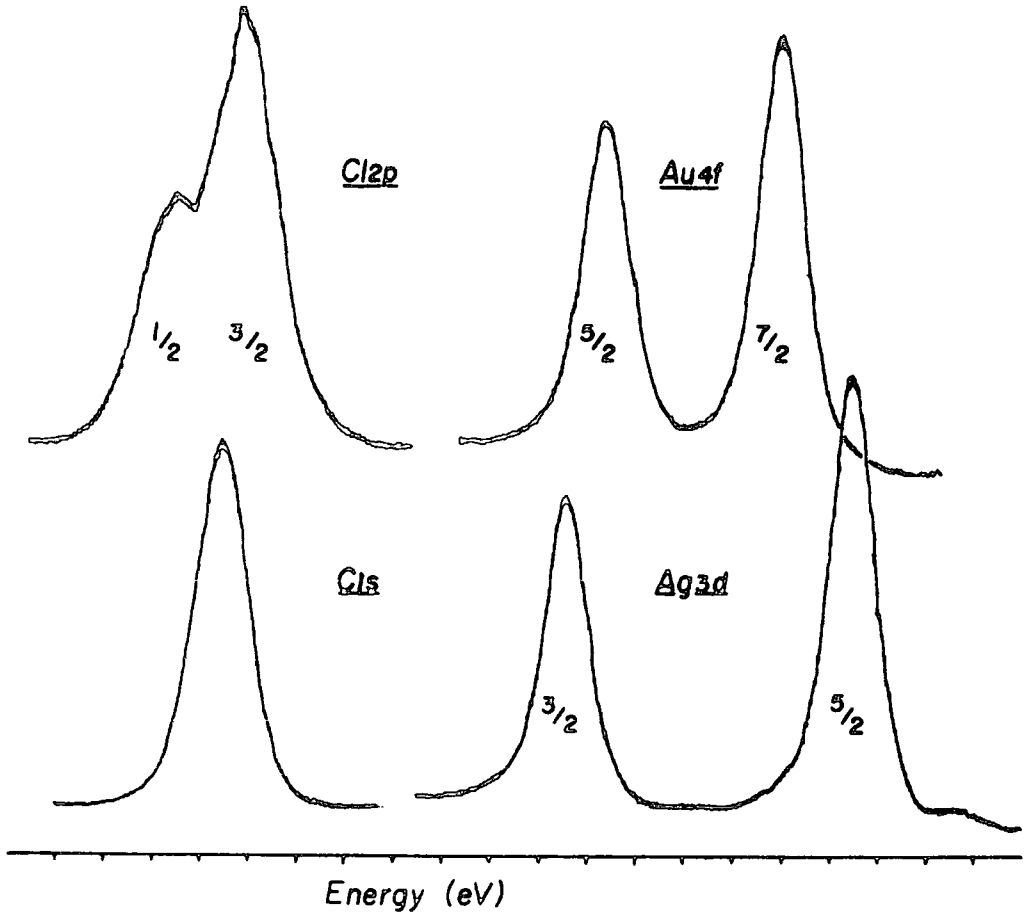

Figure 2.4.5 Examples of Spin-Orbit Splitting in the p, d and f levels

2.4.3.2 Multiplet Splitting

Multiplet splitting occurs in paramagnetic systems and is the result of interactions between unpaired electrons present in the system and the unpaired core orbital electrons remaining after photoionization. The phenomenon was predicted by Watson and Freeman[149] before being observed by Fadley and coworkers[150] for the 3s level in some fluorides and oxides of manganese and iron which contain unpaired 3d electrons. The interpretation is relatively straightforward only for s hole state.[151]

If S is the total spin of 1^n configuration in the ground state, then the two possible final states have a total spin of $S \pm 1/2$. The energy difference (splitting), ΔE between the two state $S + 1/2$ and $S - 1/2$ is proportional to the multiplicity of the ground state:

$$\Delta E = (2S + 1) K \qquad (2.4.12)$$

where K is the exchange integral between the core, c, and the valence, v, electrons under consideration and is defined by

$$K = \left\langle \phi_v(1)\phi_c(2) \left| 1/r_{12} \right| \phi_v(2)\phi_c(1) \right\rangle \qquad (2.4.13)$$

The intensities of the peaks are proportional to the degeneracies of the final states and is given by

$$\left[2 \left(S + \tfrac{1}{2} \right) + 1 \right] : \left[2 \left(S - \tfrac{1}{2} \right) + 1 \right] = (S + 1) : S \qquad (2.4.14)$$

The magnitude of the splitting for a given ion can give valuable information concerning the localization or delocalization of the unpaired valence electron in compounds;[84,152-153] the greater the spin density on an atom, the greater the splitting.

A simple example of multiplet splitting is demonstrated by Siegbahn and co-workers.[85] In a gas phase for N_2 shows no indication of splitting whilst for NO and O_2 of their 1s peaks are observably split, and this is illustrated in Figure 2.4.5. In the case of NO molecule, the single unpaired electron is delocalized over nitrogen and oxygen so that the magnitude of multiplet splitting of the O_{1s} and N_{1s} core levels will depend upon the unpaired spin densities on the two atoms. The pronounced satellite splitting (see Figure 2.4.5)

for N_{1s} but not for O_{1s} indicates that most of the unpaired spin density is on nitrogen. For the N_{1s} level, there is an energy separation of 1.5 eV; in the case of the O_{1s} level, the separation is 0.7 eV leading to line-broadening of 0.3 eV.

Figure 2.4.5 Diagram of Orbital levels in N_2, NO and O_2

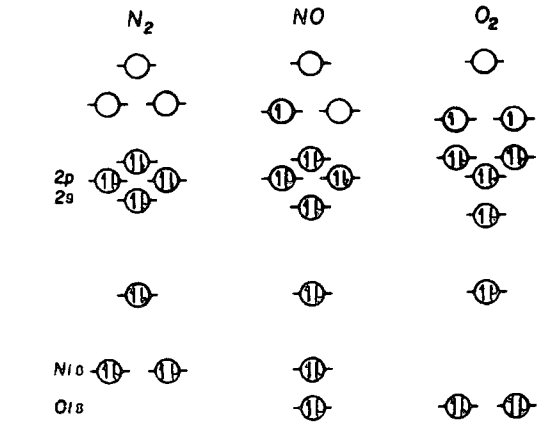

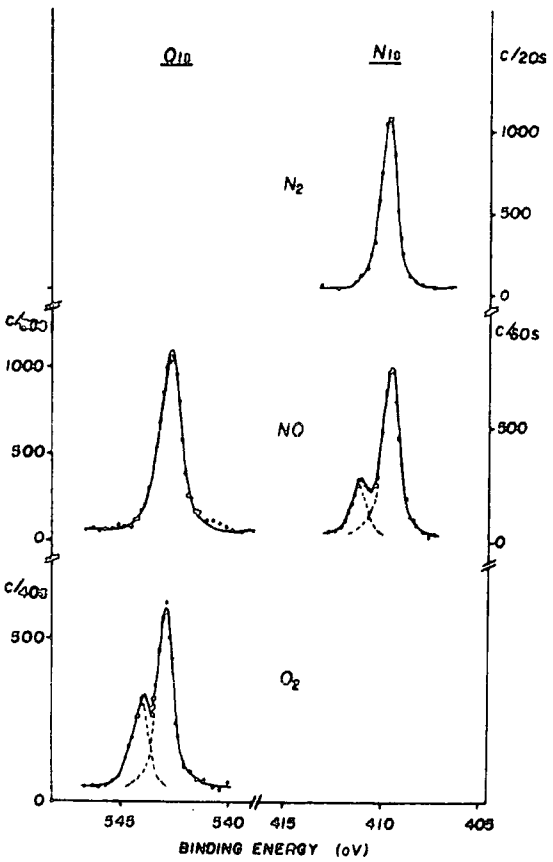

2.4.3.3 Electrostatic Splitting

Splittings in the $5p_{3/2}$ levels of uranium and thorium metals and their compounds, and some compounds of gold, have been observed.[154-155] These were interpreted as arising from the differential interaction of the internal electrostatic field with the $M = \pm 1/2$ and $M = \pm 3/2$ spin states of the $5p_{3/2}$ electrons. An example of this splitting in the $5p_{3/2}$ level of uranium, U, metal is shown in Figure 2.4.6. A definite correlation has been observed between this type of splitting and the quadrupole splittings obtained from Mossbauer spectroscopy,[156] which arise from the interaction of the nuclear quadrupole moment with an inhomogeneous electric field. Bancroft and coworkers[157] have recently observed such splitting in the spectra of the tin compounds.

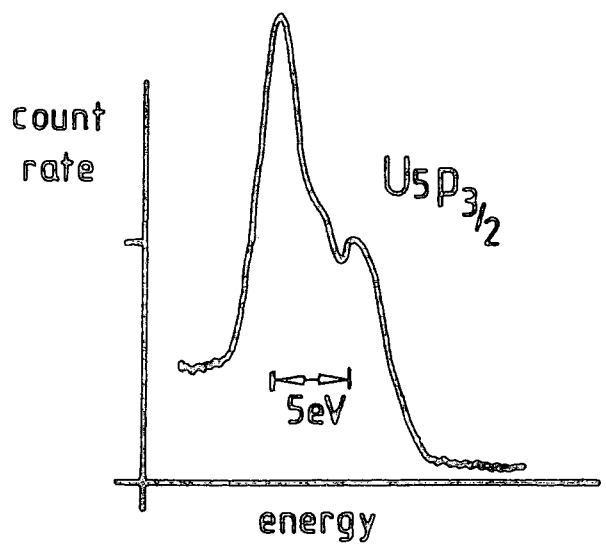

Figure 2.4.6 Electrostatic Splitting in the $5p_{3/2}$ levels of U metal

Due to the inherently amorphous structure of organic polymers it is unlikely that quadrupole fields will be induced within the bulk structure and it is therefore unlikely that electrostatic splitting will be observed in these systems. A summary of the types of splitting encountered in ESCA is shown in Figure 2.4.7.

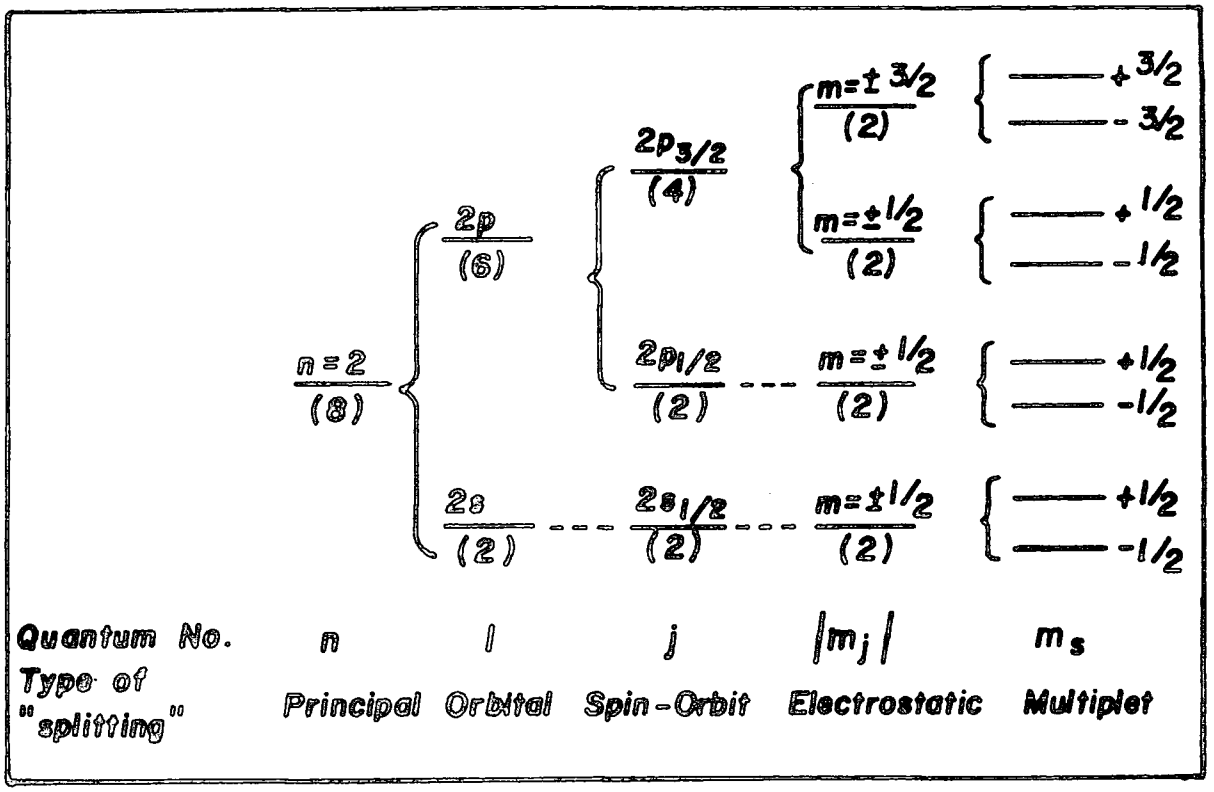

Figure 2.4.7 Splitting encountered in ESCA

2.4.4 Line Widths

The various effects contributing to the total line width ΔE_m have been discussed in Section 2.3.4. The natural line width of half maximum height peak (FWHM) of the core level under investigation, ΔE_{cl} and that of the incident radiation ΔE_x (unless monochromatization is used) depend on the Uncertainty Principle.[155]

$$\Delta E \cdot \Delta t = h/2 \qquad (2.4.15)$$

where Δt is the lifetime of the state and h is Planck's constant. From the equation 2.4.15 above, a line width of $\sim$1 eV corresponds to a lifetime of approximately 6.6×10^{-16} sec.[158] Table 2.4.8 displays some natural line widths of core levels derived from x-ray spectroscopic studies.

Table 2.4.8 Full Width at Half Maximum of Natural Line Width ΔE_{cl^2} for some Core Levels (eV)

Level	S	Ar	Ti	Mn	Cu	Mo	Ag	Au
1s	0.35	0.5	0.8	1.05	1.5	5.0	7.5	54
$2p_{3/2}$	0.10	-	0.25	0.35	0.5	1.7	2.2	4.4

Table 2.4.8 emphasizes the fact that there is no particular virtue in studying more tightly bound core levels; for Au, for example, the FWHM of $\sim$54 eV for the 1s level would swamp any chemical shift.

2.4.5 Sample Charging and Energy Referencing

The problems associated with sample charging in the ESCA studies of thick insulating samples were recognized and diagnosed at the early stage in the development of the technique by Siegbahn and coworkers.[84] For insulating samples, such as polymers, the Fermi level is not well defined analytically, but lies somewhere between the valence (occupied) and bottom of the conduction (unoccupied) energy levels. Several investigations have shown that the photoelectrons (primary photoelectrons) are rapidly slowed down by the interaction with the matter and can generate intense currents of slow 'secondary' electron clouds at the surface of the sample.[132,159-160] These secondary electrons play an

important role in establishing the electrical equilibrium at the surface and have been found to be ~20% of the photoelectron flux in a conducting sample and ~99% of the flux in an insulating sample.

For samples studied as solids three situations may clearly be distinguished. In the first the sample is in electrical contact with the spectrometer. This is usually the case for thin films deposited in situ on a conducting substrate in the spectrometer source. Since the mean free path for the incident x-ray beam is very large,[84] ~10,000 Å it is possible depending on the conditions for films of the order of ~1000 Å to have sufficient charge carriers to remain in electrical contact with the spectrometer. This can most readily be shown by the application of a D.C. bias to the sample holder. If the sample is in electrical contact the shift in energy scale will exactly follow the applied D.C. bias voltage. This technique is equally suitable for use with conducting materials and has been used[159] to determine the position of the vacuum level.

The second situation which arises is for thick insulating samples or when the sample is not in electrical contact with the spectrometer. In this case, in general it will be floating at some potential due to surface charging and indeed this process may be time dependent. An attempt has been made to study surface charging by using electron flood guns.[161] The removal of bremsstrahlung by monochromators very considerably reduces the supply of secondary electrons and may produce a shift in kinetic energy of several hundred electron volts and can be compensated by 'flooding' the sample with low energy electrons. However sample may become negatively charged and the method needs great care to achieve an accuracy comparable with that for the other methods. An alternative way of producing low energy electrons is to illuminate the interior of the sample chamber with u.v. radiation from a low pressure, low power mercury

discharge lamp via quartz viewing port.[177] Sufficient secondary electrons are generated from photoemission from the metal surfaces that sample charging is reduced to a low level. The third situation which can arise is for films 1 - 10micron thick, which have been deposited on a conducting substrate. Such films behave as 'leaky' capacitor in that they exhibit rather striking time dependent charging and discharging characteristic and follow an applied bias potential in a particular manner.[162] The investigation of the effects of electrical bias applied to the substrate as a function of thickness in the range 1 - 100 micron can provide an interesting insight to the electrical characteristic of polymer samples. This is illustrated in Figure 2.4.8.

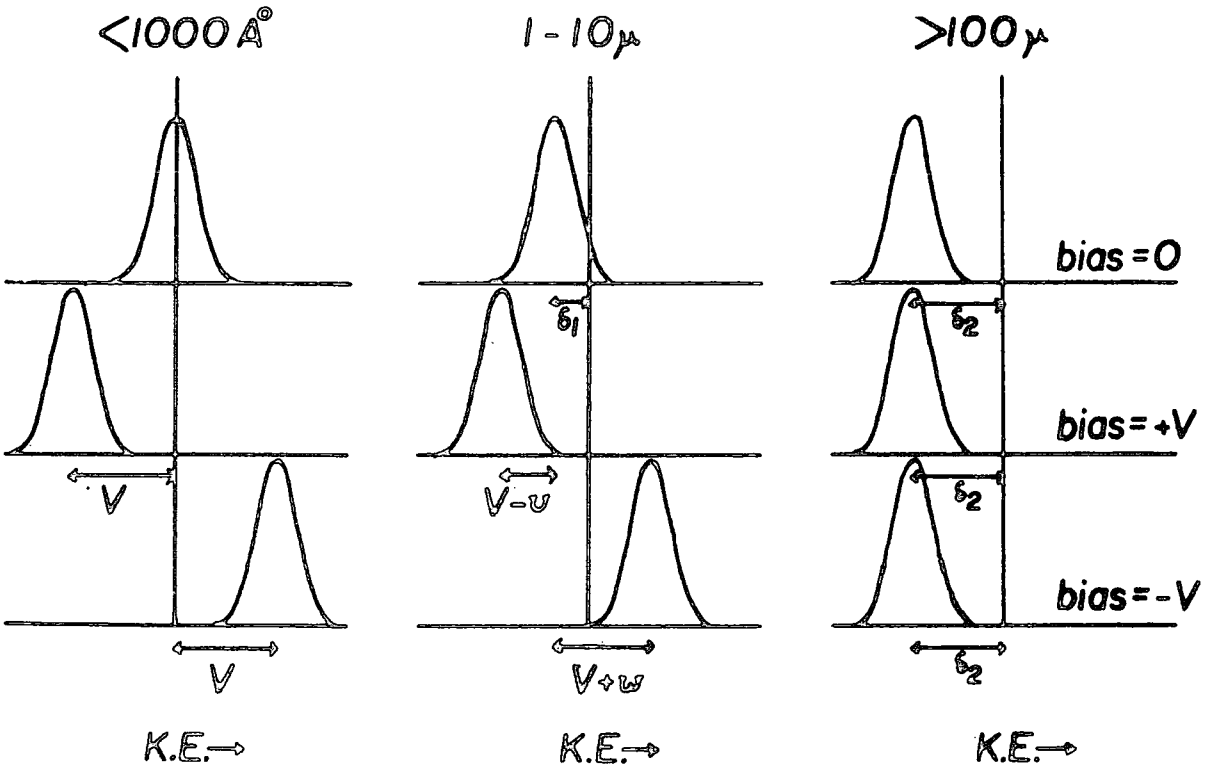

Figure 2.4.8 Typical behaviour of polymer films with an electrical bias applied to the substrate

However in practice, the problem of extracting absolute binding energies can be overcome by the use of referance standards for calibration on the binding energy scale. The most reliable method of energy referencing is to follow the slow build up of hydrocarbon contamination of the surface, which produces a peak of the C_{1s} level at binding energy of 285 eV. The second important energy referencing refers to the $Au_{4f_{7/2}}$ level at binding energy of 84 eV. The use of so-called 'gold decoration' technique[163] in particular is not recommended for organic and polymeric materials; Firstly, nucleation may be via an 'islanding' process which will almost certainly result in differential sample charging, and secondly, since gold is normally evaporated from a filament the possibility of surface damage, and other effects cannot be discounted.

Although sample charging has been widely regarded as somewhat of a nuisance which must be circumvented, recent work has shown[164-165] that sample charging is an interesting phenomena in its own right and in appropriate cases provides an important addition to the hierarchy of available information levels.

2.4.6 Line Shape Analysis

The need to line shape analysis (deconvolution) arises when the chemical shift of a level is smaller than the line width of the level. This is the most common situation encountered in ESCA and in fact, one of the major weaknesses of the technique compared to say NMR or NQR.[84] The dominant contribution to the line widths with most commercial instrumentation is the inherent width of the polychromatic x-ray photon source, although this can be improved by monochromatizing the photon source.

The measured line width for core levels may be expressed as:

$$(\Delta E_m)^2 = (\Delta E_x)^2 + (\Delta E_s)^2 + (\Delta E_{cl})^2 \qquad (2.4.16)$$

where ΔE_m is the FWHM of the observed photoelectron peak,

ΔE_x is the FWHM of the x-ray photon source,

ΔE_s is the contribution to the FWHM due to the spectrometer (i.e. the analyzer abaritions)

ΔE_{cl} is the natural width of the core level under investigation.

(For solid sample this takes into account the solid state effects not directly associated with the lifetime of the hole state, but rather with slightly differing binding energies due to differences in lattice environments.)

The contributions to ΔE_m from ΔE_x and ΔE_{cl} which are essentially Lorentzian line shapes, have been discussed in Section 2.3.4 and Section 2.4.4 respectively. While for ΔE_s is usually taken to be Gaussian in shape. The combination of the various contributions to ΔE_m produces a hybrid shape with a Gaussian distribution dominating the line shape and with a Lorentzian character to the tails. It has been shown that the assumption of a pure Gaussian shape foe the observed peaks introduces only a small error in line shape analysis.[85]

The methods employed for the resolution of complex line shape in the ESCA can be discussed under two main headings. The first involved the enhancement of resolution by mathematical manipulation of the raw data whilst the second involves curve fitting procedures in an analogue or digital fashion.

Deconvolution by mathematical methods has been reviewed by

Carley and Joyner.[166] The methods discussed are the Fourier Transform and various iterative processes, these latter often being based on Van Cittert's method. They conclude that convolution by mathematical enhancement may bring about an improvement in resolution comparable to that obtained by the use of a monochromator.

The second category involves curve fitting techniques. These produces require close control over a number of variable, for example, binding energy, line width and peak height. Therefore, the use of analogue system is more convenient than digital analysis with a large computer. The work in this thesis deconvolution was performed by analogue simulation using a DuPont 310 curve resolver. The basic approach to curve simulation is shown in Figure 2.4.9. In deconvolution by both methods a certain amount of caution is required, as it is often possible to obtain more than one solution from which the correct one must be chosen. The use of deconvolution has been discussed by Ebel and Gurker[167] and criticisms of deconvolution technique have been made by Wertheim.[168]

2.4.7 Signal Intensities

Figure 2.4.10 shows a schematic of the general geometry of the ESCA experiment employing a fixed arrangement of analyzer and x-ray source. $h\nu$ represents the incident x-rays and e^- the fraction of the photoelectrons which enter the analyzer. ϕ is the angle between the x-ray source and the analyzer entrance slit and θ describes the angle of the sample in relation to the analyzer. If the photoelectrons are emitted from a depth, d, of the sample, the true path length d' is given by:

$$d' = d / \cos \theta \qquad (2.4.17)$$

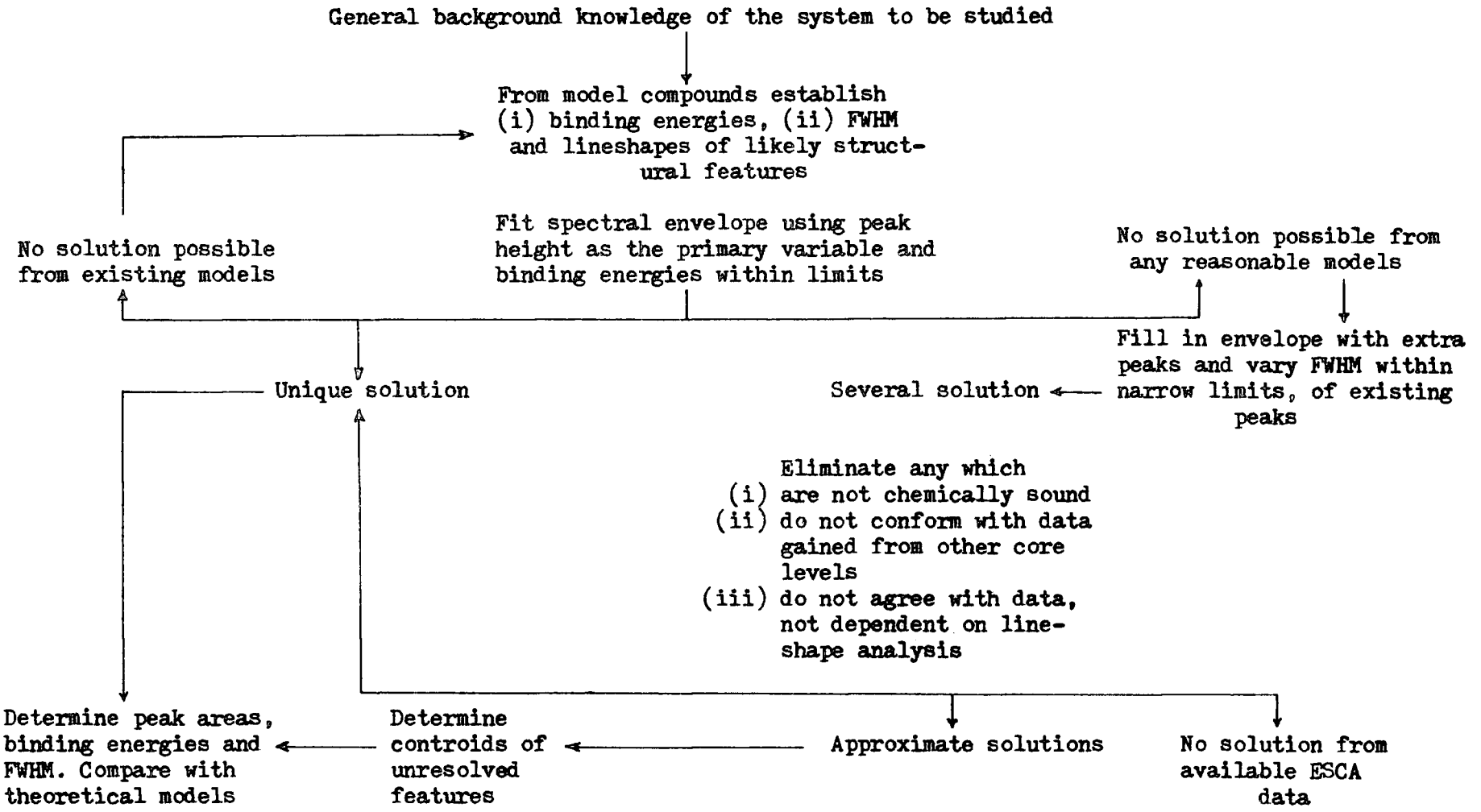

Figure 2.4.9. Line-shape analysis by curve fitting; schematic of logic procedure

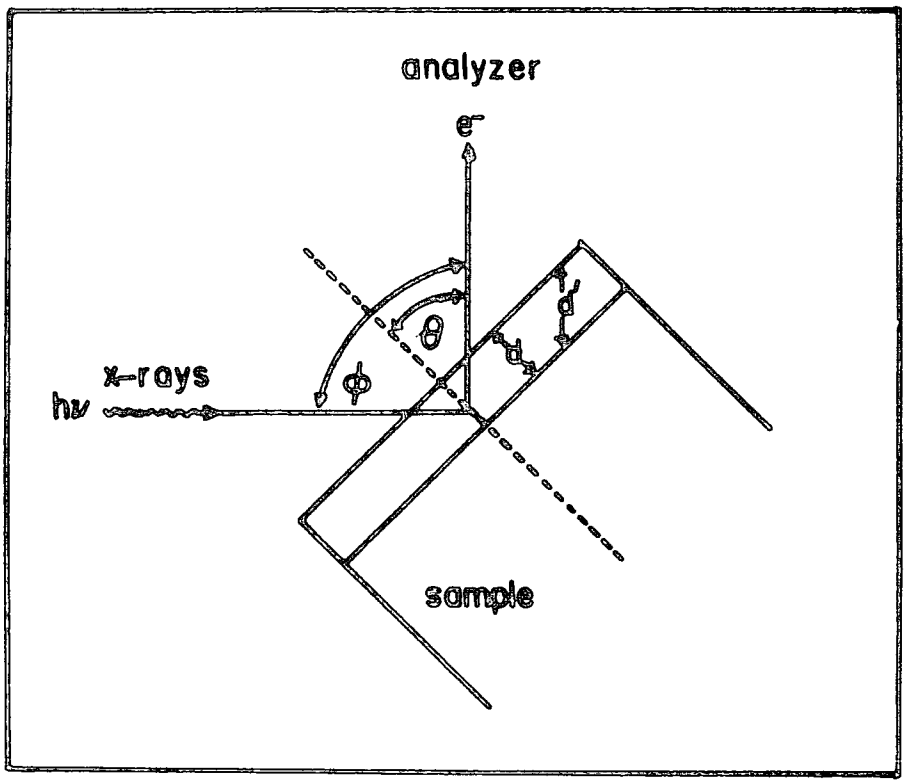

Figure 2.4.10 Geometry employed in an ESCA experiment

Due to the short mean free paths of electrons in solids (see Section 2.4.8) it is possible to study surface feature with respect to bulk and subsurface compositions by carrying out experiment at different angle of θ.[169] These parameters will be referred to in the following discussion.

2.4.7.1 Fixed Angle Studies

For an 'infinitely thick' homogeneous sample the intensity of the elastic (no energy loss) photoionization peak for photoelectrons from a core level i may be expressed as:[170-171]

$$dI_i = F\alpha_i N_i k_i e^{-x/\lambda_i} dx \qquad (2.4.18)$$

Where: I_i is the intensity arising from core level i,

F_i is the exciting photo flux,

λ_i is the cross section for photoionization of core level i,

k_i is a spectrometer factor,

N_i is the number of atoms per unit volume on which the core level i is localized, and

i is the electron mean free path.

Integration of this equation gives

$$I_i = \int_o^\infty F\alpha_i N_i k_i e^{-x/\lambda_i} dx \qquad (2.4.19)$$

and

$$I_i = F\alpha_i N_i k_i \lambda_i \qquad (2.4.20)$$

There various factors and the parameters on which they depend are discussed below.

a) X-ray Flux, F

The x-ray flux in the sample is primarily dependent on the power applied to and the efficiency of the x-ray gun. At low value of θ it has been shown that refraction of collimated x-rays in the outmost surface layers of the sample causes an effective increase in flux in the sample region as seen by ESCA, resulting in an enhancement of signal intensity. However, in practice this phenomenon is rarely experienced since samples are seldom optically flat, x-ray beams are not collimated and the angles θ, for which this applies are very small.

b) Photoionization Cross Section

The cross section for photoionization of a core level i, σ_i is a parameter which describes the probability of the core level being ionized when irradiated by photon of know energy. The parameter α_i only includes the fraction of photoelectrons eccepted by the analyzer. This a function of the core level to which it relates and the energy of the incident photon. It may be calculated from the fundamental properties of the atom,[172] or determined experimentally from the gas phase measurements.[85]

The radial distribution of photoelectrons from an atom is not uniform and α_i is a function of ϕ, the angle of detection with respect to the incident photons. The photoionization cross section, α_i is given by:[173-174]

$$\alpha_i = \alpha_i^{TOT}/_{4\pi}\left[1 - \tfrac{1}{4}\beta_i(3\cos^2\phi - 1)\right] \qquad (2.4.21)$$

where α_i^{Tot} is the total cross section of the core level i, and β_i is the asymmetry parameter of that level. For a particular spectrometer, using the same x-ray source and with a fixed value of ϕ then α_i is normally a constant. With $Mg_{k\alpha_{1,2}}$ and $Al_{k\alpha_{1,2}}$ the cross section for photoionization for core levels of most elements are within two orders of magnitude of that for the C_{1s} levels,[172] therefore ESCA is a convenient sensitivity range for most element.

c) Spectrometer Factor

The spectrometer factor, k_i which varies from one instrument to another, includes effects due to detector efficiency, analyzer

transmission characteristics (which are both dependent on kinetic energy of the photoelectrons being analyzed) and geometric factors such as the solid angle of acceptance of the analyzer.

d) Electron Mean Free Path

The electron mean free path, (sometimes referred to as the escape depth for the photoelectrons), λ_i is defined as the distance in the solid through which the photoelectrons will travel before 1/e of them have not suffered energy loss through inelestic collision. Electron mean free paths may be calculated theoretically[175] or determined experimentally.[176-177] λ_i is a function of kinetic energy of the photoelectrons and ranges from ~4 Å for electrons of about 80 eV kinetic energy to ~30 Å for electrons of about 1500 eV kinetic energy.

The sampling depth, is sometimes confused with electron mean free path, is defined as the depth from which 95% of the signal peak comes from and is related to the electron mean free path, λ by:

$$\text{sampling depth} = -\lambda \ln 0.05 = 3 \qquad (2.4.22)$$

As an example, for carbon 1s levels studied by a $Mg_{K\alpha_{1,2}}$ x-ray source the kinetic energy of the photoemitted electrons is ~960 eV and the mean free path of the electrons is ~15 Å, 95% of the signal intensity arises from the top 45 Å and 50% from the outmost 10 Å.

e) Number Density

The number of atoms per unit volume in the sample, on which core level is localized, N_i is not directly related to the density of the sample. However, it has been observed that for similar materials of different densities, the higher density material produces a large ESCA

signal for a given core level.[117] The most important consequence of N_i is that the relative signal intensities for core level in homogeneous sample are directly related to the overall stoichiometries of the atoms in the sample. Thus from the equation 2.4.20 for two core levels i and j gives:

$$\frac{I_i}{I_j} = \frac{F\alpha_i N_i k_i \lambda_i}{F \alpha_j N_j k_j \lambda_j} \qquad (2.4.23)$$

If i and j correspond to the same core in differing chemical environments then

$$k_i \alpha_i \lambda_i = k_j \alpha_j \lambda_j \qquad (2.4.24)$$

and so

$$\frac{N_i}{N_j} = \frac{I_i}{I_j}. \qquad (2.4.25)$$

if however i and j are different core levels for different elements then

$$k_i \alpha_i \lambda_i \neq k_j \alpha_j \lambda_j \qquad (2.4.26)$$

But the ratio of these can be determined experimentally using standard samples of known stoichiometry containing i and j. This ratio is usually refer to as the instrumental sensitivity ratio of the given levels.

2.4.7.2 Angular Dependence Studies

Two effects of varying the angle Θ on the x-ray flux can be observed and are important when the x-ray beam width is wider than the

width of the sample, W. These are illustrated in Figure 2.4.11.

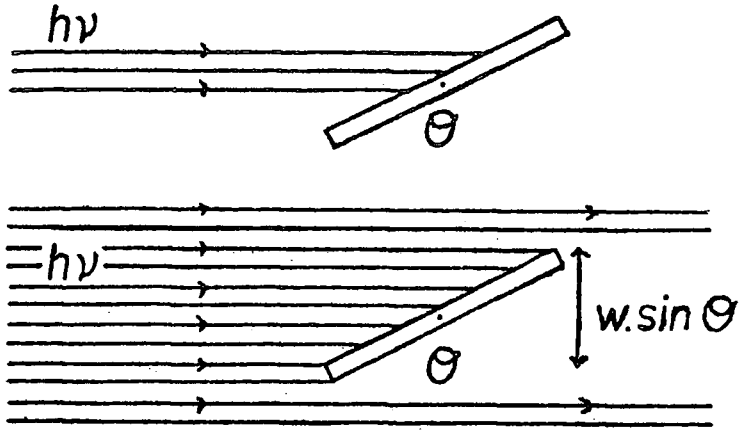

Figure 2.4.11 Narrow and Wide x-ray beams.

For the narrow beam the total flux which hits the sample is not effected by varying θ within limits. However for the broader beam the total flux hitting the sample varies as W.sin θ . Therefore as θ is increased this effect tends to increase the signal intensity. (This effect also applies for the narrow beam when θ is small). Another effect is concerned with the photoelectrons in the direction of the analyzer. For a given value of θ the entrance slit of the analyzer 'sees' a sample area proportional to W.cos θ. This effect tends to decrease the signal intensity as θ is increased. These effects have been investigated by Clark and Shuttleworth using a composite probe tip[125] containing gold plated pins set in epoxy resin. For the particular spectrometer, an AEI ES200 AA/B on which the work for this thesis was carried out, the largest contribution to the signal come from a small area of the sample, approximately 0.25 cm.^{2} out of a total area of 1.4 cm.^{2} Therefore the equation 2.4.20 may be replaced to include an overall function of θ, $F_i(\theta)$ for a core level i and becomes:

$$I_i = f_i(\theta) F \alpha_i N_i k_i \lambda_i \qquad (2.4.27)$$

where $F_i(\theta)$ can be determined empirically.

2.4.8 Analytical Depth Profiling

It is important to investigated the sample for which the surface is not representative of the bulk. As an example of this consider a single homogeneous component of thickness d on a homogeneous base as illustrated in Figure 2.4.12.

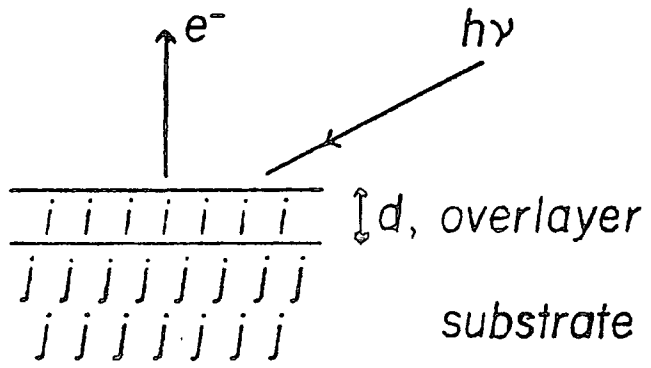

Figure 2.4.12 Substrate overlayer model

The intensity of the signal arising from the overlayer, I_i^{over} can be obtained by integrating equation 2.4.18 between x = 0 and x = d:

$$I_i^{over} = F\alpha_i N_i K_i \lambda_i \ (1-e^{-d/\lambda_i}) \qquad (2.4.28)$$

Similarly, integrating between x = d and x = ∞ gives the intensity of signal arising from the substrate, $I_j^{subs.}$:

$$I_i^{subs.} = F\alpha_j N_j K_j \lambda_j \ e^{-d/\lambda_j} \qquad (2.4.29)$$

Electron mean free path as a function of kinetic energy of photoelectrons is shown in Figure 2.4.13. It is clear that in the energy range of interest to ESCA (>300 eV) the mean free path increases

with kinetic energy. As a concequence of this, the attenuation of a signal arising from a core level in the substrate by an overlayer coverage will depend strongly on the kinetic energy of the photoelectrons. Therefore in order to use depth and angular studies for analytical purposes it is necessary to determine accurately the electron mean free path at the kinetic energies of interest, in the materials being studied. The electron mean free path most commanly used in this thesis is that of 18.5 Å for $Au_{4f_{7/2}}$ level at the kinetic energy of ~1160 eV. The electron mean free path of C_{1s} (~960 eV) and F_{1s} (~560 eV) have been recently directly determined in this laboratory by Clark and co-workers, to be ~14 ± 3 Å and 10 ± 3 Å respectively.[176]

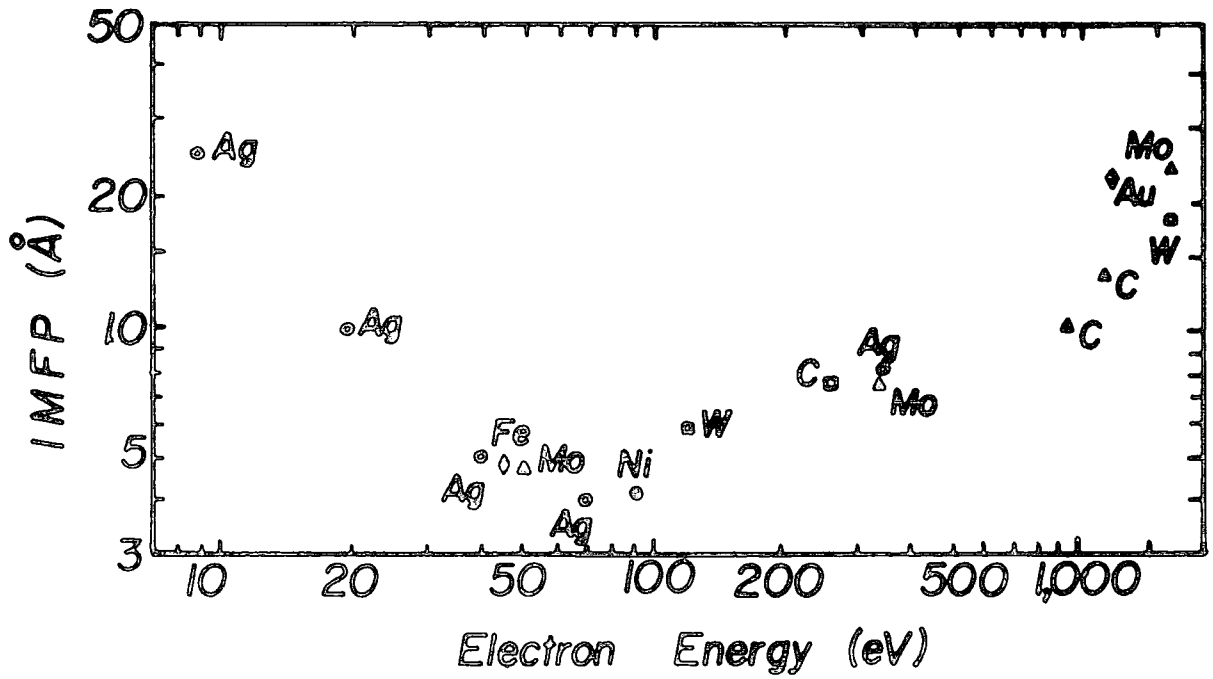

Figure 2.4.13 Electron mean free path as a function of kinetic energy

2.5 General Aspects of ESCA

2.5.1 Advantages of ESCA

ESCA is an extremely powerful tool especially with wide ranging applicability in respect of the surface studies. The principle advantages of ESCA may be summarized as follows:

1. The sample may be solid, liquid or gas and the amount required is small being approximately 10^{-3}g of solid, 0.1 μl of liquid and 0.5 cc of gas (STP).
2. The technique is essentially non-destructive, since the x-ray flux is small (0.1 millirad. s^{-1}).[123] One notable exception to this generalization is poly(thiocarbonyl fluoride) which depolymerizes rather rapidly under x-ray irradiation.
3. The technique is independent of the spin properties of any nucleus and is applicable in principle to any element of the periodic table, with the exception of hydrogen and helium for which the core levels are also the valence levels.
4. Materials may be studied 'in situ'with a minimum of preparation.
5. The technique provides a large number of information levels from a single experiment.
6. The data is often comlementary to that obtained by other techniques.
7. For solids, ESCA has the unique capability of differentiating the surface from subsurface and bulk phenomena, allowing analytical depth profiling (see Section 2.4.8.)
8. The information obtained is directly related to the molecular structure and bonding, and applies to both inner orbitals and valence orbitals of the molecule enabling a thorough analysis of electronic structure to be made.

9. The information levels are such that 'ab initio' investigations are possible and the theoretical basis is well understood.

2.5.2 Disadvantages of ESCA

However, there are surprisingly few disadvantages associated with ESCA.

1. The overall costs are quite high.
2. Whilst the technique has superior depth resolution, ~100 Å, the spatial resolution is poor and typically an area of 0.3 cm^2 is sampled.
3. If the surface layer is comparatively thick, ~100 Å, it is not possible to detemine the bulk composition by ESCA without sectioning the sample.

2.5.3 Hierarchy of ESCA Information

The hierarchy of information levels which provide the technique with such wide-ranging capabilties is as follows:

1. The technique gives absolute binding energies, relative peak intensities, shifts in binding energies, elemental analysis, analytical depth profiling, indentification of structural features, etc; allows the investigation of short range effects directly and longer effects indirectly.
2. Shake-up and shake-off satellites may be observed, monopole excited state and their energy separation with respect to direct photoionization peaks and relative intensities of components of 'singlet' and 'triplet' origin are also obtained.
3. Multiplet effect for paramagnetic systems, spin state, and distribution of unpaired electron (analogue of electron spin

resonance, ESR.) can be investigated.

4. For valence energy levels, it allows the investigation of longer range effects directly and provides a fingerprint of gross structure.

5. For solids, angular dependence studies may be carried out, providing a means of differentiating surface from subsurface and bulk effects.

6. Sample charging phenomena which provide an additional means of monitoring structure and bonding in surface regions and electrical properties of polymer films can be investigated from biasing experiments.

CHAPTER THREE

CHAPTER THREE

PLASMA POLYMERIZATION I. AN INVESTIGATION OF POLYMERS PRODUCED BY EXCITATION OF INDUCTIVELY COUPLED R.F. PLASMA IN THE PERFLUOROBENZENE AND PERFLUOROBENZENE/HYDROGEN MIXTURES

Abstract

The composition and gross structural features of plasma polymers formed in the glow regions of an inductively coupled R.F. plasma with perfluorobenzene and perfluorobenzene/hydrogen mixtures have been studied by ESCA as a function of the operating parameter. The carbon-to-fluorine stoichiometries of the perfluorobenzene polymers are similar and close to that of the starting monomor, but not for the polymers derived from perfluorobenzene/hydrogen mixtures. The rate of film deposition is shown to be dependent on the W/FM parameter. Angular and photon energy dependent studies confirm the vertical homogeneity of the plasma polymer films investigated.

CHAPTER THREE: PLASMA POLYMERIZATION I. AN INVESTIGATION OF POLYMERS PRODUCED BY EXCITATION OF INDUCTIVELY COUPLED R.F. PLASMA IN THE PERFLUOROBENZENE AND PERFLUOROBENZENE/ HYDROGEN MIXTURES.

3.1 Introduction

This chapter presents a concise summary of some aspects of ESCA studies of polymers which have been carried out to date. This will be followed by a description of the investigation of polymers synthesized from perfluorobenzene and perfluorobenzene with the addition of hydrogen by plasma techniques.

3.2 ESCA Applied to Polymers

The past few years have witnessed a growing awareness of the great potential of ESCA for investigating polymeric systems in general, and numerous reviews which appeared in the literature provide extensive background reading in this area.[117,178-179] Most of the material in this section is cited from the work which was pioneered by Clark and co-workers at the University of Durham, and covers the period from 1970 to 1981.

The early work involving ESCA has concentrated upon the study of fluoropolymer systems.[181-186] The reason for this are threefold:, Firstly, the large chemical shift in the C_{1s} core levels induced by the substituent fluorine greatly eases the problem of interpretation of the ESCA data. Secondly, fluoropolymers are academically and technologically important systems, and finally due to their insolubility and intractability

fluoropolymer systems are difficult to investigate by other spectroscopic techniques.

Since 1974 the application of ESCA to polymeric materials has been diversified to encompass non-fluorine containing systems;[196-199] a particular interest being the study of plasma polymerization and surface modification of polymers.[169,187-195,212,232] There are several distinct information levels available from the technique and the role these have played in the investigation of polymer structure is outline in Table 3.2.1.

Table 3.2.1 ESCA Applied to Polymers

(I) Aspect of Structure and Bonding

A. Static studies

1. Chemical compositions
   a. Elemental composition
   b. % comonomers in copolymers
2. Structural information
   a. Copolymers; block, alternating or random nature
   b. Domain structure in block copolymers
3. Fine structural details
   a. Structural isomerization
   b. Shake-up studies
4. Valence bands studies
5. Sample charging
6. Moropole excited states

B. Dynamic Studies

1. Surface treatments

   e.g. - by electrical discharges

   - by chemical agents

   - by grafting

2. Degradation

   e.g. - chemical; oxidation, nitration etc.

   - evironmental

   - mechanical wear

   - diffusion of additives, migration

3. In situ preparations

   - plasma polymerization

   - pyrolysis

(II) Electrical Properties

1. Mean free path as a function of kinetic energy
2. Static and dynamic of sample charging
3. Triboelectric phenomena
4. Photoconductivity of polymers.

3.3 Plasma Polymerization

3.3.1 Introduction

The rapid developing interest, from both an academic and technological point of view, in the area of plasma polymerization is clear from the extensive literature which is accumulating.[2-4,8] However, it is only in more recent times that real progress has been made as a result of systematic investigation of well-defined prototype systems, coupled with characterization techniques available to elaborate details of structure and bonding in plasma polymerized films.[200] Due to the very complex nature of the process taking place in a gas plasma and the unique structure and properties of the derived films, attention has been focussed primarily on the factors that control the overall rate of production of polymer films and its structure as a function of the starting monomer.

The bulk of the work published to date on plasmas tends to fall into three distinctive categories as follows:-

The first exemplified by relative simple systems such as plasmas excited in inert gases has been the province of the chemical physicists, and detailed studies have been made of the distribution of ion and electron kinetic energies as a function of the operating parameters of the plasma.[16] These prototype model studies are important in providing a firm theoretical foundation to the understanding of discharge phenomena in the more complicated plasmas which are of interest to the synthetic chemist or to the chemical engineer with an interest in the design of instrumentation.

The second category of research in the plasma field is exemplified by the work of chemical engineers, involved less in details of chemical reactions occurring in discharges than with detailed

considerations of the operating and design characteristics of the instrumentation involved.[29]

The final category of research work is of the chemical variety, where less attention has been paid to the instrumentation employed to produce the plasma polymers, than to the study of the polymers which are produced from a wide variety of monomers.[201-202]

It is clear even to a casual observer that reactions occurring in the gas phase or at gas/solid interphase involving the plasma state are likely to be exceedingly complex, and that progress is only likely to be made if elements of all three categories of the typical investigations which are outline above are encompassed.

Over the past few years considerable progress has been made in this 'integrated approach direction', and the pioneering researches of Yasuda and co-workers [29,203] and Bell and Shen and their co-workers [2-3] are particularly noteworthy in this respect.

Detail studies have been presented on the design and operating characteristics of typical instrumentation used for glow discharge polymerization, and the competitive nature of formation of polymer and ablation in the plasma has been emphasized. The importance of power input (W), flow rate (F) and molecular weight of the gas (M) in which the plasma excited has also been recognized, and a large amount of experimental data has been systematized by Yasuda and co-worker by mean of W/FM as an parameter of a given plasma configuration.[29]

Significant progress has been made over the past few years into the general understanding of the chemical physics aspects of plasmas excited in simple organic molecules particularly in the pioneering studies of Shen and Bell and their co-workers. [3] The potential for producing polymers from conventional vinyl monomers by plasma induced polymerization

have been recognized[204] and since such polymers often tend to be reasonably crystalline their characterization presents no great problems.

Since almost all of the work presented throughout in this thesis deals with plasma polymers which are of interest as thin films, and since the films are almost exclusively crosslinked amorphous materials their characterization poses particular problems. However, with the application of ESCA, the technique that has been mainly used for the characterization of the plasma polymer films in the studies carried out in this thesis, these problems are somewhat diminished. ESCA provides and essentially non-destructive means of studying structure and bonding in such polymer films, and the surface sensitivity also provides a convenient means for monitoring their rate of deposition.[205]

It is worthwhile at this stage to summarized the main features which have emerged from previous studies of plasma polymerization as follows:-

(1) Synthesis of ultra-thin polymer films from virtually any monomer, deposition on virtually any substrate.

(2) Solventless process, the rate of deposition can be clearly controlled, reproducible structure, deposition on complicated shapes.

(3) Films can be fabricated with a wide range of advantageous properties (chemical, physical, electrical and mechanical).

(4) Organometallic compounds can be used to obtain metal containing polymers.

3.4 Polymer Films Produced by RF Plasmas Excited in Perfluorobenzene

3.4.1 Introduction

In this section the study of polymer films produced by R.F. glow discharge techniques as revealed by ESCA is presented. The prime objective of this work being to complete the discussion of gross features of composition and structure, and of the rate of polymer deposition as a function of operational conditions for a system has been previously investigated in these laboratories, namely perfluorobenzene.

3.4.2 Experimental

For the sake of completeness, the work described in this chapter involved two polymerization reactors, one (reactor A) consisting of a reactor incorporated into a vacuum line of grease-free construction and the other (reactor C) directly attached to the insertion port of the electron spectrometer. Schematics of the reactor configurations (reactor A and C) used in this study are shown in Figure 4.2.1 in Chapter Four.

The first reactor (reactor A) consisted a pyrex tube 5 cm. in diameter, 32 cm. long, sandwiched between ground glass flanges on 'O' ring seals. This system was pumped by an Edwards ED 50 50 l. $min.^{-1}$ two stage rotary pump via a grease-free vacuum line including two cold traps. Thin films of polymer were collected by depositing onto clean Ar plasma treated gold substrates located along the bottom of the reactor in the middle of the coil region.

Since the reaction chamber (reactor C) was directly attached to the insertion port of the spectrometer, it was therefore possible to eliminate any contamination or further reaction of the sample surface,

e.g. oxidation, hydrocarbon contamination resulting from exposure to air prior to recording spectra. The reactor consisted of a pyrex tube 16 cm. long and 5 cm diameter, sandwiched between stainless steel flanges by 'O' ring seals, and enclosed in a copper mesh screen to prevent R.F. interference with the electronics of the spectrometer. The discharge was excited by a 6 μH, 9 turn, copper coil wound centrally on the pyrex tube. The deposition of polymer films was on fresh gold substrates mounted on a probe tip by double sided 'Scotch' tape. The probe of $\frac{1}{2}$" diameter and 60 cm. long stainless steel was capable of passing through the reactor, on 'O' ring seals and into the spectrometer for analysis. Reactor C was pumped by an Edwards ED 50 50 l. min.$^{-1}$ two stage rotary pump, and a cold trap was included to avoid the backstreaming of rotary pump oil.

In all cases, plasmas were excited using a Tegal Corporation R.F. Generator operating at 13.56 MHz. and associated matching network. For the purposes of this study, the power loadings employed in this work (reactor A) were in the range from 5.0 W up to 50.0 W, in attempting to shed some new light on understanding the 'CAP' process of formation of polymer in the plasma.[203]

Multiple attenuated total reflectance (MATR) IR spectra were measured for films $\sim$0.1 μ thick deposited onto high density polyethylene (HDPE) substrates (2 pieces 2 x 5 cm.^{2} in dimension). Spectra were recorded on a Perkin-Elmer 577 Grating instrument with a 25 reflaction ATR attachment. Optimization of the geometry for signal intensity and resolution lead to incident / exit angles of 45° using a KRS 5 single crystal. HDPE was chosen as a substrate for these studies since it ensures good contact of the deposited plasma polymer film with the KRS 5 crystal. The sampling depth using KRS 5 is almost certainly $\sim$ 1 μ so that the spectra are superimpositions of plasma polymer overlayer and

and HDPE substrates. Blank spectra were therefore obtained of the HDPE substrates to provide difference spectra.

Microanalyses were made by combustion for carbon, and potassium fusion for fluorine. Sufficient quantities of samples for these analyses were obtained by removing the polymer which was deposited on the walls of the pyrex reactor inside the coil region.

Spectra were recorded on an AEI ES 200 AA/B spectrometer using $Mg_{K\alpha_{1,2}}$ x-radiation. For comparison, some spectra were also recorded on Kratos ES 300 spectrometer using $Ti_{K\alpha_{1,2}}$ x-radiation source with photon energy of $\sim$4510 eV. The $Au_{4f_{7/2}}$ level at 84.0 eV and $\underline{C}H$ level at 285.0 eV binding energies were used for energy calibration. Integration of spectra was accomplished on a Du Pont 310 curve resolver. In all cases, the measured binding energies are quoted with a precision of $\pm$ 0.1 eV and area ratios to $\pm$ 5%.

The measurement of flow rates for reactor configurations A and C were discussed in Chapter Four. However, for the in situ study of H_2/C_6F_6 mixtures, flow rates for each component were step-wise determined and a total partial pressure of 200 μ for the system was maintained. Flow rates of the C_6F_6 were calculated from the decrease in the weight of initial monomer. Whilst for H_2, the flow rates were determined using a bubble flow meter, for the H_2 passing through the pumping system whilst the C_6F_6 monomer was trapped in a cold trap.

The starting monomer, perfluorobenzene was purchased from Bristol Organic Ltd. and was shown to be analytically pure by mass spectroscopic g.l.c. Prior for use, the starting monomer was degassed in an auxillary vacuum line pumped with an Edwards oil diffusion pump and and two stage rotary pump by appropriate freeze-thaw cycles. Hydrogen gas was obtained from British Oxygen Corporation and was used without further purification.

3.4.3 Results and Discussion

The R.F. glow discharge plasma polymerization of perfluorobenzene has been studied previously[206] using low power inputs (1 W — 10 W) over a pressure range of 50 μ — 200 μ . Discussion of the data on the resulting polymers was largely of a qualitative nature.[206]

The work carried out in this chapter involves polymerizations carried out over a broader range of power inputs (5 W — 50 W) and pressures of 100 μ — 200 μ in two reactor configurations (A and C). A more quantitative discussion of the polymers formed is presented here.

3.4.3.1 Polymers formed in Reactor A

Figure 3.4.1 presents the C_{1s}, F_{1s} and F_{2s} levels for plasma polymers prepared at 5 different power loadings but for the same pressure of 200 μ . Considering firstly the core levels spectra, it is possible to say that over the range of powers and at a pressure of 200 μ carried out here, the core levels of the plasma polymer obtained from perfluorobenzene are remarkably similar. But small differences are noticed when detailed line shape analysis of the C_{1s} level are considered. The C_{1s} levels (Figure 3.4.1) shows that there is an increase in the intensity of the peak at binding energy ~287 eV, corresponding to the $\underline{C}\text{-}CF_n$ components, as power input increases. It has been shown from the previous studies [206] that the line shape can be straightforwardly analyzed in terms of $\underline{C}\text{-}CF_n$, $\underline{C}F$, $\underline{C}F\text{-}CF_n$, $\underline{C}F_2$ and $\underline{C}F_3$ structural features at binding energies of ~286.8 eV, 288.6 eV, 289.4 eV, 291.7 eV and 293.9 eV respectively. A small contribution at ca. 296.0 eV is assigned to a $\pi^* \leftarrow \pi$ shake-up satellite of the dominant component centred at ~ 288.6 eV indicating the presence of $=\underline{C}F$ structural features, also observed in the MATR IR studies of polymer films deposited onto HDPE. The peak at 285.0 eV is identified

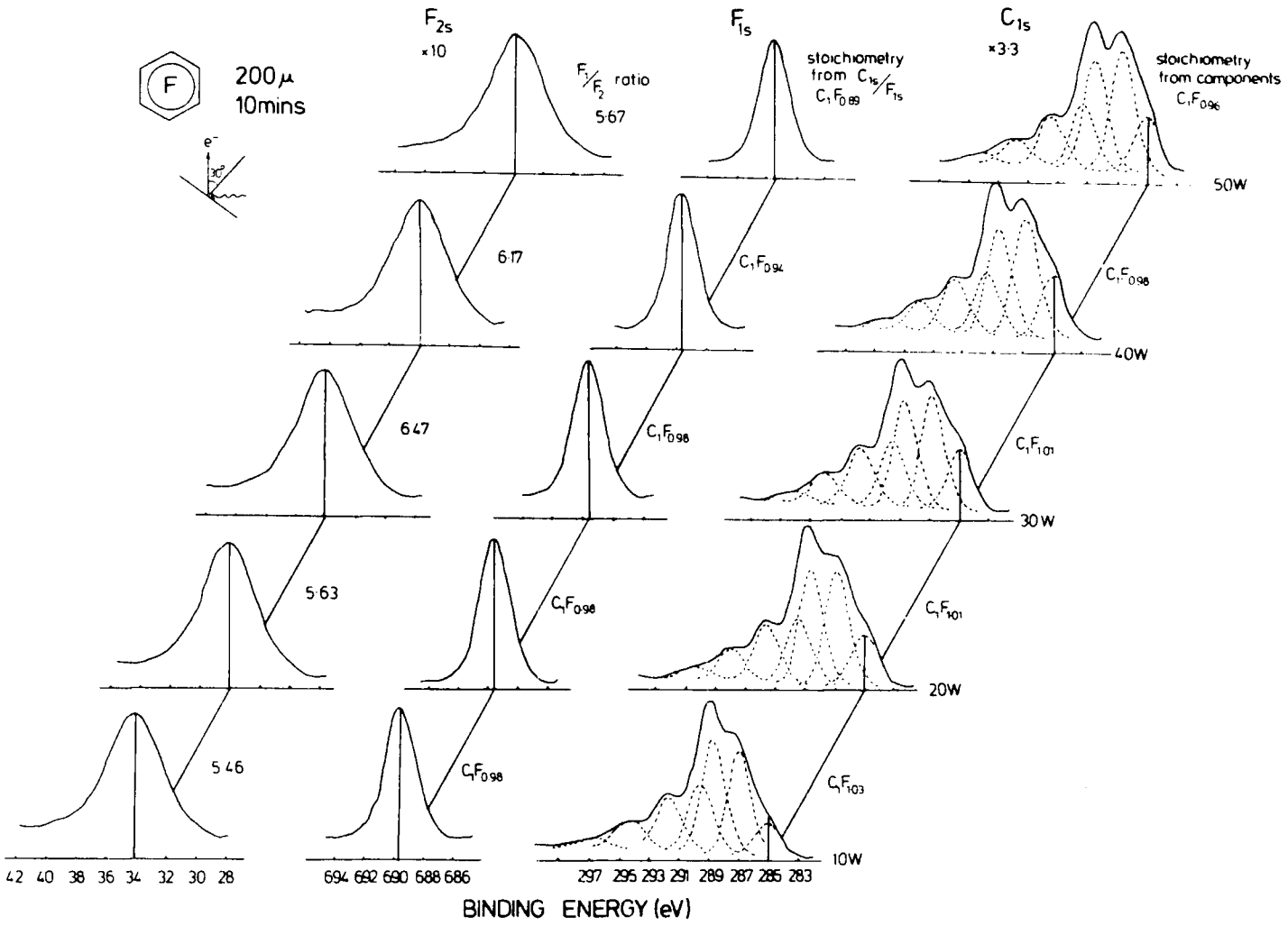

Figure 3.4.1 C_{1s}, F_{1s} and F_{2s} levels of the plasma polymer prepared in reactor A at 10, 20, 30, 40 and 50 W discharge powers and a pressure of 200 μ

from the angular dependent studies as extraneous hydrocarbon contamination. A justification for this assignment may be found in the discussion for polymers prepared in situ in a later section of this chapter.

Figure 3.4.1 also indicates the stoichiometric data for the films. The stoichiometries have been calculated by the two independent methods[207] (based on the components of the C_{1s} levels and on the relative intensities of the total C_{1s} and F_{1s} peak). In general remarkably good agreement is found between the two values. It is clear from the stoichiometric data presented that the polymer films produced in the glow regions is essentially the same as that of the starting monomer, although the core level spectra reveal evidence of extensive molecular rearrangement accompanying plasma polymerization. The data also shows the small effect that the power input has on the stoichiometry of the polymer films, although it seems that there is an increase in the C : F ratio as the power input decreases (ca. 50 W — 10 W). It is of interest to note that the previous work[206] carried out in this laboratory has also shown that the stoichiometry of polymer films produced in the glow regions is essentially the same as that of the 'monomer', with a very slight tendency to increasing C : F ratio with decreasing pressure (ca. 200 μ — 50 μ).

Considering now the F_{1s}/F_{2s} intensity ratios as indicated in Figure 3.4.1; for the polymers produced in the glow regions the relative consistency of the F_{1s}/F_{2s} ratio ca. 6.0 ± 0.4 reveals the high degree of vertical homogeneity of the samples obtained in the range of power inputs 10 W — 50 W. Microanalysis (referred to as 'bulk analysis') of the product obtained by removing the polymers deposited on the wall of the reactor indicate essentially the same stoichiometry, C : F ca. $\sim$ 1 : 1 which is consistent with the constancy of the F_{1s}/F_{2s} ratios. The F_{1s}/F_{2s} intensity ratios also indicate that the films are substantially

thicker than the effective sampling depth for both levels.

Table 3.4.1 displays data on the rate of deposition of polymers prepared in reactor A.

Table 3.4.1 Deposition rates of polymers in reactor A

C_6F_6	Pressure 200μ flow rate ∿ 3.0 $cm.^3 min.^{-1}$ (STP)				
power (W)	10	20	30	40	50
$mg.cm.^{-2} min.^{-1}$	0.027	0.035	0.042	0.045	0.038
W/FM $J.Kg.^{-1}$ ($\times 10^7$)	2.38	4.76	7.14	9.52	11.90

It is clear (from Table 3.4.1) that the rate are influenced by the W/FM parameter.[29] In this case, at a fixed flow rate ~ 3.0 $cm.^3$ min^{-1}(STP) the rate of deposition increase as the power is increased until it reaches the maximum for power input $\sim$40 W. Further increases of power (50 W), there is a decrease in the rate of deposition. This emphasizes the importance of the W/FM parameter (in this case, input power) in determining the competitive balance between polymerization and ablation. [203]

3.4.3.2 Polymers formed in situ in reactor C

Preliminary experiments were carried out on perfluorobenzene to establish a convenient range of times in order to possibly measure the attenuation of signal arising from photoemission of the gold substrate levels (Au_{4f}), thus providing a convenient means for the calculation of the initial rate of polymer deposition. In this work relative intensity changes of the $Au_{4f_{7/2}}$ level spectra using a $Mg_{K\alpha_{1,2}}$ x-ray source were

monitored to compute the rate of deposition. At this kinetic energy ($\sim$ 1170 eV) photoelectrons are assumed [177] to have a mean free path of $\sim$18.5 Å. Figure 3.4.2 shows examples of typical spectra from which the initial rates of deposition are derived. As indicated in Figure 3.4.2, at 200 μ pressure the rate of deposition is about an order greater in magnitude than at 100 μ for the same power input of 5 W. This provides clear evidence that the rates are strongly influenced by the W/FM parameter. Also indicated in Figure 3.4.2 are the stoichiometries of the polymer films derived from analysis of C_{1s} levels, these being essentially the same as the starting monomer.

The C_{1s} levels in Figure 3.4.2, were deconvoluted similarly to those for the polymers prepared in reactor A (see Figure 3.4.1). Detailed consideration of the relative intensities of the individual components of the C_{1s} levels in combination with angular dependent studies allows a relatively complete determination of structural features in the surface and subsurface of the polymer films. Reactor C was used to study the polymers deposited in situ on the spectrometer probe without exposure to atmosphere, (to avoid further reactions or contamination of the sample surface), it was therefore possible to confirm the assignment of the peak at 285 eV as being due to an extraneous hydrocarbon contamination. Figure 3.4.2 shows this evidence where at 35° take off angle the surface hydrocarbon contamination was generally not observed. But at 70° take off angle, when the samples were subjected to ESCA analysis at longer exposure times to x-radiation ($\sim$ 1 hour), the CH at 285.0 eV component is then observed. In this case the possibility of surface hydrocarbon contamination, generally submonolayer, has arisen from the x-ray cap of the spectrometer.[127] Fortunately, it provides a most convenient and accurate means of establishing a reference of binding energy for the levels being studied in this work.

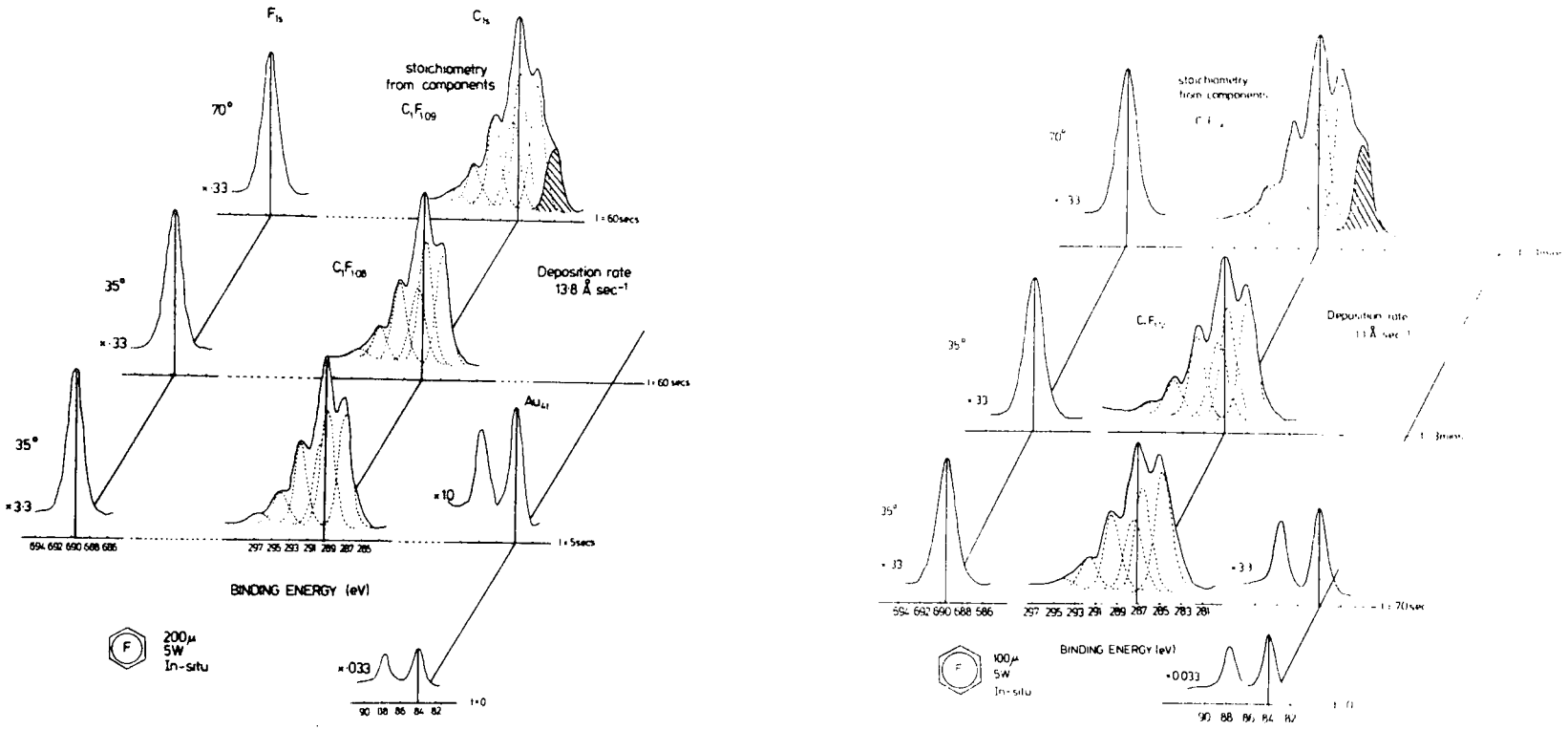

Figure 3.4.2 Au_{4f}, C_{1s} and F_{1s} levels of plasma polymerized perfluorobenzene prepared in situ

(a) at a pressure of 200 μ (b) at a pressure of 100 μ

3.4.3.3 Photon Energy Dependent Study of Polymer Films

For a variety of reasons, most of the applications in the ESCA field have employed the commonly used $Mg_{K\alpha_{1,2}}$ and $Al_{k\alpha_{1,2}}$ x-ray sources, with typical sampling depths of ~ 50 Å and ~ 90 Å respectively.† Since the facility is available for harder x-ray sources to be used, such as $Ti_{K\alpha_{1,2}}$ with photon energy of ~ 4510 eV, it is possible to sample at greater depths ~ 150 Å.[200,208] For the purpose of this preliminary investigation, the polymer films were prepared at a pressure of 200 μ and power input of 5 W for 10 minutes in the reactor A. For a comparison, ESCA spectra were recorded on a Kratos ES300 spectrometer using $Mg_{K\alpha_{1,2}}$ and $Ti_{K\alpha_{1,2}}$ photon sources, and their corresponding F_{1s} and C_{1s} core levels are shown in Figure 3.4.2, at two take off angles of 25° and 55°.

Considering firstly the C_{1s} levels studied with the $Mg_{K\alpha_{1,2}}$ x-ray source, it is apparent that the C_{1s} levels (at 5 W) resemble very closely those of the polymers prepared at higher input powers (10 W-- 50 W) for the same pressure of 200 μ . The data reveal the same, (C : F = 1 : ~ 1.0) stoichiometry.

Returning to studies of the F_{1s} and C_{1s} levels using the harder $Ti_{k\alpha}$ radiation, (see Figure 3.4.3). These studies clearly indicate the doublet nature of the exciting radiation, this is especially bourne out in the case of the F_{1s} levels, consisting as they do of intensity ratio 2 : 1 doublet with a splitting of ~ 6.0 eV. Since there are now at least 12 components which may be fitted under C_{1s} envelope, (knowing that

---

† Defined in terms of 3 λ for electrons of kinatic energy ~ 970 eV and ~ 1200 eV respectively for photoemission from C_{1s} levels where λ is the mean free path.

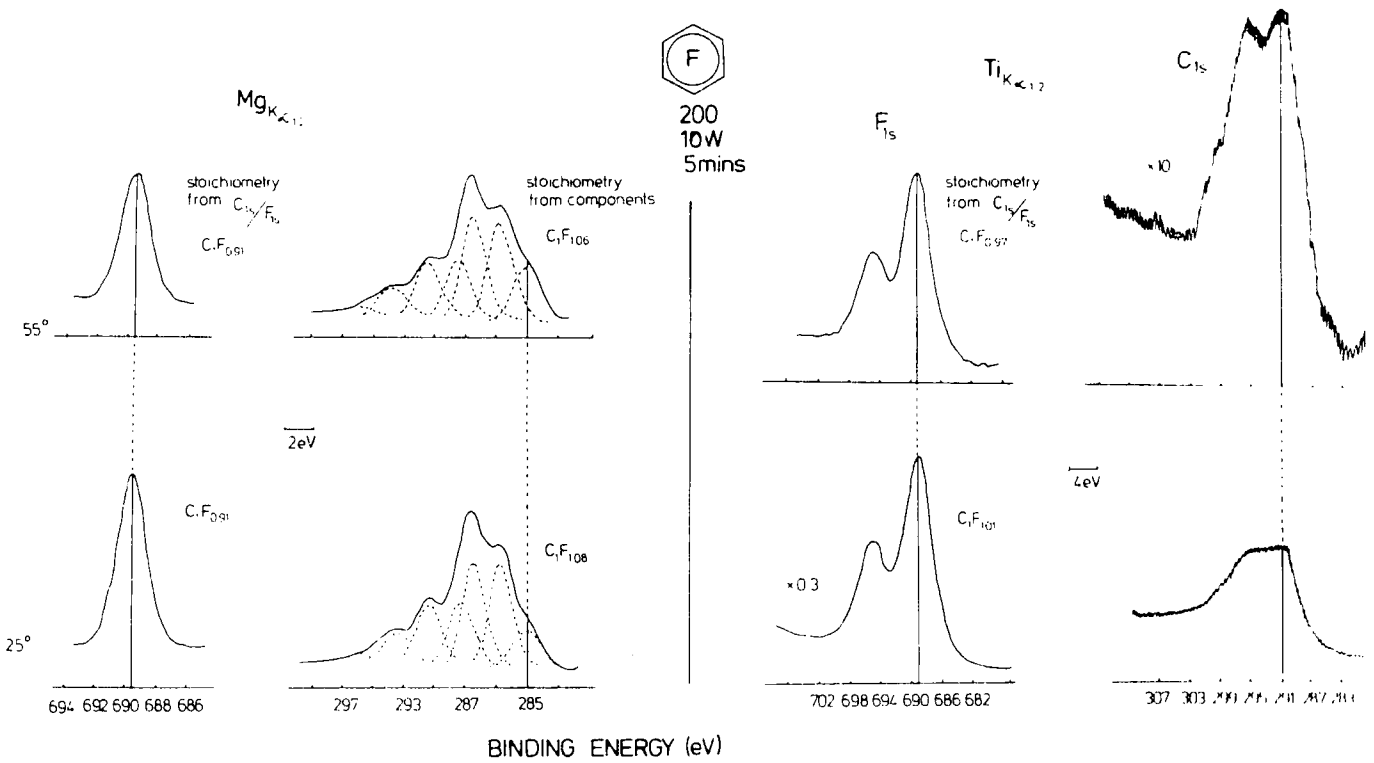

Figure 3.4.3 F_{1s} and C_{1s} levels for the plasma polymer prepared at 10 W and 200 μ

(a) spectra were obtained using photon source $Mg_{K\alpha}$

(b) spectra were obtained using photon source $Ti_{K\alpha}$

6 components can be obtained from $Mg_{K\alpha_{1,2}}$ x-ray source studies), a deconvolution of the C_{1s} core level envelope was not attempted in this case. However with a knowledge of instrumental sensitivity factors for the various core levels (C_{1s} and F_{1s} for this work) for the $Ti_{k\alpha}$ source it is possible to straightforwardly work out the stoichiometry of the polymer films. Within experimental error the stoichiometries derived from the $Ti_{K\alpha}$ and $Mg_{K\alpha}$ studies are the same $C_1F_{1.0}$. Since the sampling depths must differ quite considerably this provides evidence additional to that provided by angular dependent studies on the vertical homogeneity of the materials. It is interesting to note that low level of surface contamination evidenced from the angular dependent studies using the $Mg_{K\alpha}$ photon source is not evident from detailed line shape analysis of the $Ti_{K\alpha}$ excited spectra. This confirms the submonolayer surface coverage since the mean free paths for the $Ti_{K\alpha}$ excited spectra are such that the first monolayer contributes an insignificant proportion to the overall signal intensity and in the sampling using the higher energy x-ray source is essentially transparent. It is therefore apparent that the photon energy dependent studies can also prove an important tool in determining the vertical homogeneity of samples, when dealing with surface contaminated samples, and samples when angular dependent studies cannot be carried out, e.g. for powders and fibres.

Time dependent studies revealed no evidence for radiation damage from the harder x-ray source.

3.4.3.4 Plasma excited in Perfluorobenzene/hydrogen mixtures

(1) Introduction

It has been noted there have been relatively few systematic investigation of plasma polymerizations arising from mixtures of monomers. This contrasts with the etching field where the controlled ablation of surfaces by means of plasmas excited in various gas mixtures has been extensively studied.[209]

In this section an investigation of plasma polymers produced from perfluorobenzene/hydrogen mixtures is discussed. The main points of interest being the differences in structure and rate of deposition of polymer films compared to the pure monomer.

(2) Composition and structural features

For this studies two gas compositions have been investigated at a fixed power and pressure of 5 W and 200 μ respectively in reactor C. The corresponding core level spectra are displayed in Figure 3.4.4.

Considering firstly the H_2 : C_6F_6 gas composition of 1 : 0.7 the core level spectra bear close similarity to those displayed in Figure 3.4.1 for the pure monomer. Analysis of the relative intensities of the components provides the data in Table 3.4.2. The overall stoichiometry of C : F 1 : 0.9 indicates a small loss of fluorine for the hydrogen mixture and the component analysis reveals that this arises from a small decrease of $\underline{C}F_3$, $\underline{C}F_2$, and $\underline{C}F$ structural features and an increase of $\underline{C}$-CF structural features. The small decrease in shake-up structure shows that the polymer film has less unsaturation than that for the polymer prepared from C_6F_6. The net effect of a slight mole excess of hydrogen is therefore to modify in a subtle rather a drastic way the gross structure of the deposited plasma polymer film.

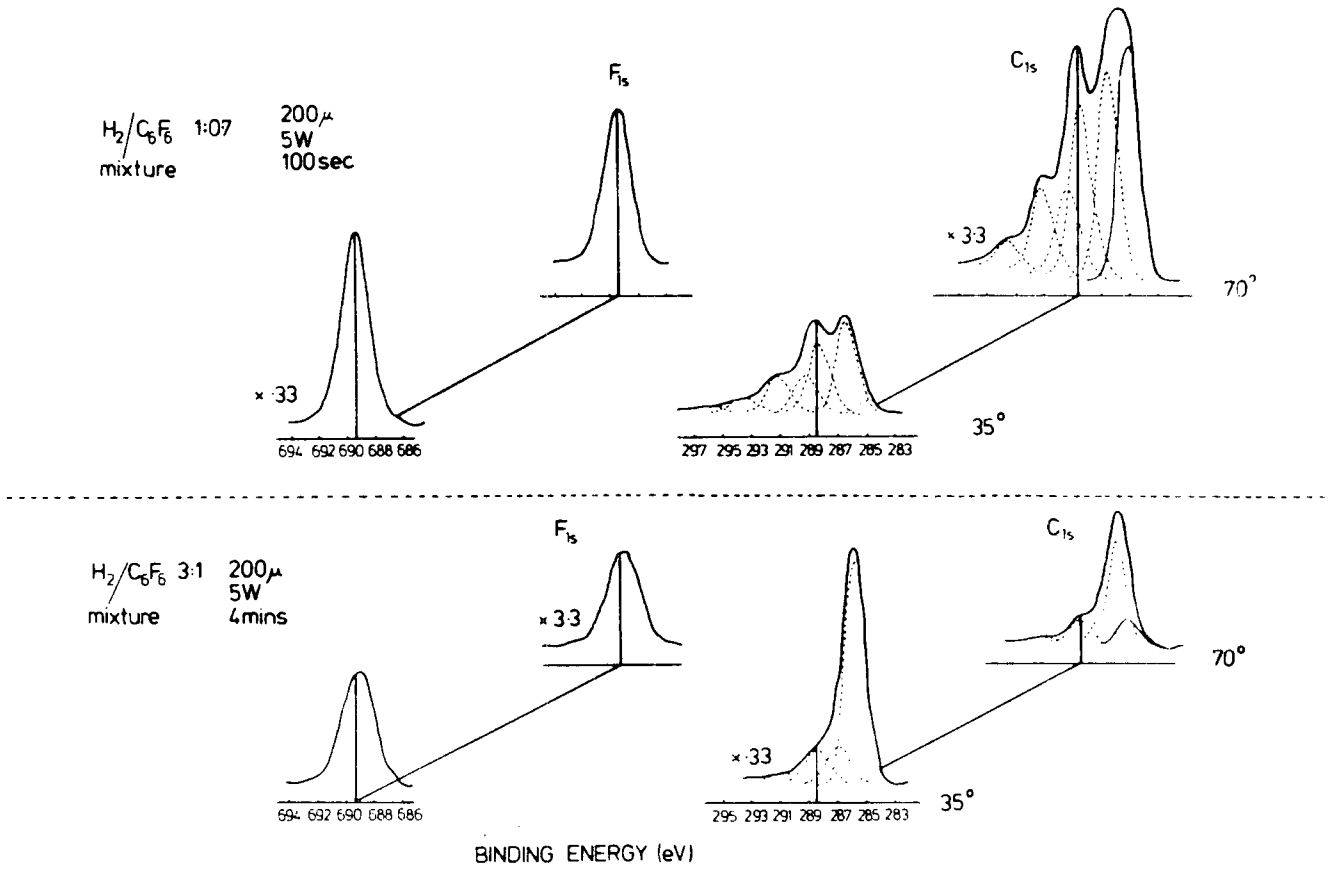

Figure 3.4.4 F_{1s} and C_{1s} spectra of plasma polymerized hydrogen/perfluorobenzene mixtures prepared in situ in reactor C at 5 W discahrge power and a pressure of 200 μ (above), 3 : 1 H_2/C_6F_6 and (below), 1 : 0.7 H_2/C_6F_6 mixtures

Table 3.4.2

Relative intensity (%) of the components of the C_{1s} levels for the plasma polymers prepared in situ in reactor C at 5 W discharge power.

Structural features (C_{1s} level)	B.E. (ev)	(%) H_2/C_6F_6 (1:0.7) 200μ	H_2/C_6F_6 (3:1) 200μ	C_6F_6 200μ	C_6F_6 100μ
$\pi \rightarrow \pi^*$	296	1	-	2	2
$\underline{C}F_3$	293.7	5.5	-	8	9
$\underline{C}F_2$	291.4	14.5	-	18	18
	290.8	-	2	-	-
$\underline{C}F\text{-}CF_n$	289.4	15.5	-	18	19
$\underline{C}F$	288.5	27.5	-	29	24
	288.2	-	13	-	
$\underline{C}\text{-}CF_n$	286.6	27.5	13	26	28
$\underline{C}\text{-}CF$	285.5	-	72	-	

Also shown in Figure 3.4.4 are spectra corresponding to the films deposited from a 3 : 1 mixture of hydrogen and perfluorobenzene. It is clear both from the overall attenuation of the F_{1s} signals and from the low intensity of the high binding energy components that the structure and composition of the film changes very substantially for around $\sim$ 4 fold change in composition of the gas mixture. The component analysis of the C_{1s} levels reveals the low level fluorine and analysis of the data provides a C : F stoichiometry of 1 : 0.2. The low level of fluorine is indicated by large descrease in $\underline{C}F_2$ and $\underline{C}F$ structural features and in consequence there is a shift to lower binding energy for both the F_{1s} levels and C_{1s} levels of a given type. This is consistent with

previous studies of highly and lightly fluorinated systems.[232] Thus the $\underline{C}F_2$ component for the polymers prepared from the two perfluorobenzene/hydrogen compositions studied here moves to lower binding energy as the fluorine composition decreases (viz. 291.4 eV for a composition of $C_1F_{0.9}$ versus 290.8 eV for a composition of $C_1F_{0.2}$. Consistent with this is the fact that the centroid of the F_{1s} levels decreases in binding energy from 689.5 eV to 689 eV. Clearly further work is necessary to delineate the exact reaction mechanism by which the hydrogen leads to elimination of fluorine however the results imply the elimination precedes the rearrangement which leads to $\underline{C}F_2$ and $\underline{C}F_3$ structural features since the activation energy for abstraction from these groups by hydrogen atoms for example is considerable.[210]

(3) Rates of Deposition

It is of interest to compare the rates of deposition of the differing plasma polymers and the relevant data are collected in Table 3.4.3. These rates have again been measured from the slope of the thickness versus time of deposition monitored from the attenuation of the Au_{4f} levels.

Table 3.4.3

Deposition rates for plasma polymers prepared in situ in reactor C

System	H_2/C_6F_6 (1:0.7; 200μ)	H_2/C_6F_6 (3:1; 200μ)	C_6F_6 (200μ)	C_6F_6 (100μ)
$\mathring{A}\ sec.^{-1}$	5.4	1.1	13.8	1.1

The raw data indicates a decrease in the rate of deposition at a constant total pressure in going from pure perfluorobenzene to the 1 : 0.7 and 3 : 1 mixtures of hydrogen and perfluorobenzene (13.8 Å $sec.^{-1}$, 5.4 Å $sec.^{-1}$ and 1.1 Å $sec.^{-1}$ respectively). If the data is reviewed however in terms of the partial pressure solely of the fluorocarbon then the effect of hydrogen ia actually to increase the rate of deposition of polymer at a given partial pressure of the monomer. Thus for the pure monomer the rate of deposition decreases as a function of pressure for a given power of 5 W an the range 200 μ -- 100 μ . For the 1 : 0.7 mixture the partial pressure of fluorocarbon is somewhat lower than for the pure monomer at 100 μ yet the rate of deposition is some 5 time higher. If a linear extrapolation is made of rate of deposition versus W/FM parameter to a partial pressure of 50 μ appropriate to the 3 : 1 H_2/C_6F_6 mixture then the observed rate of deposition is still a factor of 2 higher than that expected for the pure monomer.

The data therefore indicates that both the structure of the polymer and the rate of deposition can be substantiallly modified by inclusion of a further reactive monomer in the gas input to the plasma. It is interesting to note that although the ionization potential and excited states for hydrogen are substantially to higher energy than for the perfluorobenzene a small change in the hydrogen composition produced a substantial change in the structure of the polymer and the mechanism by which this occurs is clearly worthy of further attention.

CHAPTER FOUR

CHAPTER FOUR: PLASMA POLYMERIZATION II. A SYSTEMATIC INVESTIGATION OF THE INDUCTIVELY COUPLED R.F. GLOW DISCHARGE POLYMERIZATION OF PENTAFLUOROBENZENE

Abstract

The composition and gross structural features of plasma polymer films prepared by inductively R.F. plasmas excited in pentafluorobenzene have been investigated by means of ESCA as a function of the operating parameters. The rate of film deposition is shown to be dependent on the W/FM parameter and on site of deposition. The polymer formed in the glow region shows only small variations in structure as a function of power and pressure. Polymer films deposited in the regions away from the site of primary excitation typically have a higher fluorine content than for those formed in the coil region, the stoichiometry for the latter being comparable with that of the starting monomer.

4.1 Introduction

In this chapter a detailed ESCA investigation of polymer films produced by excitation of inductively coupled R.F. plasmas in pentafluorobenzene is described. Since there have been no previous investigations of the plasma polymers produced from fluorinated benzene monomers other than perfluorobenzene,[206] the study of the pentafluorobenzene system is of particular interest and forms the subject of this chapter. It is important to note that a systematic study on a series of related molecules (fluorobenzenes) is greatly needed to provide a basis for the more quantitative discussion of mechanism of formation of the plasma polymers. Such studies will also be discussed in detailed in the next two chapters.

The nature of glow discharge polymerization in a flow system as conventionally employed is likely to be exceedingly complex with both the structure of the resulting polymeric films and their rates of deposition dependent on the 'monomer' as well as on flow rate, power input and geometric factors associated with the given instrumental set up. Therefore a simple prototype system, pentafluorobenzene is considered in order to systematically investigate some of the features of interest in glow discharge polymerization. These can be summarized as follows:-

(a) The composition and structure of the polymer produced as a function of power and pressure at a given flow rate.

(b) The rate of deposition and structure of the polymer as a function of position in a reactor with respect to the exciting coil in an inductively coupled R.F. plasma.

4.2 Experimental

Since the prime emphasis in this work is to establish the capability of ESCA as a spectroscopic tool for elaborating the features of interest as outlined above, the study presented here entailed plasma polymerized pentafluorobenzene investigated in three reactor configurations, at a variety of input powers, pressures and flow rates and employing inductively coupled R.F. plasmas. The range of flow rates, powers and pressures employed, in the event turned out to provide convenient deposition rates for the polymer produced in the plasmas.

The three reactor configurations employed are shown schematically in Figure 4.2.1. Reactor A and B were used to produce polymer films which were subsequently transferred in air to the ESCA instrumentation for study. Reactor C however provided a capability for in situ deposition and transfer directly into the spectrometer chamber for analysis without the polymer sample being exposed to atmosphere, and was described in detail in the experimental section in the previous Chapter Three.

An obvious advantage in this work is the ability to study samples without exposure to atmosphere (reactor C) for direct comparison with those produced in reactor configurations A and B, since in a glow discharge, polymers often contain trapped radical sites.[203]

Reactor A (Figure 4.2.1) was identical to that described in the previous Chapter Three. Thin films of polymer were collected by depositing onto gold substrates, located on glass slides (3" x $\frac{1}{2}$") mounted along the bottom of the reactor in the centre of the coil. Deposition in this case was therefore somewhat below the centre line axis of the reactor.

Reactor B was specifically constructed to enable the direct investigation of the structure of the polymer and rate of deposition as

A) Short reactor

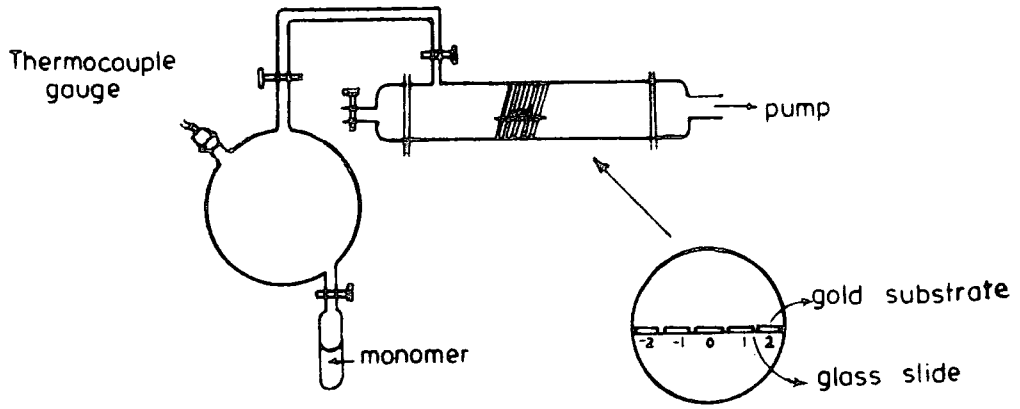

B) Long reactor

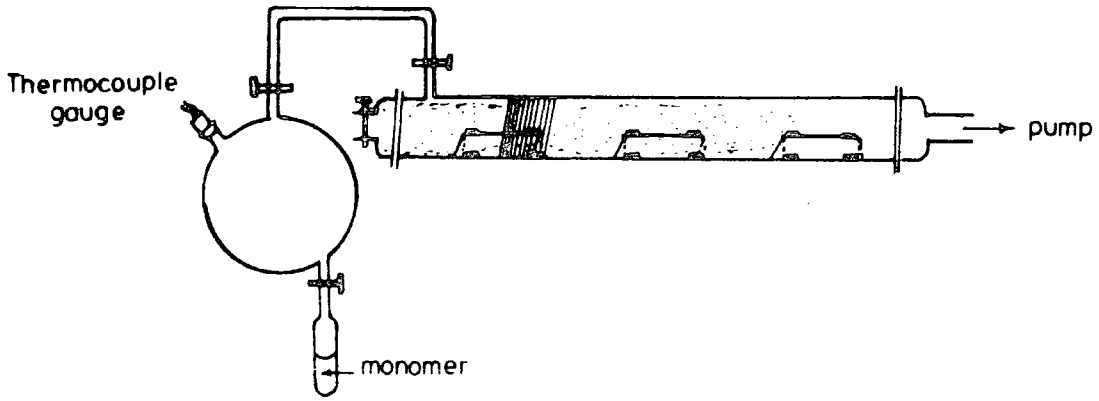

C) In-situ

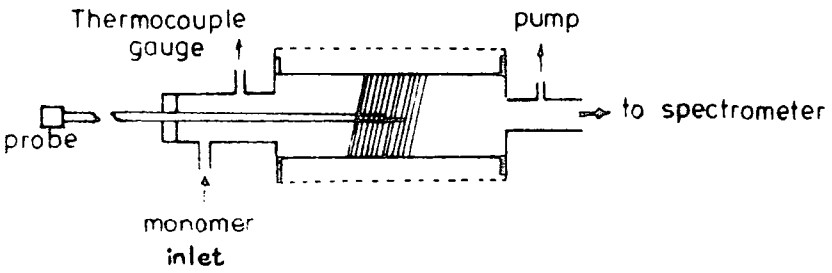

Figure 4.2.1 Schematic of the reactor configurations used in this study. (These are not to scale.)

a function of position in the reactor, both with respect to the coil region along the axis and with respect to the centre line axis and the reactor wall. Reactor B (Figure 4.2.1.) consisted of a 100 cm. long end flanged pyrex glass tube, 5 cm. in diameter. Polymer films were deposited on gold substrates at different sites located along the reactor 10, 25, 45, 60, 80 and 95 cm. from the end of the reactor as indicated in Figure 4.2.1. In this study, two different locations of gold substrates were employed to collect the polymer sample either at the wall along the bottom or along the centre line as indicated in Figure 4.2.1. The gold substrates placed along the axis of this reactor were supported by three small frames made from silica glass.

Each of the systems (reactor A and B) was pumped by an Edwards ED 50, 50 l. min.$^{-1}$ two stage rotary pump via a grease free vacuum line including two cold traps. As in the Chapter Three and for all cases, plasma were excited using a Tegal Corporation R.F. generator operating at 13.56 MHz. and associated matching network. The standing wave ratio was measured by means of a Heathkit HM 102 RF power meter. Pressure measurements for reactor A and B were made with a Pirani thermocouple gauge.

The gold substrates, (grade 2, sheet 0.3 mm. thick, Johnson Matthey, London), were cut to a convenient size for direct mounting on the probe tip of the ESCA spectrometer. All the substrates were cleaned by heating in a flame and by a discharge in O_2 then finally in Argon prior to use.

The matching network settings were optimized using the appropriate monomer at the requisite power and pressure. The matching network remained untouched for the remainder of the experiment. The

system was purged for ca. five minutes with monomer to obtain a constant flow rate before starting the actual polymerization.

Core levels spectra were recorded on an AEI ES200 AA/B spectrometer using $Mg_{k\alpha_{1,2}}$ x-radiation. The measurement of the ESCA spectra, the MATR IR studies and the microanalysis determination were as previously described in the Chapter Three.

Density measurements were performed by the floatation method using a binary solvent mixture made up from perfluorobenzene and perfluoro(methyl)cyclohexane.

For reactor A and B the degassed sample of pentafluorobenzene was attached by means of 'Cajon Ultra Torr Coupling' and $\frac{1}{2}$" OD tubing to a ballast reservoir bulb $\backsim$ 3 l. in volume. Calibration of the thermocouple gauge attached to the reservoir provided a direct measurement of the pressure of the monomer entering the reactor by means of a grease free valved inlet system indicated schematically in Figure 4.2.1. By monitoring the liquid monomer and bulb at an appropriate temperature the desired flow rates could be achieved at a given pressure without changing the pumping configuration.

Flow rates were measured by monitoring the rate of change of pressure as a function of time for the relevant closed system immediately after the monomer inlet was valved off.

For small reactor C the sample was directly vapourized into the inlet tube to the reactor, and flow rate were then measure as a function of initial rate of increase of pressure when the pumping line was valved off to the reactor whilst still connected to the monomer inlet.

The starting material pentafluorobenzene was obtained from

Bristol Organics Ltd. and was shown to be analytically pure by mass spectroscopy g.l.c.

4.3 Result and Discussion

Previous studies[52,177,212] have shown how ESCA may be used to establish the main features of structure and bonding with polymeric films in general and plasma polymer films in particular. The information levels which are of importance in this endeavour are as follows:-

(a) The relative overall intensity ratio of F_{1s} to C_{1s} levels in fluoropolymer films may be used to derived stoichiometry once sensitivity factors for the particular instrumental configuration have been established.

(b) An analysis of the overall C_{1s} line profiles with component peaks corresponding to distinctive structural features (CF_3 groups) etc. assigned by reference to previous studies of model systems also allows an independent determination of stoichiometry and and also provides information on the structural features present.

(c) Angular dependent studies in which data are recorded as a function of electron take off angle with respect to the normal to the sample surface, coupled with investigations of intensity ratios for photoemission from different levels of the same element (e.g. F_{1s} and F_{2s}) provides direct information on the vertical homogeneity of the polymer films. With $Mg_{K\alpha_{1,2}}$ photon source ($h\nu$ = 1253.7 eV) the typical sampling depth for levels of interest (3 x typical mean free paths) are F_{1s} ~ 25 Å, C_{1s} ~ 45 Å, F_{2s} ~ 90 Å [177]

(d) Monitoring of O_{1s} and C_{1s} core levels at 285 eV (C̲H) provides direct information on the low level of extraneous surface contamination of films prepared in reactor A and B and subsequently transferred to the spectrometer. Whilst for samples prepared in situ, the hydrocarbon contamination is a function of time exposed to x-ray irradiation ($\sim$ an hour) from extraneous hydrocarbon in the sample chamber of the spectrometer originating from the diffusion pump oil.[127]

(e) By monitoring substrate (Au_{4f}) and overlayer (F_{1s}, C_{1s}) core levels ESCA can be used to study the important phase of the initial rate of deposition of polymer.

It is convenient in discussing the data to consider the following points in a logical sequence;

(i) The nature of the fluoropolymer produced in the glow region in reactor A as a function of power (0 - 30 Watts) and pressure (100 - 200 μ) for flow rates in the range 0.68 - 3.04 $cm.^3$ $min.^{-1}$ (STP) and as function of cross sectional position of the substrate as illustrated in Figure 4.2.1.

(ii) The structure of the polymer deposited in situ on the spectrometer probe tip (reactor C) and its initial rate of deposition.

(iii) The structure of the polymer as a function of site of deposition in reactor B as a function of power and pressure.

Although ESCA has previously been employed on some aspects of comparable investigations, the work in this chapter represents the first systematic study of the important points covered under headings (i) - (iii) which form a necessary prerequisite to a more complete understanding of glow discharge polymerization.

4.3.1 The Gross Chemical Structure of Fluoropolymer Deposited in the Glow Regions

As previously noted in Chapter Three the distinctive, essentially additive nature, of substituent effects on C_{1s} core binding energy levels in fluoropolymers makes the analysis of complex lineshapes a relatively straightforward matter and this is illustrated in Figure 4.3.1.

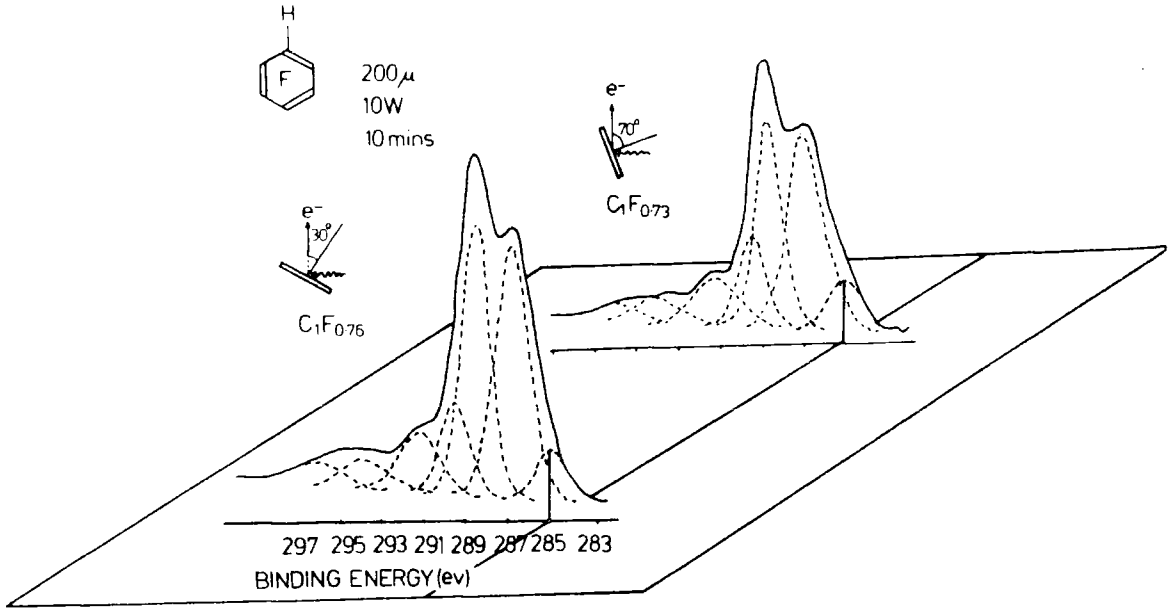

Figure 4.3.1 C_{1s} levels of plasma polymer prepared at 10 W discharge power and pressure of 200 μ for 10 minutes in reactor A

The C_{1s} levels for the fluoropolymer deposited on a gold substrate located on axis at the centre of the coil in reactor A may be analyzed in terms of seven components with well defined FWHM and peak shapes. The spectra recorded at two different take off angles are essentially the same, the only difference being a small increase in

relative intensity† of the component at low binding energy 285 eV (C̲H) which identifies this as a low level of extraneous hydrocarbon contamination at the very surface. The intensity shows that this corresponds to a fraction of a monolayer coverage and this is not unreasonable since the sample have to be removed from the reactor to be transported to the spectrometer for the ESCA investigation. In increasing binding energy the components may be assigned as C̲-CF, (viz. carbons not bearing fluorine but with an adjacent CF group), C̲F, C̲F-CF_n, C̲F_2 and C̲F_3 structural features. The component at a very high binding energy ~296 eV is too high in energy to be associated with a direct photoionization peak and corresponds to a $\pi^* \leftarrow \pi$ shake up satellite of the dominant component centred at ~ 288.4 eV indicating the presence of =C-F structural features. (A shake up energy of ~7 eV is predicted for such transitions on the basis of previous studies on model systems.)[117] The angular dependence indicates the uniformity of the films in terms of vertical homogeneity and the C:F stoichiometry derived from the analysis of the C_{1s} components of 1:0.76 (30°) and 1:0.73 (70°) confirms this. (The error limits based on the line shape analysis are probably ± 5% so that the stoichiometries are within experimental error - the same and correspond quite closely to the fluorine content of the starting material, C:F 1:0.83).

The spectra closely reveal evidence, for extensive molecular rearrangement accompanying polymerization. The shake-up

---

† It should be noted that the convolution of factors contributing to the measured absolute intensities are such that count rates for the higher take off angle are substantially lower.

intensity although small in absolute magnitude is an appreciable percentage (~6%) of the corresponding direct photoionization peak CF centred ~ 288 eV. This suggest a substantial contribution of conjugated systems to the overall structure for the polymer deposited under these conditions. Indeed films show significant absorption in the UV. For example deposition of films over a period of 1 minute at 200 μ with a power input of 5 W produces a sufficiently thick film for direct recording of the UV spectrum and the broad longer wavelength band is centred at ~270 nm. compared to about 260 nm. for the free monomer studied in the solution phase, (see Figure 4.3.2). MATR IR spectra of films ~ 0.2 μ thick on the HDPE substrate (~100μ) confirm the presence of CF structural features, the main absorption being a broad band between 1400 and 900 $cm.^{-1}$

Figure 4.3.2 UV transmission for plasma polymerized pentafluorobenzene

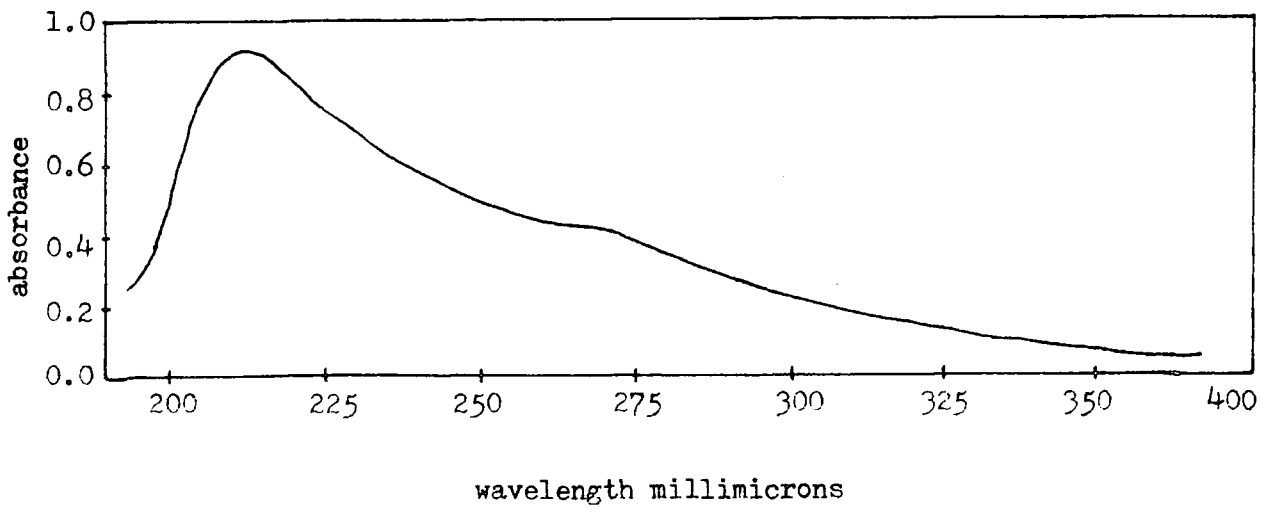

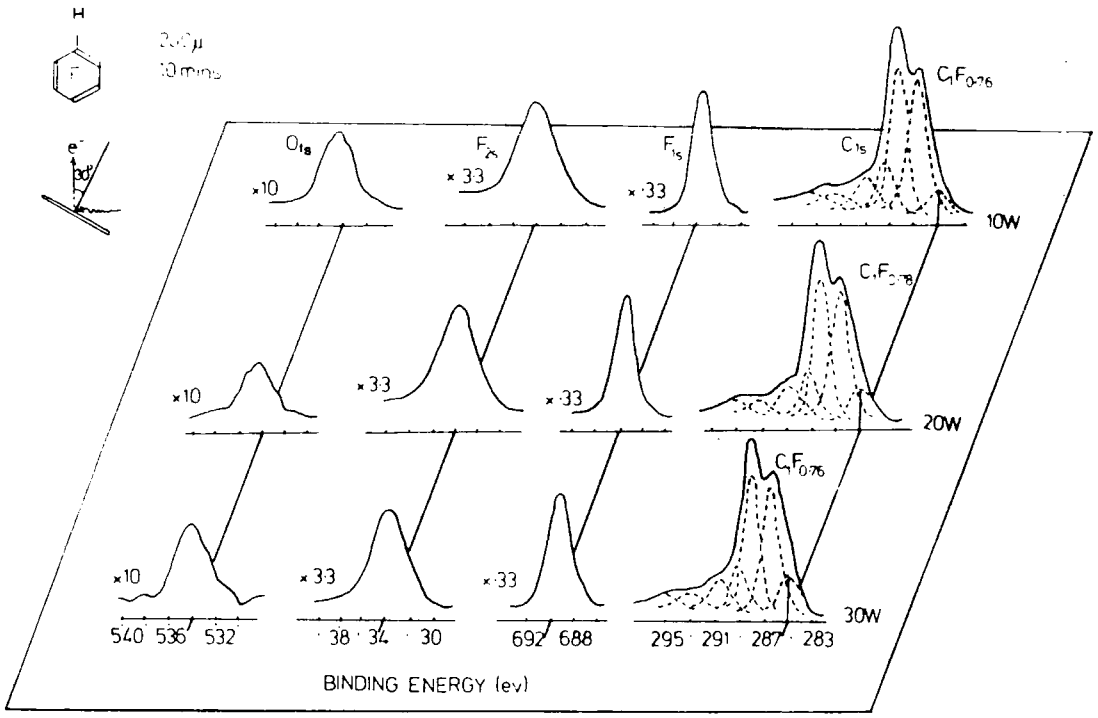

Figure 4.3.3 C_{1s}, F_{1s}, F_{2s} and O_{1s} spectra of the plasma polymer prepared in reactor A at 200 μ and three discharge powers

The gross chemical composition and structural features of fluoropolymers deposited in the glow region have been investigated at different flow rates and input powers, and the results for fluoropolymers deposited in the centre of the glow region at an input pressure of 200 μ and power inputs of 10, 20, 30 W are displayed in the Figure 4.3.3 above. In each case a low level signal is observed for the levels O_{1s} and this certainly arises for the most part from reactions in the surface regions on exposure of the sample to the atmosphere subsequent to preparation. As will become clear, samples deposited and studied in situ in reactor C exhibited much lower levels of O_{1s} signal.

To put matters in perspective the angular dependent studies show that the oxygen functionalities are primarily at the sample surface and with instrumentally determined sensitivity factors the stoichiometry

corresponds typically to one oxygen for every 50 carbons. The tendency for slightly higher oxygen contamination to be associated with higher power input also perhaps suggests the ablation of oxygen containing species from the reactor walls may be of some importance.

The component analysis of Figure 4.3.3 suggests that the basic structure of the polymer is constant within experimental error at a given pressure (200 μ) over the range of power inputs employed 10 - 30 W.

The rate of deposition of fluoropolymer was such that in the power range 10 - 30 W. at an inlet pressure 200 μ a sufficient thickness of films was deposited to enable microgram quantities to be collected for microanalysis and density measurement. (Typical deposition rate $\sim$ 20 $\mathring{A}.s.^{-1}$ at 200 μ and 5 W.)

The F_{1s}/F_{2s} intensity ratios may be used to independently establish the vertical homogeneity of the samples as has previously been described;[201] whilst the C_{1s} : F_{1s} ratio provides an independent means of establishing the overall stoichiometry. The difficulty of accurately obtained stoichiometries of fluoropolymers by means of combustion analysis and by potassium fusion are well known to microanalysts. The difficulty is compounded in analyzing small quantities scraped from thin films deposited onto glass substrates since it is inevitable that contamination will occur arising from removal of non-polymeric material at the interface. The stoichiometries derived from analysis of the C_{1s} components indicated in Figure 4.3.3 may be compared with those derived from microanalysis the value being C:F, 1:0.72, 1:0.72, 1:0.71, for 30, 20 and 10 W. depositions respectively. The differences are small and the microanalysis seems to slightly underestimate the fluorine content. The error limits are such that the two independent methods of elaborating stoichiometries by means of ESCA (viz. from the components of the C_{1s} levels and from the C_{1s} : F_{1s}

intensity ratios) are to be regarded as closely similar (viz. C : F stoichiometry of ~0.8 in each cases). The results indicate a stoichiometry close to that of the starting monomer with no strong dependence on the power input over the range studied. The overall C_{1s} band profiles and the derived components reinforce this conclusion.

The low hydrogen content of both the starting monomer and almost certainly the fluoropolymer makes the establishment of stoichiometry with respect to hydrogen difficult to determine by microanalysis. (Hydrogen content of monomer 0.20%, from combustion analysis compared with the theoretical value of 0.67, error limit for a relatively highly fluorinated sample being ±0.5% for hydrogen.) For the fluoropolymer films hydrogen was not detected by microanalysis, however, the error limits noted above are such that a low hydrogen content cannot be entirely ruled out. The density of 1.80 as measured by the floatation method may be compared with the density of conventional fluoropolymers e.g. PTFE 2.28,[213] PVF_2 1.74 and PVF 1.34. The density is therefore somewhat higher that for the PVF_2 linear homopolymer of somewhat greater fluorine content and this is consistent with a crosslinked structure.

The components of the C_{1s} levels as a function of power and pressure are shown in Figure 4.3.4. For a given initial pressure the components do not show a strong dependence on power and a comparison with data for in situ deposition (reactor C) at a much lower power input (1 and 5 W.) at the same pressure indicates that essentially the same polymer is deposited at a given pressure over a power range from 1 - 30 W. The qualification must be made in this respect is that flow rate, flow patterns and power densities will not be comparable in different reactor configurations.

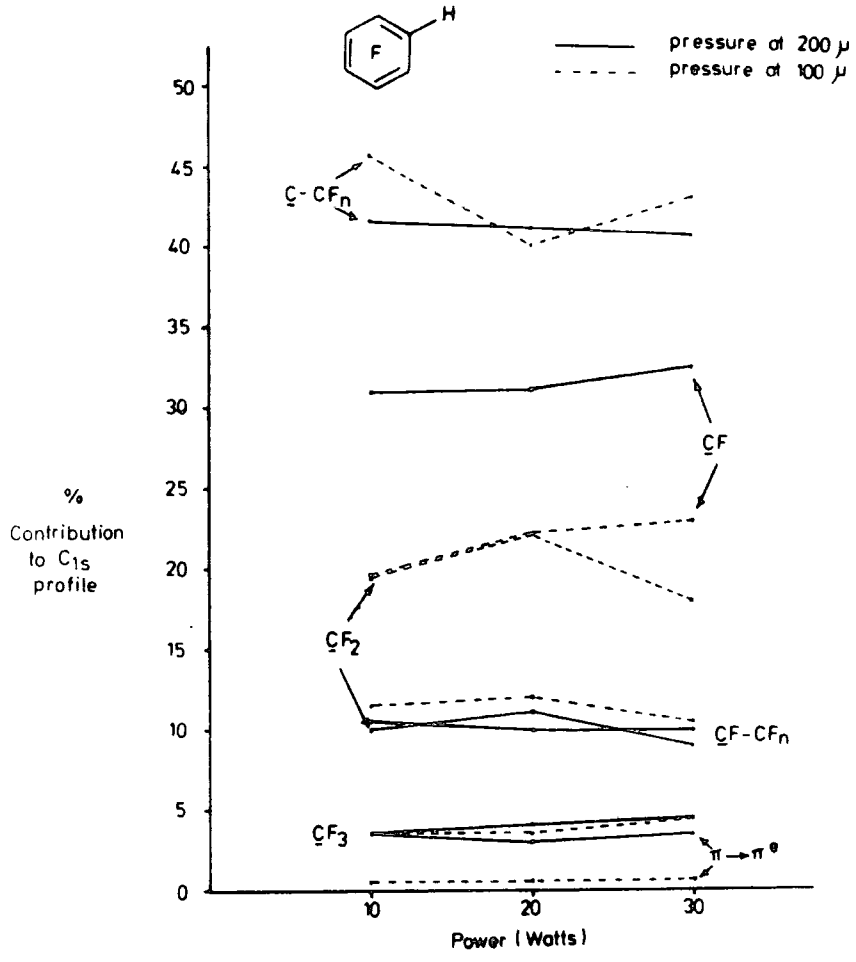

Figure 4.3.4 Percentage contribution to C_{1s} envelope for various structural features in the plasma polymers prepared in reactor A

The CF_3 and CF_2 structural features typically constitute ~15% of the C_{1s} band profile and in keeping with this the surface has a low surface energy isevidenced by contact angle measurements. For example sessile drops exhibited contact angles of 92°, 82°, 74°, 50° and 14° with water, glycerol, formamide, methylene iodide and n-hexadecane respectively. Analysis of this data provides a critical surface tension of ~27.5 dyne $cm.^{-1}$ For comparison purposes the corresponding figures for typical linear fluoropolymer systems are 31, 28, 25, 18.5 dyne $cm.^{-1}$ of polyethylene (PE), poly(vinyl fluoride) (PVF), poly(vinylidene fluoride) (PVF_2) and polytetrafluoroetylene (PTFE), respectively.[64] For comparison purposes it is interesting to note that for plasma polymers produced from

perfluorobenzene the CF_3 and CF_2 structural features constitute ~25% of the C_{1s} profile whilst for perfluorocyclohexane the corresponding figure is 55%. As previously discussed[206] the glow discharge polymerization of perfluorobenzene and perfluorocyclohexane small differences in overall band profiles were noted as a function of pressure. The data in Figure 4.3.4 reveal that for pentafluorobenzene plasma polymers with greater $\underline{C}F_2$ components and lesser $\underline{C}F$ are produced at lower pressure. In consequence the shake-up intensity decreases at lower pressure. The main feature evident from the C_{1s} band profile (which remains essentially constant as a function of power input) is the general smearing out effect associated with a decreasing $\underline{C}F$ component with concomitant increase in $\underline{C}F_2$ component. The overall stoichiometry is slightly higher for the fluoropolymer produced at lower pressure (av. ~0.84 at 100 μ compared with 0.76 at 200 μ). The spectra therefore suggest that greater molecular rearrangement takes place at lower pressure and this may be associated with the greater mean free path and somewhat higher mean energy of the electrons.

4.3.2 Fluoropolymer Deposition as a Function of Position in the Glow Region.

Having established the gross chemical structure and composition of fluoropolymer films deposited in the coil (but not on the centre line axis), considering now the structure as a function of site of deposition in the glow region. Figure 4.2.1 shows reactor configuration A with the provision of deposition sites on the centre line axis of the coil in a horizontal plane. For sites 2 and -2 the deposition region is close to the walls and it might be anticipated that the flow pattern would be somewhat different than for position 0 at the centre of the cylindrical reactor. Experiments have therefore been carried out to investigate the

gross features of the chemical structure of fluoropolymer films deposited in horizontal plane. The experiments were carried out with an initial monomer pressure of 200 μ and 5 W input power (deposition time 5 minutes) and the C_{1s} spectra for the films deposited on gold substrates are displayed in Figure 4.3.5 below.

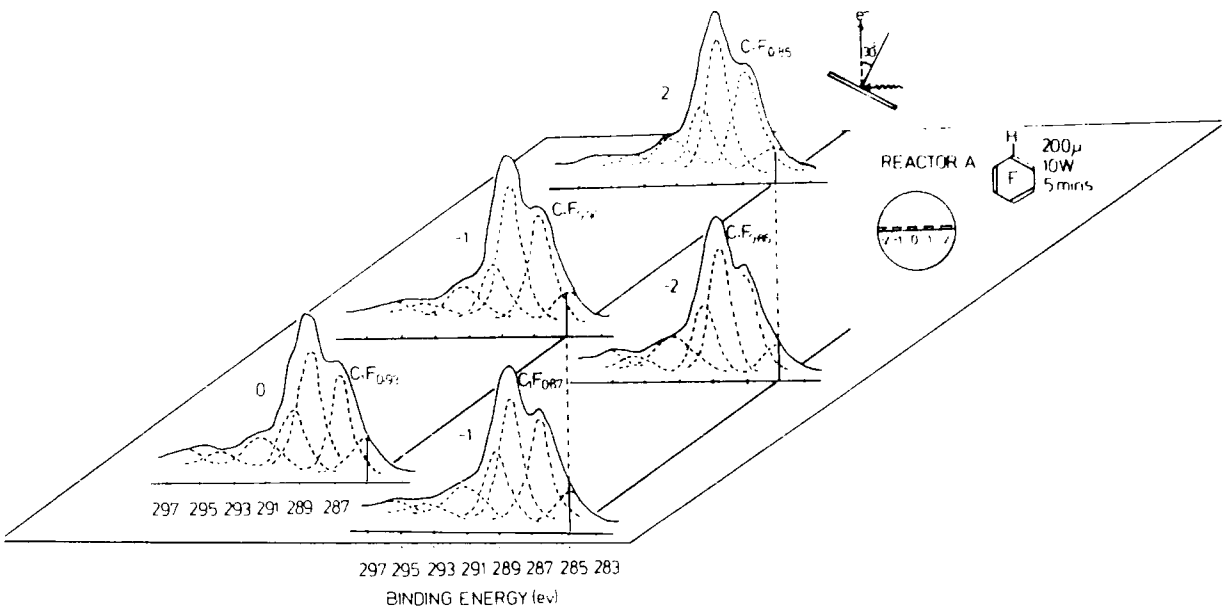

Figure 4.3.5 C_{1s} spectra for plasma polymers from five deposition sites

It is clear from a cursory comparison of the overall band profiles that the component contributions from the various structural features are very similar for all sites of deposition. The overall signal intensities are also very similar indicating that in all cases the film thicknesses are very much greater than the typical mean free paths for photoemitted electrons.

The analysis of the component peaks of the C_{1s} levels is detailed in Figure 4.3.6. The salient feature may be summarized as follows:- (a) The spectra bear a marked resemblance to those displayed

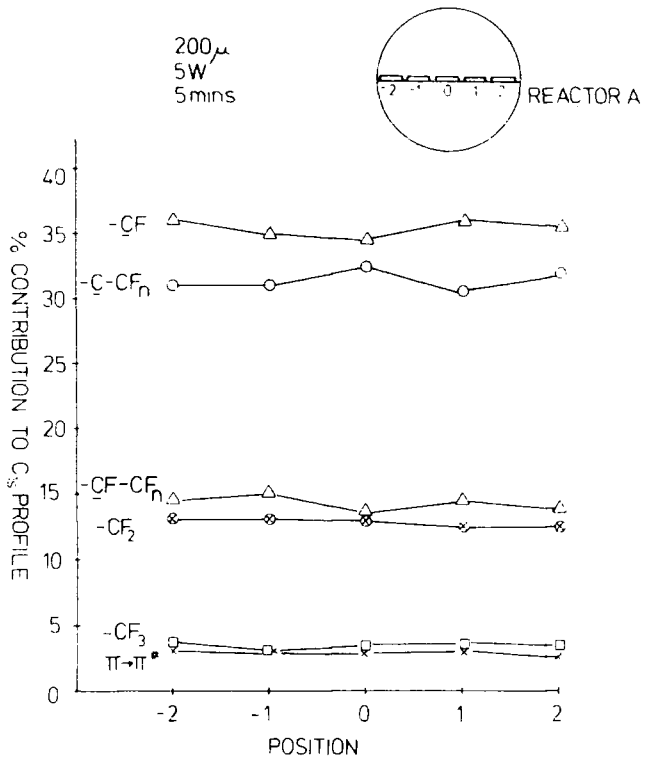

Figure 4.3.6 Percentage contribution to C_{1s} envelope for structural features in the plasma polymer from five deposition sites.

in Figure 4.3.3, however the somewhat lower power and difference deposition site leads to a small but significant difference in overall band profile. The main difference is associated with an increase in $\underline{C}F\text{-}CF_n$ groups and a decrease in $\underline{C}\text{-}CF_n$ groups, the shake-up intensities, $\underline{C}F_3$, $\underline{C}F_2$ components being closely similar to those detailed above. The next effect is the overall fluorine content is very slightly higher for the samples deposited near the centre of the reactor. (The site of deposition for the samples pertaining to the spectra in Figure 4.3.3 was vertically beneath the centre line horizontal plane at a distance somewhat between that appropriate to deposition sites 1 (=1) and 2 (=2). These results suggest that there are subtle differences in overall structure of fluoropolymer films deposited within the glow region with films closer to the centre line axis having

C : F stoichiometry slightly greater than for the pentafluorobenzene 'monomer' whilst off axis the stoichiometry tends to be same or even slightly lower than for the monomer.

To summarize it is clear that over a range of power inputs and sites of deposition within the glow region the gross chemical composition and structural features evidenced by ESCA data show subtle rather than dramatic differences. Plasma polymers deposited at lower pressures for a given power input show distinctive differences in structural features but the overall stoichiometry remains closely similar to fluoropolymer films produced at higher pressure. With this background an investigation of the in situ deposition of films in reactor C and ESCA determination of initial rates of deposition was continued.

4.3.3 In situ Deposition and ESCA Determination of Initial Rates of Deposition

Previous papers[201,213] have described a plasma reactor configuration which may readily be interfaced to the ESCA spectrometer, enabling to be deposited in situ on the spectrometer probe without exposure to atmosphere. The flow rates employing this reactor configuration are significantly lower than for reactor configuration A and B. Thus for plasma initiated at 200μ the flow rates ($cm.^3$ $min.^{-1}$ STP) were 3.0, 3.2 and 0.7 for reactor configuration A, B and C respectively. By using lower power inputs in the range 1 - 5 W. and pressure 100, 200 and 500μ it is possible to cover a substantial range in the (W/FM) operational parameter as defined by Yasuda[29] At the lower end of value of 4×10^6 J Kg^{-1}

(500 μ , 1 W.) was employed in reactor configuration C extending to 1.3×10^{8} J Kg^{-1} for the same reactor configuration at lower pressure and higher power (100 μ , 5 W.) For comparison purposes the lower and upper ranges for reactor configurations A and B were 2.6×10^{7} J Kg^{-1} (200 μ , 10 W) and 3.5×10^{8} J Kg^{-1} (100 μ , 30 W. reactor A) and 2.1×10^{8} J Kg^{-1} (100 μ , 25 W. reactor B).

Previous investigation have obtained mean free paths for electrons of a given kinetic energy for fluoro plasma polymer films and it therefore becomes a straightforward matter to monitor the attenuation of the substrate signal to obtain estimates of film thickness in the range 0 - 100 Å encompassing the initial stages of deposition.[177] Before considering this however, it is of interest to note that the ESCA spectra for fluoropolymer film deposited on axis on the probe tip in reactor C is entirely consistent with the data for the longer reactor configuration A described above. Figure 4.3.7 for example shows the core level spectra

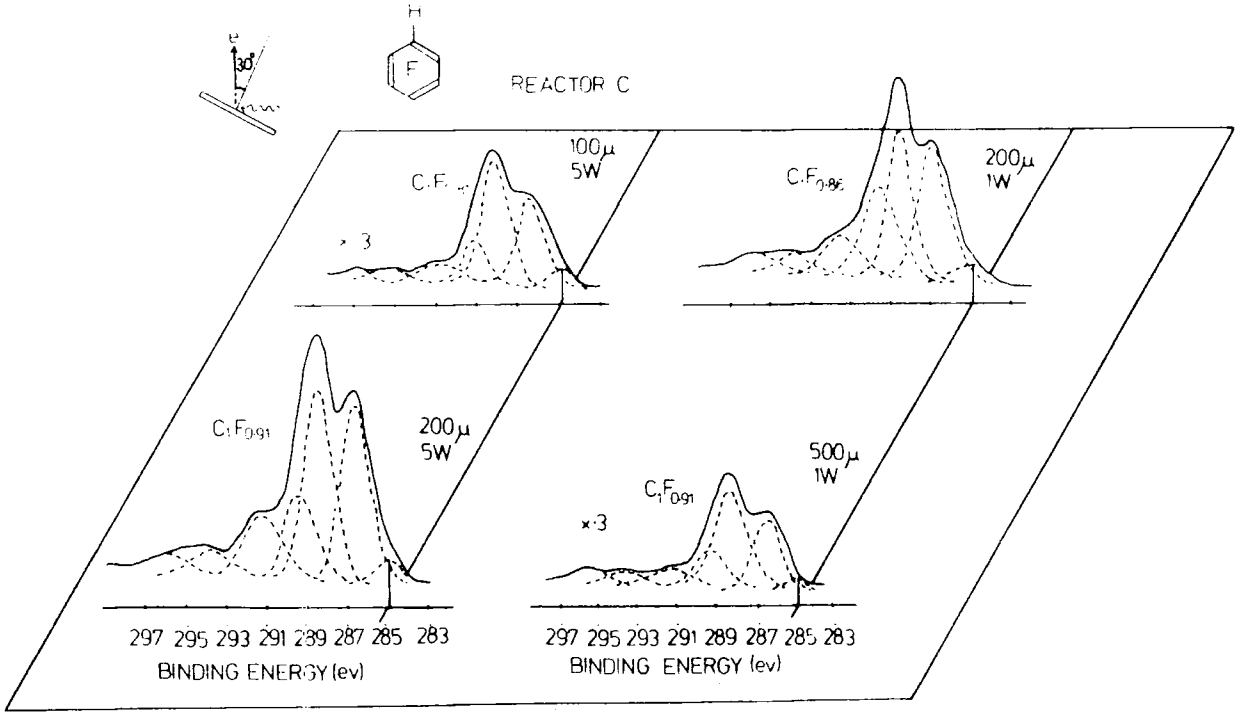

Figure 4.3.7 C_{1s} spectra for plasma polymer prepared in situ

and component analysis for a variety of powers and pressures for films deposited in situ. The distinctive feature compared with the previous spectra is a very low level of hydrogen contamination of the surface for the in situ deposition. It should perhaps re-emphasized therefore that even for depositions in the free standing reactor configuration and subsequent transfer to the spectrometer the hydrocarbon contamination is at the sub-monolayer level.

The basic philosophy in obtaining initial deposition rates by means of ESCA is illustrated by the data in Figure 4.3.8. The plasma polymers were deposited onto flamed gold substrates and the intense Au_{4f} levels were employed as monitors of film thickness. At the kinetic energy corresponding to photoemission of the Au_{4f} electron with a $Mg_{K\alpha_{1,2}}$ target ~1170 eV the mean free path in the fluoropolymer film is ~18.5 Å and the attenuation of the signal as fluoropolymer film is deposited is readily apparent from the data. It is interesting to note that the mean free path for photoemission from the F_{1s} levels is so short that after 10 seconds reaction the F_{1s} intensity has already reached a plateau value, whilst the Au_{4f} levels have been sufficiently attenuated after 15 seconds deposition time that they are not detected at acceptable S/N ratios. The data Figure 4.3.8 points to a particular difficulty in obtaining initial rates of depositions when this are very high e.g. ~10 Å $s.^{-1}$ Since the minimum time for the deposition with the instrumentation involved in this work is ~5 seconds. This becomes more evident from the compilation of data shown in Figure 4.3.8 which provides details of the measured rates of deposition. For a given power input (e.g. 1 W.) the rate of deposition obviously passes through a maximum in the pressure region ~200 μ. The rate of deposition in this pressure region is difficult to measure with any accuracy for reasons outlined above, but it is clear that the rate

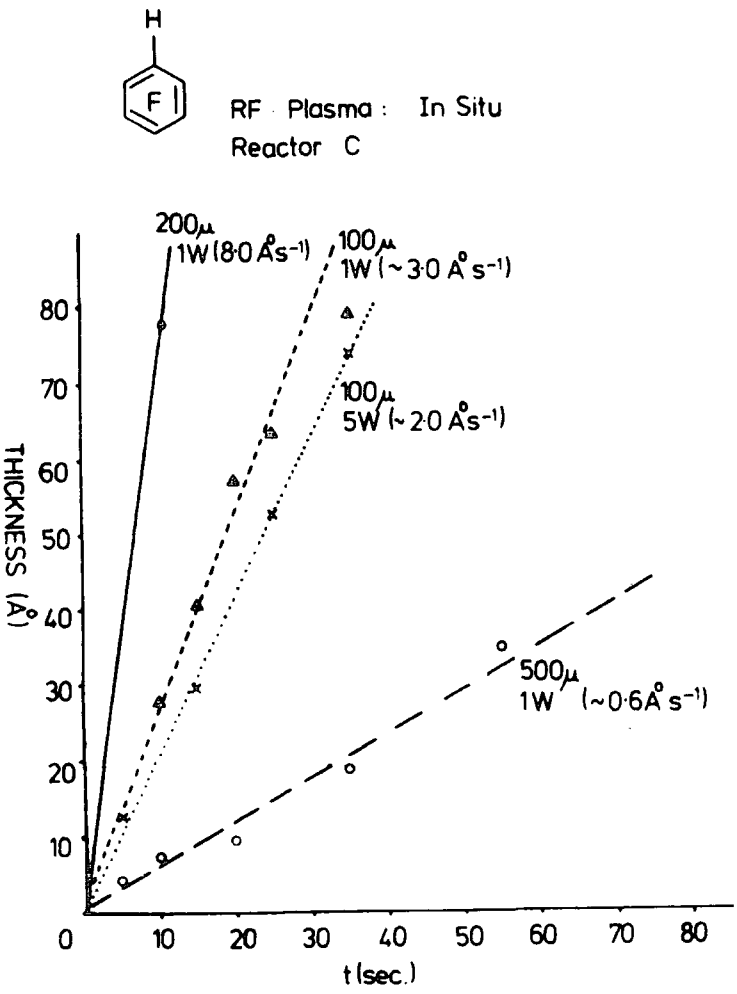

Figure 4.3.8 Thickness (Å) vs. time (sec.) for plasma polymers

is substantially higher (estimated ~ 8 Å $s.^{-1}$) than at 100 μ ~ 3 A $s.^{-1}$ and at 500 μ ~ 0.6 Å $s.^{-1}$ This illustrates the delicate balance in the competing processes of ablation and polymerization. At the extremes of low flow rate and higher power (c.f. 100 μ 1 W. and 5 W. Figure 4.3.8) and high flow rate and lower power (500 μ 1 W.) the rate of deposition is lower than for intermediate flow rate at lower power. Although the gross structural features of the plasma polymer films remain relatively constant over a range of operating parameters, the rate of deposition is strongly influenced by these parameters as has previously been pointed by Yasuda.[29,203] It is clear that with appropriate design considerations it is possible to arrange for deposition rates spanning a considerable range (for the equipment considered here typically from ~ 0.5 Å $s.^{-1}$ to ~ 20 Å $s.^{-1}$).

4.3.4. The Structure of the Polymer as a Function of Site of Deposition in Reactor Configuration B as a Function of Power and Pressure

The design of reactor B allows an investigation of deposition in both glow and non-glow regions and represents the first systematic attempt to investigate how the structure of the deposited plasma polymer depends on its site of deposition.

Glow and non-glow here refer to the usual indication of the visible component of the electromagnetic output of the plasma. This is dependent on the operating conditions but as a typical indication of the extent of this region the dotted lines in Figure 4.2.1 show the apparent area encompassed by the visible glow. At higher powers (>25 W.) the glow region extended typically throughout the whole reactor, however the intensity of emission decreased down the length of the reaction vessel away from the coil region. Polymer films deposited at 12 different sites in the reactor were investigated (6 positions, at the centre line and and bottom of reactor site of deposition) and at 2 different pressures and powers. This provides a matrix of 48 separate experiments. Representative spectra for the C_{1s} and F_{1s} levels of fluoropolymers deposited at sites located on the centre line axis of the reactor and at the bottom of the are displayed in Figures 4.3.9 and 4.3.10.

The spectra reveal straightforwardly that at sites of deposition remote from the coil region (~ 45 cm.) the centriod of the overall band profiles shifts distinctly to higher binding energy as might be expected for an increased content of $\underline{C}F_2$ and $\underline{C}F_3$ structural features. Considering firstly the overall band profiles for the polymer films deposited on gold substrates at the bottom of the reactor (shown in Figure 4.3.9) the dominant component of the C_{1s} levels for polymer deposited in the region

Figure 4.3.9 C_{1s} and F_{1s} spectra of plasma polymers deposited at 10, 25, 45, 60, 80 and 95 cm. sites at the bottom position in reactor B at 10 W discharge power and a pressure of 200 μ

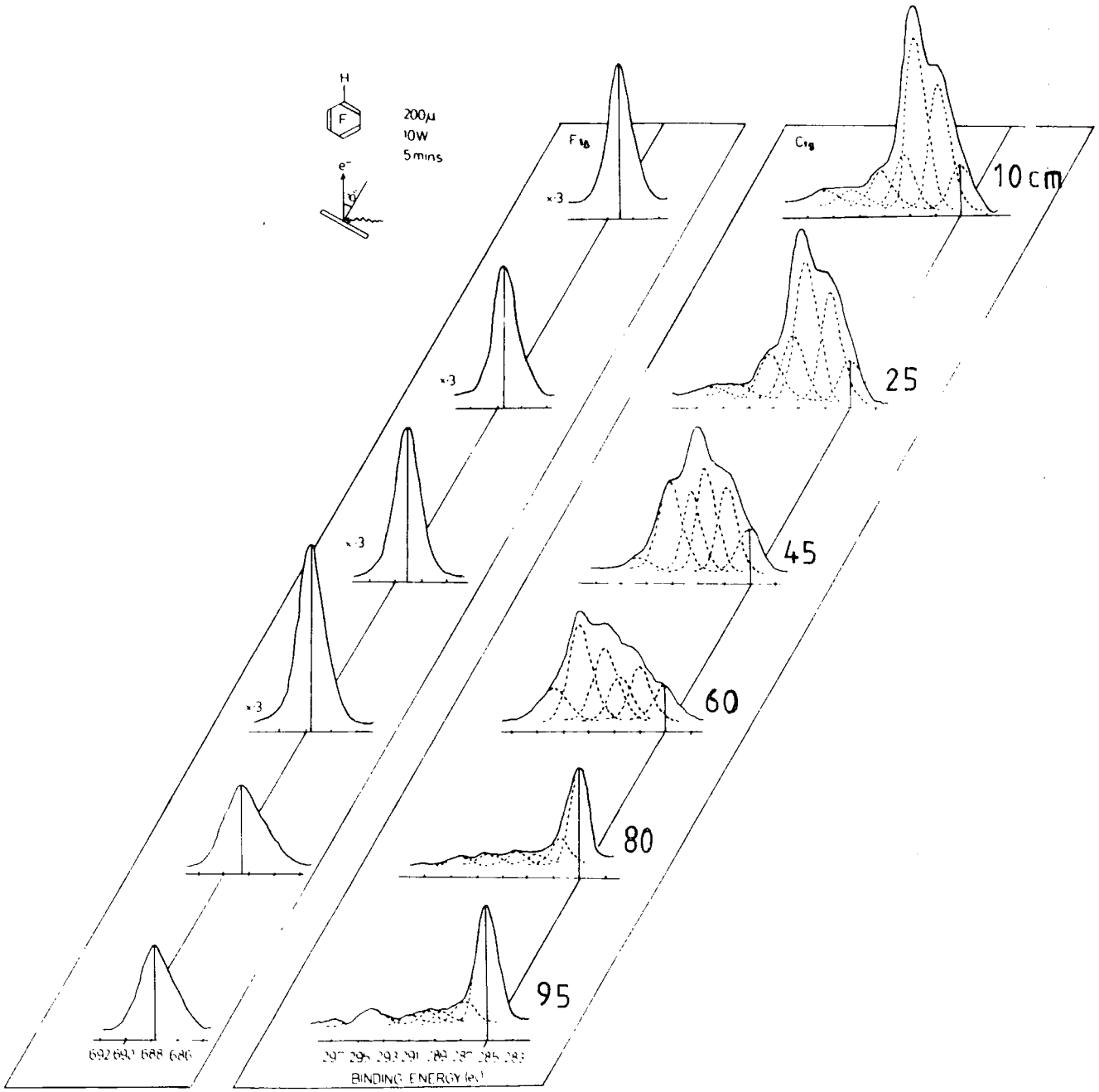

Figure 4.3.10 C_{1s} and F_{1s} spectra of plasma polymers deposited at 10, 25, 45, 60, 80 and 95 cm. sites at the centre position in reactor B at 10 W discharge power and a pressure of 200 μ

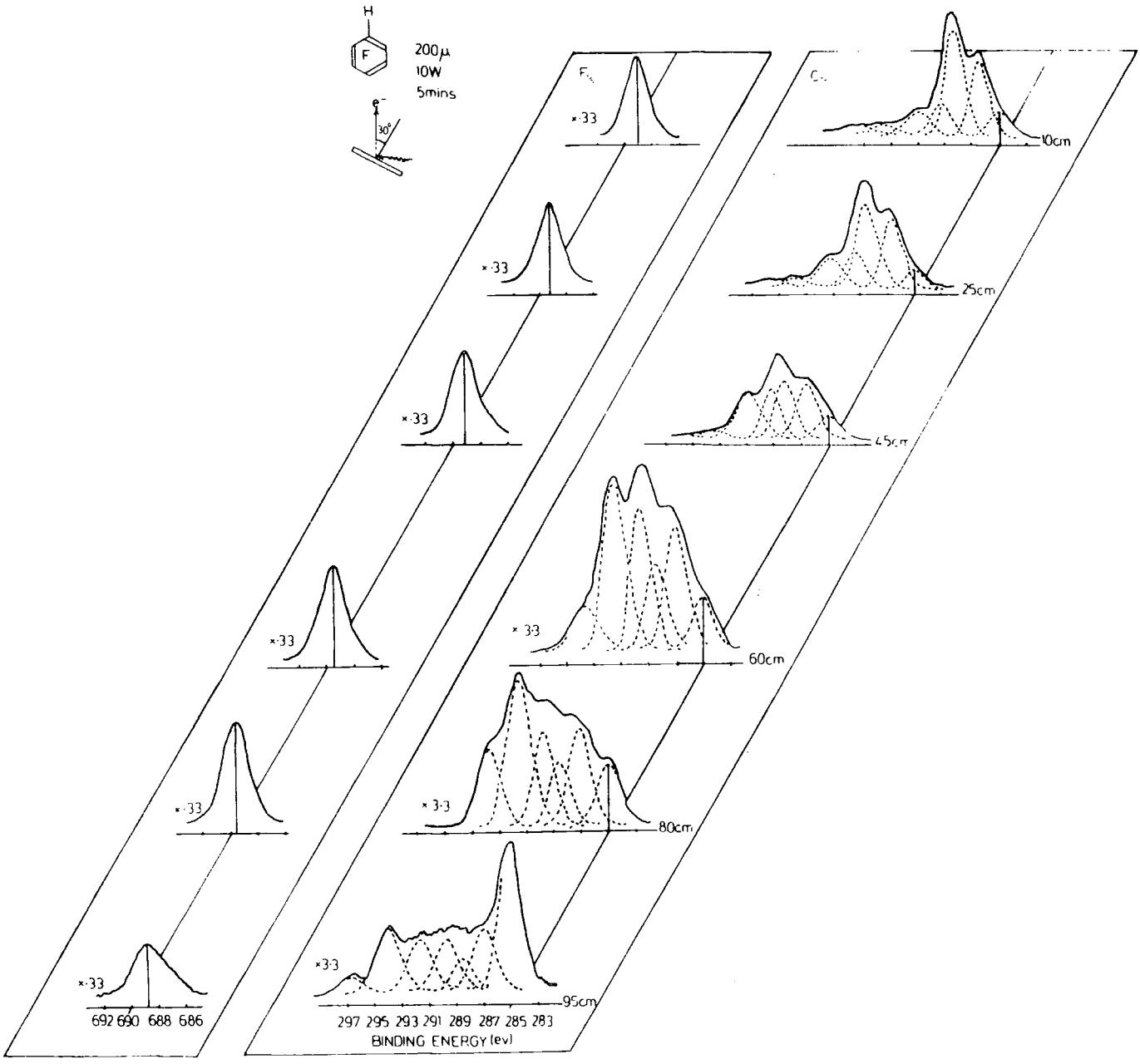

of maximum glow (10, 25 cm.) is centred at 288.4 eV corresponding to $\underline{C}F$ structural features, consistent with the overall stoichiometry which is virtually the same as for the starting monomer. By contrast at a site of deposition 60 cm. down the reactor, the dominant component is centred at ~291.3 eV corresponding to CF_2 structural features. The C_{1s} band profiles for the adjacent sites of deposition are equally revealing. Thus at the 45 cm. deposition sites the proportion of $\underline{C}F$ structural features with adjacent $\underline{C}F$ groups has increased relative to the 10 and and 25 cm. deposition sites and the component at 291.3 eV corresponding to $\underline{C}F_2$ groups has also increased. The gradual increase in $\underline{C}F_3$ functionalities is also evident whilst the very high binding energy component due to $\pi^* \leftarrow \pi$ shake-up satellites decreases in intensity consistent with the fact that as the level of $\underline{C}F_3$ and $\underline{C}F_2$ functionalities increase the degree of conjugative unsaturation decreases. The overall band profiles for the polymer deposited at 80 cm. and 95 cm. sites provides striking evidence for the 'pumping action' at the plasma in the region close to the excitation source. These plasma polymer films deposited further along the reactor are therefore very thin and the C_{1s} spectra are dominated by the extraneous hydrocarbon peak of the gold substrate. Consistent with this is the fact that the Au_{4f} signal are of considerable intensity. The higher fluorine content of the thin polymer films deposited in the region ~60 cm. is evidenced by the nature of the C_{1s} levels when due account has been taken of the component at low binding energy. The spectra then reveal a considerable proportion of CF_2 and CF_3 structural features. A similar picture emerges from the data presented in Figure 4.3.10. The generally higher deposition rate on axis and the nature of the flow pattern however does lead to a somewhat thicker fluoropolymer film being deposited in the 80 cm. and 95 cm. deposition regions. The change in gross structure

of films deposited in defferent regions is most readily followed by means of the component contributions to the C_{1s} line profiles. The component contributions to the spectra in the case of films deposited at 100 μ and 10 W. are shown in Figure 4.3.11 below.

Figure 4.3.11 Percentage contribution to the C_{1s} envelopes for various structural features in the plasma polymers prepared in reactor B, a) samples at the centre and b) samples at the bottom of the reactor.

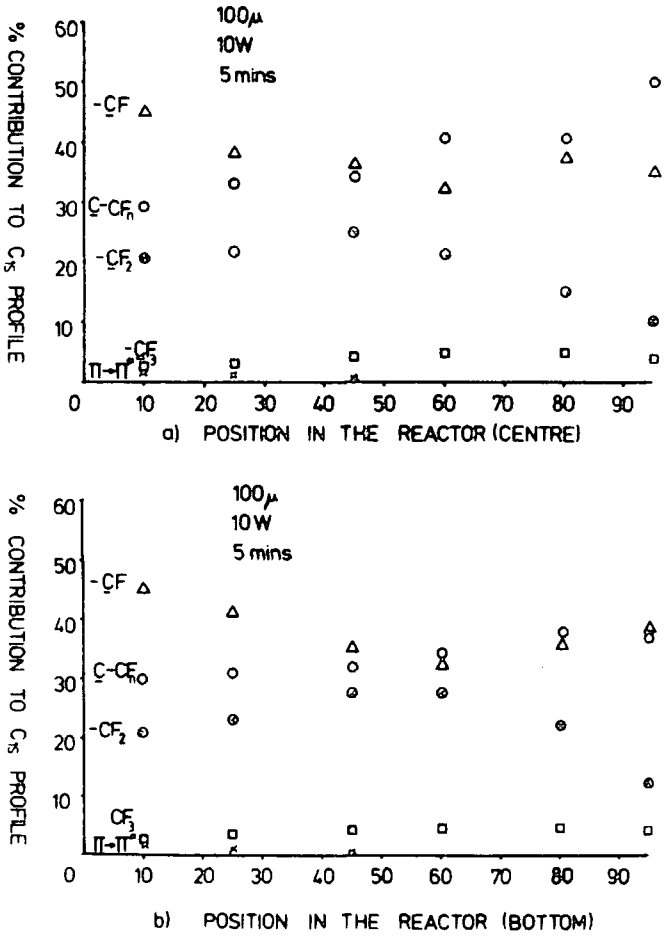

Similar trends are observed for films deposited at the centre and at the bottom of the reactor and these may be summarized as follows. CF structural features remain a relatively constant proportion ($\sim$ 40%)

of the total C_{1s} spectrum. The contribution from CF_2 groups to the overall line frofile increases to a maximum at ~45 cms. Whilst the $\underline{C}-CF_n$ carbons increase in contribution to the total C_{1s} line profile in going from the 10cm. to 95 cm. site of deposition. Shake-up components are only observed with any significant intensity for depositions in the most intense portion of the glow (viz. at 10 cms. and 25 cms.). The intensities of ~2.5% in these cases represents a significant proportion of vinylic $\underline{C}F$ groups since this corresponds to ~6% of the total $\underline{C}F$ contribution. This is around the expected intensity for the $\underline{C}F$ groups to form part of the cyclic benzoid conjugated system.[117] Until further data is accumulated on classes of molecules it is difficult to formulate any realistic discussion on the overall structure of the polymers, however it might be speculated that a possible reactive intermediate in the glow region would be tetrafluorobenzyne produced from HF elimination from the initially produced pentafluorobenzene radical cation. The shake-up intensities observed would support such a hypothesis and it is interesting to note that the Au_{4f} substrate levels observed for samples deposited at 80 cm. and 95 cm. shows distinct asymetries which are are also apparent in the F_{1s} spectra. Thus the F_{1s} spectra for samples deposited in these regions when the films is very thin e.g. 20 Å (c.f Figure 4.3.11 95 cm. deposition site.) shows component at 689 eV corresponding to CF environments and also at 687.5 eV corresponding to ionic fluorine. In the case of approximately monolayer thickness films (e.g. Figure 4.3.9, 95cm.) the F_{1s} spectrum is dominated by the low binding energy fluorine component. A curious feature evident in the C_{1s} spectra for this thin films (e.g. Figure 4.3.9, 80 cm. and 95 cm. and Figure 4.3.10, 95 cm.) is the appearance of the relatively intense high binding energy component centred ~297 eV. This is too intense in each case to be attributable to shake-up components

associated with $\underline{CF}$ structural features and it seems clear that these arise from plasmon losses.[119] Since the extraneous hydrocarbon peak at 285 eV is a sizeable fraction of the overall C_{1s} band frofile in these cases it is possible that a component at 285 eV corresponding to carbon atoms which do not have fluorine substituents either α and β is present for the fluoropolymer film. Much thicker films would be required to consider this point in detail.

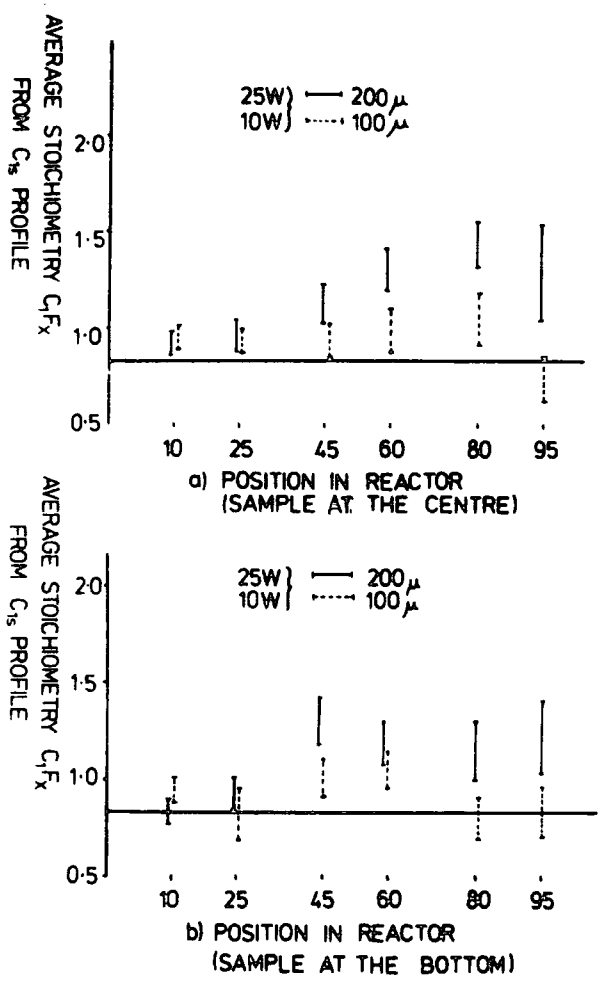

Figure 4.3.12 Average stoichiometry of plasma polymers vs. location for polymer deposited at 10 W and 25 W discharge powers and pressures of 100 μ and 200 μ ; a) samples at the centre and b) samples at the bottom of the reactor B

The stoichiometries as a function of deposition site and experimental parameters are shown schematically in Figure 4.3.12. Although the fine details of structural features varies slightly in going from 10 cm. (in front of the coil) to 25 cm. (in the middle of the coil region) the overall C : F stoichiometry remains essentially constant and is close to that for the starting monomer. In the region 45 - 80 cm. the C : F stoichiometry increases consistent with the component analysis shown in Figures 4.3.9 and 4.3.10. There are subtle differences however in deposition sites along the centre line compared with those at the wall. Thus along the centre line sites of deposition there is a uniform stoichiometry in the coil region followed by a region of increasing fluorine content such that at 80 cm. the C : F stoichiometry (at 200 μ) is $\sim$1.4 compared with $\sim$0.9 in the glow region. At lower pressure the stoichiometry differences along the reactor are not so great. For the thin films deposited at the 80 and 95 cm. sites the error limits on the derived stoichiometry are high since the total intensity of the C_{1s} levels attributable to the polymer film are of low intensity and the component analysis is thereby subject to considerable error.

4.4 Conclusions

Plasma polymer films; from the excitation of inductively coupled R.F. plasmas in the pentafluorobenzene deposited in the glow region of three reactor configurations over a range of operating parameters show very close similarity in term of overall stoichiometry and structural features. The site of deposition within the glow region does not strongly influence the gross structure of the plasma polymer film but does influence the rate of deposition. Under defined conditions it is possible

to reproducibly deposit fluoropolymer coatings at controlled rates of deposition. In the glow regions the stoichiometry of the polymer is substantially the same as for the monomer and the observation of shake-up satellites suggests that conjugated aromatic features are retained in the final structure. Deposition rate and structure of plasma polymer film are strongly influenced by the site of deposition in regions remote from the excitation source. The characteristic feature being an increased fluorine content.

CHAPTER FIVE

CHAPTER FIVE

PLASMA POLYMERIZATION III. A SYSTEMATIC INVESTIGATION OF THE INDUCTIVELY COUPLED R.F. PLASMA POLYMERIZATION IN THE ISOMERIC TETRAFLUOROBENZENES

Abstract

A systematic investigation has been made of the composition, gross structural features and rates of deposition of plasma polymer films produced from the excitation of inductively coupled R.F. plasma in the isomeric tetrafluorobenzene. ESCA data reveals that the dominant reaction involves rearrangement such that under a wide variety of experimental conditions the composition of the crosslinked products remains essentially the same as the starting monomer. Small differences in rates of deposition are observed for the different isomers and theoretical SCF MO studied at the MNDO level provides a basis for discussion of the experimental data.

Chapter Five: Plasma Polymerization III. A Systematic Investigation of the Inductively Coupled R.F. Plasma Polymerization in the Isomeric Tetrafluorobenzenes

5.1 Introduction

The development of ESCA as a tool for characterization of polymers in terms of surface chemistry is particularly important to an understanding of the complex reaction pathways which occur heterogeneously under conditions of plasma polymerization.[22] The analysis of even the grossest features of structure and composition for ultra-thin crosslinked polymer films which may readily be produced by means of plasma techniques has become routinely possible with the development of ESCA and in the previous two chapters and also in a series of papers[200] it has been shown how the technique may be applied to a systematic investigation of how the structural features present in the polymer and its ultimate composition depend on the initial starting material and the operating parameters of the plasma instrumentation.[29]

A significant feature of these previous investigations, which for a variety of reasons have centred on fluorinated starting monomers, has been the observation that structurally related materials under well defined conditions produce polymer films which are distinctive in nature and which show a structurally related deposition rate. Although the very nature of the plasma process itself involving as it does a variety of radicals, ions and excited state species inevitably leads to extensive molecular rearrangements in the route leading to the formation of film of the gas solid interface, nonetheless for a given starting material the reaction must follow a well defined pathway which is reproducible over a wide range of operating conditions.[52,200,211] The data available to date therefore is

starting to provide sufficient background of information to enable reaction pathways to be studied in some detail. As a further step in this direction a systematic study is reported here of the plasma polymers produced under a variety of conditions from the isomeric tetrafluorobenzenes. There have been no previous studies of the plasma polymers produced from the isomeric tetrafluorobenzenes, however, it is of interest to note that studies have recently been made of the emission spectra of the excited states of the radical cations produced by electron impact in the kinetic energy range 20 - 30 eV. Data are therefore available on the lifetimes and relative energies of the second and first excited states of the radical cations and therefore of relevance to the broad question of the mechanism of formation of the plasma polymers by the CAP (Competitive Ablation and Polymerization) process.

The prime objectives of this work may be summarized as follows:

(a) To investigate the stoichiometries, the distribution of various structural features for the plasma polymers produced from the isomeric tetrafluorobenzenes under identical conditions.

(b) To investigate rates of deposition of the plasma polymers as a function of the starting monomer and the operating parameters of the plasma.

5.2 (i) Experimental

The reactor configurations (A, B and C) used in this study for the plasma polymerization of the three isomers of tetrafluorobenzene have been described previously.[205] The only change was in reactor B, which consisted of a cylindrical pyrex tube 7 cm. in diameter and 60 cm long with a 6 turn 60 μH soft copper coil wound around the centre region of the reactor.

In the particular case of reactor A and B, thin films for ESCA studies were obtained by depositing the polymer onto gold substrates located at the bottom of the reactor in the middle of the coil region. Deposition in these regions was also investigated by depositing onto Al foils (2 x 1 $cm.^2$) and on pieces of HDPE (2 x 10 $cm.^2$) substrates. The rates of deposition of the polymer films were determined by measuring the weight increase of the Al foil using a CAHN electromicrobalance. Initial rates of deposition were obtained for in situ deposition in reactor C by monitoring the Au_{4f} levels of the gold substrates by means of ESCA as previously described. The RF plasma instrumentation; the measurements of flow rate; MATR IR studies and the measurement of the ESCA spectra were as previously described.[205]

A binary sovent mixture made up from perfluorobenzene and perfluorodecalin was used in measuring the density of the polymers. Microanalysis studies (reactor B) were made for carbon and hydrogen by combustion and for fluorine by potassium fusion.

Mass spectra have been measured under a variety of conditions. Electron impact induced mass spectra at 70, 30 and 18 eV primary beam energy were recorded using an A.E.I. double focussing MS 9 spectrometer. Chemical ionization mass spectra were obtained with a VG MM 16 spectrometer employing both NH_3 and CH_4. Contact angles were measured using a travelling microscope technique and critical surface tensions were estimated using empirical equations of Kim, Evans and Goring [214] using A and B values of 32 and 21 dyne $cm.^{-1}$ respectively.

Research grade sample (Bristol Organic Ltd.) of 1,2,3,5- and 1,2,4,5-tetrafluorobenzene were shown to be pure by g.l.c. and were used without further purification. Samples 1,2,3,4-tetrafluorobenzene (87% purity) were purified by preparative scale g.l.c to a purity of $\sim$ 99%.

Prior to use all starting monomers were subjected to extensive freeze thaw cycles for degassing.

(ii) Theoretical

An MNDO[215] -SCF-MO investigation has been made of the relative energies of some structural isomers of the tetrafluorobenzene ring system. Starting from estimated geometries (on the basis of previous literature studies and standard tables of bond lengths and angles) computations have been carried out such that relative heats of formation have been computed for energy optimized geometries for each system of interest. Comparison with experimental data where available shows that the theoretically calculated relative heats of formation provided a firm basis for the discussion presented in Section 5.3.

5.3 Results and Discussion

5.3.1 Introduction

It has been shown that (in Chapters Three and Four) for a given monomer, deposition of a plasma polymer at a given site depends on the W/FM parameter (where F is the flow rate, M the molecular weight of the monomer and W the power input), however, the overall stoichiometry and structure of the polymer is largely invariant to pressure and power over the typical ranges employed in the production of plasma polymers using inductively coupled R.F. instrumentation. In this work therefore, the stoichiometry and structural features of the plasma polymers deposited have been studied at a given site (the centre of the glow region) under a given set of experimental conditions to check that the previous finding

(Chapter Four) is also the case for the isomeric tetrafluorobenzenes. Under the conditions employed in this study the emission of the visible gives rise in each case to a pale blue colour which arises from the $^2\tilde{B} \longrightarrow {}^2\tilde{X}$ transition for the corresponding radical cations of the tetrafluorobenzenes.[216] This indicates that a significant tail of the essentially Maxwellian distribution of electron energies must be above the threshold ($\sim$12 eV) for the production of the second excited states of the radical cations and will consider this in some detail in a later section.

5.3.2 Structural Features

(i) 1,2,4,5-tetrafluorobenzene

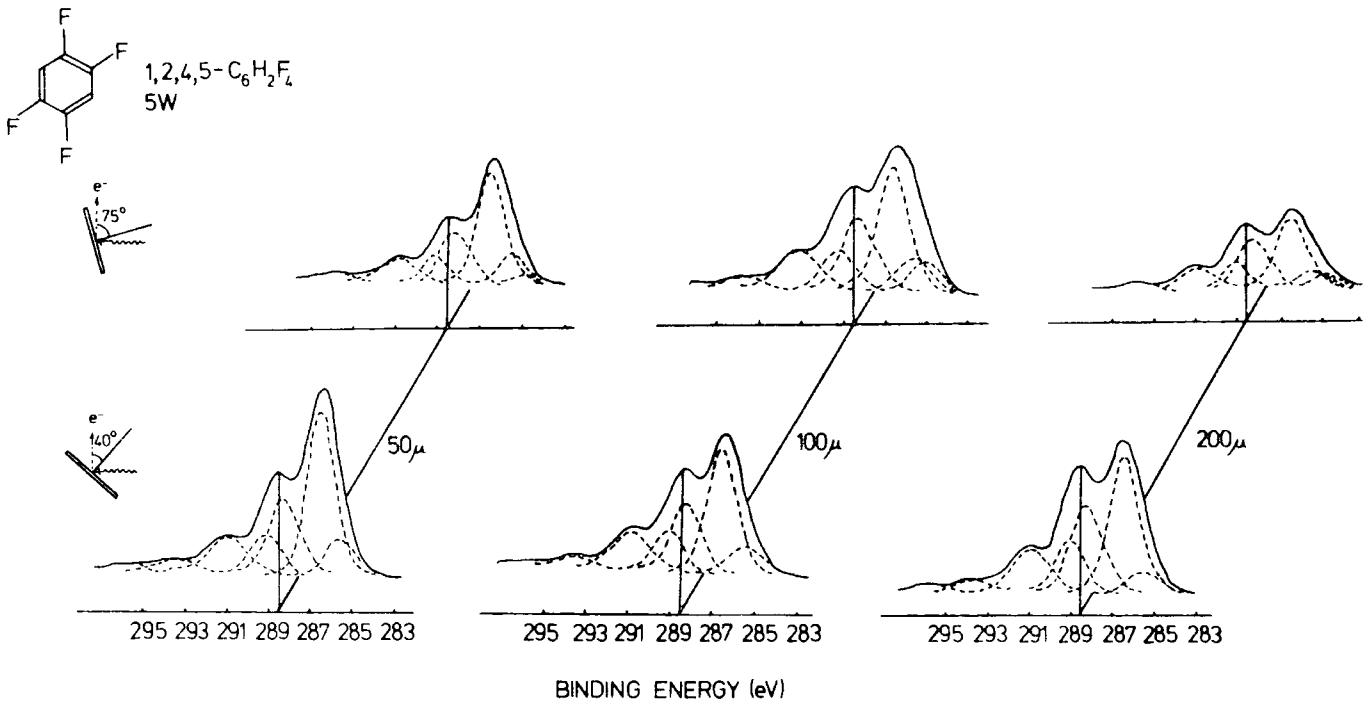

Figure 5.3.1 C_{1s} levels of plasma polymerized 1,2,4,5-$C_6H_2F_4$ prepared in situ at 5 W and pressures 50 μ , 100 μ , 200 μ

The C_{1s} core level spectra for films of plasma polymer deposited in situ on gold substrates at in put powers of 5 W and pressures of 50, 100 and 200 μ are shown in Figure 5.3.1. The spectra show little change in component analysis as a function of electron take off angle thus confirming the vertical homogeneity of the samples, the only minor difference being due to the small extent of surface hydrocarbon contamination when surface features are enhanced by going to a high take off angle. The spectra over the range of conditions studied confirm that there are subtle rather than gross changes in structure associated with changes in operating parameters for the plasma, and C_{1s} line profiles therefore fall into four distinct regions. The most intense component at lowest binding energy arises from carbons with β -fluorine substituents, a further sub-division being evident from the line shape analysis into $\underline{C}$-CF (285.6 eV) and $\underline{C}$-CF_n (286.6 eV). The shoulder to the high binding energy side than corresponds to $\underline{C}F$ structural features. These can again be sub-divided into those which have fluorine substituents in β -positions (289.2 eV) and those which do not (288.4 eV). The next higher binding energy components are assigned from their characteristic energies to $\underline{C}F_2$ and $\underline{C}F_3$ structural features. The remaining component of low overall intensity centred $\sim$296 eV can only arise from a $\pi^* \leftarrow \pi$ shake-up satellite of a lower binding energy component and on both intensity and energy grounds, the only consistent assignment is to the $\underline{C}F$ structural features at $\sim$289 eV. Since the typical transition energy for a conjugated system is $\sim$7 eV,[117] it is also conceivable that a proportion of the signal intensity attributed to $\underline{C}F_3$ structural features at $\sim$294 eV could originate from shake-up setallites of the main component at $\sim$286.6 eV. The spectra clearly show that substantial structural reorganization accompanies plasma polymerization.

(ii) 1,2,3,5- and 1,2,3,4-tetrafluorobenzenes

The corresponding C_{1s} core level spectra for the 1,2,3,5- and 1,2,3,4-tetrafluorobenzene isomers are shown in Figures 5.3.2 and 5.3.3, and show close similarities to those for the 1,2,4,5-substituted isomer. The similarities in terms of component compositions of $\underline{C}\text{-}CF_n$ (n = 1 - 3) $\underline{C}F$ (including those groups with β fluorine substituent) $\underline{C}F_2$, $\underline{C}F_3$ and $\pi^* \leftarrow \pi$ shake-up satellites for the plasma polymers produced in the pressure range 50 μ - 200 μ and at 5 W input power is clearly shown by the data in Figure 5.3.4. Whereas the $\underline{C}F_3$ and $\underline{C}F_2$ structural features remain an essentially constant proportion of the structural features as a function of pressure. There is however a tendency for a higher contribution from $\underline{C}F$ structural features at the expense of $\underline{C}\text{-}CF_n$ structural features as the pressure from 50 μ to 200 μ . In consequence the $\pi^* \leftarrow \pi$ shake-up satellite decreases in intensity and the overall carbon : fluorine stoichiometry decreases slightly (lower fluorine content) as the pressure decreases. As previously noted [205] this effect in the case of other fluorinated systems, and it has been tentatively proposed that it arises from the somewhat greater average energy for the electrons at lower pressure giving rise to somewhat greater degree of rearrangement. The component analysis at high power (10 W) is essentially the same as that in Figure 5.3.4. From starting monomers with 33% $\underline{C}\text{-}CF_n$ and 66% $\underline{C}F$ structural features, the plasma polymers show an approximate structural feature distribution of ~50% $\underline{C}\text{-}CF_n$, ~35% $\underline{C}F$,, ~12% $\underline{C}F_2$ and ~3% $\underline{C}F_3$, it is evident from this that the carbon : fluorine stiochiometries of the polymers are closely to those of the starting monomers.

Figure 5.3.2 C_{1s} levels of plasma polymerized 1,2,3,5-$C_6H_2F_4$ prepared in situ at 5 W and pressures of 50 μ , 100 μ , 200 μ

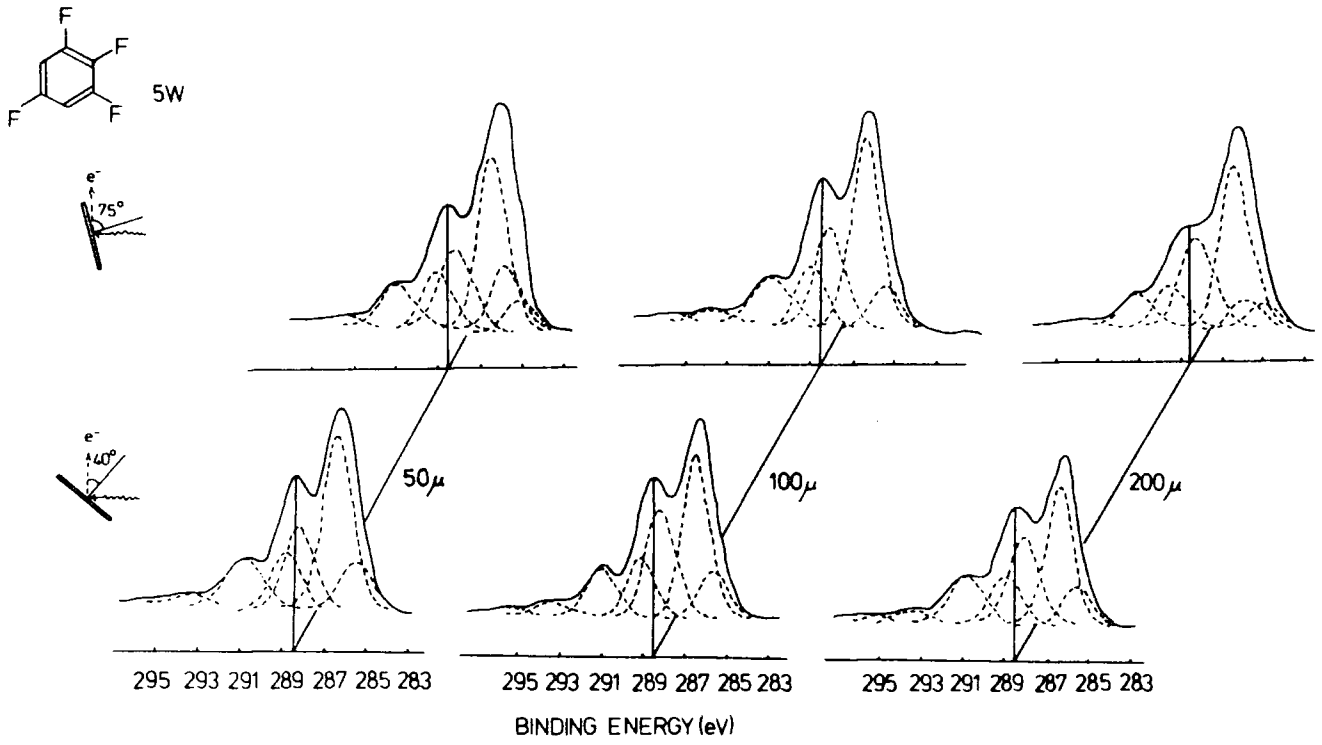

Figure 5.3.3 C_{1s} levels of plasma polymerized 1,2,3,4-$C_6H_2F_4$ prepared in situ at 5 W and pressures of 50 μ ,100 μ , 200 μ

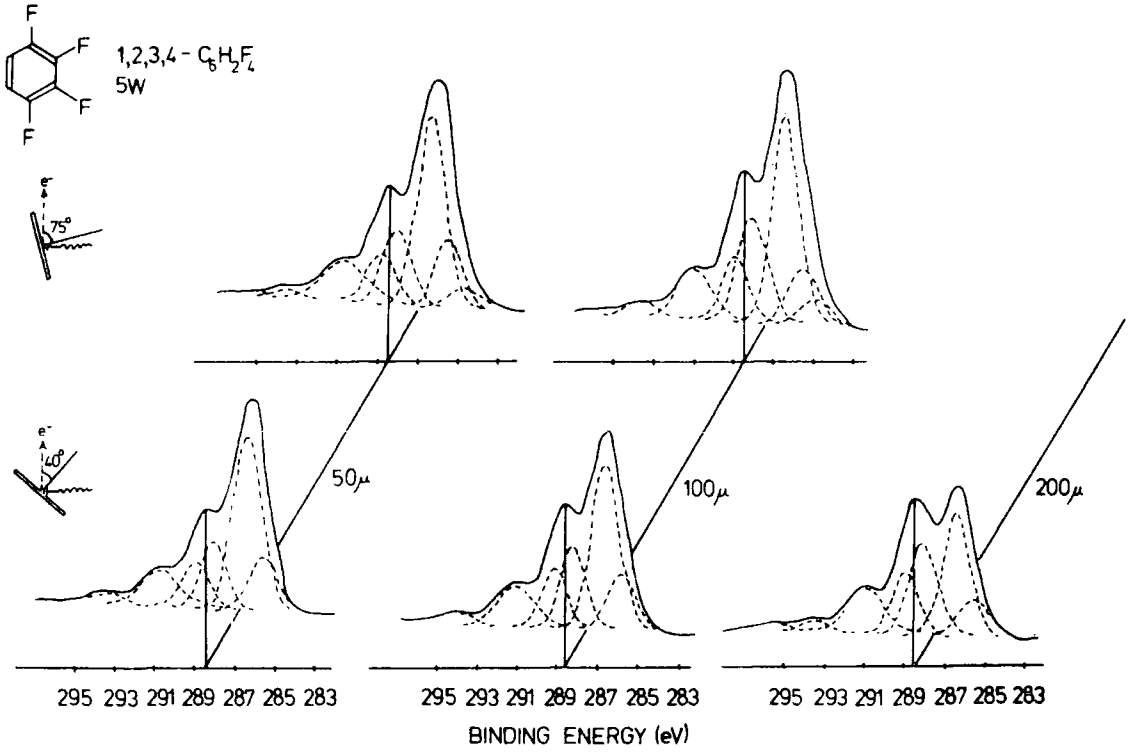

Figure 5.3.4 **Percentage contribution to C_{1s} envelope for various structural features in the plasma polymers of three isomers of tetrafluorobenzene prepared at 5 W input power and pressures of 50 μ , 100 μ and 200 μ**

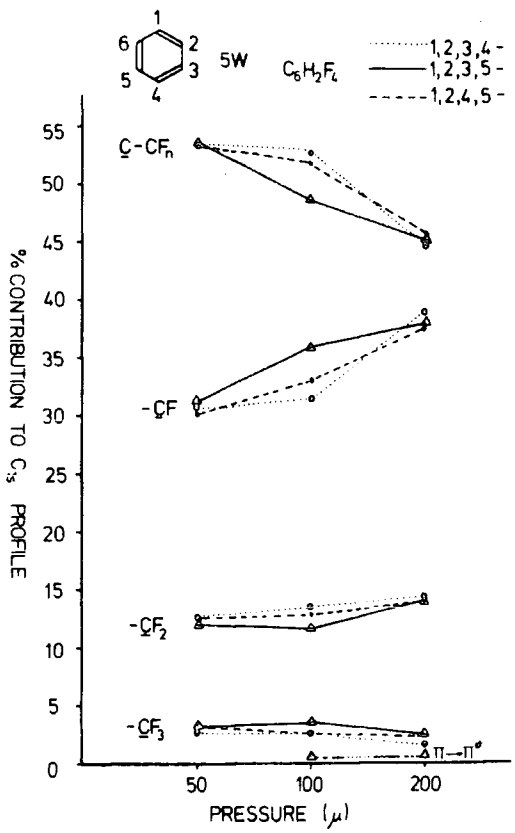

5.3.3 Stoichiometry of polymer films

The average C : F stoichiometries for the various films of plasma polymerized tetrafluorobenzene isomers studied in this work as elaborated by ESCA are detailed in Figure 5.3.5. The mean stoichiometry is in all cases very close to that of the starting monomer ($C_1F_{0.67}$). There is a tendency for lower pressure (50 μ) to give a stoichiometry slightly below that of the starting monomer, whereas at higher pressure (200 μ) the fluorine content tends to be slightly higher than that of the

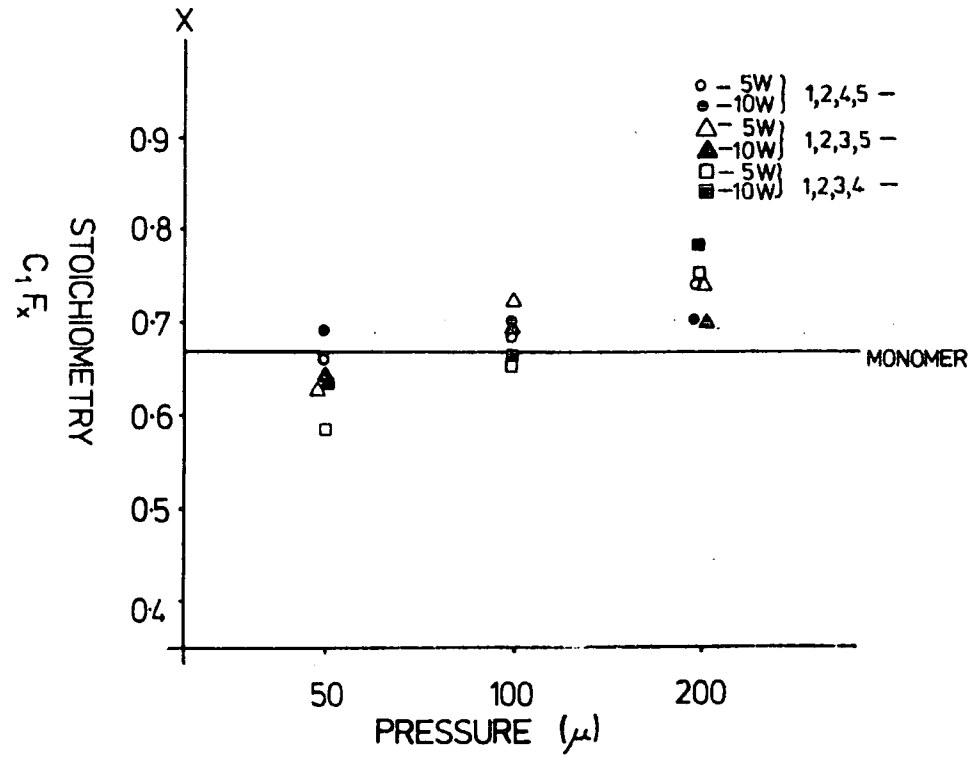

Figure 5.3.5 Average stoichiometry of plasma polymers of the isomeric tetrafluorobenzenes as a functions of power and pressure

starting monomer, although no consistent trends are evident from different isomers or from differences in power. From samples of polymer deposited in reactor B (see later) density measurements by flotation method gives a density for the films produced from the isomeric tetrafluorobenzenes of 1.8 g. cm.$^{-3}$ This identical within experimental error to the density found for the plasma polymers produced from pentafluorobenzene with slightly higher fluorine content (viz. $C_1F_{0.73}$).

Contact angle measurements give an estimated critical surface tension γ_c of ~30 dyne cm.$^{-1}$ which is slightly higher than for the plasma polymer films from pentafluorobenzene, consistent with the reduced contribution from $\underline{C}F_3$ and CF_2 structural features compared with the latter. The MATR studies confirm the presence of $\underline{C}F$ structural features, since a broad intense absorption region is evident in the range 1000 - 1400 cm.$^{-1}$

5.3.4 Rates of Deposition

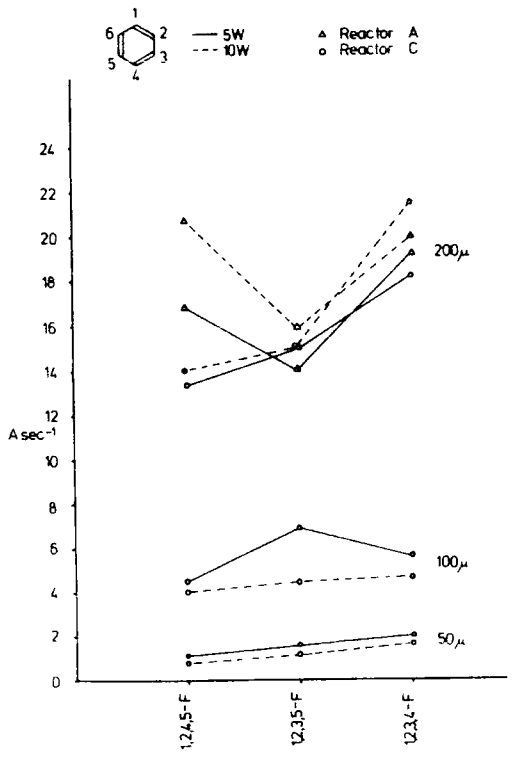

Figure 5.3.6 Rates of deposition of plasma polymers from the isomeric tetrafluorbenzenes as a functions of of power and pressure in reactor A and C

Figure 5.3.6 above displays the rate of deposition of fluoropolymer films in in situ on gold substrates which have been determined as a function of power of pressure, and typical spectra from which the data are derived are shown in Figure 5.3.7 for the particular case of 1,2,4,5-tetrafluoro-benzene. As previously noted[22,200] ESCA provides, by means of monitoring the intense $Au_{4f_{7/2}}$ levels of the gold substrate, a convenient means of measuring initial rates of deposition by this method are typically $\sim 5\%$ and it would be therefore appear that there is a statistically tendency for the 1,2,3,4-tetrafluorobenzene to deposit plasma polymer slightly

Figure 5.3.7 F_{1s}, C_{1s} and Au_{4f} levels of plasma polymerized 1,2,4,5-tetrafluorobenzene prepared in situ

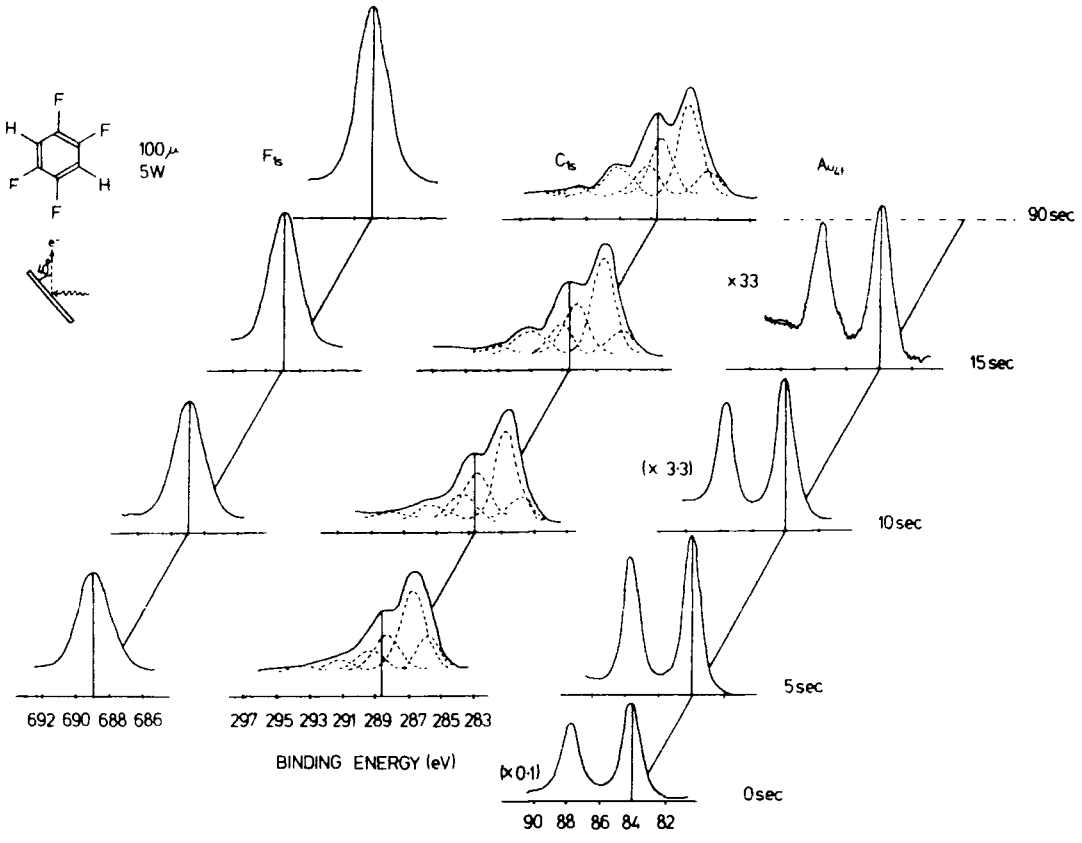

faster than for the 1,2,3,5- and 1,2,4,5- tetrafluorobenzenes overall rates of deposition increase as the pressure increases in the range 50 μ - 200 μ , however, the effect of increase in power is less dramatic. At lower pressure, high power is associated with a decreased deposition rate whereas at higher pressure (200 μ) the rate of deposition increases at higher power. This emphasizes the importance of the W/FM parameter in determining the competitive balance between polymerization and ablation.[203] It is clear from the data in Figure 5.3.6 that it is possible to exercise considerable control in the thickness of film which may be deposited under given conditions, and it is also clear that as in the case of the isomeric difluoroethylenes previously studied,[52] the rate of deposition of polymer is subtly rather than grossly dependent on the structure of the 'monomer'.

As described in the experimental section, the larger free standing reactor B has been used to investigate the efficiency of plasma polymer formation. The experiments which were carried out in this connection consisted of running a plasma in a given monomer under a given set of conditions for a fixed length of time, then recovering the totality of the polymer deposited on the walls of the reactor and the volatiles passing through the reactor into a cold trap. For the 1,2,4,5-isomer for example, material balance showed that at 200μ , (5 W), with a flow rate of $\sim$3.2 cm.^{3} min.$^{-1}$ (STP), there is close to $\sim$100% conversion to polymer with only traces of material in the cold trap located downstream of the reactor. Even over a period of three hours, during which time a substantial thickness of polymer was deposited, the quantity of liquid product accumulated in the cold trap was insufficient $\sim$20 mg. to obtain a microanalysis. Mass spectroscopic GLC investigations revealed however that the material was of relatively high molecular weight but insufficient data was obtained to present a discussion on the likely composition and structure of the material. Since it constitutes such a minor contribution to the overall conversion of the starting monomer, the discussion of this point was not pursued any further.

The plasma polymer deposited over the length of the reactor B during a three hour period is sufficient to allow material to be removed from the walls of the reactor in discrete sections, so that weight and microanalytical compositions may be investigated. The glow region typically extended $\sim$10 cms. on either site of the coil region, the coil being located centrally along the axis of the reactor. Polymer deposited in the region downstream and outside of the glow region (region V, see Figure 5.3.8) was powdery in nature compared with the film like nature of polymer deposited in region I upstream of the coil. Interestingly enough

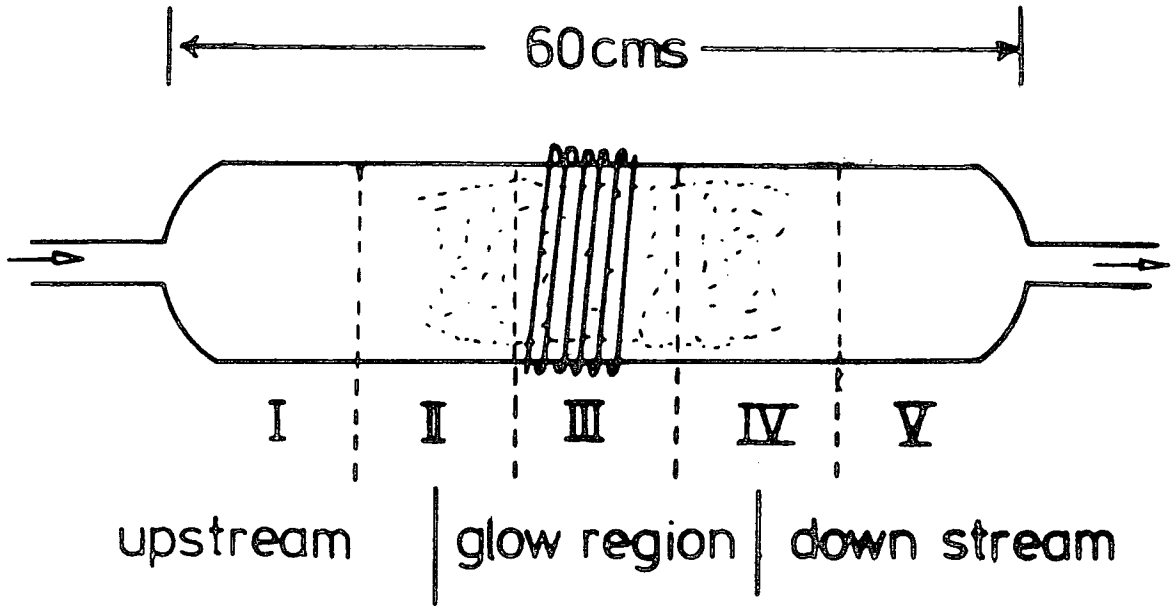

Figure 5.3.8 Schematic of glow discharge studies in the reactor B

however, microanalysis revealed that the composition of the polymer was identical in both cases, $C_1F_{0.6}$ and indeed the film samples deposited in glow region were also of the same composition. This is understandable in terms of the previous study (Chapter Four) of the structure of polymer films as a function of site of deposition in the particular case of[205] pentafluorobenzene. In Chapter Four, it has been shown that the composition composition of polymer remains constant over a region extending roughly to the dimension of the coil itself either side of the coil region, however much further downstream of the coil region, the fluorine content of polymer tended to increase. Taking the centre point of the reactor as reference, the deposition of material is roughly equally divided between the upstream and downstream regions. The interesting feature which also emerges from the analysis is that the deposition of polymer is equally divided between the regions of maximum glow (extending $\sim$20 cms. beyond the coil region) and the regions upstream and downstream. In summary therefore,

polymerization is essentially complete over the length of the reactor and the polymer is of uniform composition. However polymer deposited in the region downstream and outside of the glow tends to be somewhat powdery compared with polymer deposited elsewhere in the reactor.

The initial rate of polymer deposition in situ in reactor C may be conveniently be monitored by ESCA as has been noted in the previous Chapters Three and Four. An overall estimate of deposition rate under different W/FM conditions may be obtained from the known weight of polymer deposited in reactor B and the geometric area assuming uniform deposition throughout the reactor. This provides an estimate of $\sim$11 Å $s.^{-1}$ for a W/FM parameter of 1.4×10^7 J Kg^{-1}. The assumption of a uniform rate of deposition implies that this estimate is relatively crude. But it is interesting to note that it is comparable with the rate of deposition in situ on gold substrates mounted axially in reactor configuration C ($\sim$13 Å $s.^{-1}$) for a W/FM parameter of 6.5×10^7 J $Kg.^{-1}$ It is significant that these rates of deposition refer either to extended periods (in the case of reactor B averaged over three hours) or initial rates of deposition (ESCA analysis of deposition on gold in reactor C) and that the rates are comparable. This provides confirmatory evidence for the rapid establishment of a dynamic equilibrium involving deposition and ablation and once the gold substrate is covered to the monolayer or so level the deposition is independent of substrate, provided this is not ablated to any extent in the plasma.

To provide further confirmatory evidence on this point the rates of deposition in reactor configuration A for intermediate time periods (10 minutes) were measured by using a high sensitivity capacitance microbalance to measure the weight increase arising from polymer deposition on 2 $cm.^2$ pieces of aluminium foil substrates located at the wall in the

centre of coil region. Experiments were carried out at fixed flow rates and pressures (200 μ) but with input powers of 5 and 10 W. The overall rates of deposition are comparable with those for in situ deposition along the centre line of the reactor as obtained for configuration C, however the small variation as a function of isomer tends to be the opposite sense to that for the in situ deposition. This can most readily be appreciated by reference to Figure 5.3.6. Since the sites of deposition and W/FM parameters are different for the two reactor configurations, there could be several explanations for the small changes in the rates of deposition. It is interesting to note however that there seems to be a definite trend for the rate of deposition of polymer to increase for the 1,2,3,5-tetrafluoro isomer relative to the other isomers as W/FM increases. There is insufficient data to put this on a quantitative basis more particularly, since the flow pattern in reactor C may well be significantly different than for the other two reactors, however the data does seem to fit into a consistent pattern. Thus at high W/FM, (high power, low pressure) the rate of polymer deposition is low and differences between the isomers is small. As W/FM decreases the rate of deposition of polymer from the 1,2,3,5- isomer is slightly increased relative to the other isomers and as the parameter decreases further the relative rates of deposition for the 1,2,4,5- and 1,2,3,4-tetrafluorobenzene plasma polymers increases more rapidly (c.f. Figure 5.3.6). Separate experiments in reactor B in which rates of deposition on Al foil substrates were investigated for plasma excited at 200 μ and 5 W gave essentially identical results as for reactor A and W/FM parameters being the same. The sum total of the data on deposition rates appear to fit into a consistent overall picture and the conditions selected for polymerizations in reactor A and B are probably close to optimum in the power range which is of interest in this work viz. a plot of log W/FM

vs. rate of deposition reaches a plateau region for the lowest values of the abscissa employed in this work.

5.3.5 General Comments on Mechanism of Polymer Formation

The data presented in the previous sections has emphasized that the isomeric tetrafluorobenzenes undergo plasma polymerization a comparable rates and produce materials showing evidence for extensive molecular rearrangement accompanying polymerization. Considering now in broad outline possible routes to polymer formation. As a necessary precursor to such a discussion it is important to consider the typical range of reactive species which are likely to be present to a greater or lesser extent in inductively coupled cool plasmas in tetrafluorobenzenes.

There have been no detailed investigations of the energy distribution of electrons in plasmas in other than the simplest systems such as the inert gases and hydrogen. The result of these previous studies,[16] however can be used to present a qualitative discussion of the main features associated with the inductively coupled plasmas in the fluorobenzenes. The electron energy distributions (as discussed in Chapter One) are likely to be Maxwellian (or variant thereof, c.f. Druyvesteyn), with an average kinatic energy of a few electron volts corresponding to a Boltzmann equivalent temperature in the range of 10^4 K. The interection between the electron flux of the monomer gas when the plasma is initiated may conveniently divided into three energy regimes, corresponding to the distinct processes set out in Scheme A. A cross-section for these processes depend quite markedly on the electron energies. Thus for the tetrafluorobenzenes the cross-section for ionization is zero

SCHEME A

$M + e \longrightarrow M^-$ Electron attachment

$M + e \longrightarrow M^* + e$ Inelastic collision leading to excitation

$M + e \longrightarrow M^+ + 2e$ Ionization

$M^+ + e \longrightarrow M$ Neutralisation

until the threshold is reached at ~9.5 eV, whilst excitation is unimportant for electrons with energies below that of the first excited state (T_1) at ~ 3.9 eV (c.f. Table 5.3.1). By contrast the cross-section for electron attachment is large in the region 0 - 3 eV. It is of interest therefore to consider a typical Maxwellian or Druyvesteyn distribution for electrons with an average energy of ~2 eV. This shows that the typical percentage contributions to the distribution in the energy ranges 0 - 3 eV, 3 - 9 eV and 9 - 15 eV are~60%,~40% and ~ 0.4% respectively.

Since the plasma is overall electrically neutral (ion density probably $\sim 10^{10}$ cm.^{3}),[16] the number of electrons plus negative ions must be equal to the number of positive ions in the system.

Systematic studies have been made of the negative ion states of the fluorobenzenes by Christophorou and co-workers.[217] In the particular case of 1,2,4,5-tetrafluorobenzene isomers, negative ion states corresponding to pi radical anions derived by occupancy of the three unoccupied pi orbitals have been indentified at 0.5, 1.29 and 4.51 eV and comparison with data on both more and less heavily fluorine substituted derivatives shows[217] that similar energies would be anticipated for the other two tetrafluoro- isomers. The lifetimes of the various negative ion states as a function of pressure

Table 5.3.1

Excited state energies and lowest (π) ionization potentials for the isomeric tetrafluorobenzenes

Tetrafluorobenzene	Transition Energies (eV)				Adiabatic Ionisation Energies (eV)		
	$^3B_{1u}$	$^1B_{2u}$	$^1B_{1u}$ †	$^1E_{1u}$	$IE_1(\tilde{X})$	$IE_2(\tilde{A})$	$IE_3(\tilde{B})$ ††
1,2,3,4-	3.95	4.85	6.43	7.21	9.56	9.88	12.42
1,2,3,5-	3.93	4.79	6.2(±0.1)	7.10	9.56	9.93	12.42
1,2,4,5-	3.93	4.69	6.3(±0.1)	7.25	9.36	10.04	12.35

† Evidence has been presented for state with energy ~ 6.2 eV corresponding to excitations involving the F_{2p} lone pair.

†† Emission from the state is responsible for the colour of the plasmas excited in the fluorobenzenes.

have not been investigated in detail, however the available data suggests that for the lowest energy state the lifetime is likely to be in the range $\backsim 10^{-7} - 10^{-9}$ sec.[16] Efficient internal conversion processes suggest that if isomerizations via radical anions state are important, those involving the ground state will be dominant. Discussion of this point shall be followed after a consideration of excited states in the neutral and positive ion manifolds although it has been noted that e.s.r. studies of radical anions of benzenes provide little evidence for molecular rearrangement of the basic skeleton.[222] Very little data has been published however on pi radical anions of the fluorobenzenes.

Electron impact spectra for the fluorobenzenes have been studied in detail by Kuppermann and co-workers.[218] The data which have been reported have generally been recorded with primary electron beam energies considerably above the threshold (typically 25 eV or 50 eV), and it is by no means straightforward to extrapolate relative cross sections for excitation down to energies just above threshold. In the region from $\backsim 4 - 8$ eV five states have been identified and the transition energies are closely similar for the three isomers. The relevant data are shown in Table 5.3.1. A large number of Rydberg like states have also been observed[16] (by electron impact) at energy > 8 eV, however identification of these states has not been attempted and indeed in terms of their chemistry, there is likely to be a correspondence with the ions states with represents the convergence limit of a given Rydberg series. Molecular rearrangements involving the benzene ring system arising from excited states in the energy range up to $\backsim 6.4$ eV above the ground state have been the subject of numerous investigations.[219,220] Transformations in the gas phase involving benzvalene and prismane provide a route to the interconversion of the isomeric tetrafluorobenzenes. Thus excitation to the S_1 ($^1B_{2u}$) state can lead via the prismane skeleton to scrambling

as indicated schematically in Figure 5.3.9, whilst excitation to the S_2 ($^1B_{1u}$) state can lead to scrambling of adjacent position via the benzvalene structure or scrambling via the excited prismane produced from the symmetry allowed $\pi_{2s} + \pi_{2s}$ cycloaddition of excited state Dewar benzene.

Figure 5.3.9 Isomerizations of aromatic systems involving excited states with excitation energies < 6 eV

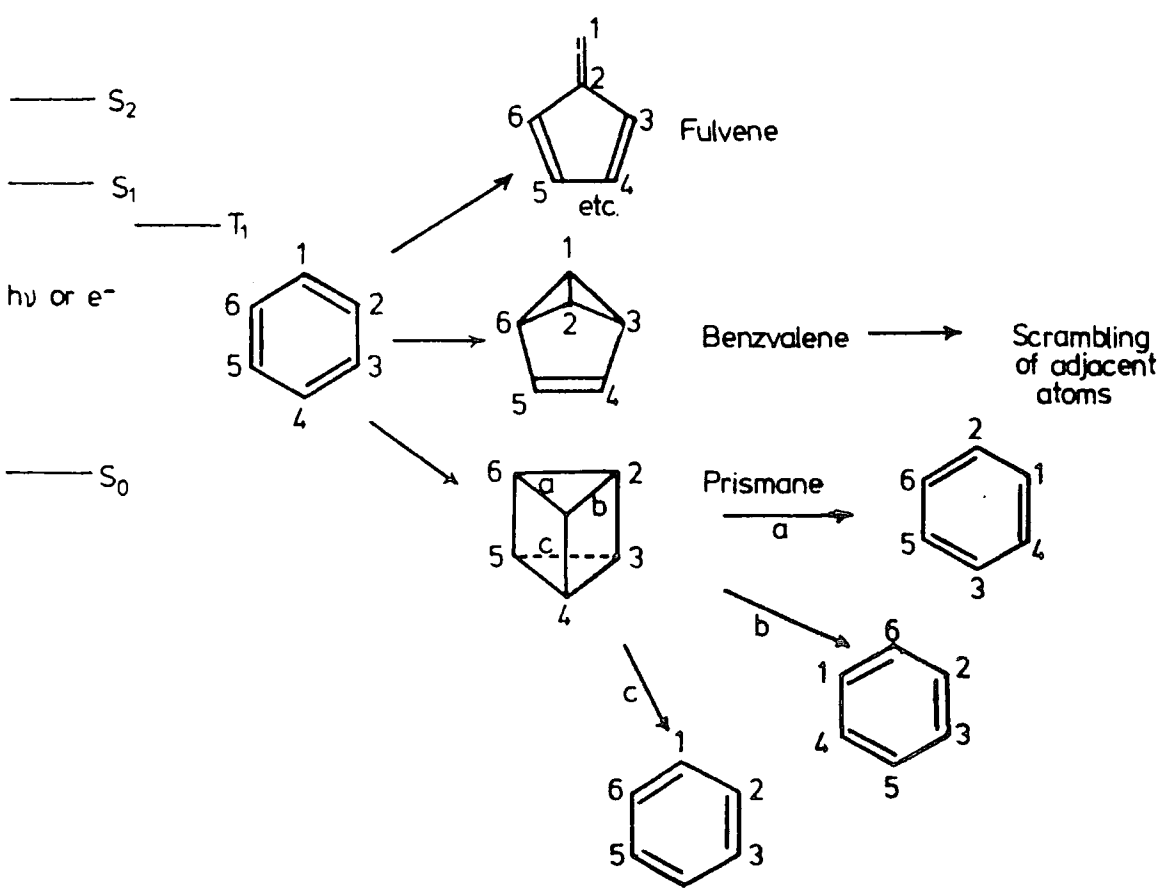

Highly substituted (prefluoro alkyl) derivatives of Dewar benzene, prismane and benzvalene have been reported,[219] however the available literature suggests that the tetrafluoro derivatives will have relatively short lifetimes and if formed in the plasma will almost certainly be involved as reactive intermediates in polymer synthesis. The energetically most favourable isomerization product from the lower excited states of benzenes is the fulvene ring system. A consistent overall picture of isomerizations involving the lower excited states of benzenes has been proposed on the basis of diradical species, related to Dewar benzene (pre-Dewar benzene) and fulvene (pre-fulvene) and this is indicated schematically in Figure 5.3.10.

Figure 5.3.10 Schematic of possible isomerization pathways from benzene to fulvene and prismane

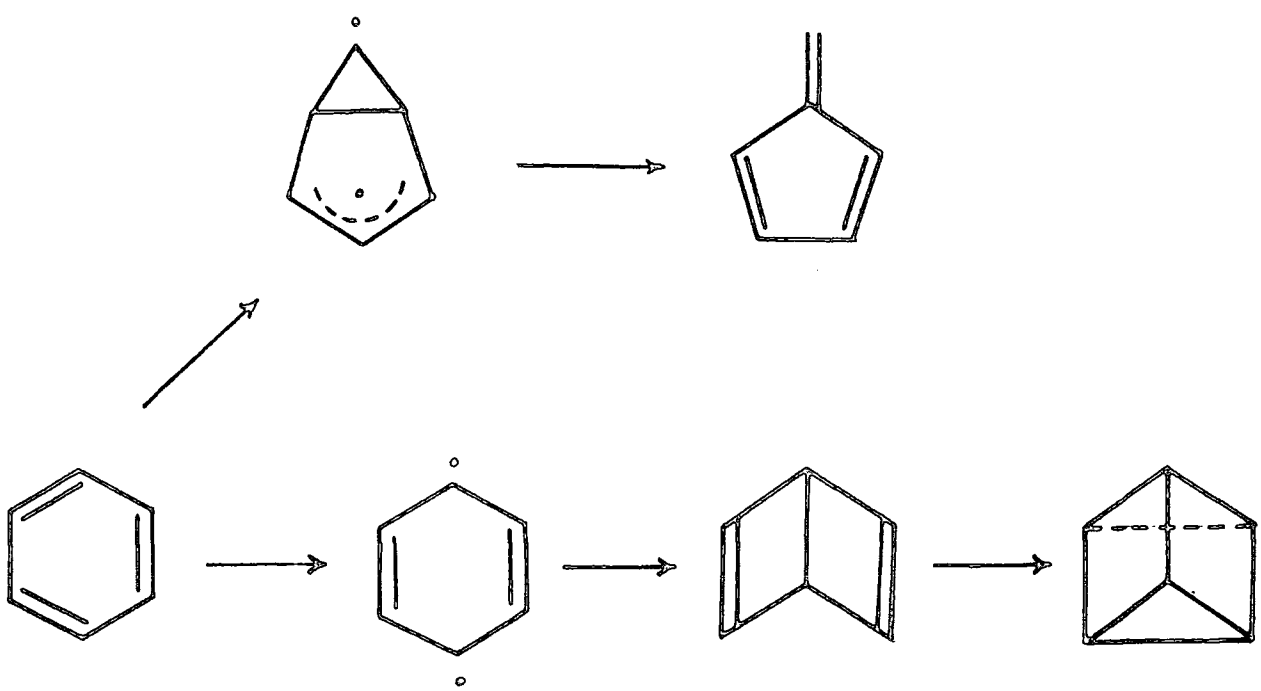

It should be noted that reactions involving pre-fulvene, fulvene and Dewar benzene intermediates provide a straightforward route to highly crosslinked materials by cycloaddition reactions. An example of such reactions are shown in Figure 5.3.11.

Figure 5.3.11 Potential reactions involving a pre-fulvene system which can lead to crosslinked product

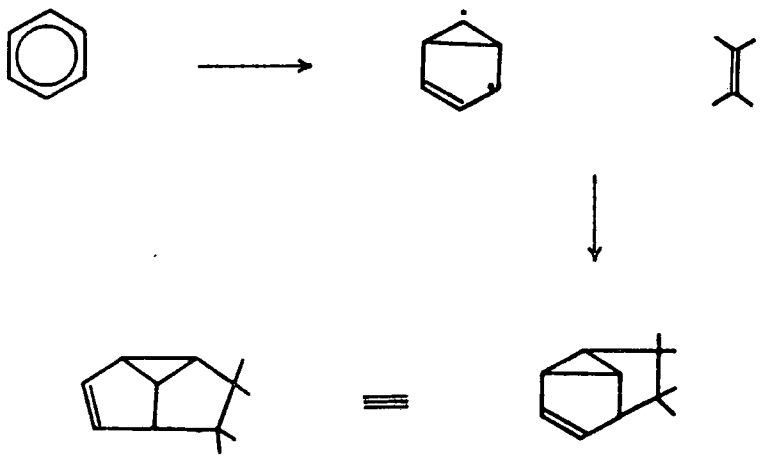

For the higher (>6.4 eV) excited state of benzenes (e.g. $^1E_{1u}$) ring fragmentation can lead to formation of isomeric hexadienynes and to fulvene and this is indicated schematically in Figure 5.3.12.

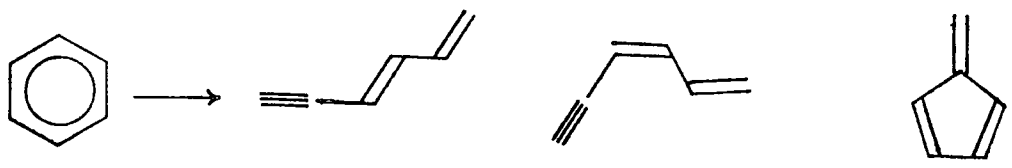

Figure 5.3.12 Isomerizations of aromatic systems involving excited states with excitation energies >6 eV.

Extensive studies[221] have been made of the ionized states of the isomeric tetrafluorobenzenes in the energy range from $\sim 9.5 - 15$ eV. The first ionization potential corresponding to removal of a pi electron is in all cases, approximately the same for the isomeric tetrafluorobenzenes ~ 9.4 eV and the A state also corresponding to removal of a pi electron is ~ 0.4 eV to lower energy. The B state, corresponding to removal of pi electron from the strongly bound a_{2u} orbital, is substantially higher in energy (~ 12 eV), however, the emission in the visible region of the spectrum for plasmas excited in the isomeric fluorobenzenes is attributed to the $\tilde{B} \longrightarrow \tilde{A}$ transition of the radical cations and indeed extensive studies have been made of the lifetimes of the B states as a function of substitution pattern.[216] The lifetimes of the B states is typically $\sim 10^{-8}$ sec. and it is clear that the excited states of both the neutral and cationic species have comparable lifetimes which are in each case somewhat shorter that the typical collision frequency in the plasma.†

In summary therefore, it is known that isomerization of positional isomers can occur via the excited state manifold in simple benzenes. Although the total electron flux, with energy above the ionization limit, is a small fraction of the total, cation states are undoubtely produced and the characteristic visible emission (~ 430 nm) from plasmas in the tetrafluorobenzenes shows that excited states of the ground state pi radical cations are present in the plasma. The lifetimes of excited states in the neutral and cation manifold are likely to be substantially shorter than the collision frequency and reactions leading to polymer synthesis are likely to be dominated by ground state species but involving the

---

† Estimates based on simple kinetic theory suggest a mean time between collisions of the massive species in the gas phase of $\sim 10^{-6}$ sec.

isomerized species (e.g. fulvene etc.). It is difficult to estimate the relative cross section for attachment, excitation and ionization, however since the plasma is overall electrically neutral, and since there is little literature data which would suggest facile rearrangement and polymerization routes via low energy negative ion states it seems likely that the reaction pathways involve reactive species derived from the excited state neutral and cation manifolds. The negative ion states nonetheless will play an important role in determining the overall energy distribution amongst the species in the plasma.

Since the greater proportion of the electron flux in the plasma is in the energy range below the thresholds for excitation and ionization, and since in the pressure regimes of interest (50 μ - 200 μ) the mean free path is short compared with the dimension of the reactor, it seems likely that neutralization (in Scheme A) would be of some importance since the cross section for these must be substantially higher than for electron attachment to the neutral species.

It is known from mass spectrometry studies of the isomeric tetrafluorobenzenes that extensive molecular rearrangement accompany ionizations and that migration of fluorine is facile (e.g. CF_3^+ is always observed as a rearrangement fragment ion in the conventional mass spectrometric analysis of the fluorobenzenes). Since the typical beam energy in a mass spectrometry experiment is substantially above threshold ($\backsim$70 eV), the observation of facile fluorine migration under these conditions is not strictly applicable to ions produced with a Boltzman equivalent temperature corresponding to embient as appropriate to the plasma. However mass spectra recorded at electron impact energies just above threshold ($\sim$18 eV) and chemical ionization using CH_4 and NH_3 show that the main fragmentation pathway of the parent ions of the isomeric tetrafluorobenzenes involved rearrangement

with migration of fluorine to produce the $C_2F_3^+$ ion (perfluorovinyl cation), (see Figure 5.3.13). There is therefore evidence for rearrangement and migration in both the neutral and cation manifolds.

Figure 5.3.13 An example of mass spectrum of tetrafluorobenzene isomers recorded at electron impact energies ~18 eV

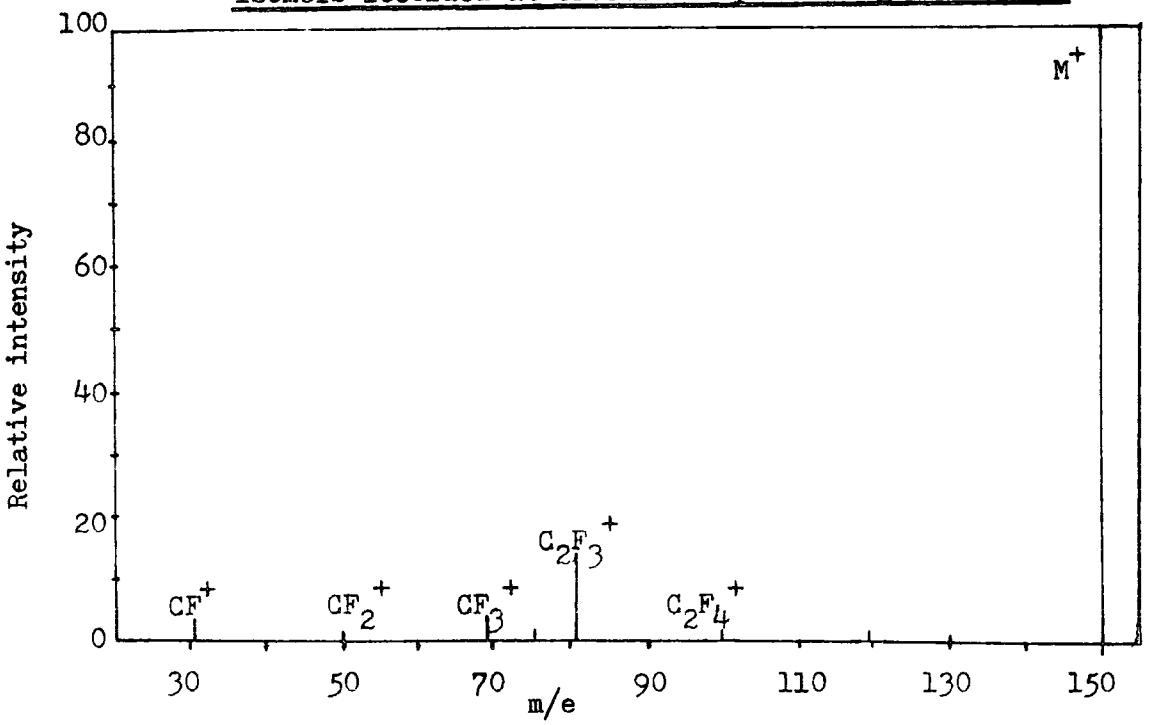

As it has been previously noted the polymerization process is extremely efficient since conversion of monomer to polymer is virtually 100% over the length of the typical reactor. Since the partial pressure in the gas phase of the monomer itself (as opposed to rearrangement products arising from the neutral excited state and cation manifolds) is likely to be high any reactions scheme must involved processes in which both rearranged intermediates and neutral ground state monomer are involved. In a previous paper [52] on reactions involving the isomeric difluoroethylenes it was pointed out that the stoichiometry of the polymers differs distinctively from that of the starting monomer in a sense which suggests that the reactive intermediates are based on species in which HF has been eliminated. A distinctive feature of the plasma polymers synthesized from the tetrafluorobenzenes however is the fact that the stoichiometry is

essentially the same as that of the monomer and this strongly suggests a polymerization route based on reactive intermediates which are skeletally isomeric with the starting monomer. The reason for this difference compared with the difluoroethylenes is twofold. Firstly there are no simple skeletally rearranged reactive intermediates on which a polymerization route could be based in the case of the difluoroethylenes and secondly the energetics for elimination of HF is substantially more favourable than in the benzene system. The significantly higher energy of a benzyne elimination as opposed to rearrangement is confirmed by detail SCF MO calculations which have been carried out in this work. The experimental data presented here for example suggests the elimination plays a relatively minor role in the overall reaction sequence since even at low pressure the C : F stoichiometry is close to that of the starting material (c.f. Figure 5.3.5). Figure 5.3.14 shows representative theoretical data for 1,2,3,4-tetrafluorobenzene. The possible tetrafluorofulvenes all have very similar energies and it seem likely therefore that isomerization of the tetrafluorobenzene skeleton to the fulvene skeleton via S_1 ($^1B_{2u}$) state will lead to a statistical distribution of all possible tetrafulvene isomers. (It should be noted that a similar energy level diagram for the cation states is qualitatively the same since the ionization potentials are all within $\pm$ 0.2 eV of one another). The isomeric tetrafluorohexadienynes also have somewhat similar energies which are still significantly below that for the elimination product (tetrafluorbenzyne and HF). With so many possible reactive species it is difficult to give a realistic discussion of reaction mechanisms giving rise to the plasma polymers but the main features can be accomodated relatively straightforwardly. Any mechanism must provide for the cross-linked nature of the polymer, for the appearance of CF_3 and CF_2 structural features, for the predominance of CF structural features and for the

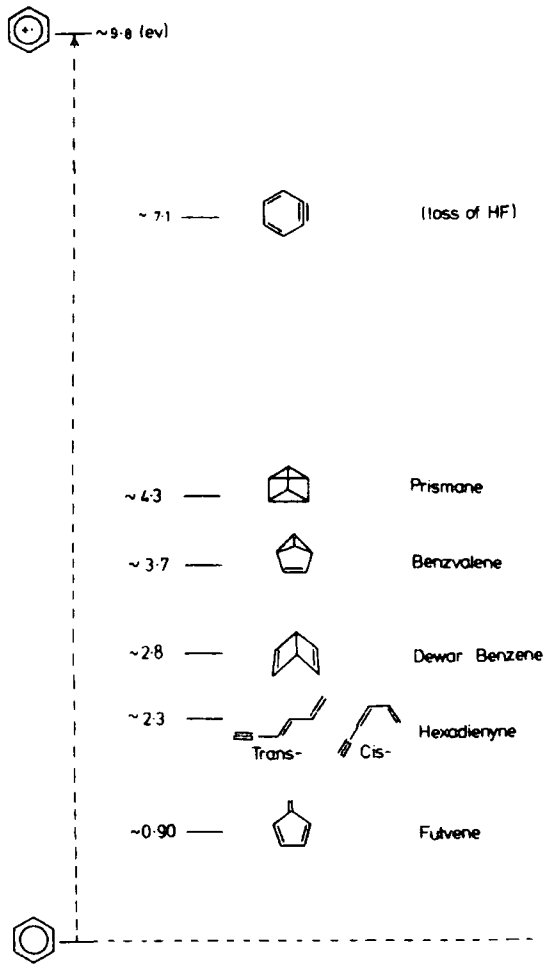

Figure 5.3.14 Relative energies of 1,2,3,4-tetrafluorobenzene and and possible isomeric species occurring in the R.F; computed using MNDO SCF MO formalism

retention of a degree of conjugative unsaturation (observed of shake-up satellites.).

The discussion presented above relates essentially to reactions occurring in the gas phase whereas except under special conditions, polymer formatioms is at the gas-solid interface either involving a substrate located in the gas stream or at the walls of the reactor. Reactions occurring at the surface will involved monomer derived reactants adsorbed at the surface and reactants diffusing to the surface from the plasma itself. The surface will be continuously bombarded with ions and

electrons in addition to electromagnetic radiation in the visible UV and vacuum UV.

The main reactions of interest as far as the tetrafluorobenzene ring system itself is concerned involves 1,2; 1,3 and 1,4 cycloaddition products. Hexafluorobenzene for example has been shown[219] to undergo both 1,2 and 1,3 addition to cis cyclo octene and similar reactions provide a route to cross linked product if the double bond component arises from an isomerized ring system such as benzvalene, fulvene or hexadienyne. Rearrangement of small (4 membered) rings containing CF_2 structural features can then give rise to CF_3 structural features. Typical reaction schemes are outline in Scheme B. Such reactions could also occur in the cation manifold, as could electrophilic reactions involving the radical cations of the tetrafluorobenzenes. From the data obtained in this work it is not possible to do other then point out the great complexity of possible routes to cross linked plasma polymer films containing the structural features identified by ESCA. However, the main conclusions from this systematic investigation of the inductively coupled R.F. plasma polymerization of the isomeric tetrafluorobenzenes presented in this chapter can be summarized as follows:

1. The isomeric tetrafluorobenzenes may be conveniently plasma polymerized in inductively couple R.F. plasma at ~100% conversion.
2. The gross structural features and compositions are closely similar over a range of W/FM parameter.
3. The isomer give rise to closely similar polymers and rates of deposition show only small variations.
4. The plasma polymers have stoichiometries essentially identical

to those of monomers.

5. The structural features present provide evidence for extensive molecular rearrangements.

Scheme B Representative cycloadditions involving the tetrafluorobenzene ring system and isomerized intermediates

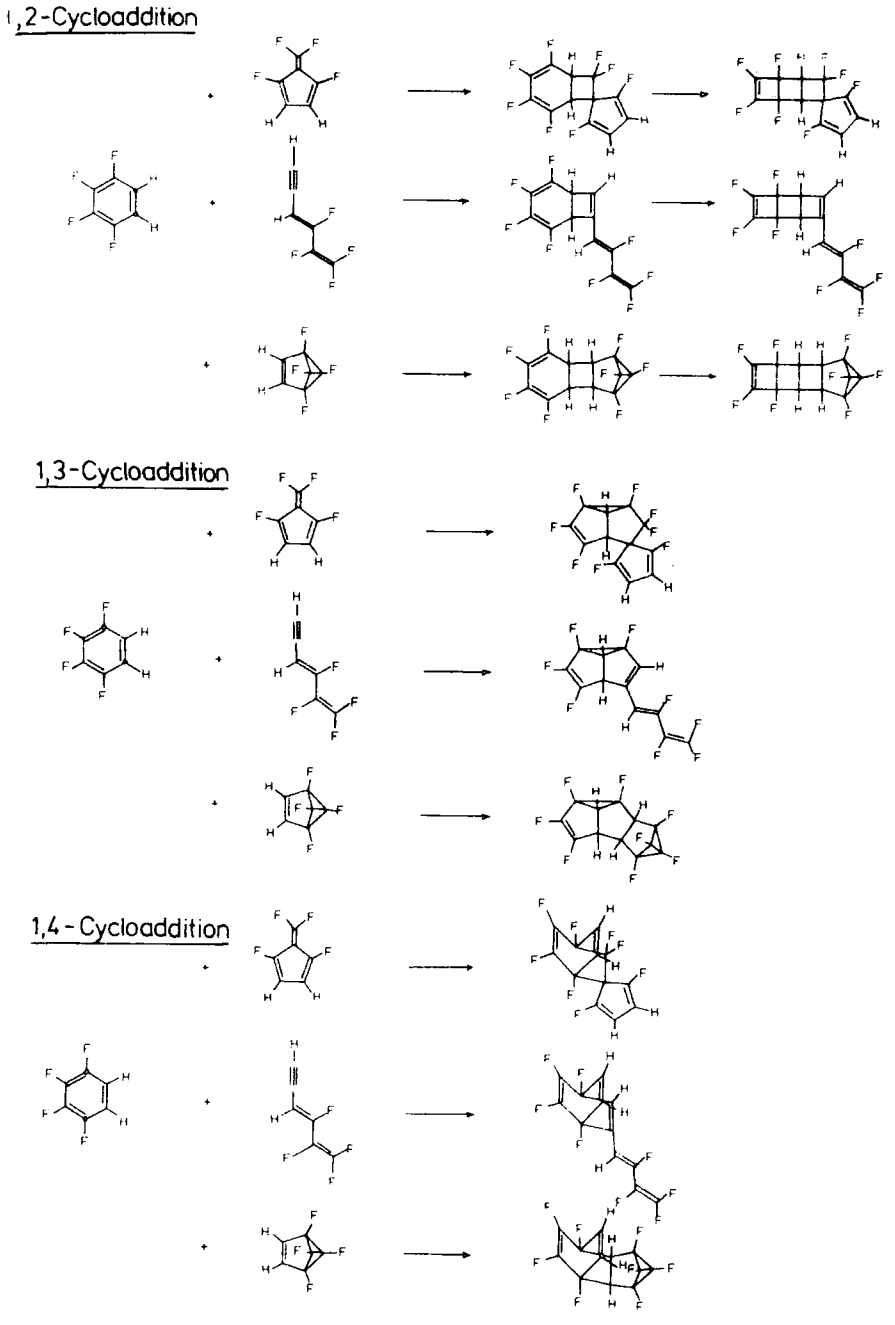

CHAPTER SIX

CHAPTER SIX

PLASMA POLYMERIZATION IV. A COMPARATIVE STUDY OF THE PLASMA POLYMERS PRODUCED FROM INDUCTIVELY CUOPLED PLASMAS EXCITED IN THE FLUOROBENZENES.

Abstract

An ESCA investigation has been made of the plasma polymers produced from the isomeric tri-, di- and monofluorobenzenes in inductively coupled plasma. Comparison is drawn with previously discussed data on perfluoro-, pentafluoro- and the isomeric tetrafluorobenzenes. The data reveals that extensive molecular rearrangement accompanies polymerization and that proportionality the C : F stoichiometry shows a decrease in fluorine content relative to the monomer in going from perfluoro- to monofluorobenzene. Internal stress, critical surface tensions and coefficients of friction are compared for the plasma polymers.

6.1 Introduction

The work presented in this chapter involves studies of the plasma polymers produced by exciting inductively coupled plasmas in the isomeric tri- and difluorobenzenes and in monofluorobenzene. The studies provided and interesting comparison with those previously described on perfluoro-, pentafluoro- and the isomeric tetrafluorobenzenes. Recent ESCA studies of fluoroalkenes [52,211] and perfluorinated aromatics,[206] alicyclics[212] and heterocyclic[223] have also started to provide the baseline information for the detailed understanding of the complex reaction sequence in a plasma. Therefore, the studies have allowed for the first time the link to be established between the structure of the monomer in which the plasma is excited and that of the polymer.

6.2 Experimental

The prime objective in this work has been to investigate some aspect of structure and bonding and rate of polymer deposition as a function of the operational parameters and of the starting 'monomer'. In order to gain quantitative information on the relative rates of polymer deposition for polymer films deposited in the glow region, experiments have been carried out under closely similar conditions for the series of variously substituted fluorobenzenes. The work described has employed the same polymerization configuration, (reactor A) as has been described previously studies of perfluoro-, pentafluoro- and the isomeric tetrafluorobenzenes.

In the measurement of rates of polymer deposition, the polymer films were deposited onto the appropriate substrates located at the bottom and in the middle of the coil region of the reactor. Thin polymer films

deposited onto clean gold substrates were employed for ESCA analysis. Deposition onto Al foil (2 x 1 cm.^{2}) substrates was employed for determination of the rate of deposition, by measuring the weight increase of the Al foil using a CAHN electromicrobalance. However, for contact angle and coefficient of friction (COF) studies, the polymer films were deposited onto HDPE (high density polyethylene) substrates and were used soon after preparation. The critical surface tension was determined by analysis[64] of the data obtained from the measurement of contact angles with water, glycerol, formamide and methylene iodide using a travelling microscope teachnique (see Appendix 3). The determination of the dynamic COF of polymer films involved a polished stainless steel platen as the counter surface to that of the plasma polymer deposited onto HDPE, employed an Instrumentors Slip/Peel Model SP-101. For the internal stress studies, the deposition of polymer films onto a flexible substrate LDPE, cause the substrate to curl. The radius of the curling substrate was measured using a travelling telescope with associated vernier scale.

ESCA spectra were recorded on an AEI ES200 A/B spectrometer with $Mg_{K\alpha_{1,2}}$ photon source. The $Au_{4f_{7/2}}$ level at 84.0 eV and the small amount of hydrocarbon contamination present at 285.0 eV were utilized for energy calibrations. Integration of spectra was accomplished with a DuPont 310 analog curve resolver. Binding energies and area ratios are quoted to $\pm$0.1 eV and $\pm$ 5.0% respectively. It should be noted that the deconvolutions presented represent envelopes that contain a number of species of similar electronic environment. These are evidenced by the broad nature of peaks typically 1.9 eV to 1.4 eV, whereas a carbon core level in a regular polymer will have FWHM of ca. 1.3 eV.[224]

The fluorobenzene starting monomers were obtained from Bristol Organic Ltd. and were shown to be pure by mass spectroscopic g.l.c. Prior to used all the starting monomer were subjected to extensive freeze thaw cycles for degassing.

6.3 Results and Discussion

6.3.1 Isomeric trifluorobenzenes

The plasma polymerizations of 1,2,4- and 1,3,5-trifluorobenzenes have been investigated at a pressure of 200 μ and power inputs of 5 W and 10 W in reactor configuration A. The corresponding core level spectra are shown in Figure 6.3.1. Before detailing the component analysis it is of interest to note the particular difficulties of obtaining C : F stoichiometries reliably from the C_{1s} line profiles in the absence of further information (e.g. stoichiometries derived independently from the C_{1s} : F_{1s} intensity ratios.)

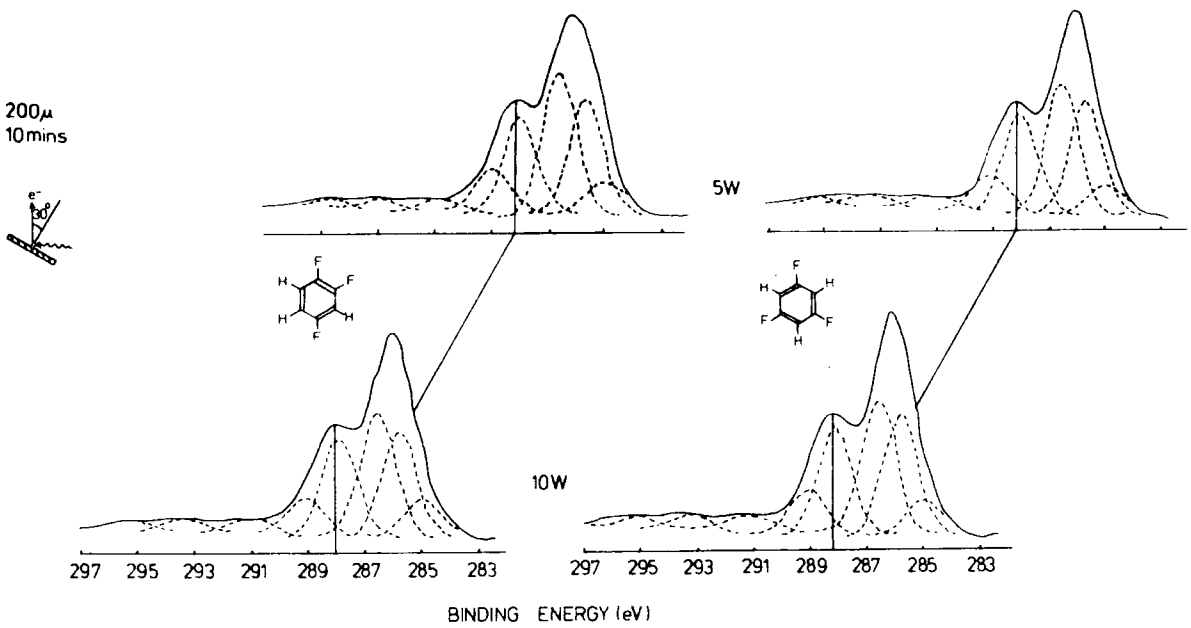

Figure 6.3.1 C_{1s} core levels of plasma polymerized 1,3,5- and 1,2,4-trifluorobenzenes prepared at 5 W and 10 W dischages powers.

For the more highly fluorinated systems[205,225] (e.g. C_6HF_5) the main component in the C_{1s} levels corresponds to $\underline{C}F$ structural features at a binding energies of ~288.5 eV with corresponding shake-up structure due to $\pi^* \leftarrow \pi$ excitations for vinylic $\underline{C}F$ groups at 296 eV well clear of components arising from $\underline{C}F_3$ and $\underline{C}F_2$ structural features (at 294 eV and 292 eV respectively). As will become apparent in a later section for the lightly fluorinated monomers (e.g fluorobenzene) the fluorine content of the plasma polymer is so low that β substituent effects are relatively unimportant and $\underline{C}F$ component at 288 eV and the main component corresponding to -$\underline{C}$-CF- environments at 285.5 eV lead to shake-up structures some 7 eV higher which do not confuse the assignment of direct photoionization from $\underline{C}F_2$ and $\underline{C}F_3$ structural features which are in any case in very low abundance. For the trifluorobenzenes however shake-up from both $\underline{C}F$ and -$\underline{C}$-CF structural features overlap with the $\underline{C}F_3$ and $\underline{C}F_2$ regions and in consequence the C : F stoichiometries obtained from the C_{1s} line profile depend on the assignment of the relative intensities of shake-up and direct photoionization components.

The spectra in Figure 6.3.1 reveal the extensive molecular rearrangement accompanying polymerization and even without the aid of the component analysis it is clear that the isomers give essentially the same polymer and there is little dependence of the structure on the power input. The assignment of the C_{1s} components in increasing binding energy are $\underline{C}H$ 285.0 eV; $\underline{C}$-CF 285.6 eV; $\underline{C}$-CF_n 286.6 eV; $\underline{C}F$ 288.2 eV; $\underline{C}F$-CF_n 289.1 eV; $\underline{C}F_2$, $\underline{C}$-CF , $\pi^* \leftarrow \pi$ 291.4 eV; $\underline{C}F_3$, $\underline{C}$-CF_n, $\pi^* \leftarrow \pi$ 293.5 eV; $\underline{C}F$, $\pi^* \leftarrow \pi$ 295.5 eV.

Assigning the whole of the components centred around 291.4 eV and 293.5 eV to direct photoionization from $\underline{C}F_2$ and $\underline{C}F_3$ groups respectively, gives rise to computed stoichiometries for both isomers of $C_1F_{0.49}$. However from the known photoionization cross sections the analysis of the C_{1s} : F_{1s}

intensity ratios give a stoichiometry of $C_1F_{0.4}$ and this indicates that $\sim$50% of the signal intensity assigned to the $\underline{C}F_2$ and $\underline{C}F_3$ components originates in $\pi^* \leftarrow\!\!- \pi$ shake-up satellites from the main components at lower binding energy arising from $\underline{C}F$ and $\underline{C}$ structural features. Micro-analysis of samples removed from the reactor after deposition for 10 min. provided a C : F stiochiometry of 1 : 0.4 indicating the homogeneity of the polymer films.

Rates of deposition have been measured by weight increase of polymer film deposited for a given period of time (10 min.) onto Al foil by means of a capacitance microbalance. For 1,2,4-trifluorobenzene the rates of deposition at 5 W and 10 W at 200 μ were 0.015 and 0.017 mg.cm.$^{-2}$ min.$^{-1}$ respectively. For comparison purposes the rates of deposition for the 1,3,5-trifluorobenzene are 0.013 and 0.014 mg.cm.$^{-2}$min.$^{-1}$ Within experimental error these are the same or indicate at most a very small dependence of rate of deposition on isomeric structure.

6.3.2 Isomeric Difluorobenzenes

The plasma polymerization of the isomeric difluorobenzenes has been studied in reactor A at a pressure of 200 μ and input powers of 5 W and 10 W. As a starting point Figure 6.3.2 shows the core level spectra for the 1,4-difluorobenzene plasma polymer at 2 take off angles (30^o and 70^o). The C_{1s} spectra show components at 285 eV, 285.7 eV, 286.5 eV, 288.1 eV 289 eV, 291.1 eV, 293.5 eV and 295.2 eV corresponding to $\underline{C}H$, $\underline{C}{=}CF$, $\underline{C}{=}CF_n$, $\underline{C}F$, $\underline{C}F{-}CF_n$, $\underline{C}F_2$, $\underline{C}F_3$ and $\pi^* \leftarrow\!\!- \pi$ shake-up. The small relative increase in intensity of the component at 285 eV at higher take off angle indicates that some at least of the $\underline{C}H$ component at 285 eV arises from very low level of surface contamination. Comparison of Figure 6.3.1

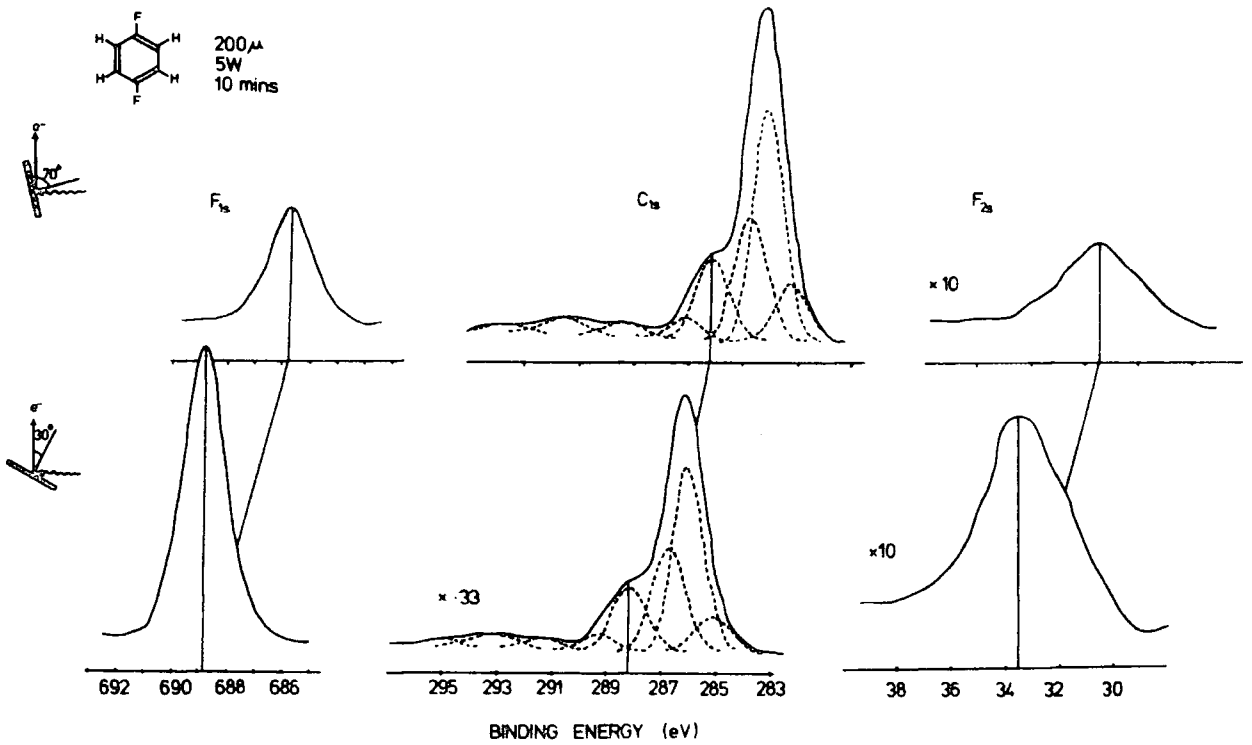

Figure 6.3.2 C_{1s}, F_{1s} and F_{2s} levels of plasma polymerized 1,4-$C_6H_4F_2$.

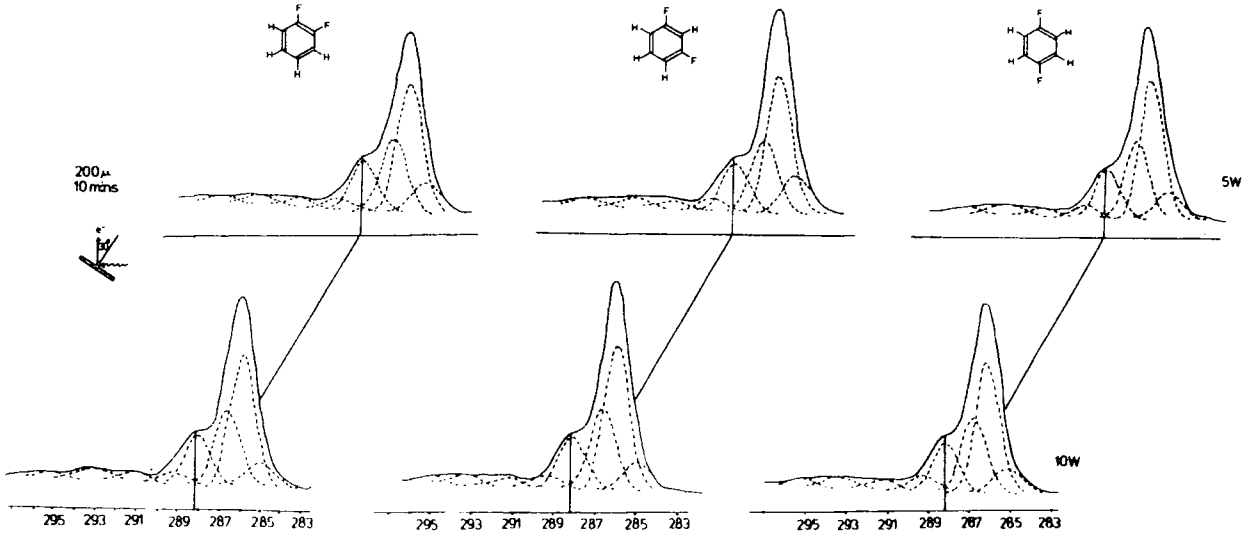

Figure 6.3.3 C_{1s} levels (at a take-off angle of 30°) of plasma polymerized difluorobenzene isomers

and 6.3.2 reveals the lower fluorine content. The C_{1s} spectra for the polymer films produced from the isomers shown in Figure 6.3.3 shows the striking similarity of the gross chemical structure of the films. Analysis of the C_{1s} and F_{1s} area ratio reveals that the stoichiometry of the films C : F 1 : 0.25 is lower in fluorine than the starting monomer (C : F 1 : 0.33). Analysis of the bulk samples removed from the reactor after 10 min. of deposition time provided a C : F stoichiometry of 1 : 0.23 in excellent agreement with that provided by ESCA. The close similarity in the plasma polymerization characteristics for the isomeric difluorobenzenes is also apparent from the measured rates of deposition (Al foil, capacitance microbalance) and these are shown in Table 6.3.1. These are somewhat comparable to those recorded for the trifluoro- isomers.

The data therefore indicate that polymerization involves a loss of fluorine and the spectra reveal evidence of the extensive molecular rearrangement accompanying the polymerization process.

Table 6.3.1

Rate of deposition (mg.cm.$^{-2}$min.$^{-1}$)

Difluorobenzene isomers	200 μ	
	5 W	10 W
1,2-	0.013	0.014
1,3-	0.008	0.013
1,4-	0.012	0.014

6.3.3 Monofluorobenzene

In the particular case of monofluorobenzene a rather more extensive study has been made of core level spectra as a function of the operating parameters. Thus for an input pressure of 100 μ studies have been made in the pawer range 5 W -- 35 W, whilst at 200 μ the study has cover the 5 W -- 45 W power range.

Considering firstly the C_{1s} core level data for polymers prepared at a pressure of 200 μ and input powers in the range 5 W -- 45 W. The data in Figure 6.3.4 reveals several interesting features. Firstly the level of fluorine retained in the polymer is substantially below that of the monomer. This most readily apparent from the low intensity of $\underline{C}F$ components $\sim$288 eV and from the F_{1s} signals. Secondly the low level of fluorine precludes the possibility of an extensive contribution from $\underline{C}F_2$ and $\underline{C}F_3$ structural features, and the broad component centred $\sim$292.5 eV is therefore clearly assigned as a $\pi^* \leftarrow \pi$ shake-up component of the main ($\underline{C}H$) peak centred $\sim$285 eV. Thirdly the relative intensity of this component decreases at higher power indicating loss of conjugative unsaturation. Thus at 5 W the shake-up component contributes 2% of the intensity of the main peak at 285 eV, and this may be compared with an intensity of $\sim$6% for the starting monomer. By contrast at 45 W the shake-up intensity has been decreased to $\sim$5%. This is the first real evidence for the dependence of the conjugative structural component of plasma polymer on the operating parameters of the plasma.

This becomes even clearer in considering the data displayed in Figure 6.3.5 which pertains to plasma polymerization at 100 μ and input powers in the range 5 W -- 35 W. At 5 W input power the shake-up intensity represents $\sim$0.5% of the main component at 285 eV, however at 35 W the intensity has all but disappeared.

Figure 6.3.4 C_{1s} levels of plasma polymerized fluorobenzene prepared at 5, 15, 25, 35, 45 W discharge powers and a pressure of 200 μ

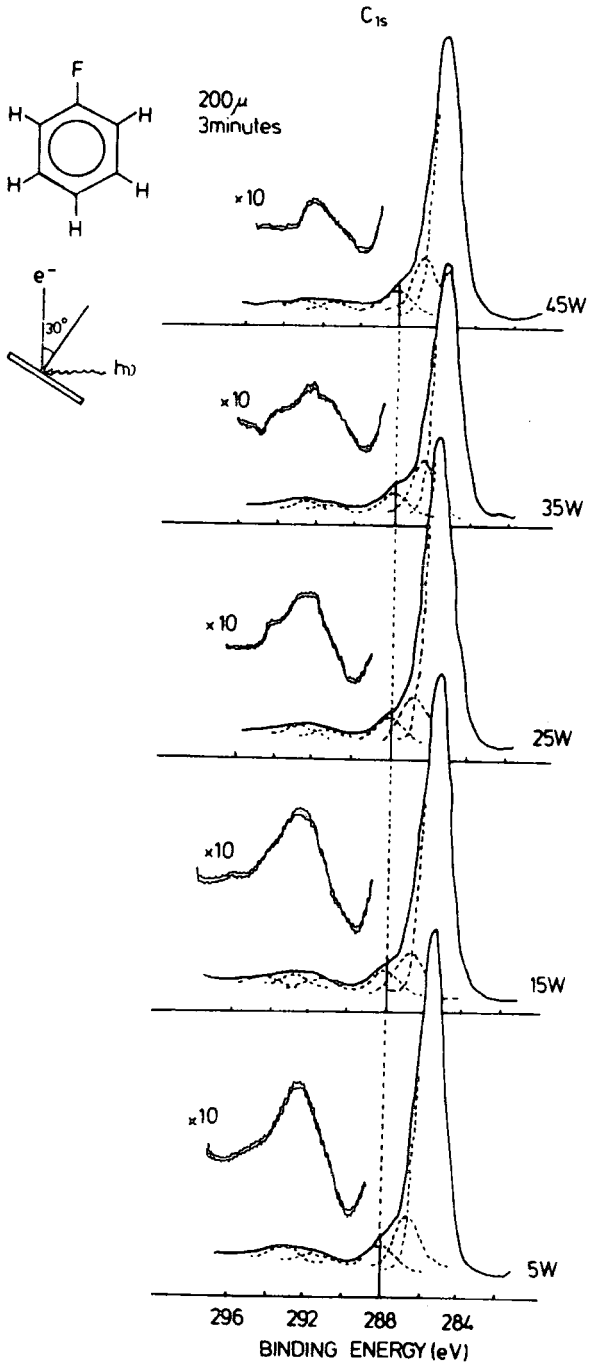

Figure 6.3.5 C_{1s} and F_{1s} levels of plasma polymerized fluorobenzene prepared at 5, 15, 25, 35 W discharge powers and a pressure of 100 μ for a deposition time of 4 minutes

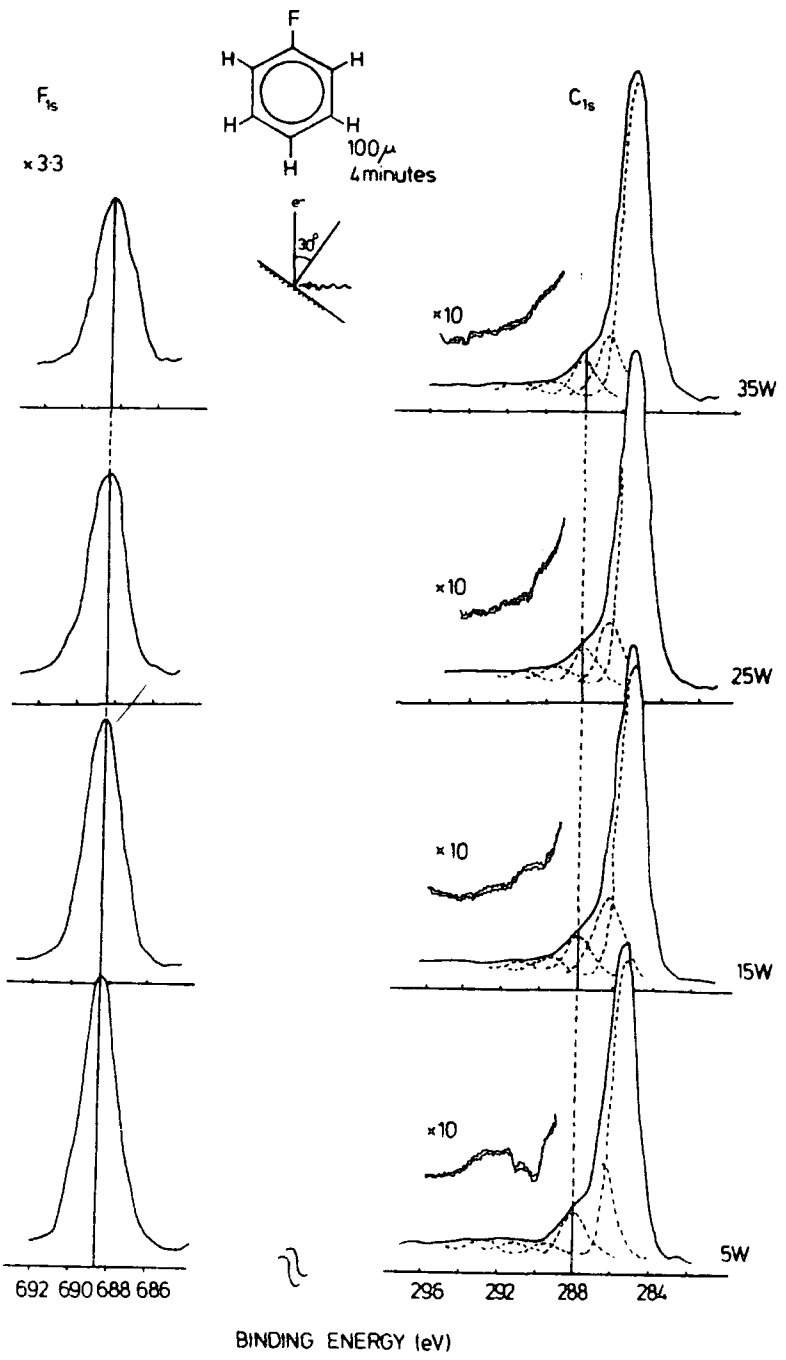

At 200 μ the C_{1s} : F_{1s} intensity ratio provides a stoichiometry of 1 : 0.06 in excellent agreement with that determined from the components of C_{1s} levels (1 : 0.05). The corresponding data at 100 μ indicates a slight tendency for a greater fluorine content at the lower pressure and this is perhaps most evident from the slightly increased contribution from the CF component at ~288 eV. The data also indicates a small increase in fluorine content at higher powers (e.g. at 200 μ C : F 1 : 0.06 and 1 : 0.05 for power inputs of 35 W and 5 W respectively.) Microanalysis which tends to be somewhat inaccurate for such low fluorine contents provides a typical bulk stoichiometry of 1 : 0.1. This compares with the stoichiometry of the monomer of 1 : 0.17.

The wide range of power inputs provides considerable variation in the W/FM parameter, and allows the direct investigation of rate of deposition (Al foil, capacitance microbalance) as a function of power and this is shown in Figure 6.3.6. The maximum in the rate of deposition at

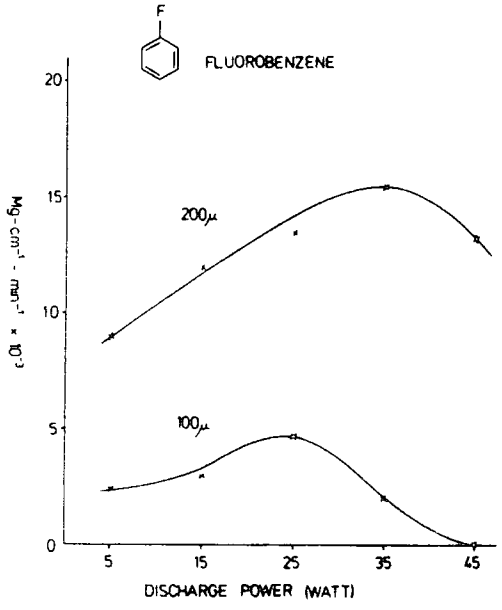

Figure 6.3.6 Deposition rate (mg.cm.$^{-2}$min.$^{-1}$) as a function of power and pressure.

100 μ occurs at lower power than at 200 μ confirming the general form of the W/FM versus rate of deposition scheme.

6.3.4 Comparison of the Data for the Fluorobenzenes

(1) Stoichiometries

Previous studies[205,225,228] have described detailed investigation of the plasma polymers synthesized from perfluoro-, pentafluoro- and the isomeric tetrafluorobenzenes and a comparison is therefore possible for the relative C : F stoichiometries for the plasma polymers compared with the starting monomers. This is most conveniently shown in graphical form (Figure 6.3.7). Whilst for the highly fluorinated systems the stiochiometry of the polymer is closely similar to that of the starting monomer, there is a loss of fluorine for the less highly fluorinated monomers.

Figure 6.3.7 Average ratio of C : F stoichiometries polymer/monomer

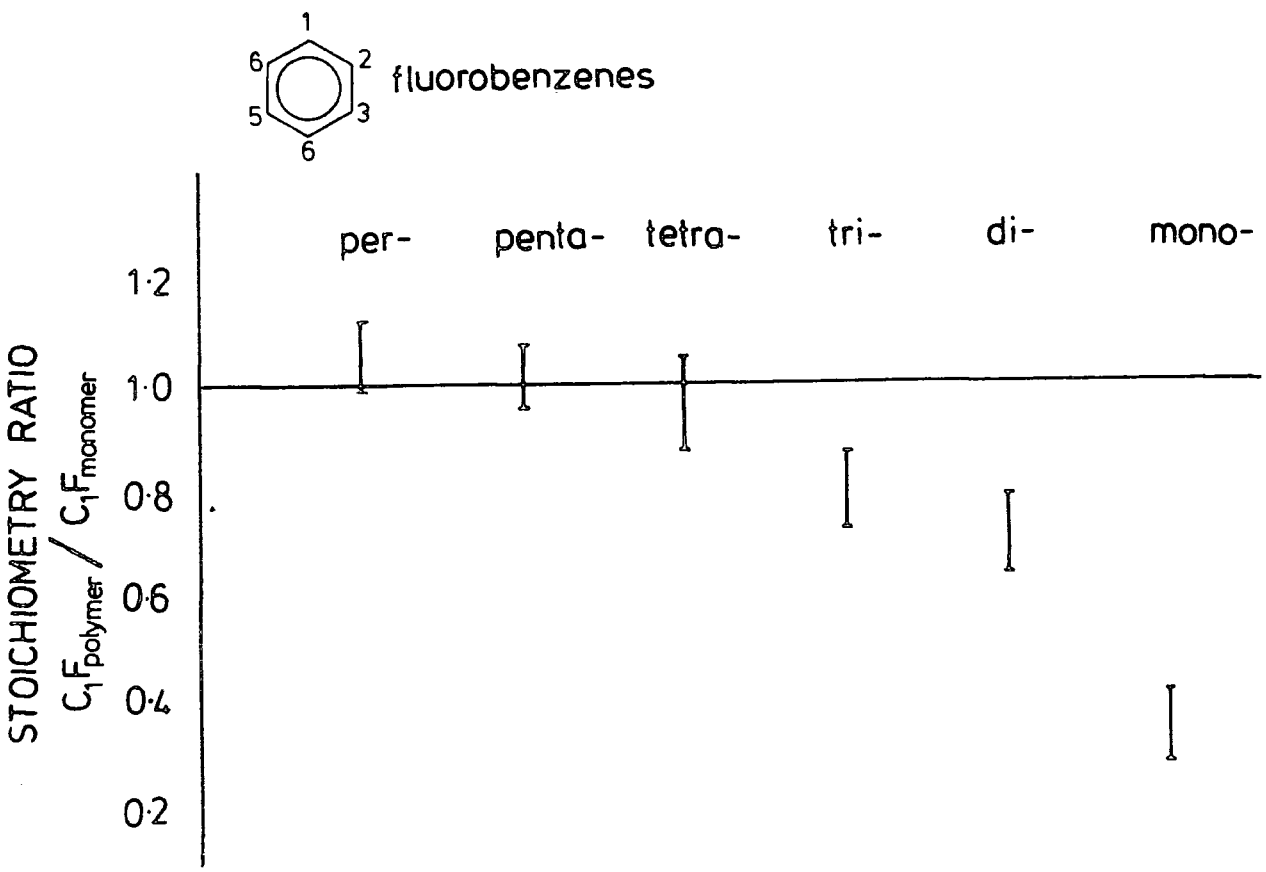

It is also interesting to note that the FWHM of the components of the C_{1s} levels and of the F_{1s} levels decreases significantly in going from the more to less highly fluorinated system as is apparent from the spectra in Figure 6.3.8. This is readily understandable in terms of the range of sites of a given type e.g. $\underline{C}F_2$ depending on the number of fluorine substituents.[226-227] Previous studies on simple prototype system have shown that under the same instrumental conditions the C_{1s} and F_{1s} levels for a system with a single environment (e.g. perfluorobenzene) have FWHM of 1.4 eV and 1.9 eV respectively. The relevant data are displayed in Table 6.3.2. The shift in binding energy for F_{1s} levels in covelently bond fluorocarbon is typically small, however the decrease in binding energy in going to tht lightly fluorinated system is evidenced by the shift in the centroid by $\sim$1.0 eV and this also indicated in Table 6.3.2.

Table 6.3.2

The FWHM and binding energy of F_{1s} and components of C_{1s} levels for plasma polymerized fluorobenzene monomers

Starting monomer (fluorobenzenes)	F_{1s} binding energy ($\pm$ 0.1 eV)	FWHM (eV) F_{1s}	Deconvolution FWHM (eV); C_{1s}
per-	689.6	2.2	1.9
penta-	689.4	2.15	1.8
tetra-	689.1	2.1	1.6
tri-	688.9	2.0	1.5
di-	688.7	1.95	1.4
mono-	688.6	1.9	i.4

Figure 6.3.8 C_{1s}, F_{1s} and O_{1s} levels of plasma polymerized fluorobenzenes prepared under the same conditions of 10 W discharge power and 200 μ pressure

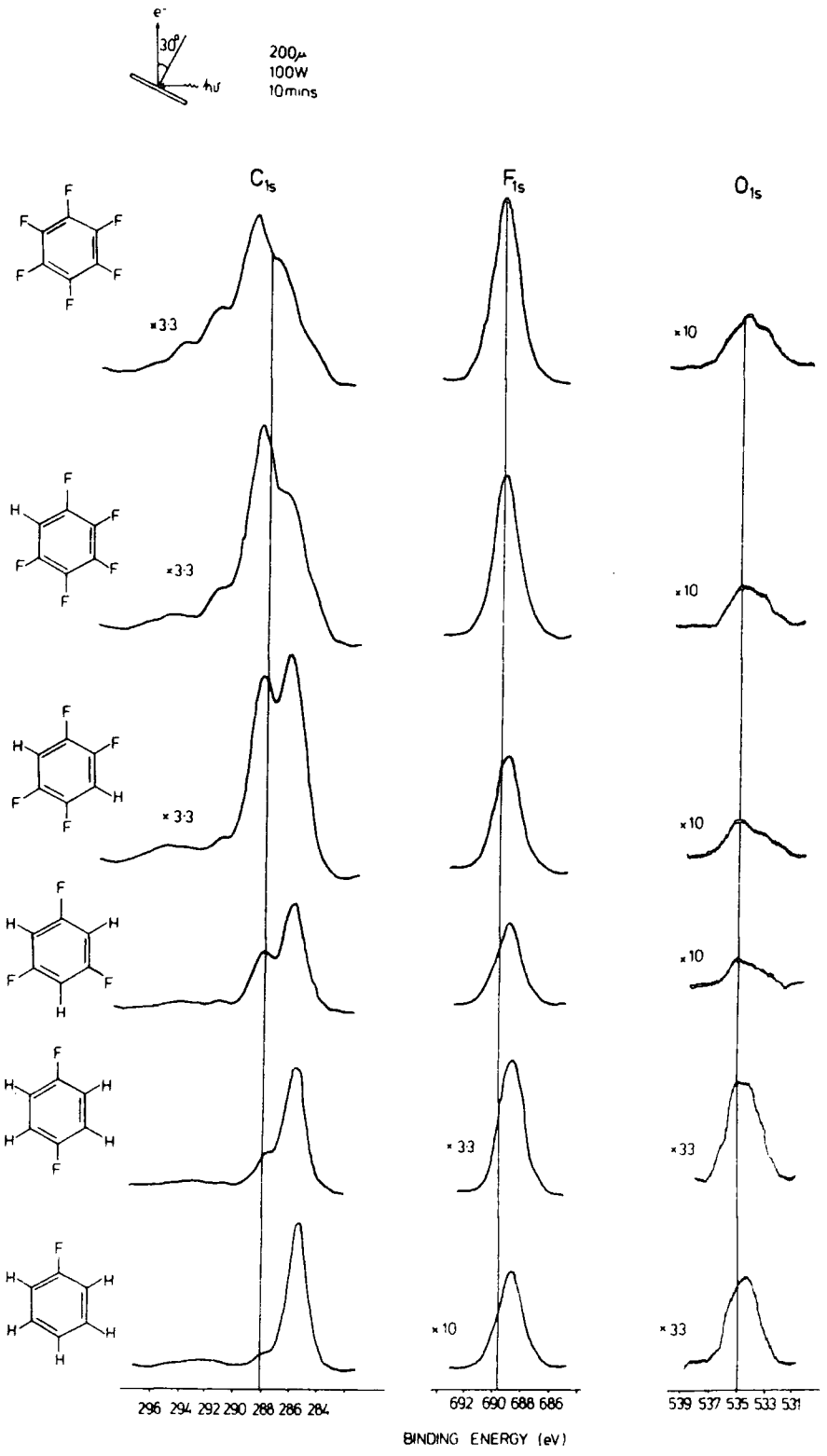

(2) Rates of Deposition

The row data for rates of deposition under comparable ranges of W/FM parameter for all of the fluorobenzenes is collected in Figure 6.3.9.

Figure 6.3.9 Deposition rate vs. W/FM parameter

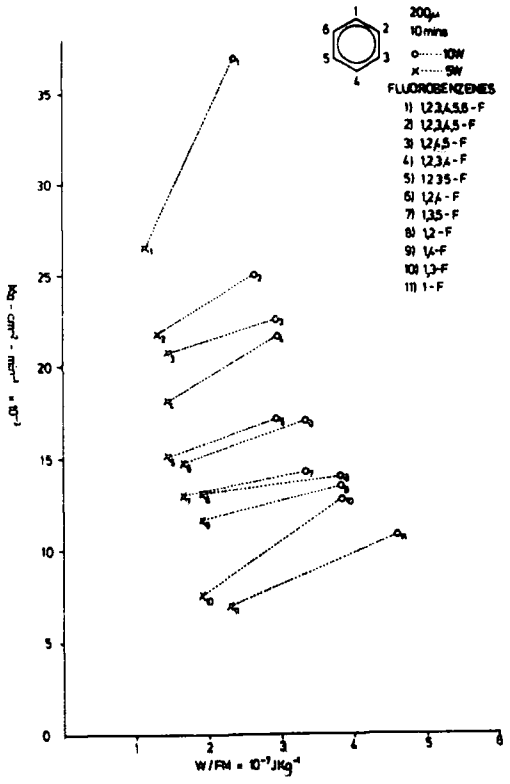

This would indicate a higher rate of deposition for the more highly fluorinated systems however, the difference is not as large as might appear at first sight since the densities for the plasma polymer films deposited from the perfluoro- and monofluorobenzenes differ significantly (viz. $\sim$1.8 versus $\sim$1.4 gm. cm.$^{-3}$).

(3) Critical Surface Tensions

By measuring appropriate contact angles for liquids of different surface tension it becames possible to extrapolate a critical surface tension[64] for the plasma polymer films prepared from the isomeric fluorobenzenes. This is shown in Figure 6.3.10.

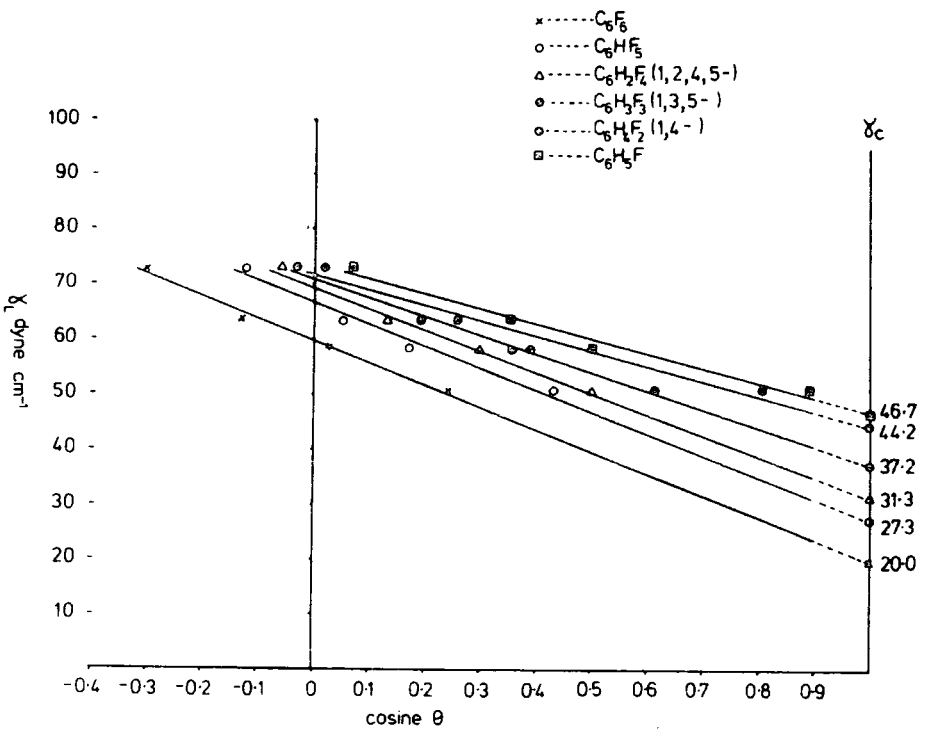

Figure 6.3.10 Surface tension γ_L of various liquids (dyne cm.$^{-1}$) vs. cosine of contact angle (θ) for plasma polymerized fluorobenzenes prepared at 10 W discharge power and a pressure of 200 μ

For the perfluoro-, pentafluoro- and tetrafluoro- based systems of C : F stoichiometry 1 : 1; 1 : 0.80 and 1 : 0.65 respectively the corresponding critical surface tensions of 20 dyne cm.$^{-1}$; $\sim$ 27 dyne cm.$^{-1}$ and $\sim$ 31 dyne cm.$^{-1}$ are consistent with a proportion of $\underline{CF}_3$ and $\underline{CF}_2$

structural features. For comparison purposes the corresponding figures for PVF_2 and PVF of C : F stoichiometry 1 : 1 and 1 : 0.5 are 25 dyne $cm.^{-1}$ and 28 dyne $cm.^{-1}$ respectively. For the lightly fluorinated systems the critical surface tension is significantly higher than for high density polyetylene. In this connection it is worth noting that the low level of oxygen signal observed in the ESCA spectra remains essentially constant across the series from perfluoro to monofluorobenzene and corresponding to ~2% of oxygen involved in the functional groups in the statistical sample provided by ESCA. From studies of the corona and plasma oxidative functionalization of polymer surfaces [22] it seems unlikely that this would substantially modify the critical surface tension at least for the more highly fluorinated systems.

(4) Internal Stress

Thick polymer films $> 1\ \mu$ prepared by plasma techniques, often tend to be brittle. This is an interesting feature which may be related to the internal stress which build-up in the films during plasma polymerization. It is of interest therefore to deposit plasma films on a flexible substrate in order to investigate the internal stress monitored in terms of a curling force. [229]

In this study, a piece of (1 x 8 $cm.^{-1}$) LDPE (thickness, D = 8×10^{-3} cm. and Young's modulus, E = 10^9 dyne $cm.^{-2}$) was used as the substrate and the plasma polymer deposition was then carried out for different time period. The film thickness was estimated from the known rate of deposition of the polymer as has previously been described in the experimental section.

The curling forces, given as $\delta_s \cdot d$ (where δ_s is the internal stress and d is the thickness) for plasma polymers prepared from the

fluorobenzenes (perfluoro- ; 1,2,4,5- and 1,4- isomers) were calculated using the empirical equation of Yasuda and co-workers.[229]

$$\delta_s \cdot d = ED^2/6R$$

where δ_s is the stress in the film

d is the film thickness,

E is the Youngs' modulus,

D is the thickness of substrate, and

R is the radius of curling substrate.

The curling forces as a function of the film thickness for the three plasma polymers studied are shown in Figure 6.3.11. This shows that the curling force in the polymer films increases with increasing thickness. It is interesting to note however, that up to a thickness of $\sim$ 6,000 Å the curling force increases linearly with thickness.

Figure 6.3.11 Curling force (δ_s.d) vs. thickness (d)

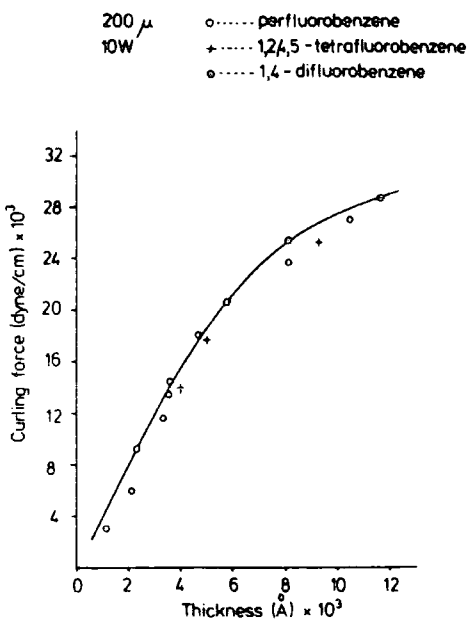

Further increase of the film thickness ($>$ 6,000 Å) shows a deviation from this linear dependence on thickness. This may be attributed to the stress in the films, where at thickness $<$ 6,000 Å the stress is a material constant, but further increases of film thickness tends to decrease the stress in the film, which implies that the film is starting to crack. Also apparent from Figure 6.3.11 is the fact that within experimental error, the stress in the plasma films derived from the three fluorobenzene monomers is essentially the same. This may also imply that the films have relatively the same morphology. At a thickness of $\sim$ 4,000 Å the stress in the plasma films prepared in this work is $\sim 3.7 \times 10^8$ dyne cm.$^{-2}$ This may be compared with the results obtained by Yasuda and co-workers[229] for plasma polymer films of thickness 4,000 Å prepared from a variety of starting 'monomers'; thiophane 2.7×10^8 dyne cm.$^{-2}$; acetylene 3.8×10^8 dyne cm.$^{-2}$; pyridine 5.2×10^8 dyne cm.$^{-2}$; and furan 7.0×10^8 dyne cm.$^{-2}$

(5) Coefficient of Friction

Dynamic coefficients of friction have been measured for the plasma polymer prepared as samples deposited on high density polyethylene strips; polished stainless steel being the counter material. The measured coefficients are displayed in Table 6.3.3 and represent the time average weightings over 10 seconds. For comparison purposes data are also included for PTFE, PVF_2, HDPE, LDPE and nylon. In general the coefficient for the plasma polymes are remarkably similar and fall between those for PVF_2 and HDPE. This almost certainly arises from the similarities in surface morphology.

Table 6.3.3

Coefficient of friction measured for time average weightings over 10 sec.

Plasma polymerized polymer 200μ, 10 W		Conventional polymer	
C_6F_6	0.18	PTFE	0.08
C_6HF_5	0.20	PVF_2	0.18
$C_6H_3F_3$ (1,3,5-)	0.19	HDPE	0.10
C_6H_5F	0.17	LDPE	0.28
		Nylon	0.32

(6) General comments on the overall polymerization processes

The previous Chapter Four has drawn attention to the variety of relative species likely to be present in a plasma excited in a fluorobenzene monomer. Thus from the lowest excited states in the neutral manifold pathways exist for ring isomerization via Dewar benzene, prismane and benzvalene[219] structures and this could well account for close similarities in polymerization products from isomeric structures (viz. the tetrafluoro-, trifluoro- and difluorobenzene derivatives). The previous Chapter Four on tetrafluorobenzene isomers has reported the MNDO[215] SCF MO computations for the neutral system which indicated the relatively small differences in heats of formation between the benzene ring system and the isomeric fulvene and hexadienyne structure which are available

from various excited states of the benzene system. Such computations have been extended to the cation manifold and the results of these MNDO SCF MO studies are indicated in Figure 6.3.12.

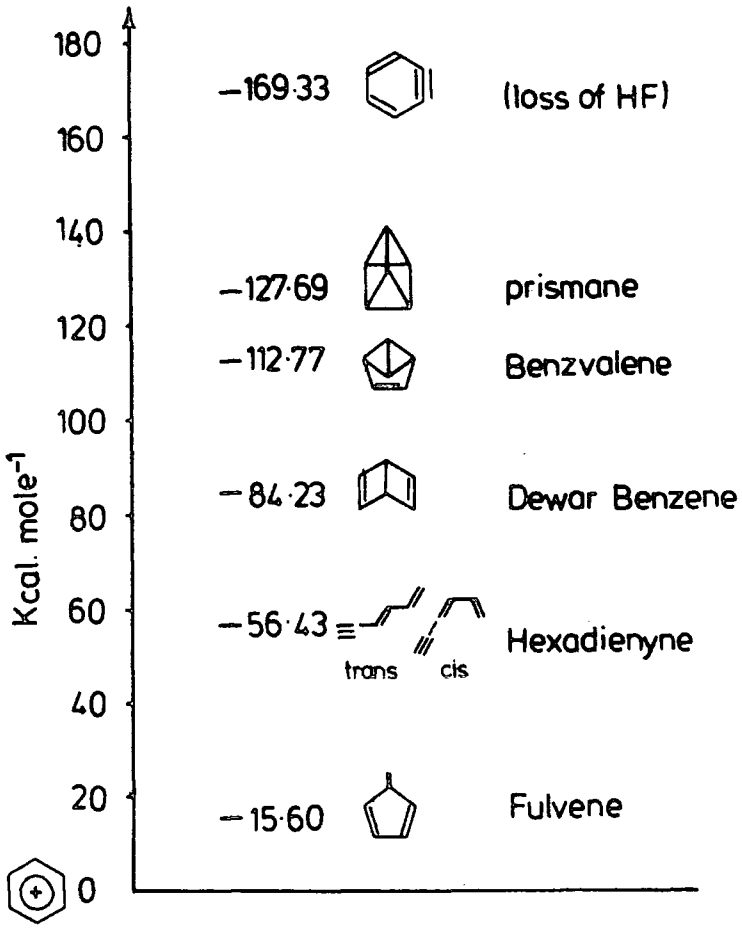

Figure 6.3.12 Relative energies of 1,2,3,4-tetrafluorobenzene cation and possible isomeric cation species occurring in the R.F. computed using MNDO SCF MO formalism

In the cation manifold the relative energies of the Dewar benzene, prismane and benzvalene isomeric structures is somewhat reduced relative to the neutral manifold and electron attachment to produce 'hot' neutrals could result in efficient conversion to the energetically preferred fulvene and hexadienyne structures. High power microwave plasmas excited in perfluorobenzene [230] have been used for the synthesis

of fluorinated acetylene most likely via the intermediacy of the hexadienyne structure and the involvement of this and the fulvene ring system provides the most straightforward explanation for the high preponderance of $\underline{C}F_3$ and $\underline{C}F_2$ structural features and for the elimination of fluorine from the lower fluorinated systems. For both the neutral and cation ma manifolds it is interesting to note that the elimination of HF to produce a benzyne is a high energy process and is in any case unlikely for excited states or π radical cation states involving as it does an elimination in the σ system. A broad scheme based on the intervention of these various reactive species and starting monomer can by a series of pericyclic reactions lead to crosslinked rearranged polymer structures however before a more detailed discussion can be given spectroscopic studies monitoring the reactive species needs to be accomplished.

CHAPTER SEVEN

CHAPTER SEVEN

PLASMA POLYMERIZATION V. AN ESCA INVESTIGATION OF THE R.F. PLASMA POLYMERIZATION OF PERFLUORO-2-BUTYLTETRAHYDROFURAN.

Abstract

Perfluoro-2-butyltetrahydrofuran has been polymerized by an R.F. glow discharge technique and detailed ESCA studies have been made of the resultant films. The rate of film deposition is shown to be sensitively dependent on the W/FM parameter and on the site of deposition. The ESCA data shows evidence for molecular rearrangement accompanying plasma polymerization and the oxygen functionality is at a significantly lower level than for the starting monomer. Under appropriate conditions plasma polymerization produces material with a C : F stoichiometry of 1 : 2 although the ESCA data shows that the polymer is drastically different from PTFE. ESCA studies are also reported on thin films of the monomer studies at low temperature.

Chapter Seven: Plasma Polymerization V. An ESCA Investigation of the R.F. Plasma Polymerization of Perfluoro-2-butyltetrahydrofuran.

7.1 Introduction

The previous four chapters have described the structural features and bonding as revealed by ESCA of plasma polymerized films prepared from a series of fluorobenzene compounds. The studies were mainly concerned with the final structure of the polymers and how it was related to the nature of the starting material, however, in certain cases, provided mechanism and kinetic information of polymer formation. The studies were also emphasized how ESCA technique allows a detailed interrogation of composition and structural features as a function of operating parameters, reactor configuration and site of deposition, as well as providing and exceptionally good technique for measuring initial rates of deposition. Such studies have quantified the differences in behavior of geometric and positional isomers in the fluoroethylene[52,211] and fluorobenzene[205,225] field respectively.

In this chapter the study of polymer films prepared from perfluoro-2-butyltetrahydrofuran by the R.F. plasma polymerization is described. It is of interest to note that pioneering studies particularly of Yasuda[29] and of Bell[2,4] and their co-workers have indicated how the facility with which a given monomer undergoes plasma polymerization is structurally based, and ground rules have been established indicating the relative propensity of for example aliphatic and alicyclic hydrocarbons compared with aromatic or acetylenic hydrocarbons to undergo plasma polymerization.[29] Important general points to arise from these studies include the fact that aliphatic and alicyclic fluorocarbons only undergo plasma polymerization with great difficulty,[2,4,29] indeed the emphasis

in the literature has predominantly been on the etching characteristics of such plasmas.[4] The other general feature, is that oxygen containing systems also show a reduced tendency to undergo plasma polymerization.[4,29] The study presented here, therefore, may provides a suitable example of an alicyclic fluorinated system which also contains oxygen. Such an investigation is particularly apposite at this time since in a preliminary report[180] on plasma polymerization of this monomer it has been suggested on the basis of infra-red evidence that a largely linear polymer is obtained with little evidence for CF_3 structural components, which have been a feature of the plasma polymerization of fluorocarbon monomers in general.

7.2 Experimental

The work presented here involves two types of reactor configuration, B and C, as described in Chapter Five. They were used without modification of those designs. Reactor B, was used for the ESCA studies the polymer films deposited on gold substrates placed along the bottom of the reactor at three different sites (-13, 0 and 13 cms. from the centre of the coil region, see Figure 7.3.10). Polymer films were also deposited onto thin Al foils (2 x 1 $cm.^2$) placed along the bottom of the reactor at five different sites located at -26, -13, 0, 13, 26 cms. from the centre of the coil region. The weight increases of the Al foils were measured using a CAHN electromicrobalance. Polymer films deposited onto high density polyethylene sample (2 x 12 $cm.^2$) placed in the coil region were employed for MATR IR and contact angle studies as described previously.

Sufficient quantities of the polymer for microanalysis and transmission IR studies were obtained by removing the polymer film which

was deposited on the walls of the pyrex reactor inside the coil region.

ESCA spectra were recorded on an AEI ES200 AA/B spectrometer using $Mg_{K\alpha_{1,2}}$ radiation and were analyzed as described in the previous chapters. Spectra of the starting material, perfluoro-2-butyltetrahydrofuran (liq.) were obtained by introducing the monomer via a heatable reservoir shaft, leaking it through a Metrosil plug and condensing it on a cooled gold substrate mounted on the sample probe while was held a temperature of $\sim 100^{\circ}C$.

The starting material, perfluoro-2-butyltetrahydrofuran was obtained from PRC (Gainesville, Florida) and was shown to be analytically pure by g.l.c. and was therefore used without further purification. Prior to use the starting material was degassed as described in the Chapter Three.

7.3 Results and Discussion

It is convenient in describing the experimental data and its analysis and interpretation to consider the monomer itself and then the plasma experiments in reactor configuration C (which allows in situ deposition and analysis without atmospheric contact) and then finally reactor configuration B (which allows and investigation of the structure and rate of deposition of plasma polymer films as a function of site.)

7.3.1 Perfluoro-2-butyltetrahydrofuran ($C_8F_{16}O$)

As a necessary prerequisite to the analysis of ESCA data for the plasma polymer films, the core level data for the starting material

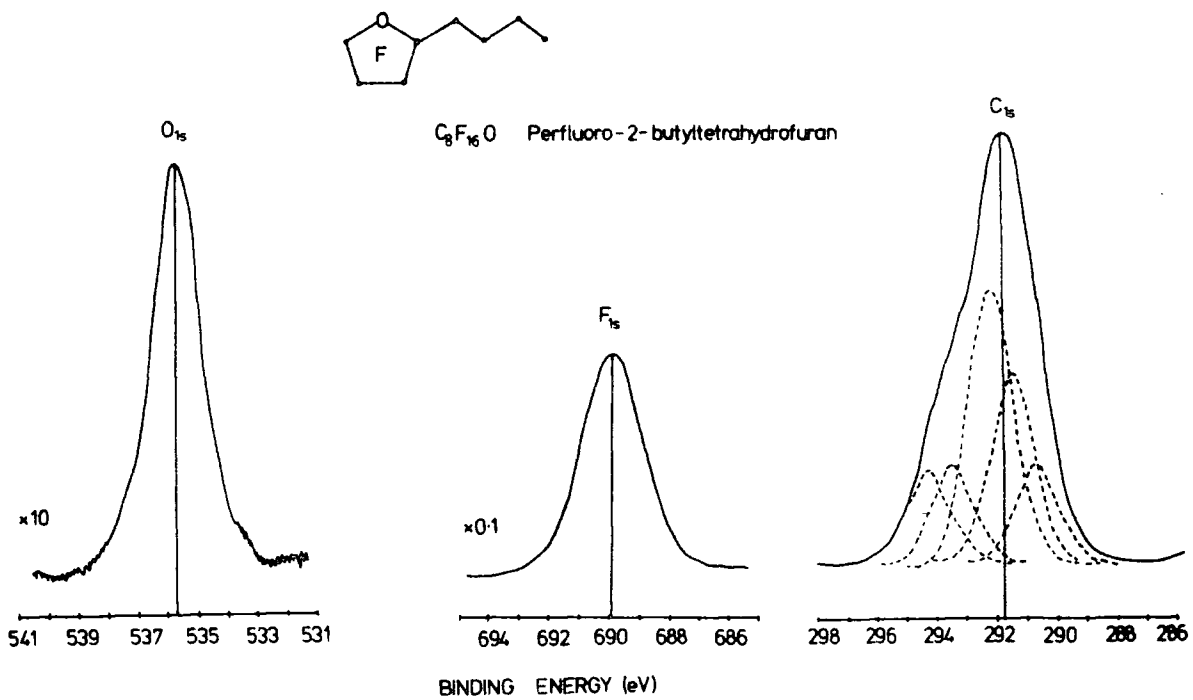

Figure 7.3.1 $\underline{O}_{1s}$, $\underline{F}_{1s}$ and $\underline{C}_{1s}$ spectra of perfluoro-2-butyltetrahydrofuran studied as a thin film in the condensed phase

has been investigated and the relevant data is displayed in Figure 7.3.1. The C_{1s} profile consists of relatively broad unresolved line shape with a distinctive asymmetry to the high binding energy side. Standard line shape analysis reveals components in the intensity ratio 1 : 1 : 3 : 2 : 1 with corresponding binding energies (BE) of 294.1 eV; 293.4 eV; 292 eV; 291.4 eV and 290.5 eV. Previous studies of perfluorinated systems allow a straightforward assignment of these components as arising from $\underline{C}F_3$-CF_2, -$\underline{C}F_2$-O-, CF_2-$\underline{C}F_2$-CF_n (two components corresponding to n = 2 and n = 1) and $\underline{C}F$ structural features of the perfluoro-2-butyltetrahydrofuran ring system. The shifts of these structural features follow a simple additivity model based on primary and secondary fluorine and oxygen substituent effects along the lines previously reported.[206,231] The F_{1s} levels show a relatively broad (FWHM 2.4 eV) unresolved peak

indicative of the small range of shifts spanned by fluorine in the various electronic environments. No attempt has been made to further analyze this spectrum in this work however the centroid of the binding energy scale at ~690 eV is consistent with previous studies of fluorocarbon systems.[71] From a knowledge of instrumentally determined cross-sections it is possible to calculate the C : F stoichiometry from the C_{1s} : F_{1s} intensity ratio. This gives a computed ratio of C : F 1 : 2 is excellent agreement with the theoretical value. The components of the C_{1s} levels also correspond exactly to the molecular formula.

The O_{1s} levels consist of a single component centred at 535.7 eV. This is at considerably higher binding energy than for a hydrocarbon ether system (c.f. O_{1s} level in polyethylene oxide 534.0 eV.) The shift to higher binding energy is consistent with a β -substituent effect for fluorine of ~0.6 eV.[71]

From previous studies of carbon oxygen containing systems may derive an apparent C : O stoichiometry based on the relative intensities of the core levels of 27 : 1 compared to the theoretical value of 8 : 1. This discrepancy is interesting in that the C : F stoichiometry from both the components of the C_{1s} levels and the C_{1s} to F_{1s} intensity ratio is entirely consistent with statistical sampling of the repeat unit. The only plausible explanation for the totality of experimental data is that if the mean free path is short enough for a given level than ESCA may not statistically sample the repeat unit. On the basis of previous studies[176-177] the mean free path for electron of ~960 eV kinetic energy, photoemitted from C_{1s} levels will have a mean free path (~15 Å) which is somewhat larger than the dimension of the molecule as a whole along its long axis. The C_{1s} levels should therefore correspond

to statistical sampling of the molecular structure. The large difference in polarity and polarizability of an ether oxygen compared with an aliphatic fluorocarbon chain could conceivably give rise to preferential orientation of the molecules at the surface of the gold substrate and the lowest surface energy configuration would then correspond to the fluorocarbon side chain being oriented normal to the surface. Scale (Dreiding) models indicate that if the mean free path for the O_{1s} photoemitted electrons, kinetic energy $\sim$720 eV, were approximately of the same dimension as the distance between the end of the perfluoroalkyl group and the oxygen atom then the observed intensity ratios would be entirely reasonable. On this basis the F_{1s} photoemitted electrons should correspond to an even shorter mean free path. However the C : F stoichiometry for the perfluoroalkyl chain and for the ring system are in any close to that for the molecule as a whole so it is entirely reasonable that the C : F stoichiometry derived from the C_{1s} : F_{1s} intensity ratios are in agreement with that for the perfluoro-2-butyltetrahydrofuran system itself.

7.3.2 In situ plasma polymerization in reactor C

(i) Gross structural features and compositions.

Preliminary experiments showed that with power inputs in the range 1 - 20 W. and pressures of 100 - 200 μ (corresponding to a range $\sim 10^7$ - 10^8 J Kg^{-1} in W/FM parameter,) convenient rates of deposition for the ESCA studies were obtained. Transparent films with very little discolouration were provided under this regime. As a starting point consider the core level spectra for a typical polymer sample deposited

in situ in reactor C as shown in Figure 7.3.2.

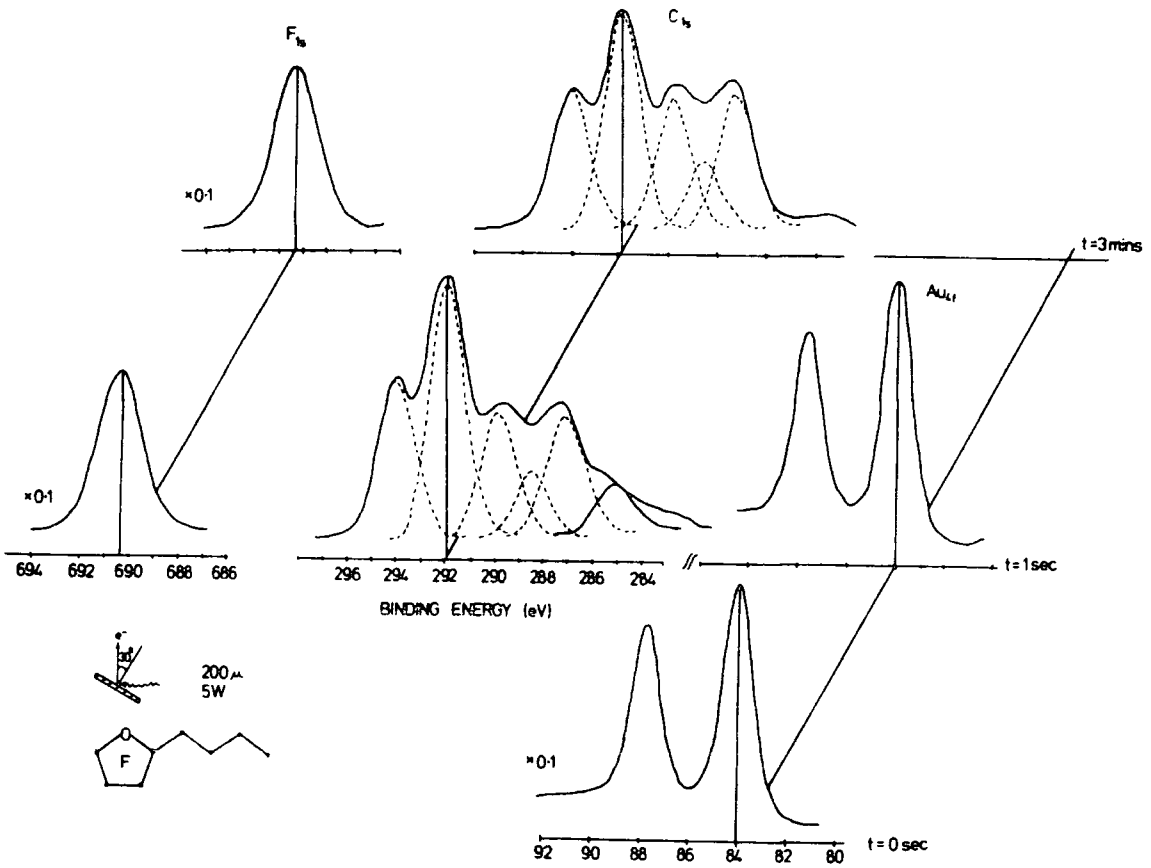

Figure 7.3.2. $\underline{F}_{1s}$, $\underline{C}_{1s}$ and Au_{4f} levels of plasma polymer prepared in situ

The F_{1s} levels show a single peak of essentially the same FWHM and the binding energy as for the starting material. The C_{1s} levels show components which extend over a binding energy range of ~7 eV which is almost double that for the starting material. The striking feature is the increased relative contribution of the high binding energy component corresponding to $\underline{C}F_3$ structural features and also the increase in low binding energy components corresponding to $\underline{C}F$ and CF_n-$\underline{C}$-CF_m structural features. It is clear therefore that polymerization is accompanied by rearrangement. The assignment of components is straightforward. Thus

the highest binding energy component at ~294 eV corresponds to $\underline{C}F_3$ structural features and constitutes ~20% of the total signal intensity. This almost double the contribution for the structural feature in the starting material. $\underline{C}F_2$ groups centred at ~292 eV constitutes ~30% of the total signal intensity compared with ~75% of the intensity for the starting material. $\underline{C}F$ structural features contribute ~25% to the total C_{1s} envelope which is approximately double that for the perfluoro-2-butyltetrahydrofuran 'monomer'. The lowest binding energy component corresponding to one fifth of the structural features corresponds to carbons which do not have fluorine attached but have several adjacent C-F bonds. The component of the C_{1s} line profile provides a stoichiometry (C : F) of 1 : 1.6 significantly smaller than for the starting monomer (1 : 2). The C_{1s} spectra for a very thin film (~30 Å, deposition time 1 sec.) also shows the characteristic low binding energy component at 285 eV attributed to hydrocarbon overlayer on the gold substrate which is useful in complementing the absolute calibration provided by the $Au_{4f_{7/2}}$ levels. After a deposition period of 3 minutes the $Au_{4f_{7/2}}$ are not observable and the data therefore shows that the polymer film is deposited extremely rapidly. It is interesting to note for the very thin film there is a significantly larger linewidth for the core levels compared with thicker films and this almost certainly arises from differences in extra molecular relaxation energies. Such phenomena in detailed investigations relating to sample charging as have previously been noted.[165]

The O_{1s} spectra show in Figure 7.3.3 reveal a single high binding energy component corresponding to a perfluoroether type environment and this is accompanied by a small component at low binding energy shifted by ~ 5 eV. This is an usually large shift for oxygen and a discussion of

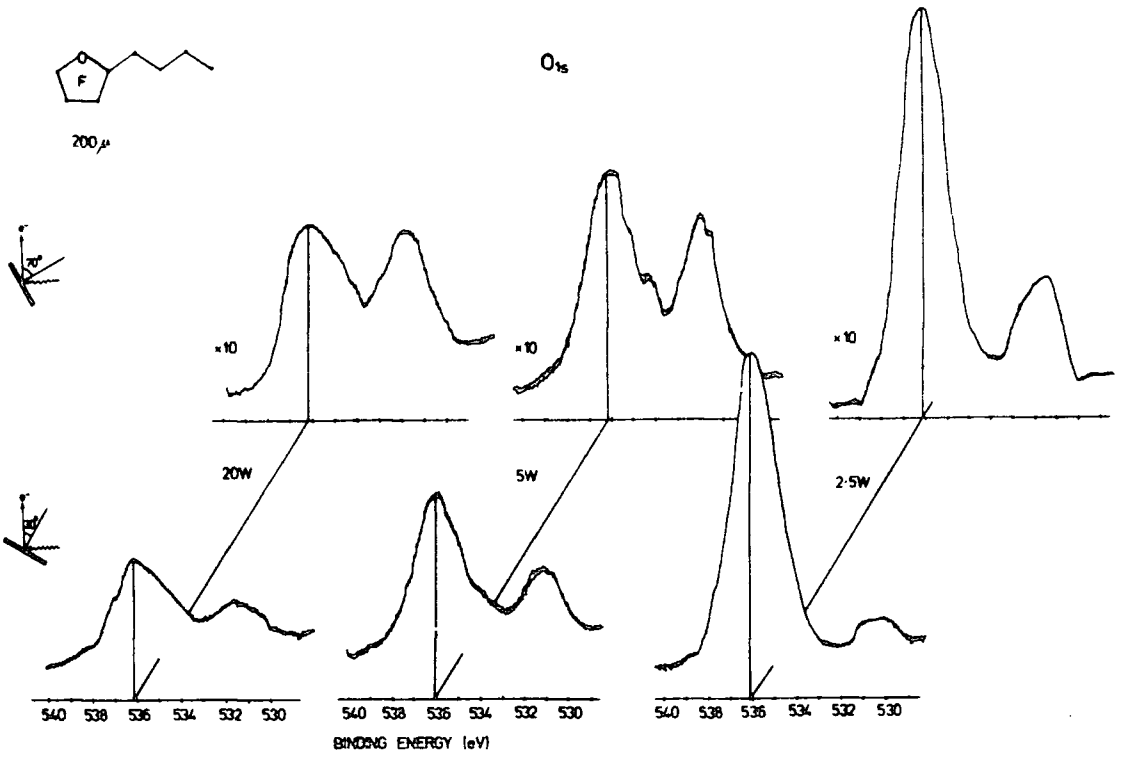

Figure 7.3.3 O_{1s} spectra of the plasma polymer prepared in situ at three discharge powers (above) at a pressure of 200 μ (below) at a pressure of 100 μ

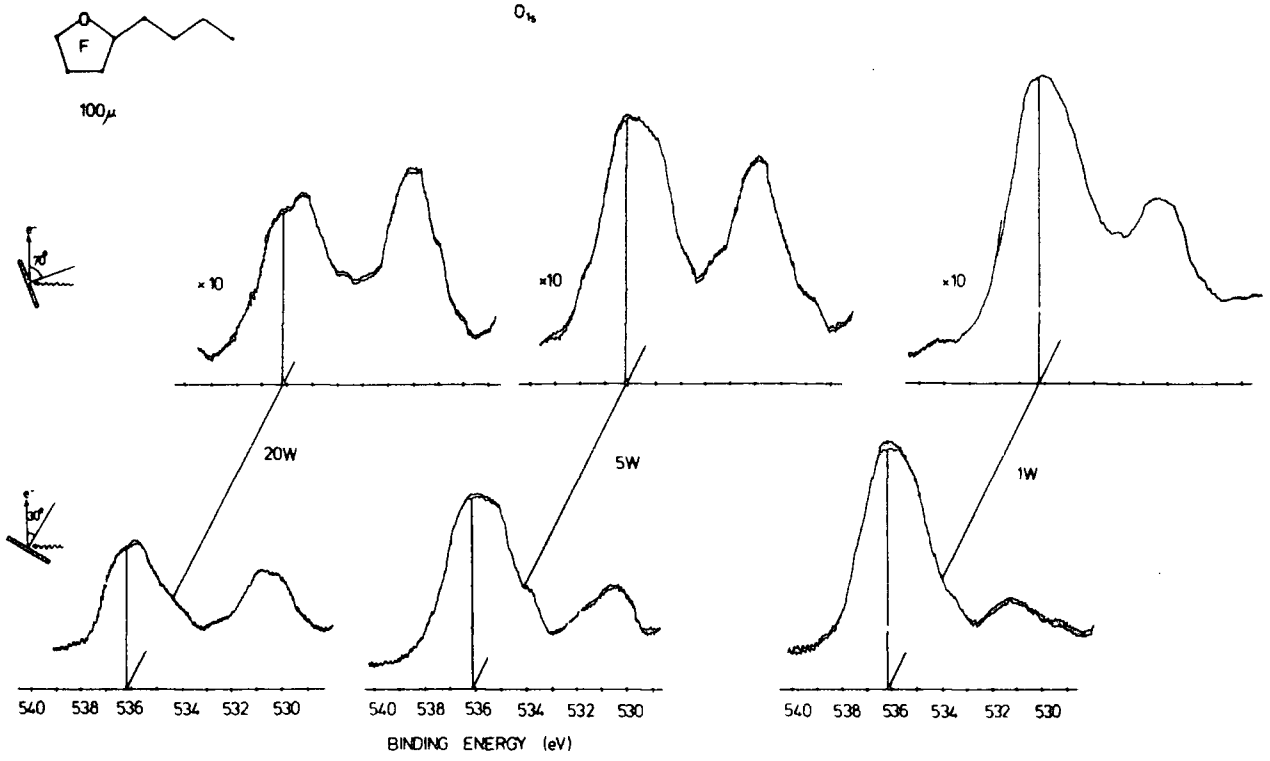

this feature will be presented in a later section. The relative intensity of the low binding energy component increases at higher take off angle indicating it surface nature. The C : O intensity ratio suggest a stoichiometry of $\sim$ 50 : 1 (the proviso being that the oxygen is in structural features which are stistically sampled by ESCA). The fact that the integrated C_{1s} : O_{1s} intensity ratios are the same within experimental error for take off angles of 30° and 70° suggests that this is a reasonable estimate of overall stoichiometry. It is clear from this therefore that plasma polymerization under these conditions is accompanied by molecular rearrangement involving loss of both fluorine and oxygen.

A detail study has been made of the structural features present in the polymer films depositied over a range of powers and pressures in situ in reactor C. The C_{1s} spectra are shown in Figure 7.3.4 and 7.3.5.

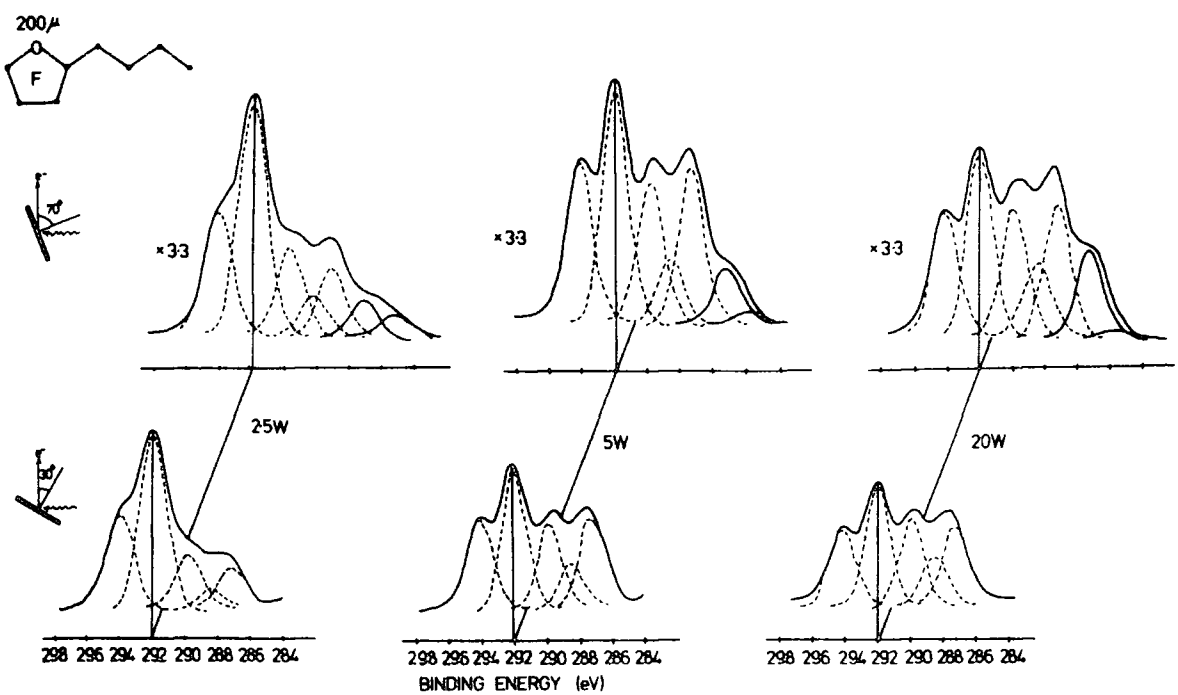

Figure 7.3.4 C_{1s} levels of plasma polymer prepared in situ at 2.5 W, 5 W and 20 W discharge powers and a pressure of 200 μ

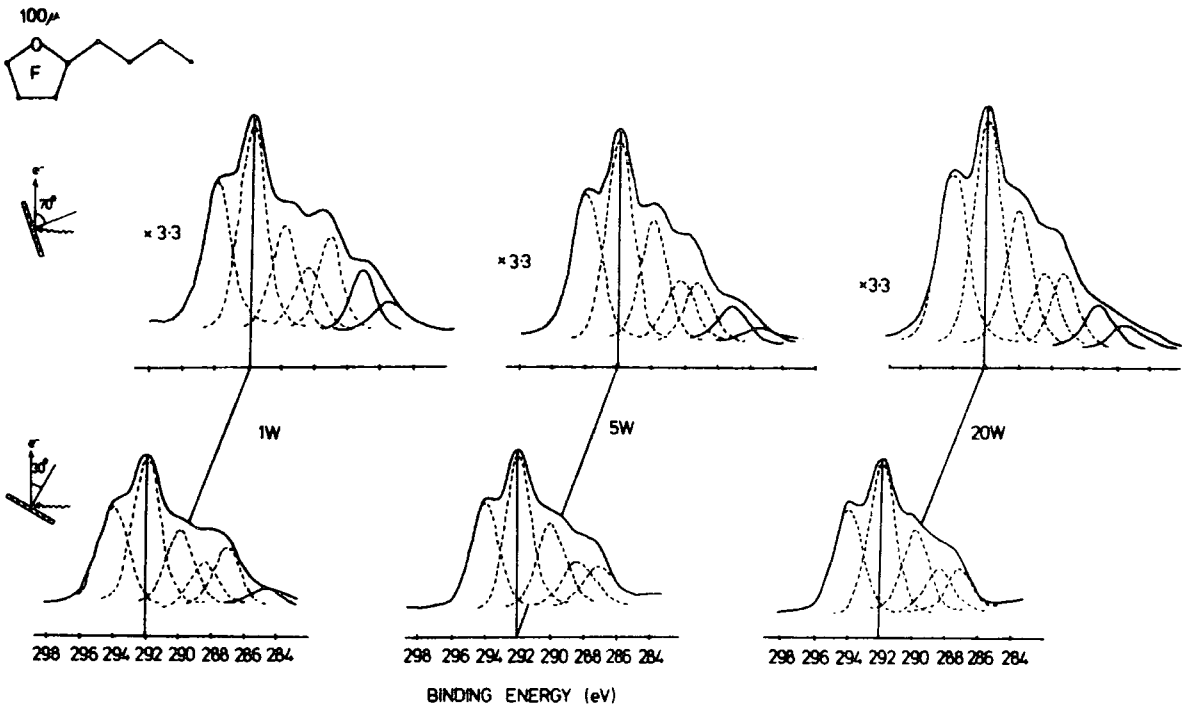

Figure 7.3.5 C_{1s} levels of plasma polymers prepared in situ at 1 W, 5 W and 20 W discharge powers and a pressure of 100 μ

The spectra taken at different take off angles reveal evidence of low levels (generally sub-monolayer) of surface hydrocarbon contamination (e.g. CH 285 eV component generally not observed at 30° take off angle but evident at low intensity at 70°). The spectra show a somewhat greater sensitivity in overall line profile to the operating parameters that has previously been found for fluorinated ethylenes[52] and benzenes[232] and this becomes more evident when the component data is considered in detail as shown in figure 7.3.6. For comparison purposes the O_{1s} signal intensity (high binding energy component) as a function of the total C_{1s} signal (at 30°) is shown in Figure 7.3.7. It is clear from these data that high pressure and low power corresponding to a low W/FM parameter gives rise to significantly higher oxygen content in the polymer film than for large W/FM (high power, low flow rate). The two extremes corresponding to power

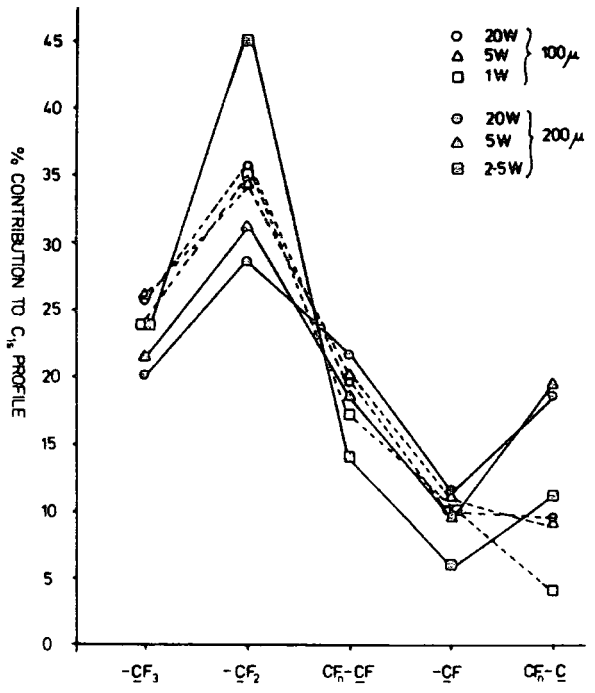

Figure 7.3.6 Percentage contribution of the C_{1s} envelope for various functionalities of the plasma polymers as a function of power and pressure in reactor C

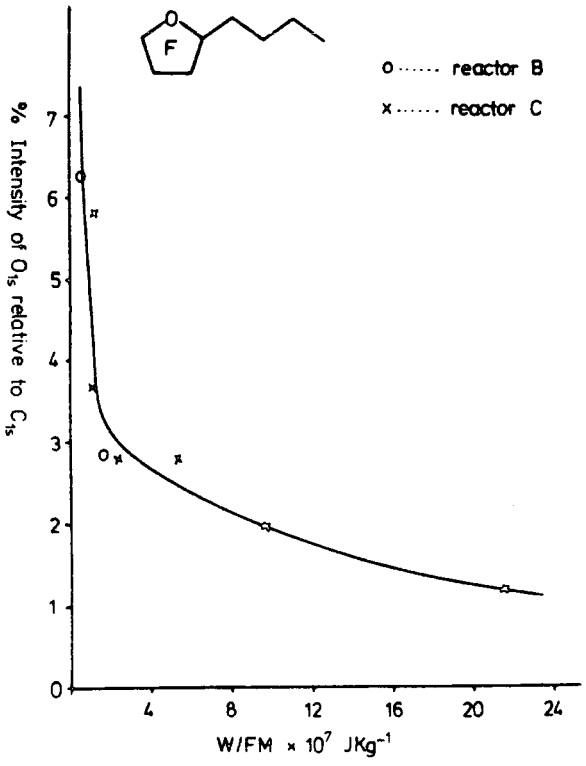

Figure 7.3.7 Percentage intensity of O_{1s} relative to C_{1s} vs. W/FM

inputs of 20 W. and 2.5 W. at pressures of 100 μ and 200 μ respectively give rise to C : O stoichiometries of $\sim$140 : 1 and $\sim$ 29 : 1 respectively. A change of W/FM parameter of $\sim$20 x therefore corresponds to a change in oxygen stoichiometry by a factor of 6 x. The low level of oxygen functionalities leads to the relatively straightforward component distribution in the C_{1s} levels shown in Figures 7.3.4 and 7.3.5. Thus the contribution from structural features with carbon directly attached to oxygen must be small. An interesting feature evident from the spectra shown in Figures 7.3.4 and 7.3.5, is the distinctive 'valley' which is evident between the $\underline{C}F_3$ and $\underline{C}F_2$ components as W/FM increases. The most likely explanation for this is that the increased oxygen content as W/FM decreases (c.f. Figure 7.3.7) is accommodated by $-O-CF_2-$ structural features at sufficiently small but significant intensity levels such that the apparent resolution between the $\underline{C}F_3$ and $\underline{C}F_2$ structural features is decreased, (c.f. Figures 7.3.1 and 7.3.4.).

The C : F stoichiometries for films deposited under different conditions follow and interesting pattern (Table 7.3.1). At 200 μ there is a tendency for the C : F stoichiometry to be relatively invariant with power input. At the lower pressure however, higher power (larger W/FM), corresponds to a greater loss of fluorine and oxygen on going from 'monomer' to polymer. As will become apparent when consider the depositions in reactor B the stoichiometry and structure of the plasma polymer is significantly more sensitive to the operating parameters than has previously been found to be the case with either the fluorinated ethylenes or benzenes.[52,232] The component analysis still reveal however subtle rather than drastic changes in the observed structural features as a function of the operating parameters as is clear from the component line shape analysis presented in Figure 7.3.4 and 7.3.5.

Table 7.3.1 C_1F_x stoichiometry of (i) plasma polymers prepared in situ in reactor C and (ii) plasma polymers prepared in reactor B

(i) In situ (reactor C)

Power	Pressure	
	100μ	200μ
20W	1.8	1.5
5W	1.8	1.6†
2.5W	-	1.8
1W	1.7	-

(ii) Free standing (reactor B)

Pressure	Power	Position		
		-1	0	1
100μ	5W	2.0	1.9	1.9
200μ	5W	1.6	1.8	1.8

The numbers in each table correspond to the CF_x stoichiometry obtained from the deconvolution of the C_{1s} profiles;

† corresponds to spectra in Figure 7.3.2.

(ii) Initial rates of in situ deposition

The initial rates of deposition were determined by monitoring the attenuation of the $Au_{4f_{7/2}}$ levels of the gold substrate on which polymer films were deposited and their relevant data are displayed in Table 7.3.2. It is clear that the rates are strongly influenced by the W/FM parameter. The rates of deposition show a stronger dependence on the

Table 7.3.2 Deposition rate (Å $s.^{-1}$) of the plasma polymer as a function of discharge power and pressure

Pressure	200μ	100μ
Power		
20W	60.0	3.0
5W	35.0	9.0

operating parameters of this system than has previously been found with fluorinated ethylenes and benzenes. At 200 μ an increase in power input from 5 to 20 W effectively doubles the rate of deposition whilst lowering the pressure to 100 μ decreases the rates significantly, that for 20 W input power actually being lower than that for 5 W.

To summarize, the overall stoichiometry of polymer films deposited in situ from R.F. plasmas excited in perfluoro-2-butyltetrahydrofuran show a much larger variation under the range of conditions employed in this work than for the fluoro aromatic systems which have previously been the subject of investigation in these laboratories.[205,225] The rate of deposition are also sensitive functions of the operating parameters and the evidence suggests that extensive molecular rearrangement is accompanied by loss of oxygen functionality the loss being greatest at high W/FM parameter. The ESCA data unambiguously demonstrates the extensive contribution to the core level spectra provided by $\underline{C}F_3$ structural features and this to some extent is at variance with increases which have been drawn in a preliminary manner from IR strudies of a related system. Although the conditions under which the films were deposited are not clear from the available literature.[180]

7.3.3 Free Standing Plasma Polymerization in Reactor B

Figures 7.3.8 and 7.3.9 displayed the C_{1s} core level spectra for 3 sites of deposition in reactor B. The spectra for samples deposited at site (-1) at 200 μ and at sites (0 and 1) at 100 μ and 5 W are distinctively different from the rest in that in each case a substantial component is evident in the C_{1s} spectra at 285 eV, corresponding to hydrocarbon contamination. At first sight this might seem somewhat puzzling, however the data are readily understandable once the rate of deposition as a function of axial location has been established. The relevant data are shown in Figure 7.3.10 and the somewhat differing flow patterns in the bigger reactor at 100 μ and 200 μ gives rise to distinctive deposition patterns. Thus at 200 μ the rate of deposition is a maximum at the centre of the coil region, whereas at the lower pressure the deposition is highest in the glow region at a site displaced some 13 cms. in front the coil.

Figure 7.3.8 C_{1s} spectra of the plasma polymers prepared at 5 W discharge power and a pressure of 200 μ from 3 deposition sites (-1,0,1)

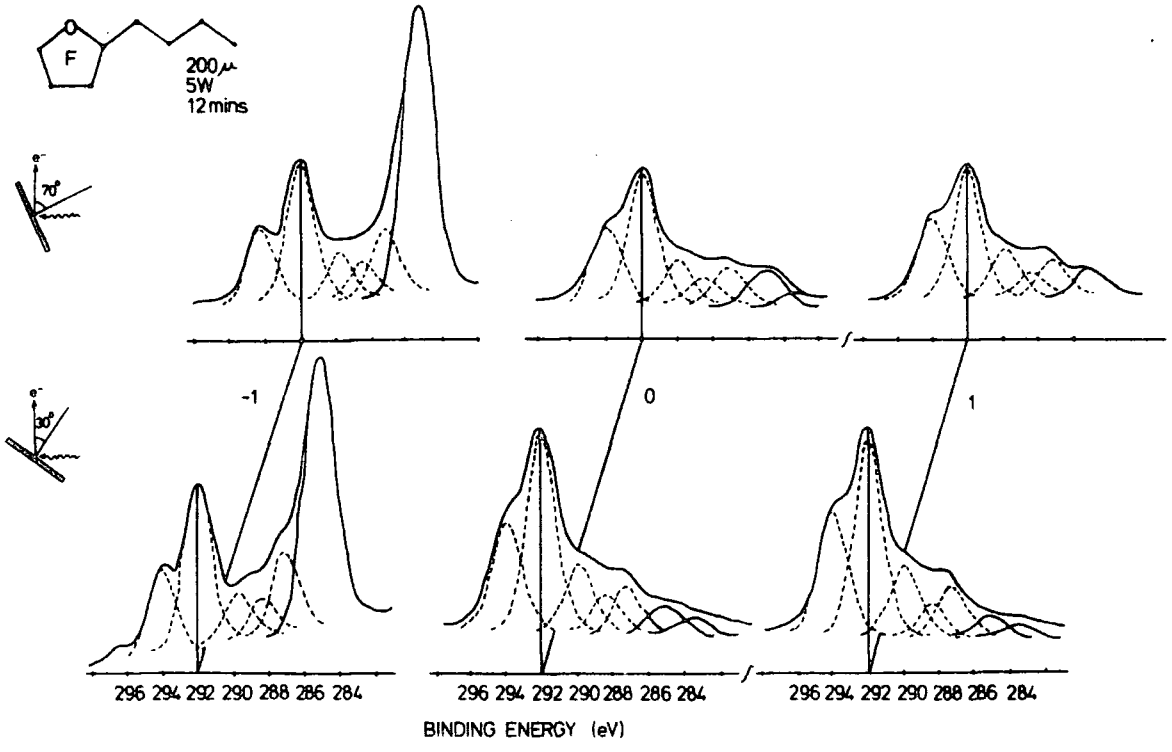

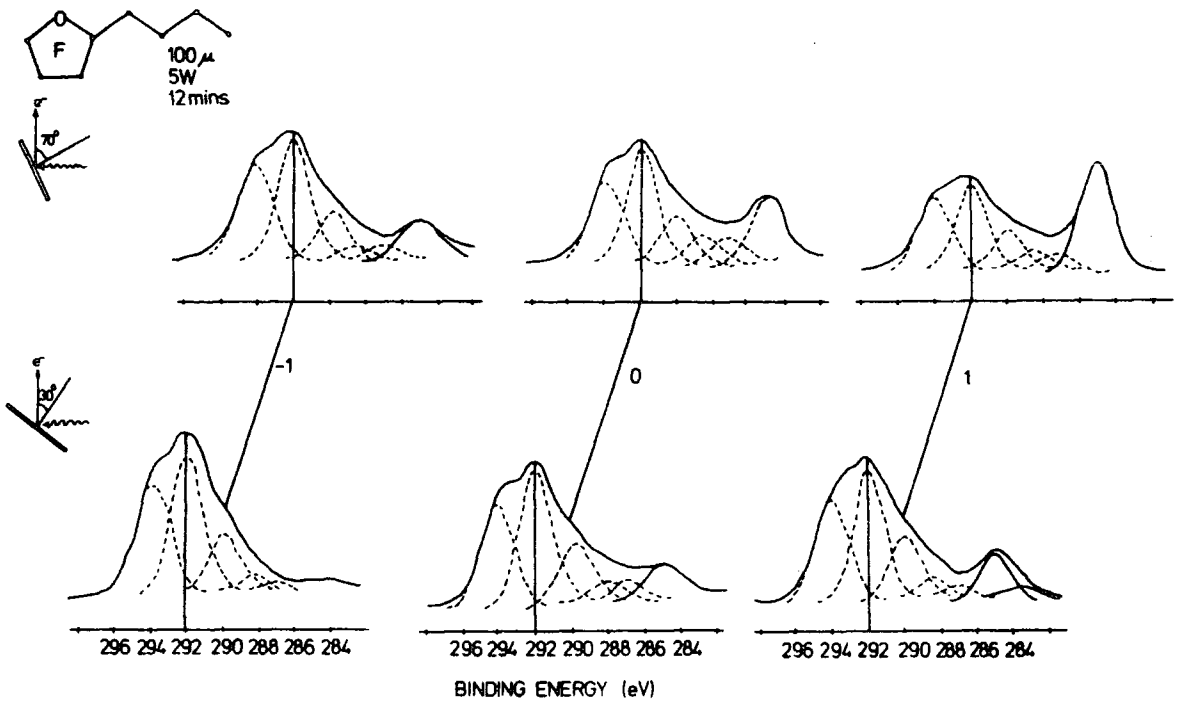

Figure 7.3.9 C_{1s} levels of the plasma polymers prepared at 5 W discharge power and a pressure of 100 μ from 3 deposition sites (-1,0,1)

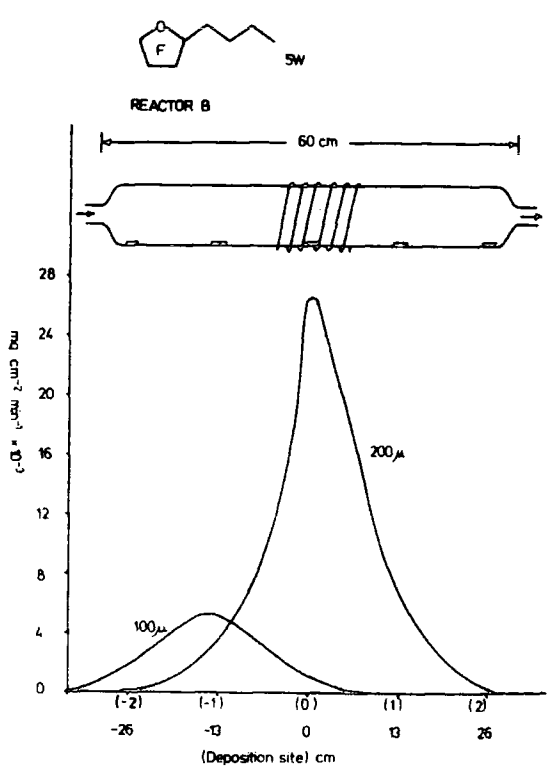

Figure 7.3.10 Deposition rate (mg. cm.$^{-2}$min^{-1}) vs. deposition site

The rate of deposition is clearly higher at the higher pressure (c.f. previous section). This behaviour is again different to that previously found (see Chapters Four and Five) for the flurobenzenes where the rate of deposition in the glow region was found to be roughly constant at a given pressure. At 100 μ therefore the films deposited at site (0 and 1) are relatively thin and in consequence the spectra reveal the characteristic 285 eV component in the C_{1s} spectra due to hydrocarbon contamination on the gold substrate. A similar situation obtains for the deposition at site -1, at the higher pressure.

Analysis of the core level spectra provide estimates of the stoichiometries as detailed in Table 7.3.1. The excellent measure of agreement as a function of take off angle reveals the vertical homogeneity of the samples.

At a pressure of 200 μ and discharge power of 5 W the C : F stoichiometry of 1 : 1.6 for site (-1) is identical to that determined for films deposited under similar conditions in situ in reactor C. In the region of maximum deposition rate the C : F stoichiometry is slightly higher and this trend is also apparent at lower pressure. Thus at 100 μ the C : F stoichiometries are close to that of the starting monomer (1 : 2) and the spectra dominated by $\underline{C}F_3$ and $\underline{C}F_2$ structural features. For the thick film deposited at site (-1) at 100 μ the C : O stoichiometry is computed to be $\sim$60 : 1 substantially lower for the starting monomer (8 : 1). The relative contributions of $\underline{C}F_3$: $\underline{C}F_2$: and CF structural features in the polymer film of 33% : 42% : and 21% may be compared with corresponding figures of 12.5% : 75% : and 12.5% for the starting monomer. Polymerization therefore involves loss of oxygen and conversion of $\underline{C}F_2$ sites in both $\underline{C}F_3$ and $\underline{C}F$ sites. Although the overall stoichiometryof the polymer prepared at 100 μ in reactor B is very similar to that of PTFE the structures are

by no means similar. Ring opening plasma polymerization undoubtely leads to branched chain material with a substantial contribution of site chain perfluoro methyl groups. In general however the polymer sample prepared from the plasma polymerization of the saturated perfluro-2-butyltetrahydrofuran system appear not to be crosslinked to the some extent as other fluoro polymer systems prepared by this route to date since sample are soluble to a small degree in the starting monomer itself.

Samples of polymer removed from the reactor walls in the glow region (site 0, 200 μ, 5 W) have been subjected to microanalysis and this provides a bulk C : F stoichiometry of 1 : 1.8 which in view of the experimental uncertainties associated with the notoriously difficult combustion analysis of highly fluorinated material is in very reasonable overall agreement with the ESCA data. Unfortunately oxygen can only be determined by difference in the microanalysis and the errors are such that it is not possible (by microanalysis) to investigate the low level of oxygen functionality. The ESCA data, Figure 7.3.11 shows that the

Figure 7.3.11 O_{1s} levels of the plasma polymer prepared at 5 W discharge power and pressures of 100 μ (site -1) and 200 μ (site 0)

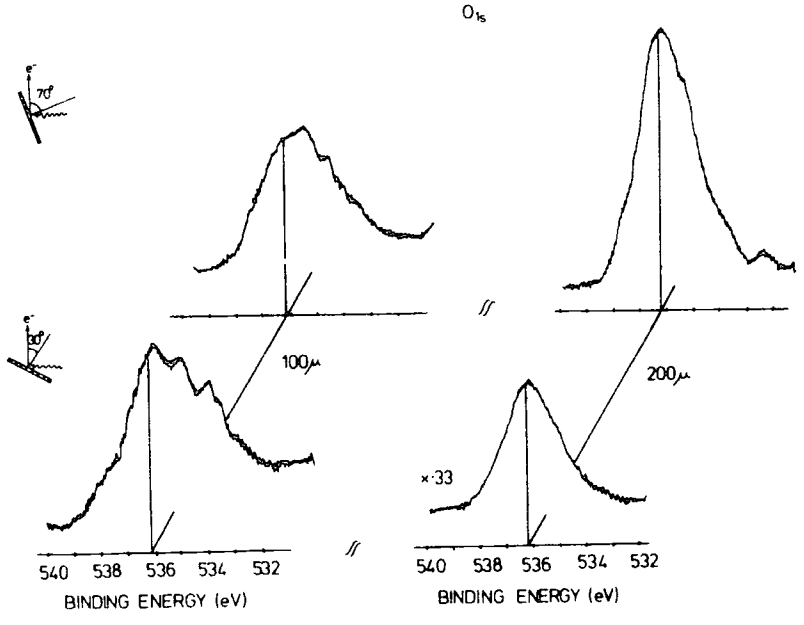

low level of oxygen functionality corresponds to a perfluorinated ether linkage, however compared to the monomer there must be a range of environments since the FWHM is substantially higher than for the starting monomer as is evident from a comparison of data in Figures 7.3.1 and 7.3.11. As these have already been noted that the O_{1s} spectra for samples deposited in situ in reactor C tend to show an additional low binding energy component centred $\sim$531 eV. It is clear from the spectra displayed in Figure 7.3.3 that the additional component is largely confined to the surface regions since its relative intensity increases on going to higher take off angle. The fact that the low binding energy component in only observed for the in situ depositions in which samples are analyzed without exposure to the atmosphere effectively rules out any likelihood that such structural features as are likelt to correspond to the low binding energy component arise from surface oxidation subsequence to preparations. It is significant to note however that the high binding energy component of the O_{1s} spectrum decreases as a function of W/FM as has previously been shown from the data in Figure 7.3.7. Analysis of the spectra show that for a 30^{o} take off angle, at the highest W/FM parameter (21.5×10^{7} J Kg^{-1}) the extraneous low binding energy component of the O_{1s} spectrum contributes 45% of the total intensity, For a W/FM parameter of 5.3×10^{7} J Kg^{-1} however with roughly double the oxygen content the contribution of the low binding energy component has dropped to 15%. For the lower values of W/FM employed in this work and for the depositions in the free standing reactor (also corresponding to lower W/FM) the lower binding energy component is unimportant. It is difficult to speculate as to the precise nature of this low binding energy component since there is a lack of reference data. The low binding energy is however only compatible with an oxyanion of some sort and corresponds to the typical

binding energies reported for the oxides.[119] The wide survey scan spectra provide no ready means of explaining what the possible counter ion could be and have not pursued this aspect of the investigation further since for the case where this structural feature is most prominent the C : O (low binding energy) stoichiometry is in excess of 100 : 1 and the contribution to the overall structure is therefore minor.

The high fluorine content of the plasma polymerized films might lead one to suspect that the surfaces would be a relatively low surface free energy. As we have already noted however the films deposited in reactor B show a low level of oxygen functionality and this clearly has a significant effect on the critical surface tension. This was calculated by analysis of the data obtained from the measurement of the contact angles with water, glycerol, formamide and methylene iodide. The relevant data for the film prepared in the free standing reactor at 200 μ and 5 W of C : F : O stoichiometry of 1 : 1.8 : 0.04 has critical surface tension of 29 dyne $cm.^{-1}$ This may be compared with values of 15, 19, 21 and 36 dyne $cm.^{-1}$ for polyhexafluoropropylene, polytetrafluoroethylene, poly (1-trifluromethyl)tetra(fluoroethoxymethylethylene) and poly(ethoxyethylene) respectively.[233]

Comparison of the transmission IR spectra of films of the monomer with MATR (KRS-5) spectra of films of the polymer is largely uninformative since the predominant feature in each case is a broad intense absorption centred $\sim$1250 $cm.^{-1}$ associated with C-F (and C-O) vibrations. The spectra look remarkably similar to those described by Kinzig[180] in the work on related systems. However the interpretation is somewhat different. The resolution and difficulty of quantifying MATR data,[234] particularly in the important C-F characteristic vibration frequency range leaves little confidence in the assertion that $\underline{C}F_3$

sturctural features can be largely discounted from the IR data. Indeed it has already been noted there is a remarkable correspondence in the region centred ~1250 $cm.^{-1}$ between the IR spectra for the starting monomer and the polymer. Comparison with standard infrared databases [235] also reveals that it is difficult on the basis of the MATR spectra to say anything other than the sample is predominantly fluorocarbon in nature, with no real means of quantifying the nature of the structural features involved. As the ESCA data reveals the plasma polymer is branched with high contribution from CF_3 structural features.

7.3.4 Mechanism of Plasma Polymer Formation

The preceding discussion has emphasized that there is a marked contrast in terms of sensitivity of gross chemical structure to site of deposition and site dependence of rate of deposition than has been found to be the case for the corresponding plasma polymerization of fluorinated ethylenes and aromatics. There is some parallel however with the previously reported plasma polymerization of perfluorocyclohexane. Polymerization in this case involves ring opening and loss of fluorine the C : F stoichiometry of the plasma polymer film being much lower than for the starting material. The resulting plasma polymer shows evidence for molecular rearrangements accompanying plasma polymerization, the structure being dominated by $\underline{C}F_3$ and $\underline{C}F_2$ structural features. At high values of W/FM, the plasma polymer produced from the perfluorinated ether also exhibits a substantially lower C : F stoichiometry than for the starting monomer. However as W/FM is reduced the stoichiometry approaches that of the starting monomer but is still deficient in oxygen. The plasma polymerization under comparable conditions of the perfluorinated ether compared with perfluorocyclohexane is some two orders of magnitude faster. Indeed the great efficiency of

the plasma polymerization route for the ether is such that strong spatial dependence is observed for both the rate of deposition and to a lesser extent, the gross structural features of the polymer film.

Electron impact studies [236] have been reported on perfluoro-2-butyltetrahydrofuran and perfluoro-2-propyltetrahydropyran. It is clear from these that the typical distribution of electron energies in the plasma will provide a significant source of fluoroalkoxy anions as well as positively charged species since the ionization potential for the oxygen lone pair is significantlt below that of perfluorocyclohexane ($\Delta E \sim 3$ eV). Mass spectrometric studies (70 eV) carried out in this work reveal extensive fragmentation with little evidence for the parent peak; the base peak corresponding to CF_3^+ with large components arising from the elimination of $C_3F_7^+$, $C_2F_5^+$ and $C_2F_4^+$ fragments. Indeed the major fragments in the positive ion mass spectrum corresponds to fluoro-alkyl fragments. By contrast the negative ion spectrum is dominated by fluoroalkoxy anions. It seems likely therefore that polymerization predominantly involves the positively charged and neutral manifold. The fact that polymerization occurs more readily than for perfluorocyclohexane and that under the appropriate conditions the stoichiometry is much closer to that of the starting monomer for the ether is readily understandable in terms of the much lower ionization potential for the ether. Moreover the oxygen radical cation produced in such a process has a variety of facile routes for elimination of oxygen and maintaining the carbon to fluorine stoichiometry (e.g. elimination of CF_2O). Rearrangement of the resulting fluorocarbon chain involving successive fluorine migrations could then account for the relative increase of $\underline{C}F_3$ and $\underline{C}F$ at the expense of $\underline{C}F_2$ structural features. The interaction of such ions with either neutral monomer or with negative ions provides a means of retaining

some low level of oxygen functionality. It is not beyond the realms of possiblity that under vacuum conditions (e.g. in situ) the large polarizable fluoroalkoxy anions could be stabilized as intimate ion pairs with fluoro-carbocation counter ions and that this could account for the unusually low binding energy observed for one component of the O_{1s} levels. An analogy might be drawn in respect of this thesis in terms of stabilized ion pairs observed in ESCA studies of frozen magic acid solutions of carbocations.[237]

The available data does not merit more detailed discussion at this stage but the basic structural features evidenced from the ESCA data are understandable in terms of conventional elimination, addition and rearrangement reactions in the cation and neutral manifold.

CHAPTER EIGHT

CHAPTER EIGHT

AN INVESTIGATION OF POLYMERS SYNTHESIZED BY R.F. GLOW DICHARGES IN METHYL ESTER 2,2,3,4,4-PENTAFLUORO-3-BUTENOIC ACID, (I); 1,1,1,3,4,4-HEXAFLUORO-2-(TRIFLUOROMETHYL)-3-BUTEN-2-OL, (II); 1,1,1,2,3,3,3-HEPTAFLUORO-2-PROPANOL,(III); AND 1,2-DIBROMO-1,1,2-TRICHLOROETHANE, (IV).

Abstract

The structural features of films formed by the plasma polymerization of I, II, III and IV have been investigated by ESCA and shown to be complex. Analysis of relative intensity of the corresponding peaks of the polymer films has revealed stoichiometries which differ from those of the starting monomers. The spectra all show evidence of extensive molecular rearrangement and elimination of atoms accompanying polymerization.

CHAPTER EIGHT: AN INVESTIGATION OF POLYMERS SYNTHESIZED BY R.F. GLOW DISCHARGES IN $CF_2=CFCF_2COOCH_3$, (I); $CF_2=CF(CF_3)_2OH$, (II); $(CF_3)_2CFOH$, (III); AND $CBrCl_2CHBrCl$, (IV).

8.1 Introduction

In this chapter a preliminary study of polymer films prepared from I, II, III and IV by R.F. plasma polymerization is presented. The considerable new insight provided by ESCA arises from the number of information levels available from a single experiment, coupled with the capability to study ultra thin films which are generally highly crosslinked and isoluble. The study will therefore concern itself with the structural features and bonding of plasma polymerized polymer films as revealed by ESCA.

The main objective of this initial study is to provide information on the final structure of the plasma polymerized polymers obtained from the aliphatic hydrocarbon monomers which contain fluorine and oxygen (I, II, III) and bromine and chlorine (IV).

8.2 Experimental

Preliminary experiments have been carried out to obtain plasma polymerized polymer films of I, II, III and IV by R.F. plasma techniques. In the previous chapters we have described the reactor configurations employed to synthesize plasma polymer films and for the work carried out in this chapter reactor B (as in Chapter Five) has been employed.

Samples prepared in the glow region were obtained by depositing onto fresh gold substrates for ESCA analysis. For IV plasma polymerized films were investigated in both the glow and non-glow regions the gold

substrate in the latter case being located 30cm from the end of the coil region. The plasma deposition and measurement of ESCA spectra (Kratos ES300) were as described previously.[232]

Starting monomers I, II, III and IV (liquids) were obtained from ICI Ltd. Cheshire. All the starting monomers were used without further purification and were degassed prior to use.

8.3 Results and Discussion

It is convenient in this section to discuss the results for each of the plasma polymers studies separately.

8.3.1 Methyl ester 2,2,3,4,4-pentafluoro-3-butenoic acid, $CF_2=CFCF_2COOCH_3$, (I).

Figure 8.3.1 shows the O_{1s}, F_{1s} and C_{1s} core levels of polymer films prepared at 10 W discharge power and a pressure of 200 μ, deposition being for 20 minutes. The C_{1s} spectra exhibit considerable fine structure attributable to structural features which entail and overall span in binding energy of $\sim$ 9.0 eV. However, a deconvolution of the C_{1s} level envelope was not attempted for the discussion presented here, since then large O_{1s} signal implies a substantial contribution to the C_{1s} profile from oxygen functionalities which overlap with the $\underline{C}=CF_n$ and $\underline{C}F$ components, although the spectra clearly reveal the evidence of $\underline{C}F_2$ and $\underline{C}F_3$ structural features. From the previous discussion there is little doubt that there are at least 9 different electronic environments within the C_{1s} profile; 6 with fluorine; 2 with oxygen; and 1 with hydrogen. However, the component at highest binding energy $\sim$ 293.9 eV, (contributing $\sim$ 8.0% the total intensity of C_{1s} envelope, FWHM = $\sim$ 1.9 eV) corresponds

unambiguously to $\underline{CF}_3$ structural features. As there are no $\underline{CF}_3$ structural features in the starting monomer, there is clear evidence for rearrangement accompanying polymerization.

Considering now the stoichiometry of polymer films derived from the intensity ratios for O_{1s}, F_{1s} and C_{1s} levels (having previously determined the apparent instrumental sensitivity factor for these levels); these provide stoichiometries for C : F of 1 : 0.68 and C : O of 1 : 0.31 compared with 1 : 2 and 1 : 0.4 for the starting monomer respectively. This provides clear evidence that the polymerization proceeds via elimination of fluorine and oxygen, with the former being more facile.

Figure 8.3.1 $\underline{C_{1s}}$, $\underline{F_{1s}}$ and $\underline{O_{1s}}$ levels for plasma polymers prepared from methyl ester 2,2,3,4,4-pentafluoro-3-butenoic acid, (I).

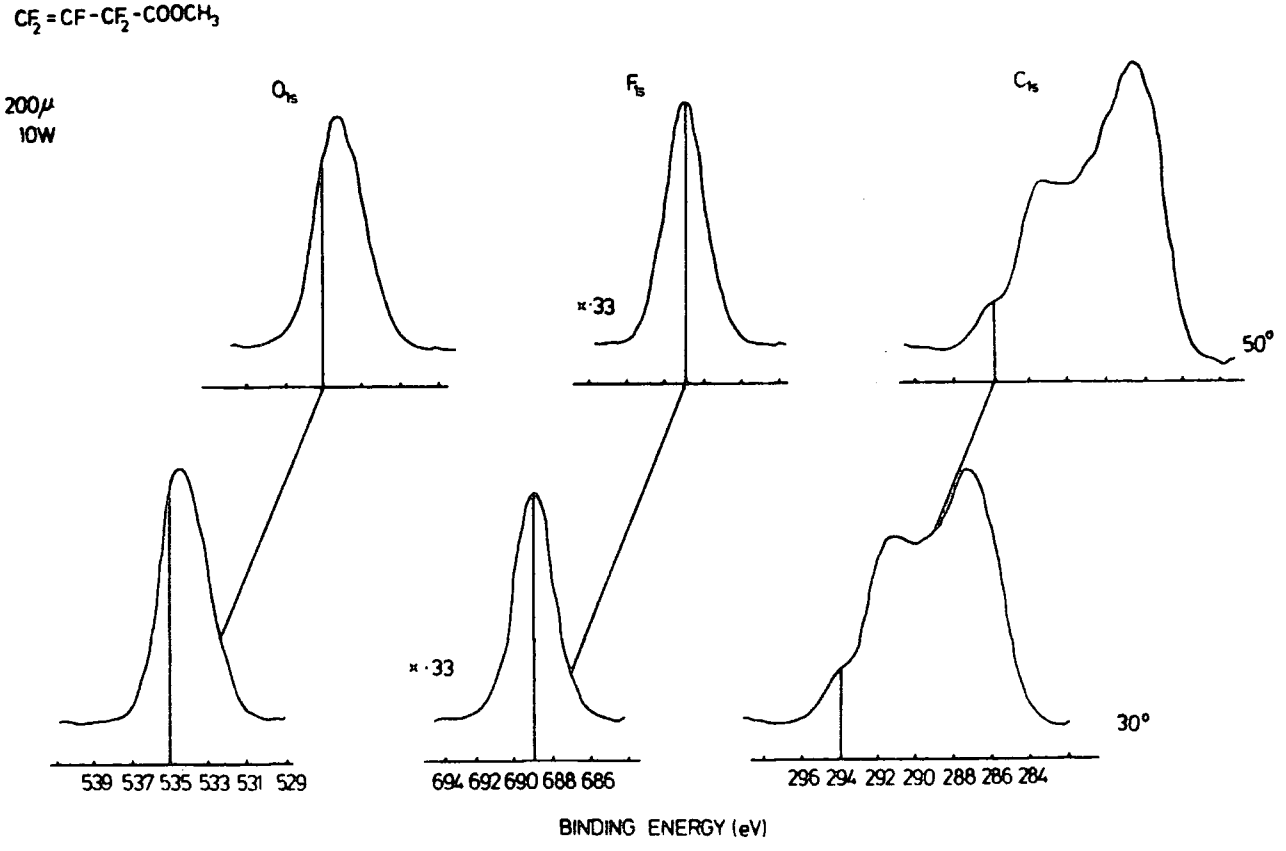

8.3.2 1,1,1,3,4,4-hexafluoro-2-(trifluoromethyl)-3-buten-2-ol; $CF_2{=}CF(CF_3)_2OH$, (II).

Figure 8.3.2 shows the O_{1s} , F_{1s} and C_{1s} levels of polymers formed in the glow region at 10 W input power and a pressure of 200 μ For the C_{1s} core levels, a distinctive peak is apparent at binding energy $\sim$ 294.0 eV corresponding to $\underline{C}F_3$ structural features, which contribute $\sim$ 24 % to the total intensity for the C_{1s} levels. As expected these to some extent arise from the $\underline{C}F_3$ structural features in the starting monomer. However, the theoretically calculated percentage contribution of 40% in the monomer for the $\underline{C}F_3$ structural features to the total intensity of C_{1s} profile, suggests a rearrangement process with associated elimination of $\underline{C}F_3$ structural features during polymerization.

Figure 8.3.2 $\underline{C_{1s}}$, $\underline{F_{1s}}$ and $\underline{O_{1s}}$ levels for plasma polymers prepared from $\underline{CF_2{=}CF(CF_3)_2OH}$, (II)

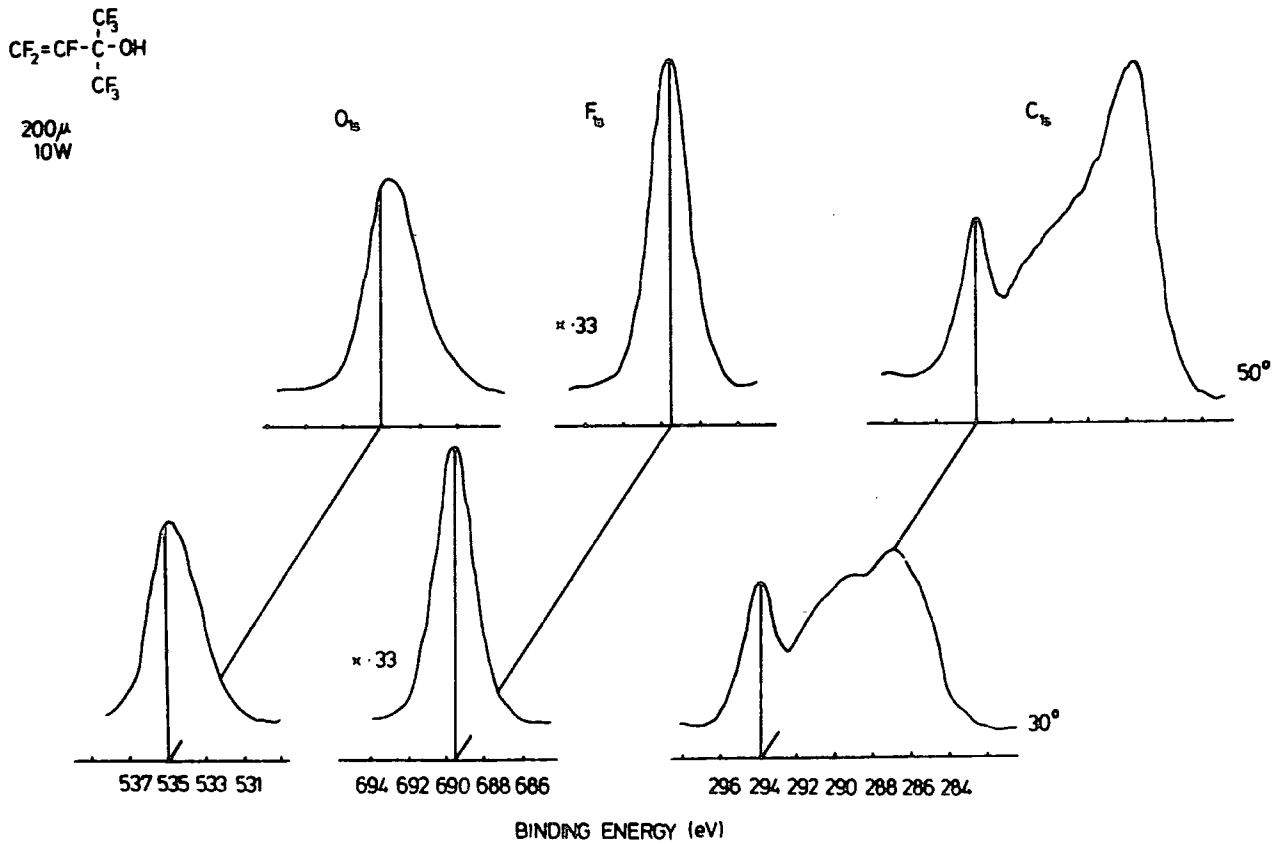

The stoichiometry of the polymer films was found to be $C_1F_{0.97}$ and this may be compared with $C_1F_{1.8}$ for that of the starting monomer. This also shows that elimination process leads to the loss of fluorine during polymer formation.

However the C : O stoichiometry is somewhat higher $C_1O_{0.28}$ compare with that of the starting monomer $C_1O_{0.2}$, indicating a higher level of oxygen incorporation in this system. From the evidence discussed above, it is clear that elimination and rearrangement accompany polymerization, with the later being more favourable.

8.3.3 1,1,1,2,3,3,3-heptafluoro-2-propanol; $(CF_3)_2CFOH$, (III)

Figures 8.3.3a and 8.3.3b shows the O_{1s}, F_{1s} and C_{1s} levels of of polymer formed in the glow region at 10 W input power and pressures of 200 μ and 300 μ respectively. Considering firstly the spectra in Figure 8.3.3a. As seen earliar in the C_{1s} envelope, it is possible to assign the peak at $\sim$294.0 eV to $\underline{C}F_3$ structural features. This peak (FWHM $\sim$ 1.9 eV) give a contribution of $\sim$27% to the total intensity for the C_{1s} profiles, compared to the theoretically calculated percentage contribution of 66.7% for the starting monomer. This indicates that the mechanism of polymer film formation is associated with molecular rearrangement and considerable loss of $\underline{C}F_3$ structural features. The C : F stoichiometry of 1 : 1.01 shows a substantially lower fluorine content for the polymer film when compared with that of the starting monomer, $C_1F_{2.33}$. However within the experimental error, the oxygen content in the polymer films is essentially the same as that of the monomer, $C_1O_{0.33}$. The broad nature of the O_{1s} level (FWHM = 3.0 eV)

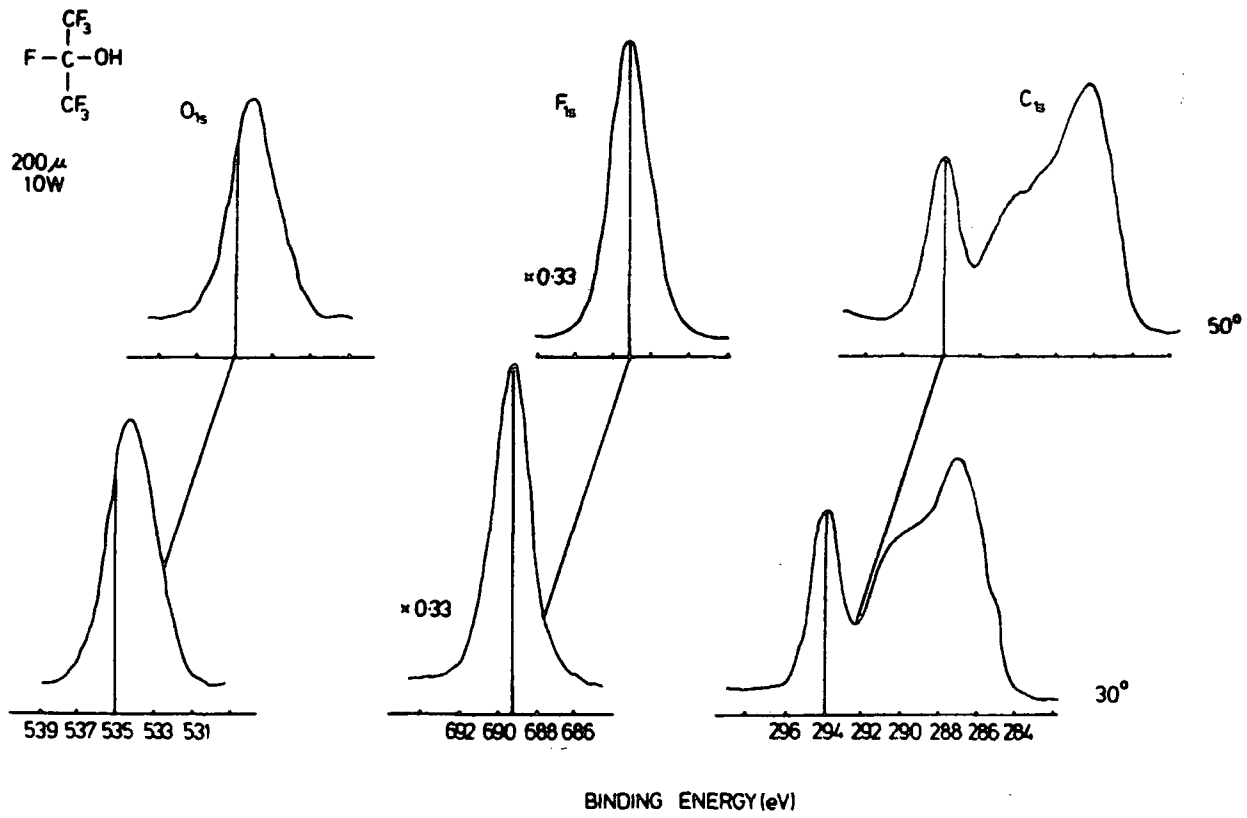

Figure 8.3.3 C_{1s}, F_{1s} and O_{1s} levels of plasma polymerized $(CF_3)_2CFOH$, (III): a. (above), prepared at a pressure of 200 μ ; b. (below) prepared at a pressure of 300 μ .

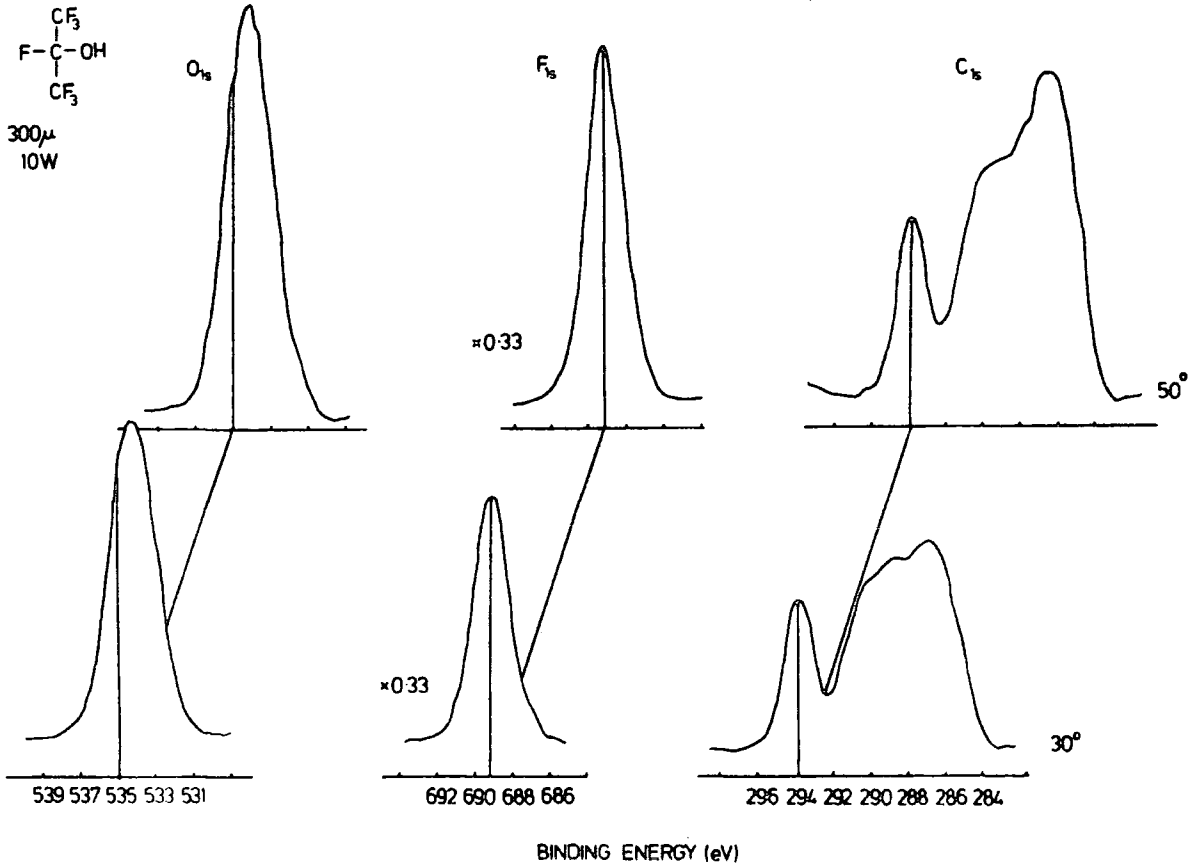

indicate that at least two types oxygen with different electronic environments are present in the polymer films, providing further evidence for molecular rearrangement involving oxygen. It is possible at this preliminary stage to say that there are substantial molecular rearrangements and eliminations of fluorine accompany polymerization.

For comparison purpose it is convenient to discuss the data in Figure 8.3.3b along the same lines as for Figure 8.3.3a. For the polymer films prepared at low input power and a pressure of 300 μ , the $\underline{C}F_3$ structural features contribute $\sim$ 22% to the total intensity (100%) of the C_{1s} profiles. This $\sim$ 5% less than for polymer films prepared at 200 μ . The C : F and C : O stiochiometries for polymer films prepared at 300 μ were found to be 1 : 0.8 and 1 : 0.41 respectively. An interesting feature to be noted here is that the polymer films show an increase in oxygen content compared with that of the starting monomer. This therefore provides strong evidence that the polymerization involves the loss of fluorine by elimination of $\underline{C}F_3$ groups etc. The data (in Figures 8.3.3a and 8.3.3b) therefore suggest that greater molecular rearrangement and at the same time greater elimination of fluorine takes place at higher pressure.

8.3.4 Plasma Polymerized 1,2-dibromo-1,1,2-trichloroethane (IV)

Preliminary experiments have been carried out on IV to study the nature of the polymer produced, (a) in the glow region and (b) in a region ca. 30 cm. beyond the end of the coil, which at higher pressures corresponds to the non-glow region. Figure 8.3.4 displays a two typical wide scan spectra for the plasma polymer produced in the glow and in a non-glow region, at a pressure of 100 μ and input power of 10 W for a

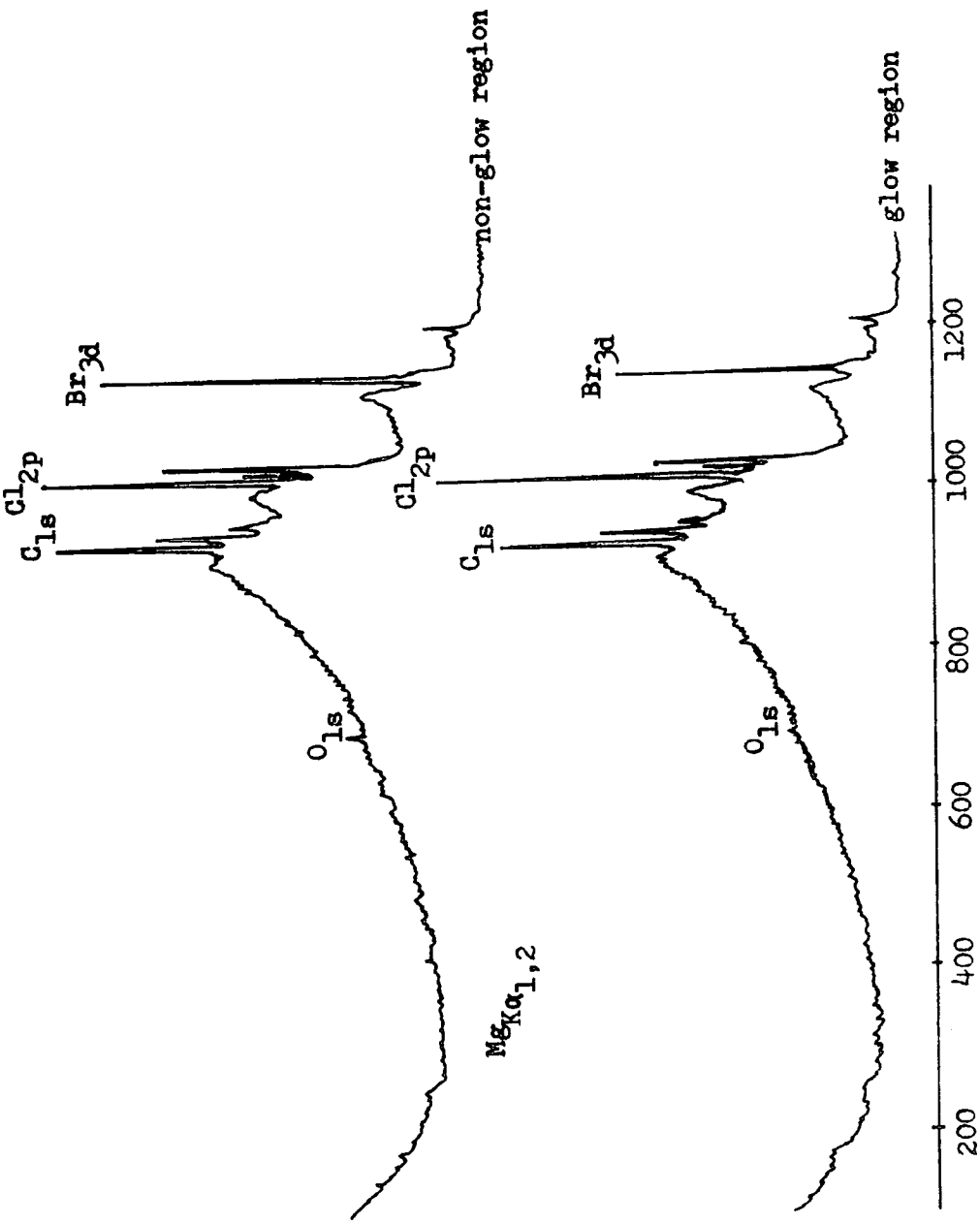

Figure 8.3.4 Wide scan ESCA spectra for plasma polymer films of $CBrCl_2CHBrCl$, (IV)

deposition period of 15 minutes. The relatively intense photoemission peaks can readily be identified as being from C_{1s}, Cl_{2p} and Br_{3d} levels. A quantitative compositional analysis of these polymers is provided from a detailed examination of high resolution spectra of these peaks. The corresponding spectra of polymer films obtained in the glow and non-glow regions are shown in Figure 8.3.5.

In previous section it has been shown that difficulties arise in the deconvolution of the C_{1s} spectra when there are a large number of atoms in different electronic environment. The problem is aggravated, since the plasma polymers were remarkably different in structure compared with the starting monomer, (c.f. previous chapters). For plasma polymer polymerized 1,2-dibromo-1,1,2-trichloroethane, deconvolution of the C_{1s} level becomes even more difficult, since chemical shifts in the C_{1s} levels arising from Cl, Br and combination of their substituents are relatively small compared with those of e.g. fluorine.[198] No attempt was therefore made to deconvolute these levels.

Considering firstly the data for polymer films in the glow region. Analysis of the relative intensities of the total C_{1s}, Cl_{2p} and Br_{3d} peak gave C : Cl : Br stoichiometries of 1 : 1.15 : 0.17. Comparing this with that of the starting monomer ($C_1Cl_{1.5}Br_1$), it is clear that elimination of chlorine and bromine and extensive rearrangement accompanies polymerization.

Turning to the polymer films prepared in the non-glow region, a C : Cl : Br stoichiometry of 1 : 0.43 : 0.27 is obtained. This indicates that the polymer produced in the non-glow region has somewhat larger bromine and slightly less chlorine in composition compared with that of in the glow region. It is of interest to consider the O_{1s} which

have a complex line shape. This can be associated with the differing oxygen functionalities (singly and doubly bonded oxygen to carbon structural features).[201] These arise from the exposure of the films to atmosphere subsequent to preparation. An increase in intensity of O_{1s} levels is seen for polymer films prepared in the non-glow region compared with that of in the glow region. This may imply that the former contains more trapped radicals than the latter (which refers to the degree of oxygen pick up from atmosphere.). It is also important to note that the polymers obtained in the non-glow region were substantially thicker than the effective sampling depth ($\sim$ 100 Å), since no signal from $Au_{4f_{7/2}}$ levels of the substrate was observed, (see Figure 8.3.4). This therefore rules out the possibility that the slight increase in intensity of the O_{1s} level may arise from the substrate.

Figure 8.3.5 C_{1s}, Cl_{2p}, Br_{3d} and O_{1s} levels for plasma polymers of $CBrCl_2CHBrCl$, (IV); prepared in glow and non-glow regions

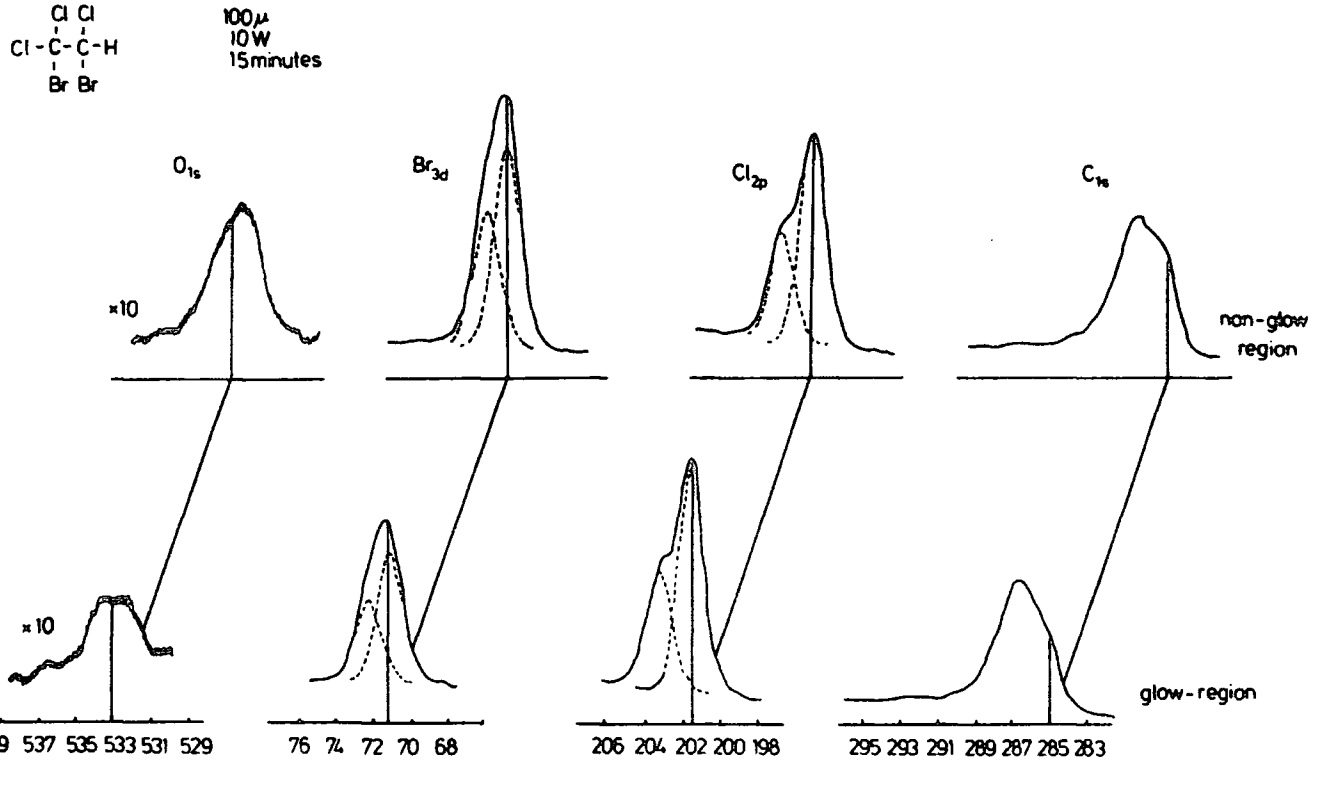

A P P E N D I X

APPENDIX ONE

REFERENCES

1. McTaggart F. K., Ed., "Plasma Chemistry in Electrical Discharges", Elsevier Publishing Co., Amsterdam, 1967

2. Hollahan J.R. and Bell A.T., Eds., "Techniques and Applications of Plasma Chemistry", Wiley, N.Y. 1974

3. Shen M., Ed., "Plasma Chemistry of Polymers", Marcel Dekker, Inc., N.Y. 1976

4. Shen M. and Bell A. T., Eds., "Plasma Polymerization" ACS Symposium Series 108, Washington D.C. 1979

5. Brondt, Deimann, van Troostwyk P. and Lauwerenburg, Ann. Chim., 21 (48), 58 (1796)

6. De Wilde P., Ber., 7,352 (1874)

7. Thenard P. and A., Compt. Rend., 78, 218 (1874)

8. Goodman J., J. Polym. Sci., 44, 551 (1960)

9. Hudis H., in "Techniques and Applications of Plasma Chemistry", Hollahan J. R. and Bell A.T.,Eds., Wiley, N.Y. 1974, Chap. 3

10. Hollahan J.R. and McKeever R.P., Adv. Chem. Ser., 80, 272 (1969)

11. Penning F.M., Ed., "Electrical Discharges in Gases", Philips Technical Library, Holland, 1957

12. C.f. McGraw-Hill Encyclopedia of Science and Technology Vol. 1, 1977, R.R. Donnelley and Sons Co. Indiana USA. pg. 729

13. Brown S. C., in "Gaseous Electronics", Vol. 1., Hirsh M. N., and Oskam H. J., Eds., Aca. Press., N. Y., 1978

14. Townsend J. S., Phil. Mag., 8, 733 (1904)

15. Crompton K.T. and Langmuir I., "Electrical Discharges in Gases. I." in Rev. Modern Physic. 2, 123 (1930)

16. Bell A.T., in "Techniques and Applications of Plasma Chemistry", Hollahan J. R. and Bell A. T., Eds., Wiley, N. Y. 1974, Chap. 1

17. Fite W. L., in "Chemical Reactions in Electrical Discharges", R. F. Gould, Ed., Am. Chem. Soc. Pubs., 1969

18. Meek J. M. and Craggs J. D., Eds., "Electrical Breakdown of Gases", Wiley, Chichester, 1978, Chap. 1

19. Franklin R. N., Ed., "Plasma Phenomena in Gas Discharges", Oxford, 1976

20. Brassem P. and Massen F. J. M. J., Spectrochimica Acta, 29B, 203 (1974)

21. Clark D. T. and Dilks A., in "A.C.S. Centennial Meeting, N. Y., April 1976, Int. Sym. On Advances in Characterization of Metal and Polymer Surfaces", Lee L. H.,Ed., 2, 101, Aca. Press, N. Y. (1977)

22. Clark D.T., Dilks A. and Shuttleworth D., in "Polymer Surfaces", Clark D. T. and Feast W. J., Eds., Wiley, N. Y. 1978, Chap. 9

23. C.f. Panel Discussion, "Symposium on Plasma Chemistry of Polymers", J. Macromol. Chem., A(10), 3 1976

24. Clark D. T. and Dilks A., J. Polym. Sci., Polym. Chem. Ed., 18, 1233 (1980)

25. Samsom J. A. R., "Technology of Vacuum Ultraviolet Spectroscopy", Wiley, N. Y. 1967

26. Dresvin S. V., Ed., "Physics and Technology of Low-Temperature Plasmas", Iowa State Univ. Press, 1977, Chap. 3

27. Yasuda H. and Hsu T., Surf. Sci., 26, 232 (1976)

28. Kay E. Int. Round Table on Plasma Polymerization and Treatment, IUPAC Symp. on Plasma Chemistry, 1974

29. Yasuda H. and Hirotsu T., J. Polym. Sci., Polym. Chem. Ed., 16, 743 (1976)

30. Koboyashi H., Bell A. T. and Shen M., Macromol., 7, 277 (1974)

31. C.f. Shen M. and Bell A. T. Eds., "Plasma Polymerization", ACS Symp. Series 108, Washington D. C. 1979, Chap. 1

32. Yasuda H. and Hsu T., J. Polym. Sci., Polym. Chem. Ed., 15, 81 (1977)

33. Vinzant J. W., Shen M. and Bell A. T., in "Plasma Polymerization", M. Shen and A. T. Bell, Eds., ACS Symp. Series 108, Washington D. C., 1979, Chap. 5

34. Yasuda H. and Lamaze C. E., J. Appl. Polym. Sci., 17, 1533 (1973)

35. Williams T. and Hayes M. W., Nature, 209, 769 (1966)

36. Yasuda H. and Lamaze C. E., J. Appl. Polym. Sci., 15, 2277 (1971)

37. Smolinsky G. and Vosile M. J., Int. J. Mass. Spectrom. Ion. Physic, 12, 133 (1933)

38. Morita S., Sawa G. and Ieda M., J. Macromol. Sci-Chem., A10(3), 501 (1976)

39. Sharma A. K., Millich F. and Hellmuth E. W., in "Plasma Polymerization" M. Shen and A. T. Bell, Eds., ACS Symp. Series 108, Washington D. C., 1979, Chap. 3

40. Westwood A. R., Euro. Polym. J., 7, 363 (1971)

41. Thomson L. F. and Mayhan K. G., J. Appl. Polym. Sci., 16, 2317 (1972)

42. Smolinsky G. and Vosile M.J., J. Macromol., Sci.-Chem., 10, 1275 (1976)

43. Denaro A.R., Owens P. A. and Crowhow A., Euro. Polym. J., 4, 93 (1968)

44. Morosoff N., Crist B., Bumgarner, Hsu T. and Yasuda H., J. Macromol., Sci.-Chem., 10, 451 (1976)

45. Carchano, J. Chem. Phys., 61, 209 (1974)

46. Lam D. K., Baddour R. F. and Stancell A.F., J. Macromol., Sci.-Chem., 10, 421 (1976)

47. Tibbitt J. M., Jensen R. and Bell A. T., J. Appl. Polym. Sci., 10, 647 (1977)

48. Suhr H., in "Techniques and Applications of Plasma Chemistry", Hollahan J. R., and Bell A. T., Eds., Wiley, N. Y., 1974, Chap. 2

49. a) Morosoff N. and Yasuda H., in "Plasma Polymerization", Shen M. and Bell A. T., Eds., ACS Symposium Series 108, Washington D. C., 1979, Chap. 10

b) Yasuda H. and Morosoff N., in "Plasma Polymerization", Shen M. and Bell A. T., Eds., ACS Symposium Series 108, Washington D. C., 1979, Chap. 17

50. Ingold J. H., in "Caseous Electronics", Hirsh M. N. and Oskam H. J., Eds., Vol. 1., Aca. Press, N. Y., 1978, Chap. 2

51. Kobayashi H., Shen M. and Bell A. T., J. Macromol., Sci.-Chem., 8, 373 (1974)

52. Clark D.T. and Shuttleworth D., J. Polym. Sci., Polym. Chem., Ed., 17, 1317 (1979)

53. Seeger M., Barrell E. M. and Shen M., J. Polym. Sci., Polym. Chem. Ed., 13, 1541 (1975)

54. Seeger M., Gritter R. J., Tibbitt J. M., Shen M. and Bell A. T., J. Polym. Sci., Polym. Chem. Ed., 15 1403 (1977)

55. Jesch K. F., Bloor J. E., Kronick P. L., J. Polym. Sci., Part. A-1, 4, 1487 (1966)

56. Kronic P. L. and Jesch K. F., J. Polym. Sci., Part. A-1, 7, 767 (1969)

57. Tibbitt J. M., Bell A. T. and Shen M., J. Polym. Sci., Polym. Chem. Ed., 13, 1541 (1975)

58. Thomson L. F. and Mayhan K. J., J. Appl. Polym. Sci., 16, 2291, (1972)

59. Dilks A., Kaplan S. and Van Laeken A., J. Polym. Sci., Polym. Chem. Ed., in press 1981

60 Kaplan S. and Dilks A., Thin Solid Films, in press 1981

61. Kobayashi H., Shen M., Bell A. T., J. Appl. Polym. Sci., 18, 885 (1973)

62. Dynes P. J. and Kaelble D. H., in "Plasma Chemistry of Polymers", Shen M., Ed., Marcel Dekker, Inc., N. Y., 1976

63. Schonhorn H., in "Polymer Science", Clark D. T. and Feast W. J., Eds., Wiley, N. Y., 1978, Chap. 10

64. Kaelble D. H. ed., "Physical Chemistry of Adhesion", Wiley, N. Y., 1971

65. Thomson L. F. and Smolinsky G., J. Appl. Polym. Sci., 16, 1179 (1972)

66. Niinomi M., Kobayashi H., Bell A. T. and Shen M., J. Appl. Phys., 44, 4317 (1973)

67. Niinomi M., Kobayashi H., Bell A. T. and Shen M., J. Appl. Polym. Sci., 18, 2199 (1974)

68. Kolotyrkin V. M. Gil'man A. B. and Tsapuk A. K., Russ. Chem. Rev., 36(8), 579 (1967)

69. Mearns A. M., Thin Solid Films, 3, 201 (1969)

70. Perez S. R. ed., "Glow Discharge Polymerization and Thin Films", Xerox, Technical Report, 1974

71. Clark D. T. 'Chemical Aspects of ESCA', in "Electron Emission Spectroscopy", Dekeyser W. and Reidel D., Eds., Reidel D., Pub. Co., Dordrect, Holland, 373 (1973)

72. Hertz H., Ann. Physik, 31, 983 (1887)

73. Leanard P., Ann. Physik, 2, 359 (1900)

74. Einstein A., Ann Physik, 17, 132 (1905)

75. Robinson H., Phil. Mag., 50, 241 (1925)

76. de Broglie M., Compt. Rend., 172, 274 (1921)

77. van Akker J.A. and Watson E.C., Phys. Rev., 37, 1631 (1931)

78. Ference, Jr. M., Phys. Rev., 51, 720 (1937)

79. Steinhardt, Jr. R.G ., Granados F. A. D. and Post G. I., Anal. Chem., 27, 1046 (1955)

80. Siegbahn K. and Edvarson K., Nucl. Phys., 1, 137 (1956)

81. Nordling C., Sokolowski E. and Siegbahn K., Phys. Rev., 105, 1676 (1957)

82. Nordling C. Hagstrom S. and Siegbahn K., Z. Physik, 178, 433 (1964)

83. Hagstrom S., Nordling C. and Siegbahn K., Phys. Lett., 9, 235 (1964)

84. Siegbahn K., Nordling C., Fahlman A., Nordberg R., Hamrin K., Hedman J., Johansson G., Berkmark T., Karlsson S. E., Lidgren I. and Lindberg B., " ESCA, Atomic, Molecular and Solid State Structure Studied by Means of Electron Spectroscopy", Almquist and Wiksells, Uppsala (1967)

85. Siegbahn K., Nordling C., Johansson G., Hedman J., Heden P. F., Hamrin K., Gelius U., Berkmark T., Werme L. D., Manne R. and Baer Y., "ESCA Applied to Free Molecules" North-Holland Pub. Co., Amsterdam (1969)

86. Siegbahn K., "Electron Spectroscopy - An Outlook" , J. Elect. Spect. and Rel. Phen., 5, 3 (1974)

87. Siegbahn K., "Electron Spectroscopy for Chemical Analysis", A Survey present at the Third International Conference on Atomic Physic at the University Colorado, Boulder, Colorado 1972

88. Siegbahn K. "Electron Spectroscopy and Molecular Structure", A Survey presented at XVIIIth Colloquium Spectroscopium International at Grenoble, Fr., Sept. 1975

89. Siegbahn K., "Electron Spectroscopy for Solids, Surfaces, Liquids and Free Molecules, Uppsala University, Sweden 1976

90. Turner D. W., Baker C., Baker A. D., Brundle C. R., Eds., "Molecular Photoelectron Spectroscopy", Wiley, N. Y., 1970

91. Clark D. T. 'Structure and Bonding in Polymers as Revealed by ESCA' in "Electronic Structure of Polymers and Molecular Crystals", Ladik J., and Andre J. M., Eds., Plenum Press, N. Y., 1975

92. Cederbaum L. S. and Domcke W., J. Elect. Spect. and Rel. Phen., 13, 161 (1978)

93. Auger P., Compt. Rend., 65, 180 (1925)

94. Lander J. J., Phys. Rev., 91, 1382 (1953)

95. Coster D. and Kronig R. de L., Physica, 2, 13 (1935)

96. Burhop E. H. S., Eds., "The Auger Effect and Other Radiationless Transitions", Cambridge Uni. Press, 1952

97. C.f. Carlsson T. A., Ed., "Photoelectron and Auger Spectroscopy", Plenum Press, N. Y., 1975

98. Hass T. W., Grant J. T. and Dooley G. J., Phys. Rev., 13(1), 1449 (1970)

99. Kowalczyk P. S., Pollack R. A., McFeely F.R., Ley L. and Shirley D. A., Phys. Rev., 13(8), 2387 (1973)

100. Grant. J. T. in "Symposium on Advances in Characterization of Metal and Polymer Surfaces", Lee L. H., Ed., Aca. Press, Vol. I, 1976

101. Chang C. C., Surface Sci., 25, 53 (1971)

102. Coad J. P., Getting M. and Riviere J. G., Farad. Disc. Chem. Soc., 60, 269 (1975)

103. Sandstrom A. E., in "Handbook of Physics XXX. X-Rays", Flugge S. F., Ed., Springer Verlag, Berlin (1975), pg. 164.

104. Bagus P. S., Phys. Rev., 139A, 619 (1965)

105. Krouse M. O., Carlson A. T. and Dusmukes R. D., Phys. Rev., 37, 170 (1968)

106. Manne R. and Åberg T., Chem. Phys. Lett., 7, 282 (1970)

107. Shirley D. A., in "Advances in Chemical Physics", 23, 85, Prigogine I, and Rice S. A., Eds., Wiley, N. Y., 1973

108. Synder L. C.,J. Chem. Phys., 55, 95 (1971)

109. Adams D. B. and Clark D. T., Theoret. Chim. Acta., 31, 171 (1973)

110. Hillier I. H. and Kendrick J., J. Elect. Spect. and Rel. Phen., 6, 325 (1975)

111. Gelius U. and Siegbahn K., Farad. Disc. Chem. Soc., 54, 257 (1972)

112. Clark D. T., Scanlan I. W. and Muller J., Theoret. Chim. Acta., (Berl)., 35, 341 (1974)

113. Koopmans T. A., Physika, 1, 104 (1933)

114. Meyer W., J. Chem. Phys., 58, 1017 (1973)

115. Levy B., Millie P. H., Ridard J. and Vinh J., J. Elect. Spect. and Rel. Phen., 4, 13 (1974)

116. Clark D. T. and Scanlan I. W., J. Chem. Soc., Farad. Trans. II, 70, 1222 (1974)

117. Clark D. T., in "Advances in Polymer Science", Cantow H. J., Ed., Springer Verlag, Berlin, 24, 125 (1977)

118. Brisk M. A. and Baker A. D., J. Elect. Spect. and Rel. Phen., 7, 197 (1977)

119. Wagner C. D., Riggs W. M., Davis L. E., Moulder J. F. and Muilenberg G. E., "Handbook of X-Ray Photoelectron Spectroscopy", Perkin-Elmer Cor. USA., 1979

120. Sunjic M., Sokcevic and Lucas C., J. Elect. Spect. and Rel. Phen., 5, 963 (1974)

121. Hooker M. P., Grant J. T. and Haas T. W., J. Vac. Sci. Technol. 13, 296 (1976)

122. Henke B. L., Adv. X-Ray Analysis, 13, 1 (1969)

123. Wagner C. D., Farad. Disc. Chem. Soc., 60, 306 (1975)

124. Siegbahn K., Hammond D., Fellner-Feldegg H. and Barnet E. F., Science, 176, 245 (1972)

125. Clark D. T. and Shuttleworth D., J. Elect. Spect. and Rel. Phen., 17, 15 (1979)

126. Eisberg R. M., "Fundamentals of Modern Physics.", Wiley, N. Y., 1961, Chap. 14

127. Clark D. T., Thomas H. R., Dilks A and Shuttleworth D., J. Elect. Spect. and Rel. Phen., 10, 455 (1977)

128. Purcell E. M., Phys. Rev., 54, 818 (1938)

129. Helmer J. C. and Weichert N. H., Appl. Phys. Lett., 13, 268 (1968)

130. Sokolowski E., Arkiv Physik, 15, 1 (1959)

131. Nordling C., Arkiv Physik, 15, 397 (1959)

132. Johansson G., Hedman J., Berudtsson A., Klasson M., and Nilsson R., J. Elect. Spect. and Rel. Phen., 2, 295 (1973)

133. Scherr C. W., Siverman J. N. and Matsen F. A., Phys. Rev., 127, 830 (1962)

134. Snyder L. C. and Basch H., J. Am. Chem. Soc., 91, 2189 (1969)

135. Schwartz M. E., Chem. Phys. Lett., 6, 631 (1970)

136. Gelius U., Basilier E., Svensson S., Bergmark T. and Siegbahn K., J. Elect. Spect. and Rel. Phen., 2, 405 (1974)

137. Muller J., Ph. D., Thesis, University of Durham, 1976

138. Vorvilain-Berger S. and Verhaegen G., Chem. Phys. Lett., 50, 468 (1977)

139. Jolly W. L. and Hendrickson D. N. J. Am. Chem. Revs., 3, 193 (1970)

140. Clark D. T. and Adams D. B., J. Chem. Soc., Farad. Trans. II., 68, 1819 (1972)

141. Adams D. B. and Clark D. T., J. Elect. Spect. and Rel. Phen., 2, 201, (1974)

142. Hehre W. J., Stewart R. F. and Pople J. A., J. Chem. Phys., 51, 2657 (1969)

143. Ditchfield R., Hehre W. J. and Pople J. A., J. Chem. Phys., 54, 724 (1971)

144. Pople J. A. and Beveridge, Eds., "Approximate Molecular Orbital Theory", McGraw-Hill, N. Y., 1970

145. Clark D. T., Briggs D. and Adams D. B., J. Chem. Soc., Dalton, 19 (1973)

146. Clark D. T. and Kilcast D., J. Chem. Soc., B., 2243 (1971)

147. Clark D. T. , Chambers R. D., Kilcast D. and Musgrave W. K. R., J. Chem. Soc., Farad. II., 2, 309, (1972)

148. Atkins P. W., in "Molecular Quantum Mechanics", Oxford, Uni. Press., London, 1970

149. Watson R. E. and Freeman A. J., in "Hyperfine Interactions", Freeman A. J. and Frankel R. B., Eds., Aca. Press. N. Y. 1967

150. Fadley C. S., Shirley D. A., Freeman A. J., Bagus P. S. and Mallow J. V., Phys. Rev. Lett., 23, 1397 (1969)

151. van Vleck J. H., Phys. Rev. Lett., 45, 405 (1934)

152. Fadley C. S., in "Electron Spectroscopy", Shirley D. A., Ed., North Holland, 1972, pg. 781

153. Shirley D. A. and Davis D. W., J. Chem. Phys., 56, 669 (1972)

154. Novakov T. and Hollander J. M., Bull. Am. Phys. Soc., 14, 524 (1969)

155. Novakov T. and Hollander J. M., Phys. Rev. Lett., 21, 1133 (1968)

156. Wertheim G. K., Ed., "Mossbauer Effect, Principles and Applications", Aca. Press, N. Y., 1964

157. Bancroft G. M., Adams I., Lampe H. and Sham T. K., Chem. Phys. Lett., 32, 173 (1975)

159. Ascerelli P. and Missoni G., J. Elect. Spect. and Rel. Phen., 5, 417 (1974)

158. Parrat L. G., Rev. Mod. Phys., 31, 616 (1959)

160. McGilp J. F. and Main I. G., J. Elect. Spect. and Rel. Phen., 6, 397 (1975)

161. Huchital D. A. and McKeon R. T., Appl. Phys. Lett., 20, 158 (1972)

162. Clark D. T., Dilks A. and Thomas H. R., J. Polym. Sci., Polym. Chem. Ed., 16, 1461 (1978)

163. C.f. Swingle II R. S. and Riggs W. M., CRC Crit. Rev. Anal. Chem., 5, 267 (1975) CRC Press, Cleveland.

164. Clark D. T., Dilks A., Shuttleworth D. and Thomas H. R., J. Polym. Sci., Polym. Chem. Ed., 17, 627 (1979)

165. Clark D. T., Physica Scripta, (Sweden), 16, 307 (1977)

166. Carley A. F. and Joyner A.T., J. Elect. Spect. and Rel Phen., 16, 1, (1979)

167. Ebel H. and Gurker M., J. Elect. Spect. and Rel. Phen., 5, 799 (1974)

168. Wertheim G. K., J. Elect. Spect. and Rel. Phen., 6, 239 (1975)

169. Clark D. T. and Dilks A., J. Polym Sci., Polym. Chem. Ed., 15, 2321 (1977)

170. Carlson T. A. and McGuire G. E., J. Elect. Spect. and Rel. Phen., 1, 161 (1972)

171. Fadley C. S. Baird R. J., Siekhaus W., Novakov T. and Bergstrom S. Å. L., J. Elect. Spect. and Rel. Phen., 4, 93 (1974)

172. Scofield J. H., J. Elect. Spect. and Rel. Phen., 8, 129 (1976)

173. Cooper J. and Zare R. N., J. Chem. Phys., 48, 942 (1968)

174. Ellison F. O., J. Chem Phys.,61, 507 (1974)

175. Penn D. R.,J. Elect. Spect. and Rel. Phen., 9, 29 (1976)

176. Clark D. T. and Thomas H. R., J. Polym.Sci., Polym. Phys. Ed., 15, 2843 (1977)

177. Clark D. T. and Shuttleworth D., J. Polym. Sci., Polym. Chem. Ed., 16, 1093 (1977)

178. Clark D. T. in "Structural Studies of Macromolecules by Spectroscopic Methods", Ivin K. J., Ed., Wiley, N. Y., 1976, Chap. 9

179. Clark D. T., in "Characterization of Metal and Polymer Surfaces", Vol. 2, Lee L. H., Ed., Aca. Press, N. Y., 1975

180. Kinzig B. J., Polymer Preprints, 21, ACS Meeting, San Francisco, (1980)

181. Clark D. T., Adams D. B., Theoret. Chim. Acta., 39, 321 (1975)

182. Clark D. T., Feast W. J., Ritchie I., Musgrave W. K. R., Modena M., and Ragazzini M., J. Polym. Sci., Polym Chem. Ed., 12, 1049 (1974)

183. Clark D. T., Chambers R. D., Kilcast D., and Partington S, J. Polym. Sci., Polym. Chem. Ed., 12, 1647 (1974)

184. Clark D. T., Feast W. J., Musgrave W. K. R., and Ritchie I., J. Polym. Sci., Polym. Chem. Ed., 13, 857 (1975)

185. Clark D. T. and Kilcast D., Nature, 233, 77 (1971)

186. Clark D. T., Kilcast D., Feast W. J. and Musgarve W. K. R., J. Polym. Sci., A1(10), 1637 (1972)

187. Clark D. T., in "Polymer Surfaces", Clark D. T. and Feast W. J., Eds., Wiley, N. Y., 1978, Chap. 16

188. Clark D. T., and Dilks A., J. Polym. Sci., Polym. Chem. Ed., 15, 15 (1977)

189. Clark D. T. and Dilks A., J. Polym.Sci., Polym. Chem. Ed., 17, 957 (1975)

190. Clark D. T., Dilks A. and Thomas H.R., in "Developments in Polymer Degradation", Grassie N., Ed., Appl. Sci. Publishers, London, 1977

191. Dilks A. and Kay E., in "Plasma Polymerization", Shen M. and Bell A. T., Eds., ACS Symposium Series 108, Washington D.C., 1979, Chap. 12

192. Millard M. M., in "Characterization of Metal and Polymer Surfaces" Lee L. H., Ed., Vol. 2., Aca. Press. N. Y., 1977, pg. 85

193. Gray J., in "Plastic; Surface and Finish", Pinner S. H. and Simpson W. G., Eds., Butterworths, London, 1971, Chap. 3

194. Clark D. T. and Dilks A., J. Elect. Spect. and Rel. Phen., 11, 225 (1977)

195. Clark. D. T., Salenek W. R. and Paton A., J. Appl. Phys., 47, 144 (1976)

196. Clark D. T. and Thomas H. R., J. Elect. Spect. and Rel. Phen., 14, 1671 (1976)

197. Clark D. T. and Dilks A., J. Polym. Sci., Polym. Chem. Ed., 14, 533 (1976)

198. Clark D. T. and Thomas H. R., J. Polym. Sci., Polym. Chem. Ed., 14, 1701 (1976)

199. Clark D. T., Peeling J. and O'Malley J. M., J. Polym. Sci., Polym. Chem. Ed., 14, 543 (1976)

200. Clark D. T., in "Photon, Electron, and Ion Probes of Polymer Structure and Properties", ACS Symposium Series 162, Washington D. C., 1981, Chap. 17

201. Clark D. T. and Dilks A., J. Polym. Sci., Polym. Chem. Ed., 16, 911 (1978)

202. Millard M., in "Techniques and Applications of Plasma Chemistry", Hollahan J. R. and Bell A. T., Eds., Wiley, N. Y., 1974, Chap. 5

203. Yasuda H., in "Plasma Polymerization", Shen M. and Bell A. T., Eds., ACS Symposium Series 108, Washington D. C., 1979, Chap. 2

204. Osada Y., Bell A. T. and Shen M., J. Polym. Sci., Polym. Lett. Ed., 16, 309 (1978)

205. Clark D. T. and AbRahman M. Z., J. Polym. Sci., Polym. Chem. Ed., in press, 1981

206. Clark D. T. and Shuttleworth D., J. Polym. Sci., Polym. Chem. Ed., 18, 27 (1980)

207. Clark D. T., Feast W. J., Kilcast D. and Musgrave W. K. R., J. Polym. Sci., 11(2), 389 (1973)

208. Clark D. T., AboShebak M. M., and Brennan W. J., in preparation

209. Kay E. and Dilks A., J. Appl. Phys., 15(11), 5676 (1980)

210. Nonhebel D. C. and Walton J. C., Eds., "Free-Radical Chemistry" Cambridge, Uni. Press, 1974, Chap. 8

211. Clark D. T. and Shuttleworth D., Euro. Polym. J., 15, 265 (1979)

212. Clark D. T. and Shuttleworth D., J. Polym. Sci., Polym. Chem. Ed., 18, 407 (1980)

213. Sperati C. A., in "Polymer Handbook", Brandrup J. and Immergut E. H., Eds., 2nd., Wiley, 1975

214. Rendall I., Converter, Sept. 22 (1974)

215. Dewar M. J. S. and Rzepa H. S., J. Am. Chem. Soc., 100, 58 (1978)

216. Allen M. and Maier J. P., Chem. Phys. Lett., 34, 442 (1975)

217. Frazier J.R., Christophorou L. G., Carter J. G. and Schweinler H. C., J. Chem. Phys., 69, 3807 (1978)

218. Frueholz R. P., Flicker W. M., Mosher O. A. and Kuppermann A., J. Chem. Phys., 70, 3057 (1979)

219. Barltrop J. A. and Coyle J. D., Eds., "Excited States in Organic Chemistry", Wiley, London, 1975, Chap. 9

220. Haller I., J. Chem. Phys., 47, 1117 (1969)

221. a). Potts A. W., Price W. C., Streets D. G. and Williams T. A., Farad. Disc., Chem., Soc., 54, 168 (1972)

b). C. f. Potts A. W., Price W. C., Gabriel A. and Williams T. A., in "Molecular Spectroscopy", West A. R., Ed., London, 1977

222. Carrington A. and McLachlan A. D., Eds., "Introduction to Magnetic Resonance", Harper and Row, N. Y., 1967

223. Clark D. T. and AbRahman M. Z., J. Polym. Sci., Polym. Chem. Ed., submitted for publication

224. Clark D. T. and Feast W. J., J. Macromol Sci., Review in Macromol. Chem., C12, 191 (1975)

225. Clark D. T. and AbRahman M. Z., J. Polym. Sci., Polym. Chem. Ed., in press, 1981

226. Clark D. T., Adams D. B., Kilcast D. and Musgrave W. K. R., J. Elect. Spect. and Rel. Phen., 1, 227 (1972/73)

227. Clark D. T. and Muller J., J. Chem. Phys., Chem. Phys. Lett., 30, 394 (1975)

228. Clark D. T. and AbRahman M. Z., J. Polym Sci., Polym. Chem. Ed., submitted for publication

229. Yasuda H, Hirotsu T. and Olf H. G., J. Appl. Polym. Sci., 21, 3179 (1977)

230. Bieri G., in "Conf. Proc.-Int. Symp. Plasma Chemistry. 4th", Veprek S. and Hertz J., Eds., 2, 467, 1979

231. Clark D. T.,Cromarty B. J. and Dilks A., J. Polym. Sci., Polym. Chem. Ed., 16, 3173 (1978)

232. Clark D. T. and AbRahman M. Z., J. Polym. Sci., Polym. Chem. Ed., to be submitted

233. Shafrin E. G., in "Polymer Handbook", Brandrup J. and Immergut E. H., Eds., 2nd. Edn., Wiley, 1975

234. Willis H. A. and Zichy V. J. in "Polymer Surfaces", Clark D. T. and Feast W. J., Eds., Wiley, London, 1978, Chap. 15

235. "Selected Infrared Spectral Data", Haas C. W., Ed., American Petrolium Institute Research Project 44, Thermodynamic Research Center, Texas, 1008, 1976

236. Heone J. and Hickam W. M., J. Chem. Phys., 32, 876 (1960)

237. Olah G. A., Mateescu G. D. and J. L. Riemenschnieder, J. Am. Chem. Soc., 94, 2529 (1972)

APPENDIX TWO

LECTURES AND SEMINARS ATTENDED DURING THE PERIOD 1978-81

15 September 1978

Professor W. Siebert (University of Marburg, West Germany), "Boron Heterocycles as Ligands in Transition Metal Chemistry".

22 September 1978

Professor T. Fehlner (University of Notre Dame, U.S.A.), "Ferraboranes: Syntheses and Photochemistry".

12 December 1978

Professor C.J.M. Stirling (University of Bangor), "Parting is Such Sweet Sorrow" - the Leaving Group in Organic Reactions.

14 February 1979

Professor B. Dunnel (University of British Columbia), "The Application of N.M.R. to the Study of Motions in Molecules".

16 February 1979

Dr. J. Tomkinson (Institute of Laue-Langevin, Grenoble), "Properties of Adsorbed Species".

4 March 1979

Dr. J.C. Walton (University of St. Andrews), "Pentadienyl Radicals".

20 March 1979

Dr. A. Reiser (Kodak Ltd.), "Polymer Photography and Mechanism of Cross-Link Formation in Solid Polymer".

25 March 1979

Dr. S. Larsson (University of Uppsala), "Some Aspects of Photoionisation Phenomena in Inorganic Systems".

25 April 1979

Dr. C.R. Patrick (University of Birmingham), "Cholorofluorocarbans and Stratospheric Ozone: An Appraisal of the Environmental Problem".

1 May 1979

Dr. G. Wyman (European Research Office, U.S. Army), "Excited State Chemistry in Indigoid Dyes".

2 May 1979

Dr. J.D.Hobson (University of Birmingham), "Nitrogen-centred Reactive Intermediates".

8 May 1979

Professor A. Schmidpeter (Institute of Inorganic Chemistry, University of Munich), "Five-membered Phosphorus Heterocycles Containing Dicoordinate Phosphorus".

9 May 1979

Dr. A.J. Kirby (University of Cambridge), "Structure and Reactivity in Intramolecular and Enzymic Catalysis".

9 May 1979

Professor G. Maier (Lahn-Giessen), "Tetra-tert-butyltetrahedrane".

10 May 1979

Professor G. Allen, F.R.S. (Science Research Council), "Neutron Scattering Studies of Polymers".

16 May 1979

Dr. J.F. Nixon (University of Sussex), "Spectroscopic Studies on Phosphines and their Coordination Complexes".

23 May 1979

Dr. B. Wakefield (University of Salford), "Electron Transfer in Reactions of Metals and Organometallic Compounds with Polychloro-pyridine Derivatives".

13 June 1979

Dr. G. Heath (University of Edinburgh), "Putting Electrochemistry into Mothballs - (Redox Processes of Metal Porphyrins and Phthalocynanines".

14 June 1979

Professor I. Ugi (University of Munich), "Synthetic Uses of Super Nucleophiles".

20 June 1979

Professor J.D. Corbett (Iowa State University, Ames, Iowa, U.S.A.), "Zintle Ions: Synthesis and Structure of Homopolyatomic Anions of the Post-Transition Elements".

27 June 1979

Dr. H. Fuess (University of Frankfurt), "Study of Electron Distribution in Crystalline Solids by X-ray and Neutron Diffraction".

21 November 1979

Dr. J. Muller (University of Bergen), "Photochemical Reactions of Ammonia".

28 November 1979

Dr. B. Cox (University of Stirling), "Macrobicyclic Cryptate Comlexes, Dynamics and Selectivity".

5 December 1979

Dr. G.C. Eastmond (University of Liverpool), "Synthesis and Properties of Some Multicomponent Polymers".

12 December 1979

Dr. C.I. Ratcliffe (University of London). "Rotor Motions in Solids".

19 December 1979

Dr. K.E. Newman (University of Lausanne), "High Pressure Multinuclear NMR in the Elucidation of the Mechanisms of Fast, Simple Inorganic Reactions".

30 January 1980

Dr. M.J. Barrow (University of Edinburgh), "The Structures of some Simple Inorganic Compounds of Silicon and Germanium - Pointers to Structural Trends in Group IV".

6 February 1980

Dr. J.M.E. Quirke (University of Durham), "Degradation of Chlorophyll-a in Sediments".

23 April 1980

B. Grievson B.Sc., (University of Durham), "Halogen Radio-pharmaceuticals".

14th May 1980

Dr. R. Hutton (Waters Associates, USA), "Recent Developments in Multi-milligram and Multi-gram Scale Preparative High Performance Liquid Chromatography".

21st May 1980

Dr. T .W. Bentley (University of Swansea), "Medium and Structural Effects in Solvolytic Reactions".

10th July 1980

Professor P. des Marteau (University of Heidelburg), "New Developments in Organonitrogen Fluorine Chemistry".

7th October 1980

Professor T. Felhner (Notre-Dame University, USA), "Metallo-boranes - Cages or Coordination Compounds"

15th October 1980

Dr. R. Adler (University of Bristol), "Doing Chemistry Inside Cages - Medium Ring Bicyclic Molecules".

12th November 1980

Dr. M. Gerloch (University of Cambridge), "Magnetochemistry is about Chemistry".

19th November 1980

Dr. T. Gilchrist (University of Liverpool), "Nitroso Olefins as Synthetic Intermediates".

3rd December 1980

Dr. J.A. Connor (University of Manchester), "Thermochemistry of Transition Metal Complexes".

18th December 1980

Dr. R. Evans (University of Brisbane, Australia), "Some Recent Communications to the Editor of the Australian Journal of Failed Chemistry".

18th February 1981

Professor S. F. A. Kettle (University of East Anglia), "Variations in the Molecular Dance at the Crystal Ball".

25th February 1981

Dr. K. Bowden (University of Sussex), "The Transmission of Polar Effects of Substituents".

4th March 1981

Dr. S. Craddock (University of Edinburg), "Pseudo-Linear Pseudohalides".

11th Marth 1981

Dr. J.F. Stoddard (I.C.I. Ltd./University of Sheffield), "Stereochemical Principles in the Design and Function of Synthetic Molecular Receptors".

17th March 1981

Professor W. Jencks (Brandsis University, Massechusetts), "When is an Intermediate not an Intermediate?".

18th March 1981

Dr. P. J. Smith (International Tin Research Institute), "Organotin Compounds - A Versatile Class of Organometallic Compounds".

9th April 1981

Dr. W. H. Meyer (RCA Zurich), "Properties of Aligned Poly-acetylene".

7th May 1981

Professor M.Gordon (Essex University), "Do Scientists Have to count".

10th June 1981

Dr. J. Rose (I.C.I. Plastics Division), "New Engineering Plastics".

17th June 1981

Dr. P. Moreau (University of Montpellier), "Recent Result in Perfluoroorganometallic Chemistry".

Conferences Attended During The Period 1978 - 1981

1. Royal Institute of Chemistry/Chemical Society Annual Congress, Durham, April, 1981.

2. Polymer Characterization Symposia, Durham, July 1981.

APPENDIX 3

Determination of Contact Angles from Dimensions of Liquid Drops

a) $\theta < 90^\circ$

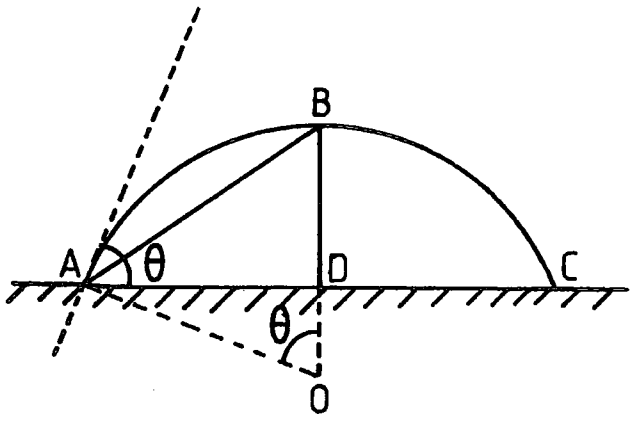

b) $\theta > 90^\circ$

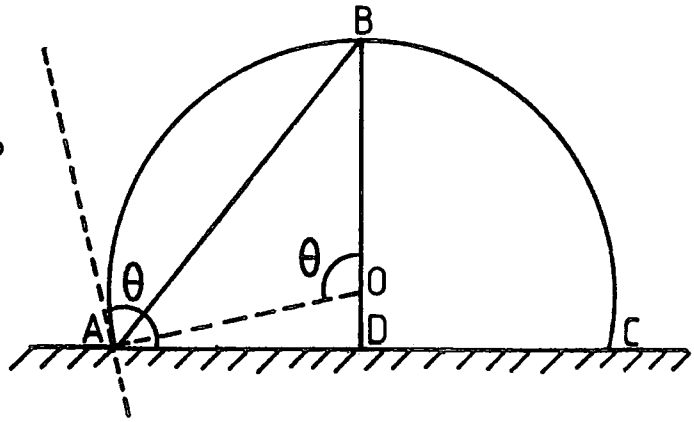

$$\theta = 2 \tan^{-1} \frac{BD}{AD}$$